HEAT TRANSFER AND FLUID FLOW STUDIES ON FLAT HEAT PIPE

THESIS

Submitted to

THE UNIVERSITY OF CALICUT

in fulfilment of the requirement for the award of the degree of

DOCTOR OF PHILOSOPHY

in

MECHANICAL ENGINEERING

by

C. MURALEEDHARAN

Department of Mechanical Engineering

Calicut Regional Engineering College

CALICUT - 673601, KERALA

JUNE 2001

CERTIFICATE

This is to certify that the thesis entitled **"Heat Transfer and Fluid Flow Studies on Flat Heat Pipe"** being submitted by **C. Muraleedharan** to the University of Calicut, for the award of the degree of **Doctor of Philosophy,** is a record of the bonafide research work carried out by him under my supervision and guidance. The results contained in this thesis have not been submitted to any other University or Institute for the award of any Degree or Diploma.

Department of Mechanical Engineering
Calicut Regional Engineering College
Calicut 673 601

Dr. S. Jayaraj
Assistant Professor
Department of Mechanical Engineering
Calicut Regional Engineering College
Calicut – 673 601

Date: 18 - 6 - 2001

Forwarded to the University

18/06/2001

Dedicated

To

My Parents

ACKNOWLEDGEMENT

I express my profound gratitude to my research guide Dr. S. Jayaraj, Assistant Professor, Department of Mechanical Engineering for his invaluable guidance, tremendous support and constructive suggestions during the research work. I will always remain grateful to him for the fruitful end of this work.

I wish to express my sincere thanks to Dr. C. Robert Samuel, former Professor, Department of Mechanical Engineering for attracting me towards this topic and guiding me at the early stages of the research work. The financial assistance provided by A.R.D.B, Govt. of India (Project No. 443) is also acknowledged which was useful in setting up the experimental test rigs.

I express my sincere thanks to Dr. N.M. Nagarajan, Professor and Head, Department of Mechanical Engineering, for providing all the helps and facilities for completion of the research work.

I wish to express my sincere thanks to Dr. M.P. Chandrasekharan, Principal and former Head, Department of Mechanical Engineering for providing all the requisite facilities and encouragement rendered without which the research work would not have been completed.

I wish to thank Dr. K. Prabhakaran Nair, Professor, Department of Mechanical Engineering, Dr. C.B. Sobhan, Assistant Professor, Department of Mechanical Engineering, Dr. P. Syamala, Assistant Professor, Department of Civil Engineering and Dr. E. Gopinathan, Professor and Head, Department of Electronics Engineering, the

Members of the Doctoral Committee for reviewing the work and extending valuable suggestions regarding my research work.

I would like to extend my thanks to Dr. P. M. Abdul Majeed, Dr. K. N. Dutta, Dr.V. George and Dr. R. Ravindran Nair former Heads, Department of Mechanical Engineering for the helps rendered during the course of the research work.

I am very much thankful to Mr. Ghulam Jilani, Lecturer, Department of Mechanical Engineering for the fruitful discussions with him. I am also thankful to the M. Tech students Mr. P. S. Hariharan, Mr. Jayee. K. Varghese, Ms. Krishna Priya, Mr. Soumitra Mahato and Mr. Krishna Prasad.

I am very much thankful to Mr. P. Anilkumar, Mr. Joseph George, Mr. T. P. Balan and all the other Technical Staff, Department of Mechanical Engineering for their helps rendered in completing the experimental part of the research work in time. I am thankful to Mr. N.M. Jayachandran, Draughtsman, Department of Mechanical Engineering for the neat preparation of drawings related with the work.

I am thankful to all my colleagues in the Department of Mechanical Engineering for their encouragement during the course of the research work.

Finally, I am very happy to appreciate my wife P. S. Sathidevi and children Aparna and Murali Gopal for their encouragement and wholehearted co-operation for the completion of the research work.

C. Muraleedharan

ABSTRACT

Heat pipe is a simple heat transport device having very high 'effective thermal conductance'. Due to its significant advantages like compactness, light weight and passiveness, heat pipe finds a wide range of applications to dissipate heat. Some of the applications of heat pipe are cooling of electronic components, flattening of temperature in aerospace vehicles, waste heat recovery from exhaust gas, etc. Flat rectangular heat pipes can economically be employed for handling large heat transfer rates when weight and space are major constraints.

The working medium which is entrapped within the heat pipe experiences phase transformations from liquid to vapour and vice versa. The vapour working medium which is formed by the vaporisation of liquid at the evaporator region by absorbing heat from the heat source, flows to the condenser section through the vapour core. The vapour condenses at the condenser zone by rejecting heat to the sink and returns to the evaporator through the porous wick structure utilising capillary pumping pressure for re-evaporation.

The working fluid experiences pressure drop both in the wick region and vapour channel. The simple theory of the heat pipe states that the capillary pressure developed in the wick should be greater than the sum of the pressure drops in the vapour core and in the wick structure. If the heat pipe is not horizontal, then gravitational head will also play a role in the pressure balance.

In low capacity heat pipe designs, the pressure drop in the vapour core is generally neglected. However in flat heat pipes which carry large heat fluxes, this pressure drop will be significant. The heat pipe is hypothetically an isothermal device. That is, it is capable of working without any temperature drop along the heat pipe.

However, in practice depending upon the temperature difference between the evaporator and the condenser, a temperature gradient can exist in the heat pipe. Many research works were done on cylindrical heat pipes. Investigators like Busse (1967 and 1989), Bankston and Smith(1973), Tien and Rohani (1974), etc. analysed the flow in the vapour core of the circular heat pipe. A noticeable work reported on flat heat pipe was by van Ooijen and Hoogendoorn (1979 and 1981). They investigated the flow of vapour in the flat heat pipe both theoretically and experimentally. Vafai *et al.*(1992,1995 and 2000) and Sobhan *et al.* (1997 and 2000) analysed numerically both the liquid flow and vapour flow in flat heat pipe. But a detailed analysis of the liquid flow was not reported in any of these investigations. Abhat and Nguyenchi (*cf.* Dunn and Reay, 1982) and Strel'tsov (*cf.* Dunn and Reay, 1982) are a few who have investigated on fluid inventory in gravity assisted heat pipes. However the work on this area is found to be inadequate. The present work envisages the theoretical and experimental analyses of fluid flow, both liquid and vapour and heat transfer characteristics of nonsymmetrical flat heat pipes. The following are the three main objectives of the present work.

(i) Experimental investigations of the performance of the flat heat pipe.
(ii) Application of Poiseuille approximation model for the flat heat pipe.
(iii) Development of two dimensional numerical model for the flat heat pipe.

The present study is aimed to obtain the following characteristics of the flat heat pipe.

(i) Theoretical velocity distribution in the vapour core and wick region.
(ii) Theoretical temperature distribution in the vapour core and wick region.
(iii) Experimental temperature distribution along the heat pipe.
(iv) Pressure variation in the heat pipe.
(v) Effect of amount of working fluid in the heat pipe performance.
(vi) Effect of wick porosity on the performance of heat pipe.

The heat transfer and fluid flow in flat heat pipe has been analysed by experimentally and theoretically. The experimental investigations have been conducted on two different test rigs. The first one is a stainless steel flat heat pipe with axially grooved wick, which can employ either water or acetone as working fluid. The important performance characteristics like temperature distribution and pressure variation along the heat pipe have been obtained at various heat fluxes while using both the working fluids. The effect of amount of the working fluid on the performance of this heat pipe is also studied using water and acetone as working substances. The experiments have been carried out on the heat pipes not only with the normal charges, but with undercharge and overcharge also.

The effect of porosity of the wick structure on the performance of the heat pipe has been investigated on an aluminium flat heat pipe with acetone as working fluid. This heat pipe has been fabricated with provision to change the wick structure. Wick structures with different wire screen meshes, axial grooves and their combinations (with porosity values 0.75, 0.70, 0.65 and 0.50) have been tested on the aluminium - acetone flat heat pipe.

Poiseuille theory can be used to determine the velocity and the pressure drop in the flow of working fluid in the flat heat pipe. Liquid flow in the wick and vapour flow through the vapour core are assumed to be laminar and incompressible. A two dimensional situation for the flow is created by considering the width of the heat pipe to be very large compared to the thickness of the heat pipe.

The flow of vapour through the vapour core obtained by Poiseuille model can easily be shown as parabolic. The mean velocity is linearly increasing at the evaporator zone due to mass addition by evaporation of the liquid medium, uniformly at the adiabatic section and finally linearly decreasing at the condenser zone due to

condensation of vapour. Similar liquid velocity distribution is available for the flow of liquid medium through the wick, with the major difference of change in the direction of flow. At condenser zone of the liquid wick velocity increases due to mass injection by condensation and depletes at the evaporator by evaporation of liquid from liquid wick matrix.

The complex mechanism of fluid flow and heat transfer inside the heat pipe has been analysed numerically. The working medium flows from the evaporator to the condenser through the vapour core as vapour and returns to the evaporator through the wick structure as liquid. A two dimensional model for nonsymmetrical flat heat pipe of rectangular in cross section under steady state operating conditions has been developed. The vapour flow in the vapour channel and the liquid flow in the porous wick structure have been analysed separately here. They have similar governing equations. However, the boundary conditions are distinct with common interface conditions.

The flow of vapour through the vapour core is similar to any fluid flowing in a flat rectangular passage, while the liquid working medium flows through the *porous* wick structure. In addition to the two dimensional continuity and momentum equations, energy equation has also been considered in both cases. These equations have been solved adapting the stream function - vorticity approach. The governing equations have been discretised using Alternating Direction Implicit (ADI) finite difference scheme.

The variation of pressure and the distribution of temperature along the stainless steel heat pipe have been obtained with water and acetone as working fluids for different Reynolds number (Re) values. The temperature at evaporator, adiabatic and condenser zones are experimentally found to be almost constant at the respective

sections except in low heat fluxes. The distribution of temperature and pressure have been studied with various amount of charges with both the working fluids. The working fluid quantity has influence on the performance of the heat pipe. The surface temperature of the heat pipe is found to be minimum and effective thermal conductance is maximum with the optimum charge in the heat pipe. Mainly the temperature characteristics are studied in the aluminium - acetone heat pipe with various wick structures. It has been observed that as the porosity of the wick decreases the temperature of the heat pipe increases. The high thermal conductivity of the container material causes a temperature gradient to exist from the evaporator end to the condenser end. Pressure build up has been observed in the vapour flow when acetone is used as the working fluid in the stainless steel flat heat pipe.

The velocity distribution along the vapour core and through the wick structure have been found out for various Reynolds numbers using Poiseuille model. The pressure drop in the liquid is estimated by Darcy's equation. The pressure drop in the vapour flow is also determined by considering the frictional and inertial terms separately. When Re>5, the pressure in the condenser zone can build up due to domination of the inertial component.

Numerical results have been obtained with different Reynolds number values for a stainless steel flat heat pipe which employs water as the working substance. Stream lines, velocity vector plots, velocity profiles, velocity distribution, isotherms, temperature distribution and pressure variations have been plotted for both the vapour flow and liquid flow. It has been observed that the velocity profile in the vapour at low Re values are parabolic. But at high values Re of the profile has deviation from this. The temperature in the evaporator, adiabatic and condenser zones are virtually uniform in the wick region when low conducting material is used for the container.

The effect of porosity on velocity, pressure and temperature in the flat heat pipe has also been analysed numerically. The evaporator temperature has been found to be increasing, pressure drop increases and axial velocity increases with decrease in porosity. The temperature distribution along the stainless heat pipe has been compared with that of van Ooijen (1981) and found to be similar in nature. The pressure drop estimated using Poiseuille model has been compared with the values obtained from experimental and numerical results.

The investigations carried out on flat heat pipe reveal that the vapour pressure drop must be taken into account in the compact design of large capacity heat pipes. Poiseuille model is only an approximate method to estimate the pressure drop. The pressure drop in the vapour core which has been obtained experimentally and numerically have similarities and larger in magnitude than that obtained by Poiseuille model.

The axial velocity distribution obtained numerically in the vapour core and wick region are like that assumed in Poiseuille model. The velocity in the vapour core increases due to mass addition eventhough it is not linear in the evaporator zone by evaporation and decreases at condenser zone by condensation. The velocity distribution in the liquid wick region has direction opposite to the former one. It has also been observed that at low Reynolds number values the axial velocity profile is parabolic in nature in the vapour core but has deviation at higher Re values.

The pressure drop in the wick and temperature in the heat pipe have been found to be increasing with decrease in porosity of the wick structures. Though the temperature distribution along the heat pipe is unchanged in the respective zones using low conducting container wall, there is temperature drop from one end to the other end when a highly conducting material like aluminium is used for the container.

The experimental temperature characteristics reveal that the amount of working fluid has effects on the performance of the heat pipe.

The present research work leads to the following noticeable contributions. Stream function- vorticity approach has been employed in the vapour core of the heat pipe by a few investigators, but in the present work this has been applied to liquid wick region of the flat heat pipe also. In addition to that, a detailed analysis of liquid flow in flat heat pipe has been presented here which was not much studied. The temperature distributions obtained by numerical and experimental studies have been found to be matching. The numerical and experimental temperature distributions at various porosity values are comparable. Experimentally it has been established that the temperature at no zone will remain constant when highly conducting material is used for the container of the heat pipe. The heat pipe shall be charged with the optimum amount of working fluid for the best performance.

CONTENTS

NOMENCLATURE

English Alphabets

Ar - Aspect Ratio (Ratio of Thickness to Length)

C - Specific Heat, kJ/kg K

C_E - Ergun's Constant

C_p - Specific Heat at Constant Pressure, kJ/kg K

d - Wire Diameter, m

Da - Darcy's Number

h - Thickness, m

h_{fg} - Enthalpy of Evaporation, J/kg

k - Thermal Conductivity, W/m K

K - Wick Permeability, m^2

l - Dimensional Length, m

L - Nondimensional Length

M - Liquid Transport Factor or Merit Number, W/m^2

N - Number of Nodes

Na - End of Adiabatic Section

Ne - End of Evaporator Section

NX - Number of Nodes in X-direction

NY - Number of Nodes in Y-direction

p - Dimensional Pressure, N/m^2

p_C - Capillary pressure, N/m^2

p_∞ - Reference Pressure, N/m^2

P - Nondimensional Pressure

P′ - Nondimensional Pressure Drop

P^+ - Nondimensional Pressure Drop With Respect to the Effective Pressure Drop

Pr - Prandtl Number

q - Heat Flux Intensity, W

r_C - Capillary Radius, m

r* - Nucleation Radius, m

r_h - Hydraulic Radius, m

R - Thermal Resistance

Re - Reynolds Number

RHC - Ratio of Specific Heats

t - Dimensional Time, s

T - Dimensional Temperature

u - Dimensional Velocity Component in X-direction, m/s

U - Nondimensional Velocity Component in X-direction

u_o - Vertical Velocity at Wick-Vapour Interface, m/s

v - Dimensional Velocity Component in Y-direction, m/s

V - Nondimensional Velocity Component in Y-direction

$\forall$ - Volume of Working Fluid

W - Width of Heat Pipe, m

x,y - Dimensional Cartesian Co-ordinates

X,Y - Nondimensional Cartesian Co-ordinates

z - Impedance

Greek Symbols

α - Thermal Diffusivity, m^2/s

β - Momentum Correction Factor

δ - Groove Width, m

Δq - Axial Heat Conduction Along the Container, W

ε - Porosity of Wick

E - Error

ϕ - Angle of Contact, Degree

γ - Inclination of Heat Pipe, Degree

μ - Dynamic Viscosity, N s/m^2

ν - Kinematic Viscosity, m^2/s

θ - Nondimensional Temperature

ρ - Density, kg/m^3

σ - Surface Tension, N/m

τ - Nondimensional Time

Ω - Nondimensional Vorticity

ψ - Nondimensional Stream Function

Subscripts

a - Adiabatic

B - Boiling

c - Condenser

C - Capillary

e - Evaporator

eff - Effective

E - Entrainment

f - Frictional

g - Gravitational

i - Location in X-direction

in - Inertial

j - Location in Y-direction

l - Liquid

m - Mean

S - Sonic

so - Source

si - Sink

v - Vapour

V - Viscous

w - Wick

Superscripts

n - Time Level

n +1/2 - Time Level

n +1 - Time Level

* - Value at Previous Time Level

LIST OF FIGURES

LIST OF TABLES

INTRODUCTION

C. Muraleedharan “Heat transfer and fluid flow studies on flat heat pipe ” Thesis. Department of Mechanical Engineering, Calicut Regional Engineering College , University of Calicut, 2001

Chapter 1

INTRODUCTION

1.1 Introduction

The heat exchanging devices are used in numerous thermal systems ranging from the modern power generation systems to domestic heating and air conditioning systems. Smaller and more compact devices are preferred in most of the applications. The heat pipe is a simple and novel device that allows the transfer of substantial quantities of heat through small surface or cross sectional area. It finds many applications like cooling of electronic components, temperature evening-out in satellites, recovery of waste heat, etc. In addition to the objectives of the research work, the basic principles and heat transport limits of flat heat pipe are discussed in this chapter.

1.2 Thermosyphon and Heat Pipe

In thermosyphon, a small quantity of a liquid (say, water) is kept in an evacuated vertical tube. When the lower end is heated up, water gets evaporated. The vapour moves to the cold end of the tube where it gets condensed rejecting heat. The condensate is returned, to the hot lower end by gravity. This is the working principle of 'thermosyphon'. Since latent heat of vaporisation of the fluid is utilised in thermosyphon, large quantities of heat can be transported easily. This leads to high 'effective thermal conductance'. The main limitation noticed in thermosyphon is that

for returning the condensate gravity force is utilised. This restricts the position of the thermosyphon to be vertical and always the heat is absorbed at the lower end.

The heat pipe has similarities with thermosyphon. The schematic diagram of a heat pipe is shown in Fig. 1.1 The inner region of a heat pipe consists of a vapour core and a wick structure. The wick structure is generally made of a few layers of fine mesh is fixed at the inner surface of the container. The capillary pumping force developed in the wick structure returns the condensate to the evaporator from the condenser. Hence there is no restriction on the location of the heating or cooling end and orientation of the heat pipe. The term 'heat pipe' itself is used to indicate its 'high thermal conductance'.

1.3 Working Principle of Heat Pipe

Conventionally heat pipes are circular in section. Rectangular heat pipes can also be used to effect large heat transfer rates in the place of several cylindrical heat pipes. The present work deals exclusively with flat rectangular heat pipes. The inner surface of the metallic container has a lining with a wick. The ends of the container are sealed off with end caps after evacuating and saturating the wick structure with a working fluid.

Functionally, any heat pipe has three zones (see Fig. 1.2). The part of the heat pipe which is in contact with the heat source is the evaporator. The other end which is communicating with the heat sink is the condenser. In between these two zones the adiabatic section exists whenever the heat source and sink are separated by a distance. When the heat pipe is not operating, the temperature of the heat pipe is same as the ambient and the pressure inside the heat pipe is the saturation pressure of

the working fluid at the ambient temperature. When the heat source is brought in contact with the evaporator and heat sink with the condenser, the heat pipe begins to operate.

The saturation pressure of the working fluid is higher at higher temperatures. At the vapour core of the evaporator region in the heat pipe, a higher vapour pressure corresponding to evaporator temperature prevails. However, at the condenser a low vapour pressure tend to be established. As the vapour space is connected, this results in the flow of vapour from evaporator to condenser region tending to equilise the pressure. This leads to a situation where the vapour core pressure is less than the saturation pressure at the evaporator temperature and greater than saturation pressure at the condenser temperature. This results in evaporation of liquid at the wick into the vapour core of the evaporator and condensation of vapour at the condenser side. Evaporation of liquid at the evaporator exposes tiny pores of wick which maintain a lower pressure of the liquid in the wick at the evaporator due to surface tension. The lower pressure of liquid in the wick at the evaporator makes liquid to flow from the condenser to the evaporator through the wick.

1.4 Selection of Materials for Heat pipe

The basic components of heat pipe are:

(i) container,

(ii) wick structure and

(iii) working fluid

It is essential that suitable combination of different materials is selected for a given application. A review of available materials and their significance are elaborated in the following sections.

1.4.1 Container

The container material should have high thermal conductivity so that heat transfer into the heat pipe at the evaporator and from the heat pipe at the condenser takes place with less temperature drops across the container wall. The container material should possess sufficient strength at the operating temperature range. The specific gravity of the material is also an important consideration in typical applications. Commonly used materials for the heat pipe container are copper, aluminium, stainless steel and nickel.

1.4.2 Wick Structure

Selection of wick includes both the wick material and the wick geometry. It is essential that the thermal conductivity of wick material should be sufficiently high. Low thermal conductivity causes high temperature drop across the wick which can lead to burn out. The geometry of the wick should be selected so that it produces maximum capillary pumping pressure. Though smaller pore radius provides larger capillary pressure, the frictional pressure drop in the liquid phase is inversely proportional to the pore size.

There are three principal capillary geometries as depicted in Fig. 1.3

(i) wick consisting of porous structure made up of interconnecting pores, like wire mesh, felts, sintered powder wick, etc.

(ii) open grooves which may be constructed at the bottom plate itself and

(iii) covered grooves, consisting of an area for liquid flow closed by a fine mesh capillary structure, which are called as composite wicks.

1.4.3 Working Fluid

The working fluid of the heat pipe selected for a particular application should satisfy the following conditions.

(i) The triple point and critical temperature of the working fluid should be outside the operating temperature range of the heat pipe

(ii) The working fluid should be compatible with the wick and container materials.

(iii) The working fluid should be stable in the operating temperature range of the heat pipe.

(iv) The working fluid should possess good thermophysical properties (Tables C.1 and C2 give the thermophysical properties of acetone and water respectively).

Below the triple point, the working fluid is in solid state. The enthalpy of evaporation is very less near the critical temperature. Table 1.1 gives the useful temperature range for different working fluids which are used for heat pipe applications. The compatibility has two aspects namely chemical reaction between the working fluid with the wick and container materials and the deposition of materials in the wick structure. The latter affects the proper working of the wick and development of hot spots is noticed. Gas generation within the heat pipe is also reported in such cases. The compatibility data for low temperature heat pipe working

fluids is given in Table 1.2. Thermally unstable working fluids decompose and lead to the production of non-condensable gases which will impair the unhindered operation of the heat pipe. The working fluid should have high surface tension as the capillary pumping force is obtained due to surface tension of the working fluid. The major pressure drop is the frictional pressure drop of the working fluid in the wick and hence the working fluid should be having low liquid viscosity. The enthalpy of evaporation should be large enough to carry maximum heat per unit charge. For working fluids with high density, for same mass flow rate, velocity is less and hence the pressure drop is decreased.

A good heat pipe working fluid should have low viscosity, high surface tension, large density and high enthalpy of evaporation. No working fluid will possess all these properties simultaneously. Thus a combined parameter called 'Liquid Transport Factor' or 'Merit Number' (M) is defined as,

$$M = \frac{\rho_l \ \sigma_l \ h_{fg}}{\mu_l} \tag{1.1}$$

It is obvious that higher value of the merit number is desirable for working fluid used in heat pipe application. All the above properties vary with temperature and hence the merit number is a function of temperature. The variation of Merit number against temperature for different working fluids is shown in Fig. 1.4.

1.5 Heat Transport Limits of Flat Heat Pipe

The basic data required for the design of a heat pipe is the heat flux to be handled. The design of a flat heat pipe is quite complicated. The dimensions of the

heat pipe and the materials used for construction are usually selected as per the application. The designed heat pipe need to be checked for the various limitations.

The heat transport capacity of a heat pipe is limited by different mechanisms which depend on the geometry, wick structure, vapour channel space, working fluid and operating temperature. The maximum heat load permitted by these phenomena is known as the limit (or limitation) of heat pipe. The various limits of a heat pipe are listed below.

(i) Capillary limit (Wicking limit)

(ii) Viscous limit.

(iii) Entrainment limit.

(iv) Sonic limit.

(v) Boiling limit.

(vi) Wall thermal resistance limit

1.5.1 Capillary Limit

When the heat pipe is under normal operation, the working fluid which flows in the heat pipe experiences phase transformations by timely absorption and rejection of heat from the heat source and the sink respectively. While flowing along the heat pipe the vapour and liquid working mediums face pressure drops and there exists a pressure balance for normal functioning of the heat pipe.

For the heat pipe to operate steadily, the maximum capillary pumping pressure p_c must be greater than the total pressure drop in the heat pipe.

$$p_c + p_g \geq \Delta p_l + \Delta p_v \tag{1.2}$$

where Δp_l is the liquid pressure drop,

Δp_v is the vapour pressure drop and

p_g is the gravitational pressure head (which may be positive, zero or negative).

The driving forces are summed up and equated to the pressure drops. Re-arranging these the capillary limit of a flat heat pipe is obtained as (Robert Samuel 1991),

$$Q_c = \frac{h_{fg} W(2\sigma_l / r_c)\cos\theta + \rho_l g \sin\alpha}{12\mu_v / h_v^3 \rho_v + \mu_l / 2Kh_w \rho_l} \tag{1.3}$$

where Q_c is the capillary limit.

The parameter appearing in the denominator of Eq. (1.3) is defined separately for wire screen mesh and rectangular grooves.

(i) Wire screen mesh $$K = \frac{d^2 \varepsilon^3}{122(1-\varepsilon)^2} \tag{1.4}$$

where $$\varepsilon = 1 - \frac{\pi SNd}{4} \tag{1.5}$$

(ii) Rectangular grooves $$K = \frac{2\varepsilon r_{hl}^2}{f_l \, Re_l} \tag{1.6}$$

where $$\varepsilon = \frac{w}{\delta} \tag{1.7}$$

The parameter $f_l Re_l$ in the denominator of Eq. (1.6) is to be determined from the Fig. 1.5 (Chi, 1976).

1.5.2 Viscous Limit

At low temperatures viscous forces are dominant in the vapour flow through the vapour of the heat pipe. Busse (1973) has shown that the axial heat flux increases as the condenser pressure is reduced, the maximum heat flux occurring

when the condenser pressure is reduced to zero. He carried out a two-dimensional analysis and obtained a relation for viscous limit in circular heat pipe. The corresponding viscous limit for flat heat pipe is (Robert Samuel, 1991),

$$Q_v = \frac{h_v^{\,3} W \rho_v p_v h_{fg}}{24 \mu_v l_{eff}} \tag{1.8}$$

where Q_v is the viscous limit.

1.5.3 Entrainment Limit

In a heat pipe, the vapour flows through the vapour core from the evaporator towards the condenser at a particular velocity. The wick has many pores with liquid exposed to the vapour region. The flowing vapour tends to shear off the liquid from the wick. This tendency is resisted by the surface tension of the working fluid. If the magnitude of the shear force is greater than the surface tension force, the liquid droplets from the wick are carried by the flowing vapour. This depletes the wick of enough liquid that is being returned to the evaporator. This phenomenon is known as the entrainment in the heat pipe operation. Due to entrainment the evaporator can be starved of liquid and hence the heat pipe fails to function properly.

The Weber number, We, which is the ratio of inertial vapour force and surface tension force is used as a convenient scale to measure the tendency of entrainment.

i.e. $$We = \frac{\rho_v v_v r_{hv}}{2\pi\sigma_l} \tag{1.9}$$

Here r_{hv} is the hydraulic radius of the vapour core. When a value of unity is assigned to We, the condition

$$v_v = \left[\frac{2\pi\sigma_l}{\rho_v r_{hv}}\right]^{1/2} \tag{1.10}$$

is obtained. This value of v_v is used in the equation for heat capacity and the entrainment limit of flat heat pipe (Q_E) is obtained as (Robert Samuel, 1991),

$$Q_E = Wh_v h_{fg}\left[\frac{2\pi\rho_v\sigma_l}{r_{hv}}\right]^{1/2} \tag{1.11}$$

1.5.4 Sonic Limit

In the evaporator of the heat pipe, the mass flux increases in the direction of vapour flow while in the condenser the mass flux decreases. This is analogous to a converging – diverging nozzle. Hence the vapour flow in a heat pipe is happening like compressible fluid flow through a converging–diverging nozzle and there is a possibility of the occurance of choking phenomena in the vapour region. This puts a limit to the maximum heat transport (Q_s), known as the sonic limi and given by (Robert Samuel, 1991), the expression

$$Q_S = 0.5h_v Wh_{fg}[\rho_v p_v]^{1/2} \tag{1.12}$$

1.5.5 Boiling Limit

As there is heat transfer into the heat pipe, a temperature gradient exists across the wick and the temperature at the wick-container interface is higher than vapour temperature at the evaporator zone. However, the pressure of liquid in the wick is less than the vapour pressure in the core by the amount of capillary pressure and hence the whole system is not in thermodynamic equilibrium. The liquid near the container

has excess energy proportional to the temperature difference between the interface and the wick. This excess energy tends to make the liquid flash into vapour. However, at normal operation, when transverse heat flux is low, flashing may not occur. The increase in the temperature difference with the increase in heat flux and at a stage vapour bubbles may be formed in the wick near the container. As the bubble has low thermal conductivity, the heat transfer is further reduced and the temperature gradient is greatly increased leading to burn out in the heat pipe. The heat pipe load (Q_B) that can initiate burn out is termed as the boiling limit (Robert Samuel, 1991)

$$Q_B = \frac{2 W l_e k_w T}{h_w h_{fg} \rho_v}\left[\frac{2\sigma}{r^*} - p_c\right] \qquad (1.13)$$

Here r^* is the nucleation radius which may be assumed to be of the order 2.5×10^{-7}m. The boiling limit can be avoided by reducing the heat flux. This is often done by increasing the length of the evaporator section.

1.5.6 Wall Thermal Resistance Limit

The heat carried by the heat pipe has to pass across the evaporator wall, through the vapour core and across the condenser wall. The temperature variation in the heat pipe and corresponding thermal circuit are in Figs. 1.6 and 1.7, respectively. The heat transfer path has various thermal resistances as listed below.

(i) R_{eo} = Convective resistance at the outer wall of the evaporator

(ii) R_{et} = Conduction resistance across the container at the evaporator

(iii) R_{ew} = Conduction resistance across the wick structure at the evaporator

(iv) R_v = Resistance for heat transfer through the vapour core

(v) R_{ew} = Conduction resistance across the wick structure at the condenser

(vi) R_{ct} = Conduction resistance across the container at the condenser

(vii) R_{co} = Convective resistance at the outer wall of the condenser

(viii) R_k = Conduction resistance along the heat pipe wall

The wall thermal resistance limit for heat transport is the maximum possible heat transfer through the heat pipe which is limited by the wall thermal resistance for the given source and sink temperatures.

$$Q_t = \frac{T_{so} - T_{si}}{R_t} \tag{1.14}$$

Here the equivalent thermal resistance (R_t) of the heat pipe is given by,

$$R_t = R_{co} + R_{co} + \frac{1}{\frac{1}{R_k} + \frac{1}{R_{et} + R_{ct} + R_{ew} + R_{cw} + R_v}} \tag{1.15}$$

The equation (1.15) excludes the thermal resistances at the wick vapour interface at the evaporator and condenser as these resistances are very small compared with other resistances considered. The thermal resistance offered for flow through the vapour core is small in conventional heat pipes. In addition, the heat transfer along the container from the evaporator to the condenser is negligible in most conventional heat pipes. The resulting simplified thermal resistance for the heat pipe is,

$$R_t = R_{eo} + R_{co} + R_{et} + R_{ct} + R_{ew} + R_{cw} \tag{1.16}$$

The individual heat transfer resistances for a flat heat pipe are given as,

$$R_{co} = \frac{1}{Wl_e h_o} \tag{1.17}$$

$$R_{co} = \frac{1}{Wl_c h_o} \tag{1.18}$$

$$R_{ct} = \frac{t_t}{W l_e k_t} \tag{1.19}$$

$$R_{ct} = \frac{t_t}{W l_e k_t} \tag{1.20}$$

$$R_{cw} = \frac{h_w}{W l_e k_w} \tag{1.21}$$

$$R_{cw} = \frac{h_w}{W l_e k_w} \tag{1.22}$$

The maximum possible heat transfer (Q_t) through the heat pipe limited by the wall thermal resistance limit for flat heat pipe is obtained as (Robert Samuel, 1991),

$$Q_t = \frac{W l_e l_c (T_{so} - T_{si})/(l_e + l_c)}{1/h_o + t_t/k_t + h_w/k_w} \tag{1.23}$$

1.6 Advantages of Heat Pipe

The heat pipe has the following outstanding advantages:

(i) It is simple in construction and operation.

(ii) The heat pipe has very high 'equivalent thermal conductance' (several times the thermal conductivity of copper).

(iii) It is a passive device (*i.e* no external power is required to activate the heat pipe).

(iv) It does not require an extensive coolant circuit (as in the case of convective cooling).

(v) The heat pipe is very compact in size and light in weight.

1.7 Applications of the Heat Pipe

Some of the areas of application of heat pipe are listed below. The special characteristics of the heat pipe is utilised in each of the following applications.

(i) Separation of heat source and sink

(ii) Temperature flattening,

(iii) Heat flux transformation,

(iv) Temperature control,

(v) Thermal diodes and

(vi) Energy conservation.

The high effective thermal conductivity of heat pipes enables heat to be transferred at high efficiency over considerable distances. In many applications it may be inconvenient to dissipate the heat through a heat sink or a radiator located in the immediate neighbourhood to the heat generating component. For example, heat dissipation from a high power device within a module containing other temperature-sensitive components would be effected by using the heat pipe to connect the component to a remote heat sink located outside the module.

The heat pipe tends towards operation at a uniform temperature. It maybe used to reduce thermal gradients at different locations within the body. For example, the outer skin of a satellite which is facing the sun will be hot whereas the opposite side under shadow will be cooler.

In thermionics, the heat transfer of a comparatively low heat flux, as generated by radio active isotopes into sufficiently high heat flux capable of being utilised effectively in thermionic generators has been attempted.

The temperature control can effectively be achieved using a variable conductance heat pipe. This can be used to control accurately the temperature of devices mounted on the evaporator section of the heat pipe. This method is extensively used in aircraft and cooling in integrated circuit packages.

Thermal diodes are used where heat transport in one direction only is required. Examples are space vehicles and cryogenic applications. Thermal switches enable the heat pipe to be switched off and on to permit flow of heat in one direction only.

Heat pipes can effectively be used in tapping solar energy. The heat pipe assisted solar collectors have many advantages over conventional solar collectors. The cooling and thereby freezing by recirculation which is common in ordinary solar collectors, is avoided in heat pipe assisted solar collectors. In addition to that the maintenance cost will also be less in such collectors. Heat pipes can be used for recovering waste heat even from fluids with very small temperature difference. Large waste heat recovery boilers can be operated with the help of heat pipes.

1.8 Objectives of the Present Work

Commonly used heat pipes have circular cross section and many researchers have studied on this type of heat pipe in detail. For applications in confined space, large heat transfer can be effected with flat heat pipes having rectangular cross section. Such heat pipes have less unit weight and hence find use especially in aerospace applications.

The heat pipe is theoretically an isothermal device. That is, it can work without considerable temperature variation. But there can exist a temperature gradient in the adiabatic section depending upon the temperature difference between

the evaporator and condenser zones. The container of the heat pipe is normally made of materials having high thermal conductivity in order to transmit heat at evaporator as well as the condenser zones. Hence, some amount of heat will be transmitted through the container walls and wick material also directly from the evaporator to the condenser region.

The working fluid within the heat pipe experiences liquid phase pressure drop in the wick and vapour phase pressure drop in the vapour core. In addition, the working fluid undergoes pressure losses during acceleration and deceleration. Over and above it is subject to the gravitational head in heat pipes which are not kept horizontal. The capillary rise in the evaporator draws the fluid from the condenser end of the heat pipe overcoming the above pressure drops. Though these pressure losses are small, they are significant as far as the operation the heat pipe. The amount of heat transfer depends very much on these pressure drops.

In most heat pipe designs, vapour core area is made large so that the vapour phase pressure drop is insignificant. Where space or weight considerations control the selection of heat pipe, the vapour core area is reduced thereby compromising on the vapour phase pressure drop. Majority of the work available in literature are carried out with respect to circular heat pipes. Busse (1967 and 1989), Bankston and Smith (1973), Tien and Rohani (1974) etc. have estimated the pressure drop in the vapour core of cylindrical heat pipe. A noticeable work done on flat heat pipe are by van Ooijen and Hoogendoorn (1979 and 1981). They investigated theoretically and experimentally the vapour flow in flat heat pipe. They have obtained the temperature distribution along the bottom plate of the heat pipe also.

The liquid working fluid reaches the evaporator from the condenser because of capillary pumping pressure developed in the porous wick. During the flow through the wick structure liquid also experiences pressure drop. The liquid pressure drop depends upon the pore radius and porosity of the wick structure. In addition to the pressure variation,fluid flow in the wick structure will have effect on the temperature distribution along the heat pipe. Vafai (1992, 1995 and 2000) and his colleagues have investigated the flow of working medium in the flat heat pipe. They analysed both liquid and vapour flows in the flat heat pipe. Sobhan *et al.* (1997 and 2000) numerically analysed the liquid flow and vapour flow in the flat heat pipe. They also studied the influence of wick porosity incorporating the axial heat conduction along the container wall on the heat pipe performance. But so far no detailed report about the liquid flow along the wick structure in flat heat pipe have come out.

The amount of working fluid (charge) required for a particular heat pipe has to be estimated using various parameters like length of the heat pipe, area of cross section of the wick structure, porosity of the wick and area of cross section of the vapour core. The optimum charge of a heat pipe is the amount of working fluid which is required just to saturate the porous wick structure and to fill the vapour core and other charging lines. It is essential to charge the heat pipe carefully with the exact amount of working substance. If the amount of the working medium in a heat pipe is less or greater than the optimum charge there will be the change in the performance of heat pipe. Rarely investigators have worked on this particular problem. Abhat & Nguyenchi (*cf.* Dunn and Reay, 1982) and Strel'tsov (*cf.* Dunn and Reay, 1982) are a few who investigated the fluid inventory in gravity assisted heat pipes. However, the work on this area is found to be quite inadequate.

The present work is mainly aimed at studying the flow of vapour working medium in the vapour core and liquid flow in the wick region of nonsymmetrical flat heat pipes. Heat transfer characteristics of flat heat pipes are to be analysed theoretically and experimentally, which will help in developing the optimum design of flat heat pipes. The effects of the amount of working medium and axial conduction along the container wall on the heat pipe performance are studied experimentally. The influence of wick structure i.e. wick porosity on the performance of the flat heat pipes is also analysed by both numerically and experimentally. Numerical analysis for both the flow of vapour in the vapour channel and the liquid flow through the wick structure in flat heat pipe are carried out and compared with the experimental results.

1.9 Outline of the Thesis

The present chapter intends to convey the basic principles of heat pipes. The working principle of the heat pipe, its components, the heat transport limits, advantages and important applications are discussed. The significance of the present work and the main objectives are also stated in detail. In the following chapters a brief review on existing literature, the programme of the present work, the results and discussions, conclusions and scope for future work and the contributions of the research work are discussed.

Before detailing the actual work, it is essential to give an overview of the existing literature on heat pipes. Most of the works connected with heat pipe in literature are on cylindrical heat pipes. However, there are some recent reports on flat heat pipes also. The analysis of heat transfer characteristics, vapour flow and

liquid flow in heat pipes (both cylindrical and flat heat pipes) are discussed in **Chapter 2**.

The programme of the work consists of three sections (see Fig.1.8). They are

(i) the experimental studies on the flat heat pipe,

(ii) the Poiseuille model and

(iii) numerical model.

Chapter 3 describes the experimental studies conducted on two flat heat pipes. One heat pipe was constructed with stainless steel having cavity dimensions of 550mm x 80mm x 10mm. Both water and acetone are used as working substances in this heat pipe. Another heat pipe was constructed with aluminium as the container and having size 440mm x 50mm x 14mm. Experiments were conducted with acetone as working fluid in this heat pipe. Extensive experimentations (see Figs.1.9 and 1.10) were conducted on both the heat pipes for the sake of obtaining the vapour pressure drop along the flat heat pipes, temperature characteristics and influence of wick porosity and fluid inventory on the heat pipe performance.

In **Chapter 4** the Poiseuille model applied to flat heat pipe is discussed. This is an approximate method to estimate the pressure drops in the vapour core and the liquid wick region. The velocity distributions and pressure drop for various Reynolds numbers and porosity values estimated in the vapour flow and liquid flow are compared with other results.

In **Chapter 5** the numerical model of the flat heat pipe is analysed in detail using the basic continuity, momentum and energy equations. Two dimensional steady state solution is obtained for the vapour flow in the vapour space and liquid flow

through the wick using Alternating Direction Implicit (ADI) finite difference scheme employing the stream function – vorticity approach.

In **Chapter 6** the various results of the experimental investigations, Poiseuille model and numerical studies are presented. Comparison of these results and also that available in the literature are presented in this chapter. The thesis is concluded with detailing the inferences derived based on the present work and proposing the scope for future work on this topic in **Chapter 7**. The contributions of the present research work are also highlighted in this chapter.

Table 1.1 Useful Operating Temperature of Working Fluids

Sl. No.	Medium	Melting Point (^{0}C)	Boiling Point at Atmospheric Pressure (^{0}C)	Useful Range (^{0}C)	
				Min	Max
1	Helium	-272	-269	-271	-269
2	Nitrogen	-210	-196	-203	-160
3	Ammonia	-78	-33	-60	100
4	Freon-11	-111	24	-40	120
5	Pentane	-130	28	-20	120
6	Freon-113	-35	48	-10	100
7	Acetone	-95	57	0	120
8	Methanol	-98	64	10	130
9	Ethanol	-112	78	0	130
10	Heptane	-90	98	0	150
11	Water	0	100	30	200
12	Toluene	-95	110	50	200
13	Thermex	12	257	150	395
14	Mercury	-39	361	250	650
15	Caesium	29	670	450	900
16	Potassium	62	774	500	1000
17	Sodium	98	892	600	1200
18	Lithium	179	1340	1000	1800
19	Silver	960	2212	1800	2300

Table 1.2 Compatibility Data

Wick Material	Water	Acetone	Ammonia	Methanol
Copper	RU	RU	NU	RU
Aluminium	GNC	RL	RU	NR
Stainless Steel	GNT	PC	RU	GNT
Nickel	PC	PC	RU	RL

RU – Recommended by past successful usage
RL – Recommended by literature
PC – Probably compatible
NR – Not recommended
GNC – Generation of gases at all temperatures
GNT – Generation of gases at elevated temperatures.

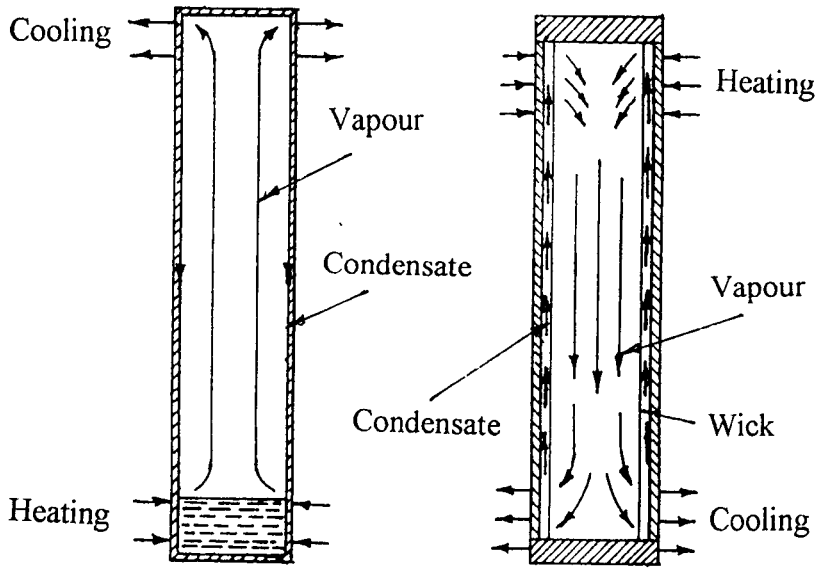

a) Thermosyphon b) Heat Pipe

Fig.1.1 Thermosyphon and Heat Pipe

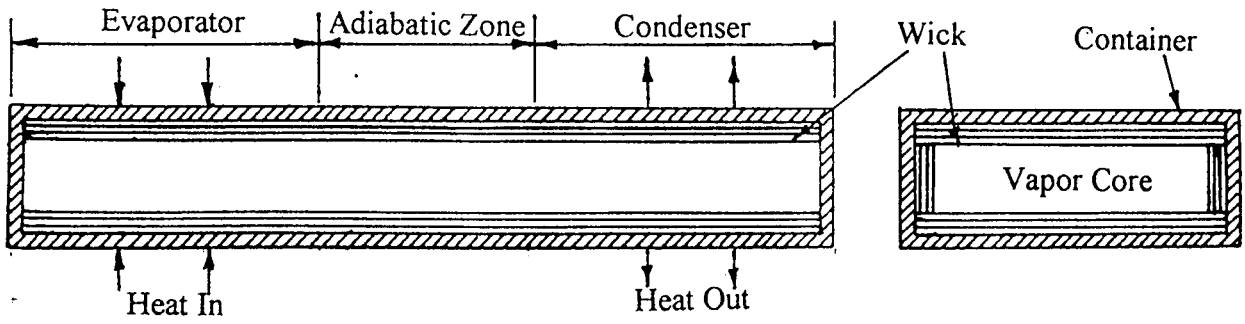

Fig.1.2 Rectangular Heat Pipe

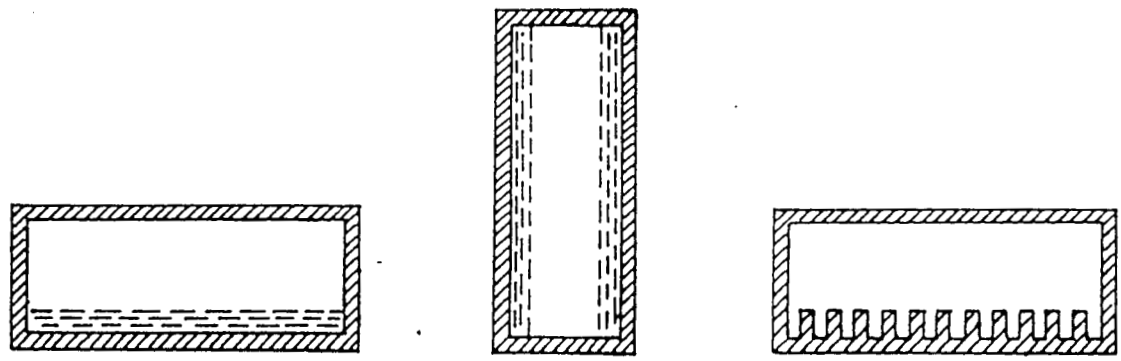

a1) Wire Screen

a2) Wire Screen

b) Axial Grooves

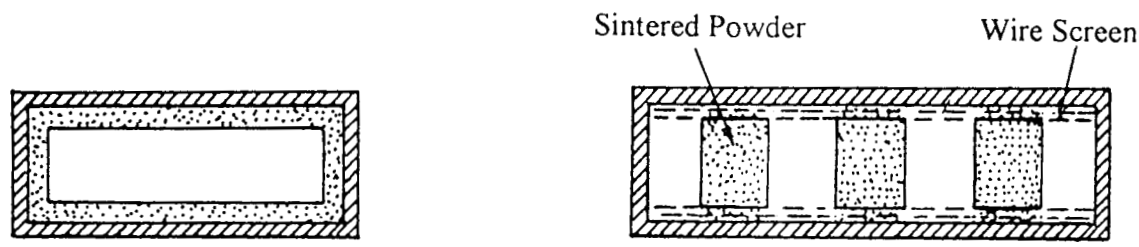

c) Sintered Metallic Powder

d) Composite Wick

Fig.1.3 Different Types of Wick Structures

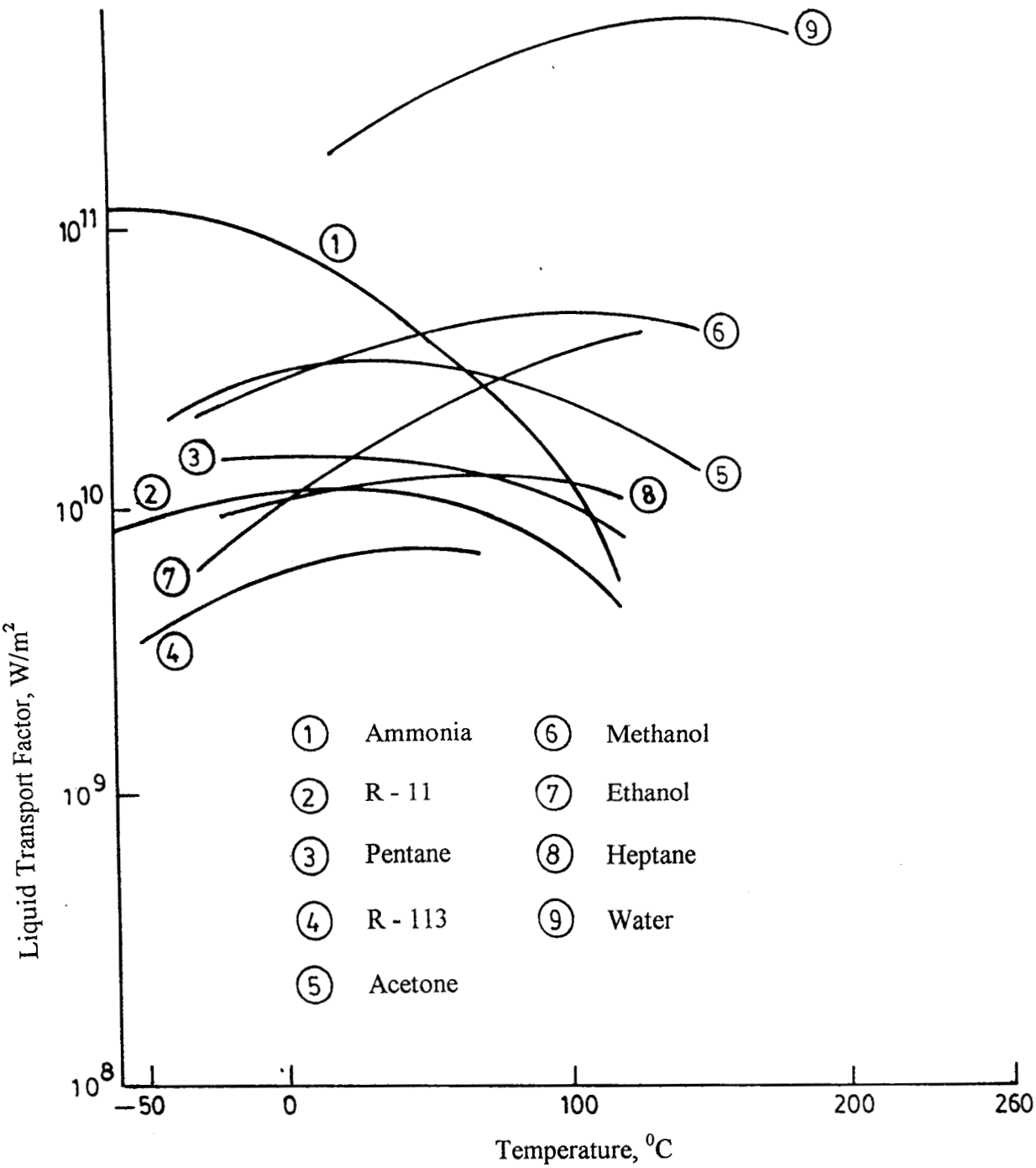

Fig.1.4 Liquid Transport Factor for Low Temperature Working Fluids

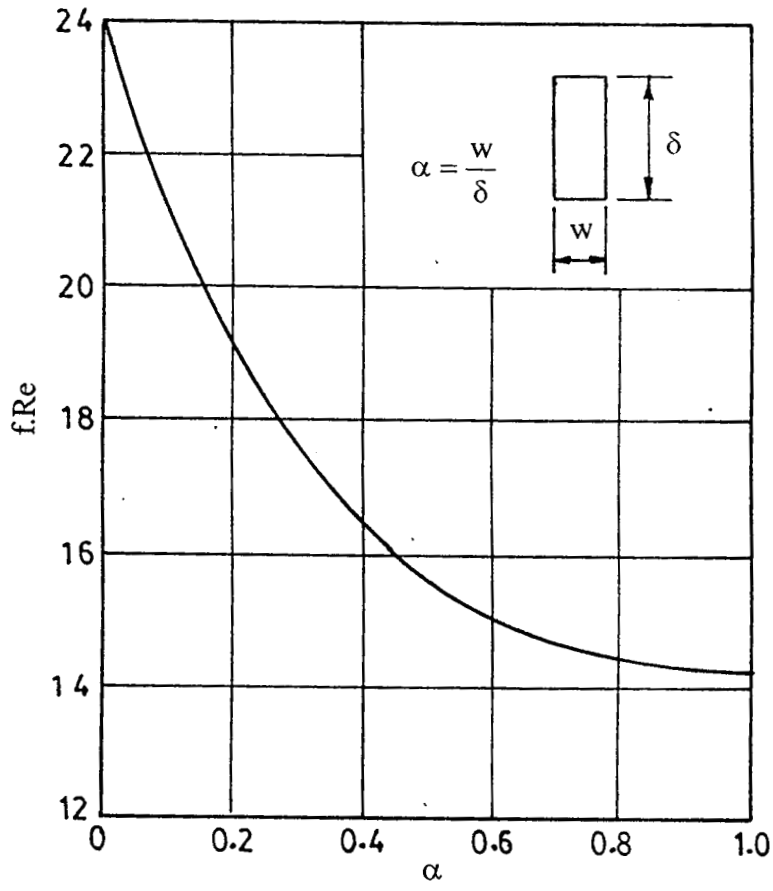

Fig.1.5 Frictional Coefficients for Laminar Flow in Rectangular Passages

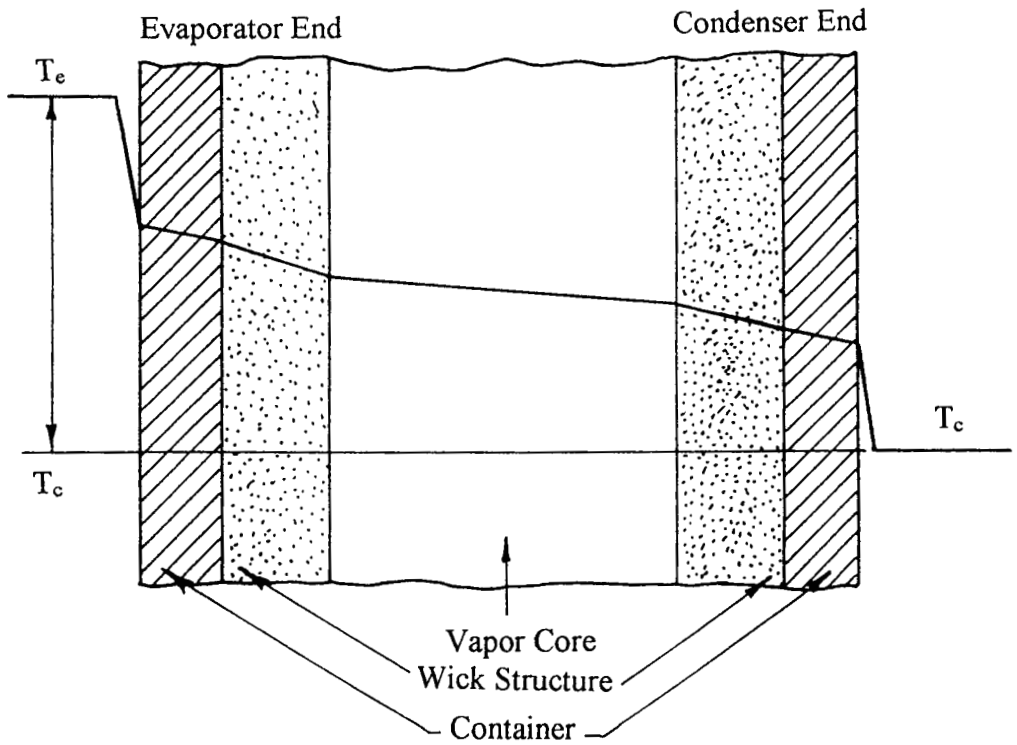

Fig.1.6 Temperature Variation in Heat Pipe

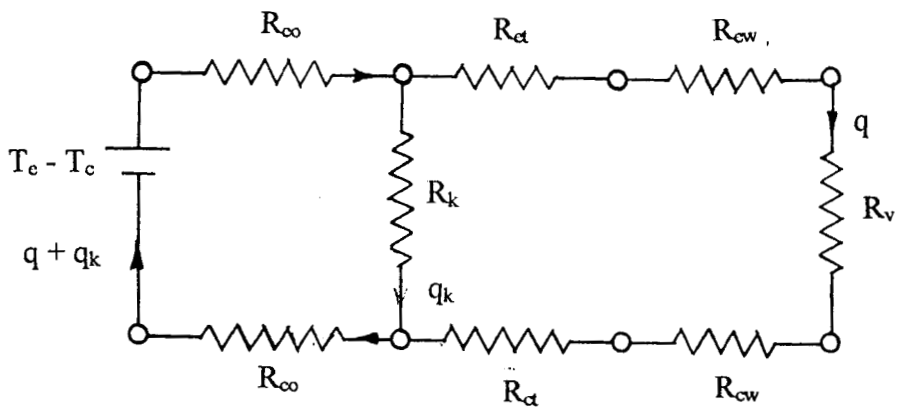

Fig.1.7 Thermal Circuit for Heat Pipe

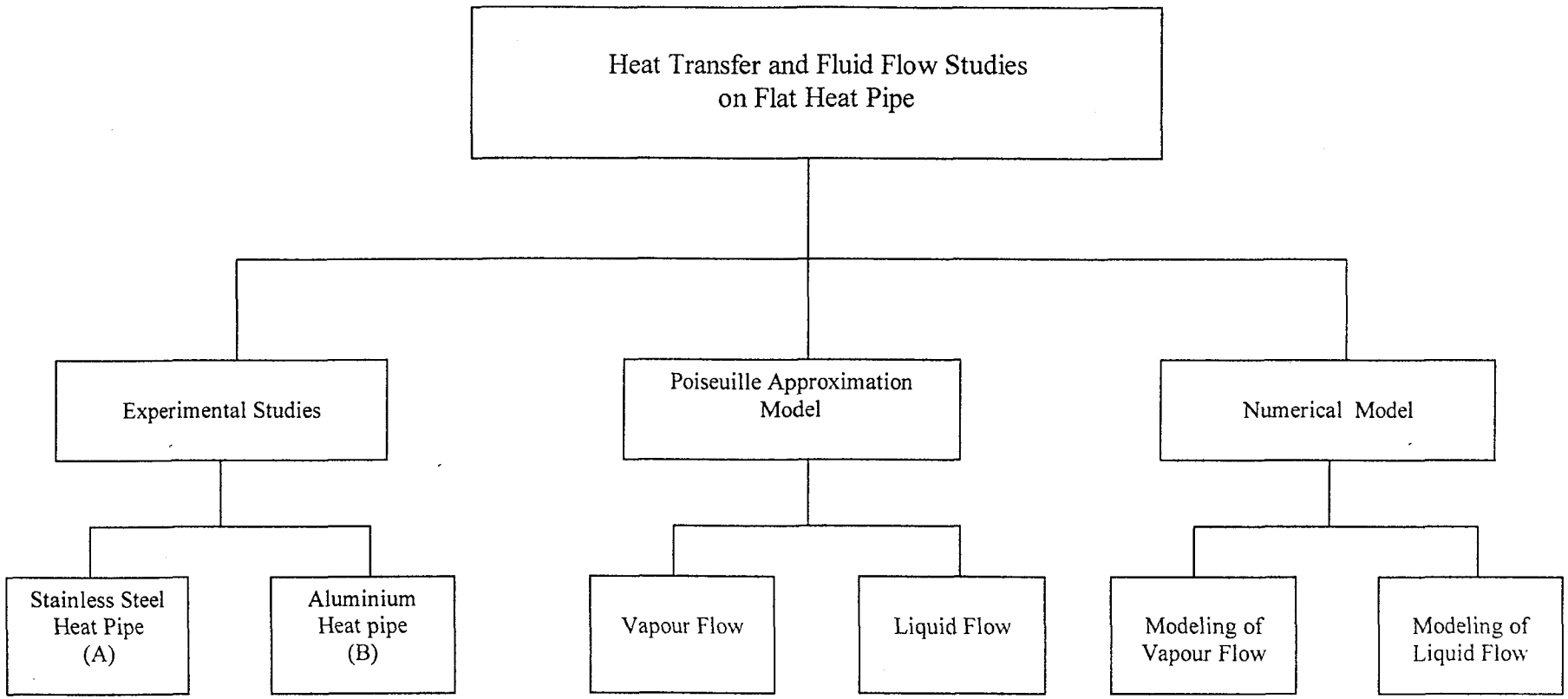

Fig.1.8 Schematic Diagram of Programme of the Present Work

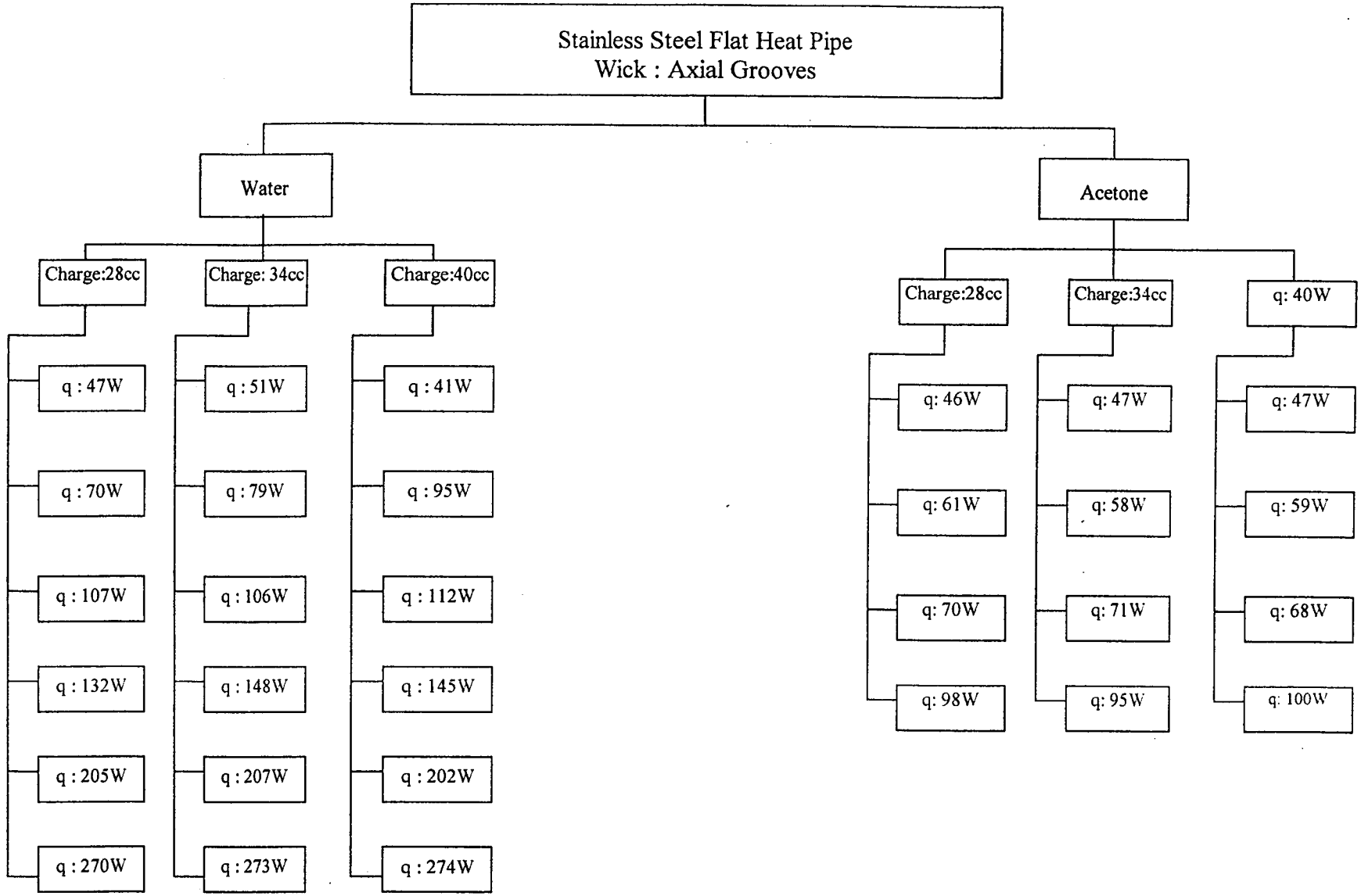

Fig.1.9 Schematic Diagram of Experiments Carried Out on Stainless Steel Flat Heat Pipe

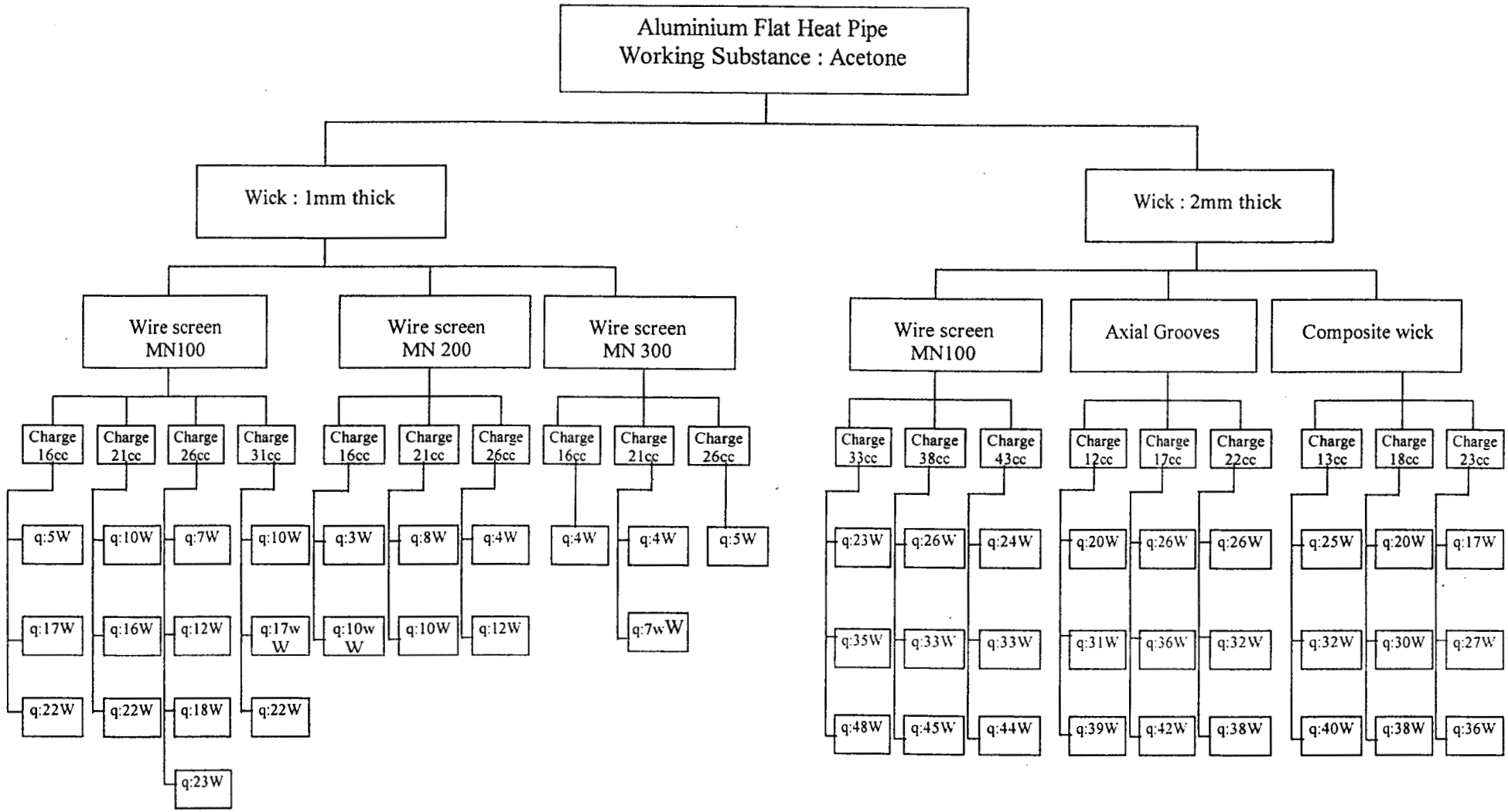

Fig.1.10 Schematic Diagram of Experiments Carried Out on Aluminium Flat Heat Pipe

LITERATURE REVIEW

C. Muraleedharan “Heat transfer and fluid flow studies on flat heat pipe ” Thesis. Department of Mechanical Engineering, Calicut Regional Engineering College , University of Calicut, 2001

Chapter 2

LITERATURE REVIEW

2.1 Introduction

The concept of the heat pipe was first introduced by Gaugler in 1942 (*cf.* Dunn and Reay, 1982). According to Gaugler, the objective of his invention was "to cause absorption of heat, or in other words evaporation of the liquid to a point above the place where the condensation or giving off heat takes place without expending upon the liquid any additional work to lift the liquid to an elevation above the point at which condensation takes place". A capillary structure was proposed as the means for returning the liquid from the condenser to the evaporator.

However, it was not widely publicised until 1963 when Grover (*cf.* Dunn and Reay, 1982) reinvented the concept. Grover demonstrated it as a high performance heat transmission device, named it "The Heat Pipe" and developed its application at Loss-Alamos Laboratory, New Mexico.

After Grover's publication, extensive work on heat pipe was carried out at UK Atomic Energy Laboratory in Harwell and at ISPRA in Italy. The areas of application of the heat pipe extended from thermionic emitters and refrigeration purposes to satellite cooling, air conditioning, cooling of electronic components, engine cooling, etc. Several types of wick structures were proposed and many working fluids were used. Along with the conventional heat pipes increasing interests are also found now

a days in the area of flat rectangular heat pipes, disk type heat pipes, rotating heat pipes, flexible heat pipes and micro heat pipes.

2.2 Literature Review

Large number of theoretical and experimental investigations have been carried out with heat pipes and the reports are available in literature. The majority of the publications are on the flow of working fluid that too in the vapour core and heat transfer in cylindrical heat pipes. Some literature are also available on the flow of liquid through the capillary wick structure. Researchers and experimenters have recently started showing interest in the combined analysis of vapour core and liquid wick regions of the heat pipe. This chapter gives an overview of the important literature available on the heat pipes. Both the works done on cylindrical heat pipes as well as on flat heat pipes are reviewed here.

2.2.1 Cylindrical Heat Pipes

Traditionally, heat pipes are cylindrical in shape. Hence, majority of the investigations are done in the area of circular heat pipe. The working principle, the fluid flow and heat transfer mechanism are similar in any heat pipe (irrespective of the shape). Therefore the review of the works on cylindrical heat pipes is done here with respect to fluid flow and heat transfer mechanism in a heat pipe.

In the field of circular heat pipes the contribution of Busse is invaluable. Under the leadership of Busse, ISPRA, Italy had become the focal point of heat pipe activities in Europe. Busse first analysed (1967, 1970 and 1973) the problem of pressure drop in laminar vapour flow in a long cylindrical heat pipe. Poiseuille

velocity profile was assumed. The analysis leads to similarity profiles for the evaporation zone and variation of profiles with the axial distance in the condenser zone.

Busse *et al.* (1970) have developed high temperature cylindrical heat pipes for thermionic converters. Niobium, Zirconium and Tungsten were the container materials used. The working substances used were Lithium, Lead, Bismuth and Barium. The temperature range selected was between 1500°C and 2000°C for the operation of their heat pipes. Busse (1973) presented the ultimate limit of heat transfer for the cylindrical heat pipes with laminar vapour flow. The heat transfer in the heat pipe is limited either by insufficient return flow of condensate or by vapour flow limitation. Busse has proved that, if the return flow is guaranteed by a suitable wick, the heat flux is ultimately limited by vapour flow effects only. He described the two different regimes of vapour flow as inertia flow regime and viscous flow regime. Busse predicted approximate expressions to compute these heat transfer limits. His analysis shows that, the ultimate limit of heat transfer is of the viscous type below a certain temperature. Busse (1980 and 1982) have reported about the analysis of dry-out mechanism in gravity-assisted cylindrical heat pipes with capillary flow. Busse and Loehrke (1989) have presented further a method for the prediction of laminar subsonic flow in cylindrical heat pipes. They have described about the velocity profiles, including strong flow reversals occurring within the heat pipe. The calculation of pressure recovery at the condenser section was also reported by them.

Chun (1972) carried out an experiment to predict the dry out limits on screen wick. A new model was proposed by him for the wick dry out. Chun found that his model predicts with in 10 percent of the experimental dry out heat inputs which are

below the values that would be expected if the evaporator wick were fully saturated with liquid. Tien and Rohani (1972) have established a theoretical frame work for predicting the steady state operational characteristics of a two component heat pipe. They showed the variation of temperature and pressure along the heat pipe by applying the law of conservation of mass and energy as well as thermodynamic equilibrium relations. In order to substantiate the validity of the theoretical model, a series of experiments were carried out on a horizontal cylindrical heat pipe with water and ethanol mixture as the working fluid.

Tien and Rohani (1974) have also studied the effects of vapour pressure drop on vapour temperature, evaporation and condensation rates on a cylindrical heat pipe. Stream function-vorticity approach was used to solve the two dimensional axi-symmetric problem. In addition, they introduced the energy conservation equations and thermodynamic equilibrium equations to couple the vapour pressure and the temperature. Variation of temperature and pressure were presented up to a radial Reynolds number of 36. Bankston and Smith (1973) reported the two dimensional analysis of a cylindrical heat pipe. For laminar flow the mass and momentum equations are solved with finite difference computational method based on stream function vorticity approach, thus eliminating pressure as a separate variable. The results are reported over a wide range of Reynolds number (Re) values, from very small to very high. For different ranges of Re values, the convergence and accuracy of the method depended largely on the appropriate choice of the vorticity boundary conditions. In each particular range of increasing Re values deviations from Poiseuille flow become evident first in the condenser. Flow reversal is encountered for Re values greater than 2.

Faghri and his co-workers have done a lot of research work on heat pipes. Faghri and Thomas (1989) fabricated and tested successfully a newly designed concentric annular heat pipe. They carried out theoretical and experimental studies to predict the capillary limit on concentric annular heat pipe. A significant increase of the heat capacity per unit area was found compared to conventional circular heat pipes. Cao and Faghri (1990) have studied the phase change mechanisms in the heat pipe, numerically. They have presented the two dimensional model for compressible flow analysis with respect to high temperature cylindrical heat pipes also.

A numerical model was presented by Chen and Faghri (1990) for the overall performance of the cylindrical heat pipes with single or multiple heat sources. The analysis includes the heat conduction through wall and liquid wick regions considering the compressibility effect of the vapour inside the heat pipe. The two dimensional governing equation and thermodynamic equilibrium relations with appropriate boundary conditions are solved. The axial temperature and pressure obtained and compared with the existing experimental results. Faghri and Buchko (1991) carried out experimental and numerical analyses of the effects of heat load distribution on the vapour temperature, wall temperature and heat transfer capacity for heat pipes with multiple heat sources. An optimization of heat distribution of such heat pipes was performed and found that the heat capacity can be increased by redistribution of heat loads.

Jang and Faghri (1991) have reported a one dimensional transient analysis on cylindrical heat pipe, treating the vapour as compressible using an implicit finite difference scheme. In addition to the pressure variation with respect to time, velocity and temperature distribution against axial distance at steady state conditions have also

been obtained. Faghri and Harley (1994) have described two dimensional models of conventional circular and gas loaded heat pipes. In both the cases the axial conduction through the wall was incorporated in the analysis. By lumped analysis of conventional heat pipe, they have obtained the temperature distribution at transient and steady state conditions. Comparison of numerical solutions with the experimental data was also given. The mathematical model detailed by Khrustalev and Faghri (1995) describes the heat transfer through liquid films in the evaporator of heat pipe with capillary grooves. The model accounts for the effects of interfacial thermal resistance, pressure and surface roughness for a particular contact angle. The free surface temperature was determined and the expression for interfacial resistance was given by kinetic theory.

Shibayama and Morooka (1979) have studied the evaporation mechanism within the evaporator of the heat pipe. They evaluated the effects of working pressure, working substance, heat pipe inclination and production of non condensable gases. Water and F113 were the working fluids used. Heat transfer coefficients were obtained from the experimental analysis. They have also worked to determine the operating limits of heat pipes (1980). The experimental analysis was on wick characteristics corresponding to maximum heat transfer rates. Sintered metallic powder was used as wick along with working substances water and F113. They have studied the wick characteristics, friction losses in the heat pipe and capillary properties. A simplified model was also developed to predict the maximum heat transfer for capillary limits. Maximum heat flux in the heat pipe was measured and presented.

The natural convention in vertical porous cylinder with uniform heat generation and side wall cooling was reported by Rao and Wang (1991). Their analysis was using partial Galerkin method and finite difference method. The stream lines, isotherms and vertical velocity profiles were obtained. The objective of another investigation by Issacci (1991) was to find the dynamic behaviour of the vapour flow in heat pipes during its start-up phase. The complex vapour flow was analysed using a two dimensional model treating it as compressible flow in an enclosure with inflow and outflow boundary conditions. Using the implicit finite difference method, the heat flux development and variation of temperature, pressure and velocity of flow were discussed.

A one dimensional model of the vapour flow in heat pipe which is different from previous models was reported by Bowman and Beran (1993). The vapour flow was assumed to be incompressible with space even though compressibility with respect to time is considered. The vapour densities predicted by them indicates that ideal gas behaviour can deviate greatly from saturated vapour densities. El-Genk and Huang (1993) studied the transient response of water heat pipe at different heating rates. Mainly the temperature distribution along the heat pipe, *viz.* in the vapour core and through the wall, was studied. A cylindrical heat pipe made of copper with copper wire screen of mesh number 150 was used for their experiment.

Tournier and El-Genk (1994) have presented the results of two dimensional transient heat pipe model and the experiment conducted on a cylindrical copper heat pipe using water as the working fluid. The outcome of the work includes the transient and steady state characteristics of vapour flow and liquid flow and variation of temperature and pressure in the heat pipe. They have found out the axial distribution

of vapour and liquid pressure. The analysis of start up of sodium heat pipe from frozen state has also been presented by them in another paper (1996). The calculated temperature at different times during start up are found in good agreement with the measured values.

Hsiao *et al.* (1994) have analysed numerically the steady state convection in an inclined porous cavity with a discrete heat source on a wall. Non-Darcy and thermal dispersion effects are considered in the momentum and energy equations. Wall effects on porosity, permeability and thermal dispersion are also taken into account. The numerical solution procedue employed was finite difference method on stream function - vorticity approach. Imura *et al.* (1994) conducted extensive experimentation on screen wick to find out the effective pore radius. The capillarity of stainless steel and phospher bronze screen mesh was measured with water, ethyl alcohol and F 113 as test liquids. The experimental data showed that the contact angle of the liquids are much different from the values that were assumed. An expression for the capillary pressure was also presented in their paper.

Sun *et al.* (1995) proposed an approximate method to calculate the effective length of a flat heat pipe when the strip heater is partially covering the evaporator section. They found that a higher capillary transport limit can be achieved, if the heat source is placed symmetrically at the centre of the evaporator section. Evaporative heat transfer at the evaporator section of grooved heat pipe has been presented by Khrustalev and Faghri (1995) and Kobayashi *et al.* (1996). Numerical results presented by the latter indicate that a large heat flux of the order of MW/m is transported in the narrow micro region which is close in contact to the solid wall. Kobayashi *et al.* (1996) investigated the evaporative heat and mass transfer

phenomena at the liquid meniscus edge in the evaporator of a grooved heat pipe. They proposed an analytical model to simulate this phenomena. Numerical results were obtained for ammonia as the heat pipe liquid. Optical measurement was conducted at the meniscus edge to confirm the existence of the non-evaporative liquid film and to identify the thickness in the order of few nanometres.

Hall and Doster (1990) have presented a transient model for liquid metal heat pipes. Their contribution is the calculation of evaporation and condensation accommodation coefficients. Abhat and Seban (1974) studied the heat transfer mechanism by boiling and evaporation from the wicks with water and acetone as working substances. Bairamov and Toiliev (1981) used the diode property of the heat pipe in the application in solar collectors. Bilegan and Fetcu (1981) conducted study on heat pipe with axially grooved wicks. They have reported that using the inexpensive axial grooves for the wick structure, high heat transfer rates can be achieved. The working substance used was R12. The performance has been studied with various parameters like operating temperature, heat pipe inclination and length of the heat pipe. Bilegan and Fetcu (1981) concluded that the heat pipe can be effectively used in waste heat recovery systems.

Very few investigators have studied the effect of the amount of working fluid on the performance of heat pipe. Larkin (1981) has presented one of the early reports which explains about the effect of fluid quantity in the heat pipe. He has studied the performance of heat pipe in a compact air-to-air heat exchanger. R22 was used as the working fluid in his studies. Temperature profiles, pressure and heat transfer coefficients in the heat pipe were obtained. Peretz (1981) also have studied the heat transfer effectiveness of a heat pipe exchanger using NTU method.

Thermodynamic analysis of heat pipe has been done by Vasiliev and Konev (1981), Richter and Gottschlich (1994) and Zuo and Faghri (1998). Vasiliev and Konev (1981) analysed the heat transfer for dry, moist and superheated vapour as well as in the subcooled fluid phase. Richter and Gottschlich (1994) showed an approach to the general operation and performance of heat pipes from fundamental thermodynamic considerations. In contrast with the classic heat pipe theory in which the circulation of the working fluid occurs due to the capillary pumping pressure and the pressure difference of vapour and liquid working medium, an attempt has been made to analyse this by conversion of thermal energy into kinetic energy. Zuo and Faghri (1998) also provided a unique view into the physics behind the heat pipe operation which was considered as a thermal network of various components. Many investigations have been reported on the compatibility of materials used for the wick and working substance. Acton (1981) studied the flow and heat transfer through metal felt in the heat pipe. Experimentally, he has predicted the effective thermal conductivity, capillary radius and permeability of the sintered metal felt wick of copper, nickel and stainless steel.

Feldman and Kenney (1981), Munzel and Krahling (1981), and Petrick (1993) investigated the heat pipe mechanism with ferrous metal wicks when water is used as the working substance. Petrick (1993) proposed empirical relations for the production of hydrogen gases as a function of time and temperature when water is used in stainless steel heat pipe. He has inferred that continuous or repeated removal of hydrogen will stop the mid-way ceasure of the operation of heat pipe. Munzel and Krahling (1981) also worked with different grades of stainless steel and water at various operating temperatures. Feldman and Kenney (1981) has conducted lot of

experiments with the combination of mild steel and water. They noticed that the thermal resistance is lowered by using mild steel as the heat pipe material. However, production of noncondensable gases in their experiments is reported. Nevertheless, the performance of the heat pipe was quite satisfactory in a temperature range between 150 and 300°C. Abhat , Nguyenchi and Strel'tsov (*cf.* Dunn and Reay, 1980) investigated the fluid inventory on gravity assisted heat pipes. Li *et al.* (1993) theoretically analysed the flow and heat transfer in a wickless rotating heat pipe. Ideal charges and working conditions are also estimated from the film thickness. The effect of fluid quantity on the performance of the heat pipe was investigated.

2.2.2 Flat Heat Pipes

The present work deals with flat rectangular heat pipe only. Obviously, the literature review on flat heat pipes assumes more significance. Important published articles on flat heat pipes, are detailed in this section. Comparatively, the literature on flat heat pipe is quite less.

van Ooijen and Hoogendoorn (1979) have conducted an analytical study on the pressure profiles for a steady laminar incompressible two dimensional vapour flow in a flat plate heat pipe with adiabatic top plate. Continuity, Navier – Stokes and energy equations were solved for uniform evaporation and condensation rates. The stream lines, vapour velocity profiles and vapour pressure profiles were obtained at various values of the Reynolds number. They noticed reversed flow at the condenser when Re=10 and the pressure drop is more than three times that of the Poiseuille pressure when Re=50. They have also investigated experimentally (1981), the vapour pressure drop and temperature profiles on a flat heat pipe with adiabatic top plate.

They compared the results thus obtained with the earlier results from the numerical solution. They measured the vapour pressure drop and presented the longitudinal pressure profiles in the rectangular vapour channel for different values of Reynolds number values.

In the past few years Vafai and his colleagues have contributed noticeable results on flat heat pipe. Vafai and Wang (1992) made an in depth integral analysis revealing various physical aspects of an asymmetrical flat plate heat pipe. They presented a pseudo three dimensional vapour flow model due to asymmetrical nature of heat source and sink. The vapour velocity profiles, axial temperature variation, and pressure distribution were brought out. Vafai *et al.* (1995) presented the two dimensional investigation and conceptual design of a disk shaped asymmetric heat pipe. They studied the incompressible vapour flow and liquid flow in this heat pipe using conservative formulation. The vapour velocity profile, the vapour and liquid pressure distribution and vapour temperature variation obtained in asymmetric heat pipes are compared with those of rectangular heat pipes.

Zhu and Vafai (1998) carried out numerical study for the steady in-compressible vapour and liquid flow in an asymmetrical flat plate heat pipe. The three dimensional model developed is extended to account for the vapour flow reversals, the liquid flow in the vertical wicks, the coupling of the liquid flow with the top and bottom wicks, the non-Darcian effects of the liquid flow through the porous wick and also the gravitational effects. The velocity profiles and pressure distribution, both in vapour and liquid regimes are found to be in good agreement with the experimental results. They have developed an analytical model (1998) for the start-up transient of asymmetrical flat plate and disk shaped heat pipes. A quasi-

steady state pseudo-three dimensional approximation is presented to model the heat transfer within the wall and liquid wick regions coupling with vapour phase at the vapour liquid interface.

Wang and Vafai (2000) conducted experimental studies to investigate the thermal performance of a flat plat heat pipe. The temperature along the pipe wall surface is quite uniform. The results indicate that the porous wick of the evaporator section creates the main thermal resistance resulting in the largest temperature drop. This has profound effect on the performance of the heat pipe. Vafai and Wang (2000) conducted experimental studies on flat plate heat pipe to predict its performance during start up and shut down operations. They have established that the wick at the evaporator region provides the maximum resistance for heat transfer. They have also shown that the input heat has a substantial effect on the temperature increase of the heat pipe.

Unnikrishnan and Sobhan (1997) obtained the transient distribution of field variables in the vapour and wick regions of a flat heat pipe. Their analysis was two dimensional employing a finite difference procedure based on SIMPLER algorithm. This numerical experimentation revealed that the wick porosity does not have a significant effect on the velocity and pressure distributions in the vapour core region. However, it is reported that the temperature distribution is slightly influenced by wick porosity. The transient model of a flat heat pipe developed by Sobhan *et al.* (2000) involves the solution of two dimensional continuity, momentum and energy equations coupled with equation of state in the vapour core, transport equations for the porous wick medium and two dimensional heat equation for the container wall. Using finite difference method the variation of temperature, pressure and velocity

fields are obtained. The effect of axial conduction through the pipe wall and wick which causes heat to flow into the interior of the externally adiabatic section, thus affecting the velocity distribution in the wick and vapour core is established.

2.3 Summary

Though the conventional heat pipes are circular, flat heat pipes are also used widely for carrying large heat fluxes. It was already mentioned that most of the literature available on heat pipes are in connection with circular ones. Some important works on cylindrical heat pipe connected to the present research have been discussed. Some articles on the compatibility between the working medium with the wick and container materials are also discussed. Very less investigations have been carried out on the effect of fluid inventory in the heat pipe. A few examples of the same have been mentioned in this chapter. Some published articles on flat heat pipe have also been described briefly.

Very little investigation has been carried out to study the performance of flat heat pipes, though researchers recently turned their attention to the same. The results of the literature review on heat pipes indicate the necessity and scope for further theoretical and experimental studies on flat rectangular heat pipes. The present work is an attempt to study the steady state operation of the flat rectangular heat pipes, both theoretically and experimentally. It also aims at the study of the influence of the amount of working medium and wick porosity on the performance of heat pipes.

EXPERIMENTAL STUDIES ON FLAT HEAT PIPES

C. Muraleedharan “Heat transfer and fluid flow studies on flat heat pipe ” Thesis. Department of Mechanical Engineering, Calicut Regional Engineering College , University of Calicut, 2001

Chapter 3

EXPERIMENTAL STUDIES ON FLAT HEAT PIPES

3.1 Introduction

The main objective of the present experimental analysis is the determination of vapour pressure profiles and temperature characteristics of flat rectangular heat pipe. In addition, the influence of the amount of working fluid and the porosity of wick structure on the heat pipe performance are also investigated. These investigations are conducted on two different test rigs. The vapour pressure drop studies, heat transfer characteristics and effect of the amount of the charge on the heat pipe performance are studied on a stainless steel flat heat pipe which employs either water or acetone as the working fluid. The influence of wick structure on the heat pipe performance is studied on an aluminium flat heat pipe using acetone as the working medium.

3.2 Design of Flat Heat Pipe

The overall design of the flat heat pipe from basic principles is quite complex. However, for a particular application the various materials for the heat pipe and its dimensions can be selected. The selected heat pipe may then be subjected to the check for various limitations as explained in Section 1.5. Required changes, if any, may be incorporated further in the design.

The heat pipe design should be essentially, based on capillary limit criterion. The functions of the capillary wick structure in the heat pipe are:

(i) To generate the necessary capillary pressure for the operation of the heat pipe and

(ii) To provide return path of low fluid resistance for the flow of liquid from the condenser to the evaporator.

The maximum capillary head developed by the wick structure increases with decreasing pore size, while this results in increase of liquid pressure drop due to friction. However, the wick permeability, another desirable feature, increases with increase in pore size. Hence for homogeneous wicks there is an optimum pore size at which maximum capillary pumping pressure is provided with minimum flow resistance.

Increasing the wick thickness obviously raises the heat transport capability of the heat pipe. But the increased thermal resistance of the wick created due to larger wick thickness will work against the increased heat transport capability and will lower the allowable maximum evaporator heat flux. So the wick thickness should also need to be optimized.

The wick and container materials should be compatible with the working fluid. Incompatibility can cause chemical reaction between the working fluid and container or wick material, may lead deposition of materials in the wick thereby ceasing of operation of the heat pipe. The container should possess high mechanical properties also at the working temperature range of the heat pipe.

The working fluid for the heat pipe should have the best thermophysical properties at the operating temperature range of the heat pipe. It should be easily

available and cheap. The working fluid which has the highest 'liquid transport factor' at the operating temperature is tentatively selected for a purpose (explained in Section 1.4.3).

3.3 Selection of Materials for the Present Work

For carrying large amount of heat, flat rectangular heat pipes can be used where space and weight are constraints. When the capacity is high, the mass flow of working fluid is considerably large. When the vapour core cross sectional area is reduced, the pressure drop in the vapour phase is not insignificant. The present experimental work is aimed at studying the vapour pressure drop and heat transfer characteristics on flat heat pipes. The performance of the flat heat pipe with different amounts of working fluid is also analysed experimentally.

The experimental studies conducted involve the following two sections:

(i) The study of the vapour pressure drop and heat transfer characteristics of the flat heat pipe and

(ii) the effect of wick structure and amount of working fluid on the heat transfer characteristics of the flat heat pipe.

The experiments are conducted on two different heat pipes *viz.* a stainless steel flat heat pipe of cavity dimensions of 550mm x 80mm x 8mm with axial grooves as wick structure of size 0.50mm wide and 2mm deep and aluminium flat heat pipe of cavity size 440mm x 50mm x 13mm with screen wick, rectangular grooves and composite wick.

3.3.1 Stainless Steel Flat Heat Pipe

In addition to the investigation of vapour pressure drop and heat transfer characteristics, the influence of fluid inventory (both water and acetone) are also studied on the stainless steel flat heat pipe. The internal dimensions of the stainless steel heat pipe are:- length – 550mm, width – 80mm and height –10mm, with external dimensions of 600mm x 140mm x 22mm. The length of the evaporator and condenser zones are 200mm each and that of adiabatic section is 150mm. Stainless steel is selected as the wall material and also for the capillary structure due to its low thermal conductivity (20W/m K at 50°C). The wick structure is in the form of axial rectangular grooves machined at the bottom surface of the heat pipe.

The working fluid compatible with stainless steel and commonly available are water, ammonia, acetone and F11. Water has high 'Liquid Transport Factor' (see Fig.1.4). It may produce noncondensable gases (Hydrogen) with stainless steel at high operating temperatures. At the working temperature range proposed (below 75°C) water is selected as the working fluid. Later acetone is also used as working fluid in the stainless steel heat pipe and performance characteristics are analyzed. Ammonia is superior to many working fluids based on its properties and 'Merit Number'. Nucleation occurs more readily in Ammonia and this is another positive aspect with respect to the operation of the heat pipes . But the handling of ammonia in high purity is difficult and it is hazardous substance. Hence for the present experimentation ammonia is not used. Table 3.2 gives the design details of the stainless steel flat heat pipe tested in the present work.

3.3.2 Aluminium Flat Heat Pipe

Selecting flat rectangular section for the heat pipe, it can be made compact and light without any reduction in heat transport capacity. Though the pressure drop of working fluid in the vapour core region is significant for flat rectangular section, this is suitable for aerospace applications. The density of the container material will also affect significantly on the overall weight of the heat pipe. Using light metals like aluminium as container material the heat pipe can be fabricated more light in weight. Depending upon the thermophysical properties of the container material, the heat transfer characteristics can be expected different for such heat pipes.

As mentioned before in addition to the experimentations on the stainless steel heat pipe, some investigations are also made on an aluminium flat heat pipe. The aluminium flat heat pipe used has internal dimensions of 440mm x 50mm x 14mm. The length of the evaporator zone, adiabatic region and condenser section are 130mm, 180mm and 130mm respectively. The influence of porosity on the heat pipe performance is studied on this set up. Temperature distribution along the heat pipe and pressure drop are measured in this heat pipe. Aluminium is selected as the container material due to fact that it is very light compared to stainless steel. The wick structures used are wire screen made up of stainless steel and axial grooves made in brass. Since water is not compatible with aluminium, acetone only is used as the working fluid in this heat pipe. The effect of fluid inventory and wick structure are investigated on the aluminium flat heat pipe. Tables 3.3 – 3.6 show the design deatails of the aluminium heat pipe used in the present study.

3.4 Stainless Steel Heat Pipe Test Rig

This experimental test rig consists of a horizontal asymmetric flat heat pipe, made up of stainless steel. The schematic diagram of the stainless steel flat heat pipe test rig is shown in Fig.3.1. The heat pipe has an adiabatic wickless top plate which provides locations for pressure tappings and thermocouples. Tests can be carried out on this heat pipe by charging any compatible compatible working fluids such as water and acetone.

The longitudinal and transverse sections of the heat pipe set up are shown in Figs. 3.2 and 3.3. These figures depict the details of the stainless steel heat pipe test set up. The vapour channel width is 80mm, which is very large compared to the height of the vapour channel, 8mm. Hence a two dimensional flow situation is prevailing within the heat pipe.. The length of the evaporator and condenser zones are 200mm each. The low thermal conductivity of stainless steel (20W/mK at 50°C) restricts the longitudinal heat flow along the container. The heat source at the evaporator section consists of an aluminium block which is attached with the bottom plate. Heat sink compound is applied between the aluminium block and bottom plate to provide least resistance to heat flow. In this aluminium block 8mm diameter holes (8 numbers) are drilled in a single row. These holes act as the source which supplies heat continuously at a constant temperature by circulating hot oil through the holes. Arrangement for controlled heating of the oil with the help of electric coil heaters is available with the set up. Thermostat is provided in the oil sump aid to fix the temperature of the oil at any particular value. The oil is recirculated through the evaporator region of the heat pipe with the help of a small centrifugal pump. Two rows of 3 mm holes are drilled on the aluminium blocks at a distance of 10 mm

between rows and thermocouples are kept inside these holes. Heat flux assessment in the evaporator can be carried out by measuring the temperature at various locations within the aluminium block.

The length of the adiabatic section is 150 mm. Provision is made in the adiabatic section to measure the temperature at four locations along the bottom plate of the heat pipe. The condenser section of the stainless steel heat pipe contains an aluminium block similar to the one in the evaporator section. This also has a row of 8mm diameter holes (8 numbers) which allows circulation of cooling water. Two rows of holes (5 numbers in each row) are drilled for thermocouples. The heat rejected in the condenser can be calculated by measuring the temperatures.

The top plate of the heat pipe has a connection provided for evacuation of the heat pipe and for charging the heat pipe with the working fluid. The same line can be used to remove noncondensable gases also that may accumulate at the condenser end while the heat pipe is in operation. The wick structure is provided only on the bottom plate of the heat pipe. The wickless top plate and the bottom plate which incorporates the axially grooved wicks are held together with the help of nuts and bolts. A distance ring made up of rubberised cork is used between the plates to avoid leakage of working fluid as well as to minimise the direct conduction heat transfer from the bottom plate to the top plate.

Longitudinal grooves of width 0.50 mm and depth 2mm with a pitch of 1.0 mm, are integrally fabricated with the bottom plate of the heat pipe. This wick serves as the return passage for the liquid from the condenser to the evaporator by developing sufficient capillary pumping pressure.

There are 12 pressure tappings and equal number of thermocouples connected in the adiabatic top plate at uniform distances of 50mm. These are provided in the entire length of the vapour channel of the heat pipe. All the pressure tappings are connected to a common header. Shut off valves are provided on every tapping for making the pressure measurement conveniently from each tapping (see the assembly shown in Fig. 3.4). Figs. 3.5 and 3.6 show the photographs of the stainless steel flat heat pipe assembly and its inner details respectively. The adiabatic top plate, the bottom plate and the aluminium blocks which act as the heat source and the heat sink respectively are lagged with a thick layer of glass wool and thermocole. This is to minimise the leakage of heat to the surroundings.

The temperature measurement at 40 positions in the heat pipe set up are made by using calibrated copper - constantan thermocouples. Fig. 3.7 shows the various locations of thermocouples in the set up. The pressure at the evaporator end is used as the reference pressure. With the help of a differential pressure gauge, the pressure differences between the reference pressure and pressures at other sections are measured.

3.5 Experimentation With Stainless Steel Flat Heat Pipe

First the top plate and the bottom plate which contains the grooved wick are subjected to a high pressure stream of air, for removing metallic particles and impurities that may affect adversely the functioning of the heat pipe. The plates and the grooves are then cleaned with petrol and acetone to remove other impurities like oil, grease etc in order to get the best capillary actions. The plates are connected

together using nuts and bolts with the non-conducting distance ring in between them. The heat pipe is then checked for leakage by admitting compressed air at 10 kg/cm^2.

After assembling the whole set up with the required instrumentation, the heat pipe is evacuated upto a vacuum pressure of 750mm. The optimum charge, the amount of working fluid just to saturate the wick structure (to fill the grooves) and to occupy the tubings is calculated. The thermal and flow behaviour in the heat pipe are studied with water and acetone, and that too with undercharge, normal charge and over charge. At comparatively high temperatures water may react with stainless steel forming hydrogen, there by causing degassing problem. The heat pipe may have to be disassembled and cleaned well before charging the next working fluid.

Acetone is selected as the first working fluid and 28cc of it is charged into the heat pipe. This amount of charge is less than the calculated charge value of 34cc. The charge is introduced into the heat pipe with the help of a charging bottle.

An immersion heating coil is used to heat the oil bath and the hot oil is circulated over the evaporator region at a constant temperature. Heat transfer from the high temperature oil will occur towards the evaporator zone of the heat pipe. Hot oil is recirculated at uniform rates with the help of a small centrifugal pump. Cold water at ambient conditions and constant flow rate is circulated in the condenser side.

The temperature at various locations on the heat pipe are measured after it has attained steady operating conditions. The pressure difference at a point with respect to the pressure at the evaporator end in the heat pipe is measured by the differential pressure gauge. However, in some cases the pressure at various points are measured by using a vacuum pressure gauge which is also connected in the set up..

The heat flux at the evaporator and condenser are calculated by Fourier's conduction equation. The experiment is repeated with various heating rates by changing the hot oil temperature. The experiment is also conducted for other charges namely the calculated normal charge of 34cc and excess charge of 40cc (see Fig.1.9). Similar experimentations are conducted with water as working fluid also.

3.6 Aluminium Heat Pipe Test Rig

The work with aluminium heat pipe is aimed at studying the fluid flow and heat transfer characteristics of the heat pipe with acetone as working fluid using different types of wicks. The various wicks used in this heat pipe are:

(i) Screen wick with three different porosity values,

(ii) Axial grooves and

(iii) Composite wick

The test rig as shown in Fig. 3.8 consists of a horizontal asymmetric flat heat pipe made of aluminium. The photograph of the experimental test rig is shown in Fig.3.9. The wick of the heat pipe is fixed at the bottom surface. The adiabatic top plate provides the locations for pressure tappings and thermocouples.

The heat pipe has overall dimensions of 500 mm x 100mm x 27 mm with the cavity dimensions of 440mm x 50 mm x 14 mm. The length of the evaporator and condenser zones are 130 mm each, separated by a 180 mm adiabatic section in the middle. The electric heating element, which acts as the heat source is sandwitched at the outer surface of the bottom plate in the evaporator section. The heat input is controlled by means of a dimmerstat and the amount of heat input is measured by a wattmeter. The condenser section is provided with water cooling. The cooling water is circulated through a small tank fixed below the condenser section at ambient

temperature and constant flow rate. This cooling water takes away the heat that is rejected at the condenser section of the heat pipe. The top plate has provision for evacuation of the heat pipe and for charging required amount of working substance.

The asymmetric aluminium flat heat pipe has wick structure at the bottom surface only. The wick of the heat pipe is not an integral part of the bottom plate. Hence, it is convenient to replace the wick structure as per the requirement. The wick structure is gripped at the inner surface of the bottom plate with the help of stainless steel screws and two aluminium strips. Figs. 3.10 and 3.11 show the aluminium flat heat pipe assembly and its internal details respectively.

The various wick structures used are wire screen, axial grooves and combined wire screen - axial grooves. Fig.3.12 shows the photograph of various wick structures used for the experimentation (1. Wire Screen – MN 100, 2. Wire Screen – MN 200, 3.Wire Screen – MN 300 and 4. Axial grooves). The details of the wick structure used are shown in Table 3.1.

Table 3.1 Details of Wicks Used in Aluminium Flat Heat Pipe

Sl. No.	Wick Type	Number of Layers	Thickness (mm)
1	Wire Screen – Mesh Number 100	7	1
2	Wire Screen – Mesh Number 200	11	1
3	Wire Screen – Mesh Number 300	14	1
4	Wire Screen – Mesh Number 100	13	2
5	Axial Grooves	--	2
6	Composite Wick (Axial Grooves and Wire Screen MN 100)	1	2

The bottom plate on which the wick is attached with and the wickless top plate, are held together with the help of nuts and bolts to form the full aluminium heat

pipe. A distance ring made up of rubberised cork is provided between the plates, to avoid direct contact between the plates, thereby preventing the possibility of direct conduction heat transfer from the bottom plate to the top plate and also to avoid the leakage of working fluid. The differential pressure gauge is used to measure the pressure at the various sections of the heat pipe with reference to that at the beginning of the evaporator section. Provisions are made to measure the temperature at various points on the bottom plate of the heat pipe also. Totally temperatures at 20 points on the heat pipe are measured.

3.7 Experimentation With Aluminium Flat Heat Pipe

For proper functioning of the heat pipe no impurities should exist inside the pipe. The dirt in the heat pipe including that in the wick structure is blown off by means of compressed air. The wick structure, both the wire screen and axial grooves, is cleaned using petrol and acetone to remove oil, grease etc. After completing the assembly of heat pipe, the leakage test at all joints is done by admitting compressed air inside the heat pipe. The complete heat pipe set up was insulated using glass wool, cotton and thermocole to avoid any unwanted heat leakage.

The normal charge, the amount of working fluid which is supposed to yield, the best results is calculated for all the different types of wicks. For 1mm thick wire screen mesh the calculated amount of working fluid is 21cc. (There is slight difference in the normal charges for MN 100, 200 and 300). In 2mm thick wicks, for wire screen MN100, axial grooves and combined wick the normal charges are 38cc, 17cc and 18cc, respectively.

Experiments are conducted to study the performance of the heat pipe at various heat inputs, different wick structures and three different charges. The heat input at the evaporator section of the heat pipe is controlled by a dimmerstat and measured by a wattmeter. The amount of heat transported along the bottom plate by conduction is calculated by measuring the temperature at various locations along the bottom plate. The pressure at various sections in the vapour core and corresponding temperatures are measured. Copper – constantan thermocouples are used for the temperature measurement. Heat flux at the condenser is measured by calorimetry method.

With the calculated normal charge, the heat pipe is run for three different heat transport rates for different types of wicks and wick thickness. In addition to this, experiments are conducted with undercharge as well as over charge with all the different wicks. The total pressure drop and temperature variation for all the test runs are obtained. Experiments have been carried out with aluminium flat heat pipe employing various wicks (see Fig.1.10).

3.8 Comments on Heat Transport Limits

Since the heat pipe design used here is based on capillary limit criterion, the results obtained automatically satisfies the capillary limit. Viscous limit depends upon the vapour phase properties and the cross section of the heat pipe. If the viscous limit is not exceeded, the vapour core area of cross section can be increased. In flat heat pipes, either the height of vapour core or width or both can be increased as per the constraints. Viscous limit occurs at low temperatures. In the present work the operating temperature is around 50°C and so need not be considered. The entrainment

is caused by high vapour velocities. The vapour velocity can easily be reduced by increasing the cross sectional area of the vapour core. Alternatively entrainment can be prevented by using wick structure with smaller pore size. Obviously, this needs redesign of wick structure. Use of composite wick may also be considered to avoid entrainment in heat pipe. Since in all the cases of the work the heat flux is comparatively low and thus the velocity. So the entrainment will not happen.

Sonic limit is due to choking of vapour flow in the heat pipe. Only in liquid metal heat pipe, sonic limit is normally exceeded, because of the low sonic velocities associated with liquid metals. The sonic limit can also be avoided by reducing vapour velocity by increasing vapour cross sectional area. Since in the present analysis only and acetone are used as working substances, that too at low fluxes there is no point of sonic limit to reach. Boiling limit can be exceeded with large temperature gradient in wick caused by large heat flux in the evaporator. The temperature gradient can be reduced by increasing evaporator surface area or evaporator length. The temperature drop in the wick can also be reduced by reducing wick thickness or by selecting a wick of larger equivalent thermal conductivity. The heat fluxes and thus the temperature gradients that occur in the present study are small. So no boiling limit of heat transfer will reach in any of the cases.

3.9 Dimensionless Variables Used

Instead of fundamental dimensional variables, all the variables are expressed in a convenient nondimensional form. The dimensionless parameters used for the present work are given in the following section.

3.9.1 Calculations in Vapour Flow

The following are the nondimensional parameters used for calculations pertaining to the vapour core region.

$$Y = \frac{y}{h_v} \qquad \theta = \frac{T-T_c}{\left(\frac{\dot{q}h_v}{k_v}\right)} \qquad P = \frac{p-p_\infty}{\rho_v u_0^2}$$

$$Re = \frac{\rho_v u_0 h_v}{\mu_v} \qquad P' = P_y - P_0 \qquad P^+ = \frac{p_y - p_0}{p_l - p_0} \tag{3.1}$$

3.9.2 Calculations in Liquid Wick Region

The following are the nondimensional parameters used for calculations pertaining to the liquid wick region.

$$Y = \frac{y}{h_w} \qquad \theta = \frac{T - T_c}{\left(\frac{qh_w}{k_m}\right)} \qquad Re = \frac{\rho_l u_o h_w}{\mu_l} \tag{3.2}$$

In experimental studies the temperature distribution is obtained along the top and bottom walls corresponding to the vapour core and liquid wick of the heat pipe. The temperature at various locations are measured with the help of thermocouples connected internally on the respective walls and so they give corresponding temperature values of the vapour core and wick region.

3.10 Summary

The stainless steel flat heat pipe and aluminium heat pipe test rigs have been discussed. The experimental analysis is always complicated and involves many obstacles. In the present analysis the performance characteristics of the flat heat pipe

are obtained. The temperature characteristics and pressure variation of the flat heat pipe are determined with different capacities. In addition, the influence of fluid inventory, wick porosity and axial heat transfer along the container wall are also obtained. The various results are exhibited with the explanation in Chapter 6. A comparison of the results with that of theoretical results are also discussed.

Table 3.2 Stainless Steel - Water/Acetone Flat Heat Pipe

Material	Stainless Steel
Working fluid	Acetone
Type of wick	Rectangular axial grooves
Number of effective grooves	50
Depth of each groove	2×10^{-3} m
Width of the grooves	5×10^{-4} m
Length of the grooves	550×10^{-3} m
Width of the heat pipe	80×10^{-3} m
Height of the vapour core	8×10^{-3} m
Length of evaporator zone	200×10^{-3} m
Length of condenser zone	200×10^{-3} m
Length of adiabatic zone	150×10^{-3} m
Porosity	0.5
Effective capillary radius	5×10^{-4} m
Hydraulic radius for liquid passage	4.4×10^{-4} m
Permeability	$1 \times 10^{-8} m^2$
$F_l Re_l$	18.5
Design temperature	50^0C
Maximum capillary limit with Water	650W
Maximum capillary limit with Acetone	125W

Table 3.3 Aluminium Flat Heat Pipe (Wire Screen – Mesh Number 100)

Material of container	Aluminium
Material of wick	Stainless Steel
Working fluid	Acetone
Type of wick	Wire screen
Mesh Number	100
Depth of the wick structure	1×10^{-3} m / 2×10^{-3} m
Wire diameter	9.87×10^{-5} m
Wire spacing	1.738×10^{-4} m
Length of the wick structure	440×10^{-3} m
Width of the heat pipe	50×10^{-3} m
Height of the vapour core	13×10^{-3} m
Length of evaporator zone	130×10^{-3} m
Length of condenser zone	130×10^{-3} m
Length of adiabatic zone	180×10^{-3} m
Porosity	0.744
Effective capillary radius	1.263×10^{-4} m
Permeability	3.22×10^{-10} m^2
Design temperature	60^0C
Maximum capillary limit	26W / 52W

Table 3.4 Aluminium Flat Heat Pipe (Wire Screen – Mesh Number 200)

Material of container	Aluminium
Material of wick	Stainless Steel
Working fluid	Acetone
Type of wick	Wire screen
Mesh Number	200
Depth of the wick structure	1×10^{-3} m
Wire diameter	4.63×10^{-5} m
Wire spacing	7.78×10^{-5} m
Length of the wick structure	440×10^{-3} m
Width of the heat pipe	50×10^{-3} m
Height of the vapour core	13×10^{-3} m
Length of evaporator zone	130×10^{-3} m
Length of condenser zone	130×10^{-3} m
Length of adiabatic zone	180×10^{-3} m
Porosity	0.6995
Effective capillary radius	6.21×10^{-5} m
Permeability	6.6×10^{-11} m^2
Design temperature	60^0C
Maximum capillary limit	12.5W

Table 3.5 Aluminium Flat Heat Pipe (Wire Screen – Mesh Number 300)

Material of container	Aluminium
Material of wick	Stainless Steel
Working fluid	Acetone
Type of wick	Wire screen
Mesh Number	300
Depth of the wick structure	1×10^{-3} m
Wire diameter	3.46×10^{-5} m
Wire spacing	4.84×10^{-5} m
Length of the wick structure	440×10^{-3} m
Width of the heat pipe	50×10^{-3} m
Height of the vapour core	13×10^{-3} m
Length of evaporator zone	130×10^{-3} m
Length of condenser zone	130×10^{-3} m
Length of adiabatic zone	180×10^{-3} m
Porosity	0.66
Effective capillary radius	4.15×10^{-5} m
Permeability	2.5224×10^{-11} m^2
Design temperature	60^0C
Maximum capillary limit	6W

Table 3.6 Aluminium Flat Heat Pipe (Axial Grooves)

Material of container	Aluminium
Material of wick	Brass
Working fluid	Acetone
Type of wick	Rectangular axial grooves
Number of effective grooves	24
Depth of each groove	2×10^{-3} m
Width of the grooves	5×10^{-4} m
Length of the grooves	440×10^{-3} m
Width of the heat pipe	50×10^{-3} m
Height of the vapour core	12×10^{-3} m
Length of evaporator zone	130×10^{-3} m
Length of condenser zone	130×10^{-3} m
Length of adiabatic zone	180×10^{-3} m
Porosity	0.5
Effective capillary radius	5×10^{-4} m
Hydraulic radius for liquid passage	4.4×10^{-4} m
Permeability	$1.05 \times 10^{-8} m^2$
Design temperature	60^0C
Maximum capillary limit	42W
Capillary limit for composite wick	177 W

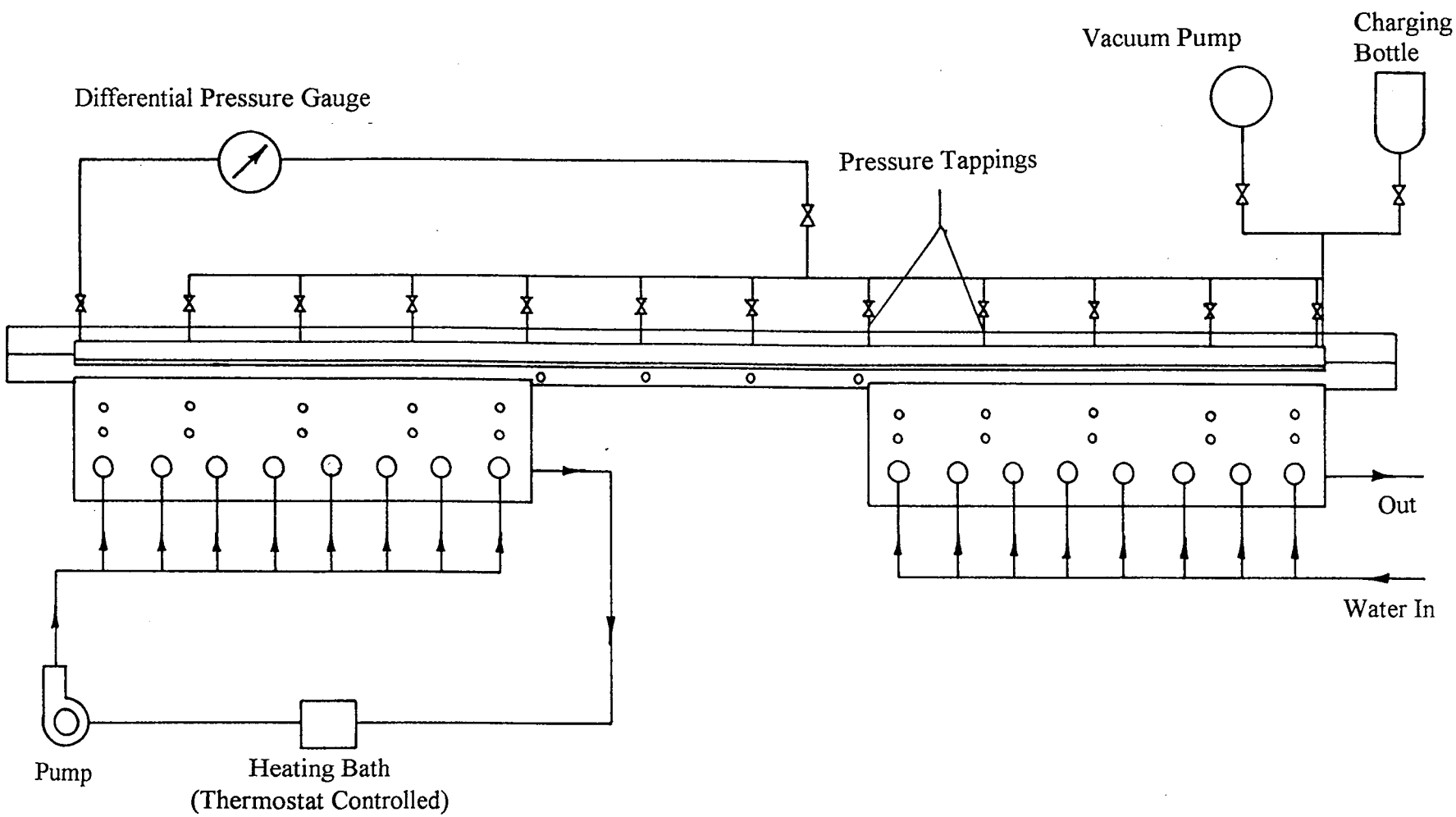

Fig.3.1 Stainless Steel Flat Heat Pipe - Test Set Up

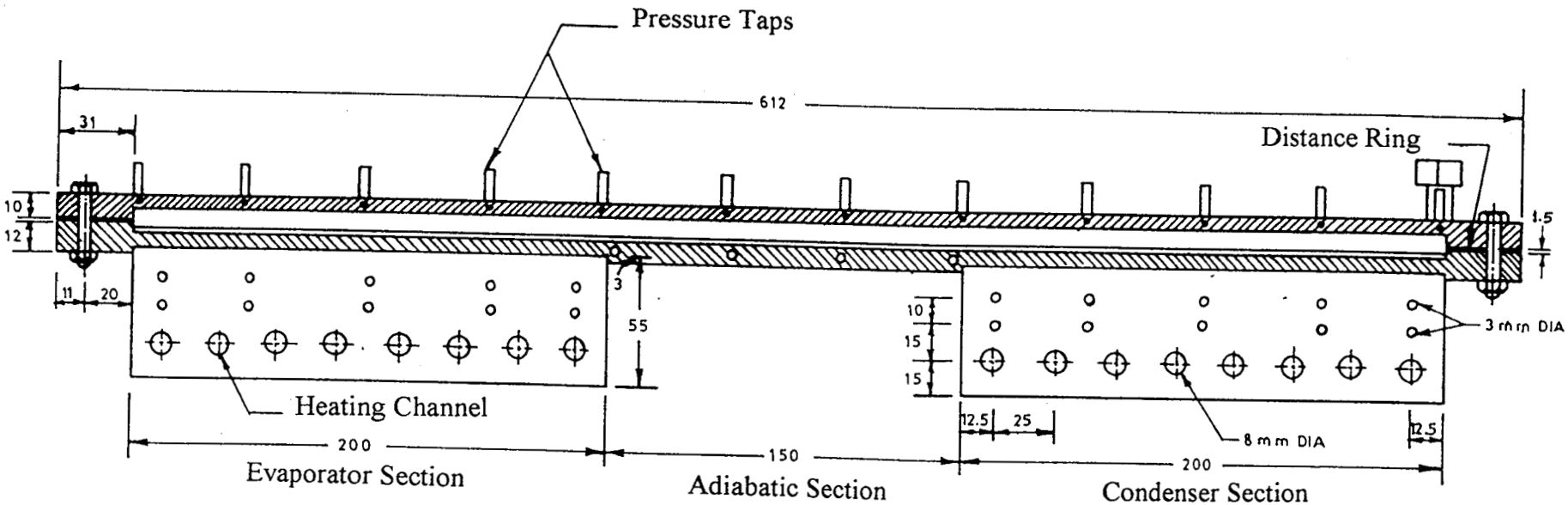

Fig.3.2 Stainless Steel - Water Heat Pipe - Longitudinal Section

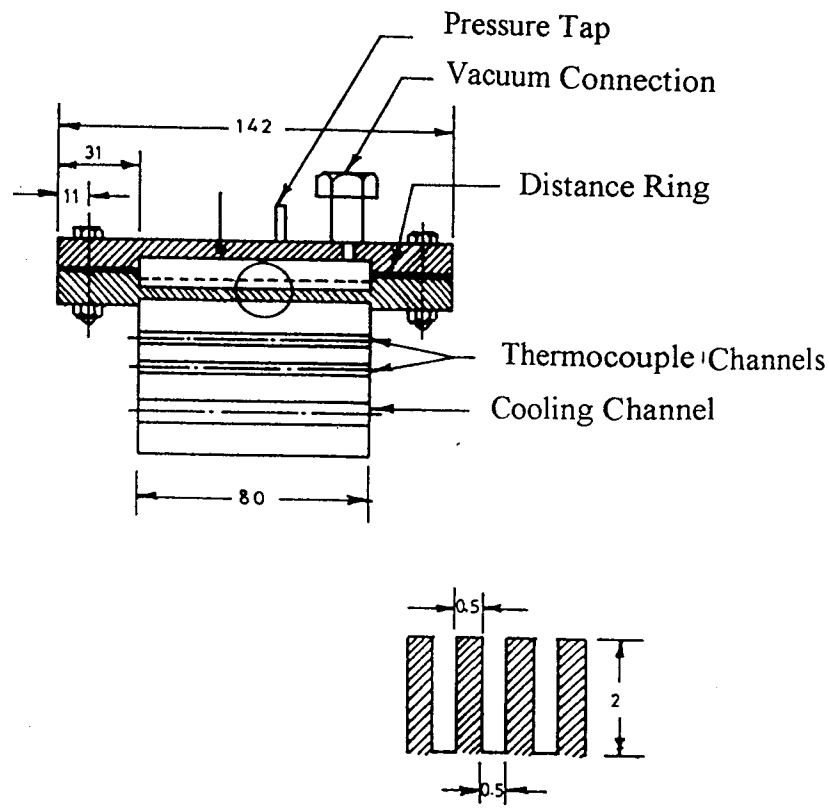

Fig.3.3 Stainless Steel Flat Heat Pipe - Transverse Section

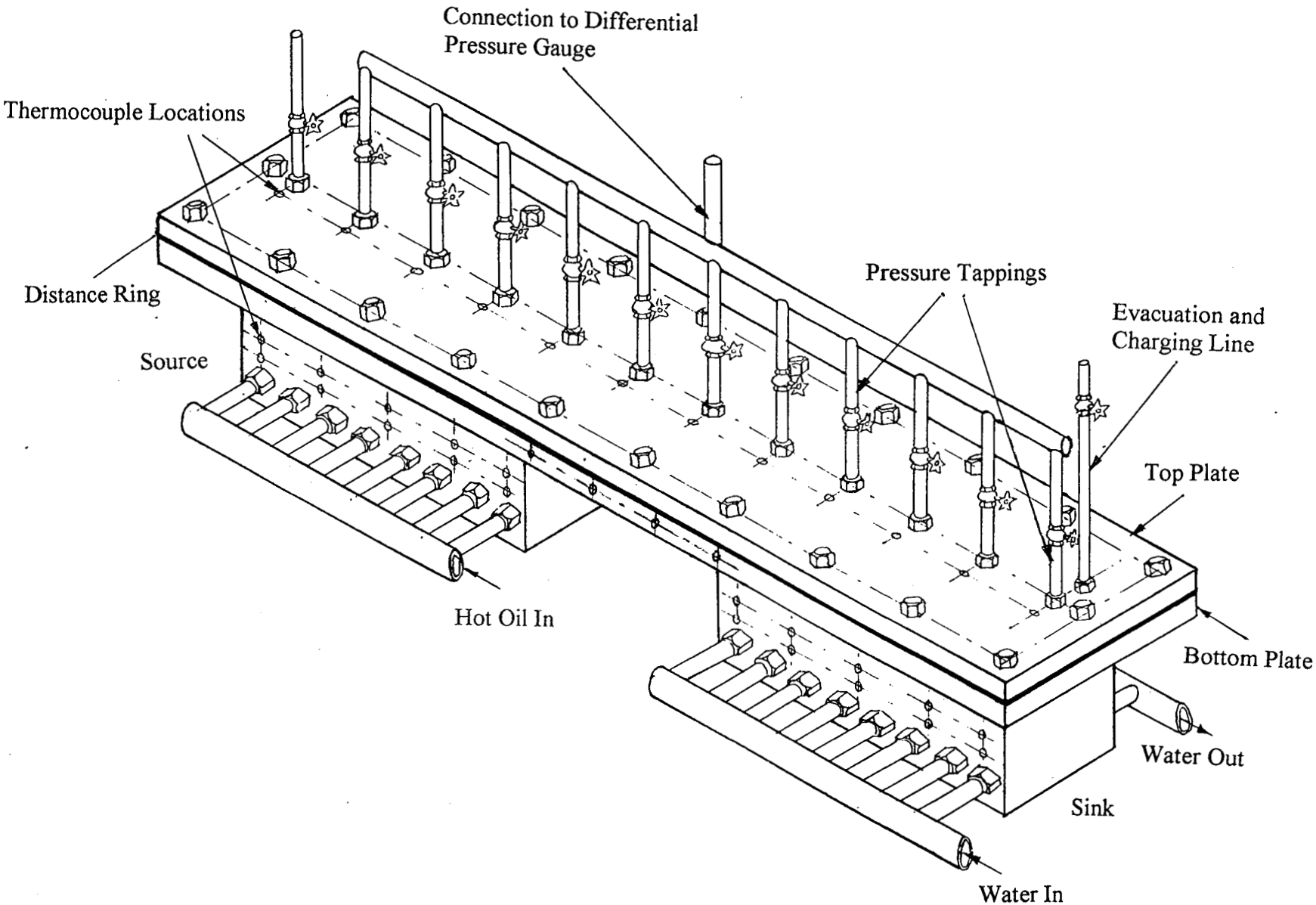

Fig.3.4 Stainless Steel Flat Heat Pipe - Experimental Set Up

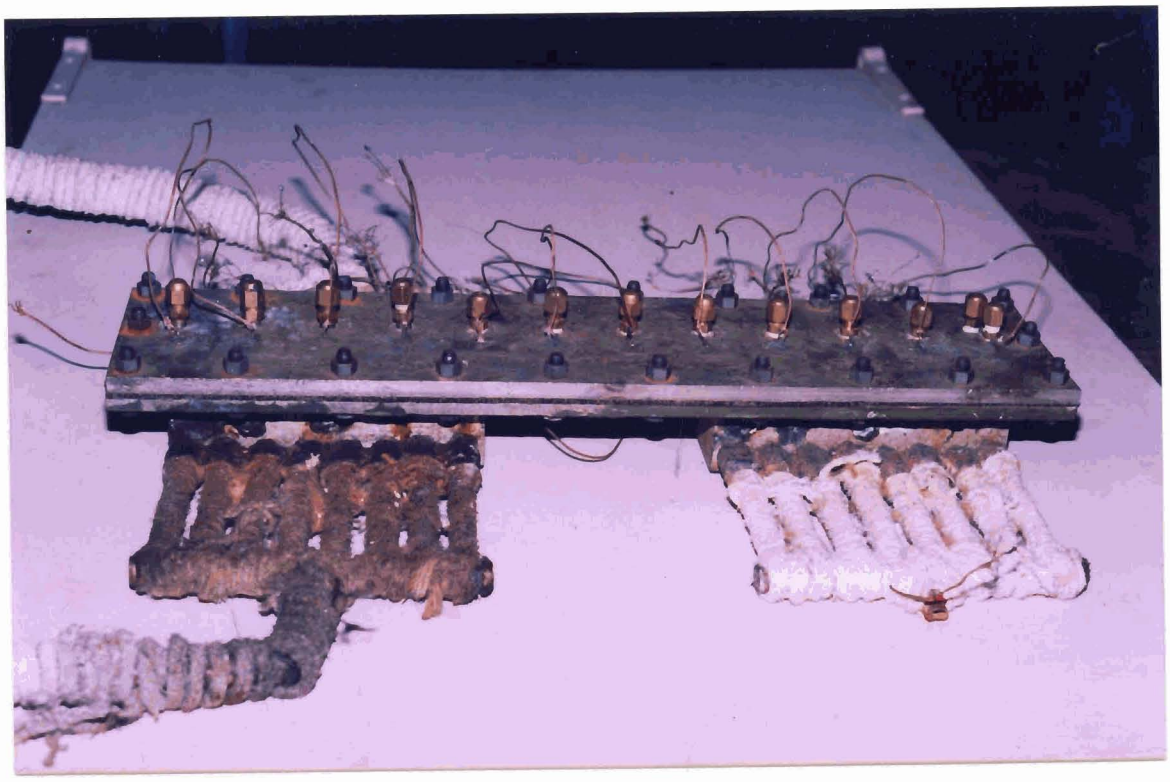

Fig.3.5 Photograph of Assembly of Stainless Steel Flat Heat Pipe

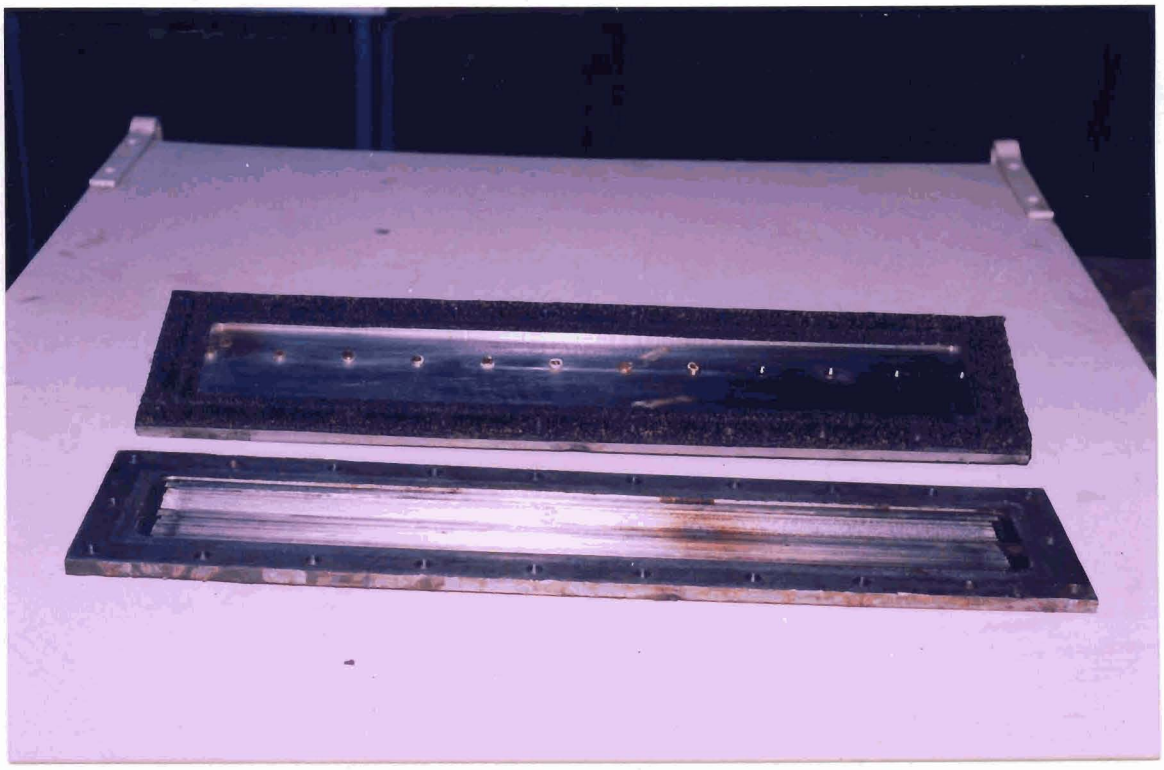

Fig.3.6 Photograph of Inner Details of Stainless Steel Flat Heat Pipe

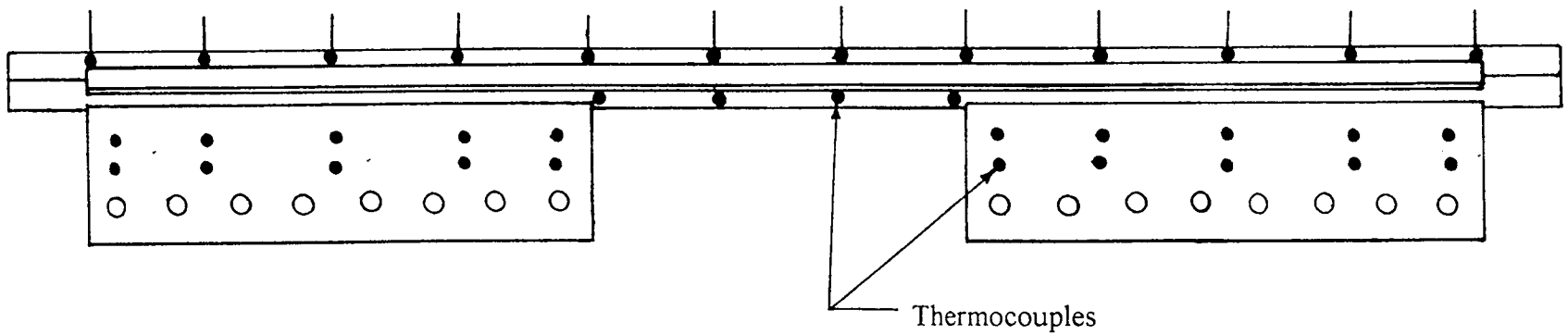

Fig.3.7 Locations of Thermocouples

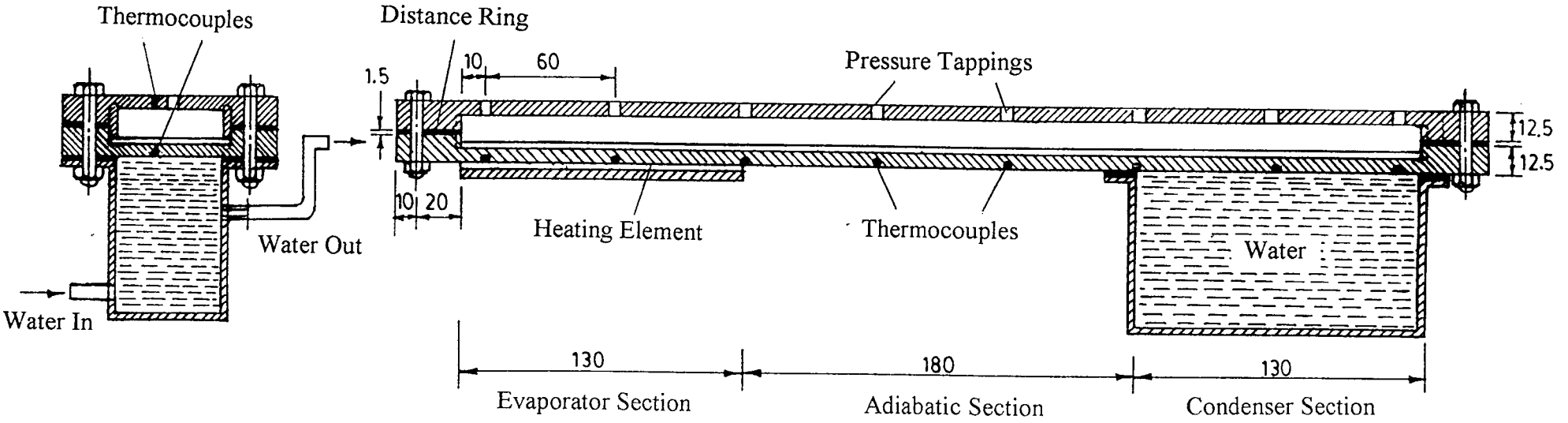

Fig.3.8 Experimental Set Up, Aluminium - Acetone Heat Pipe

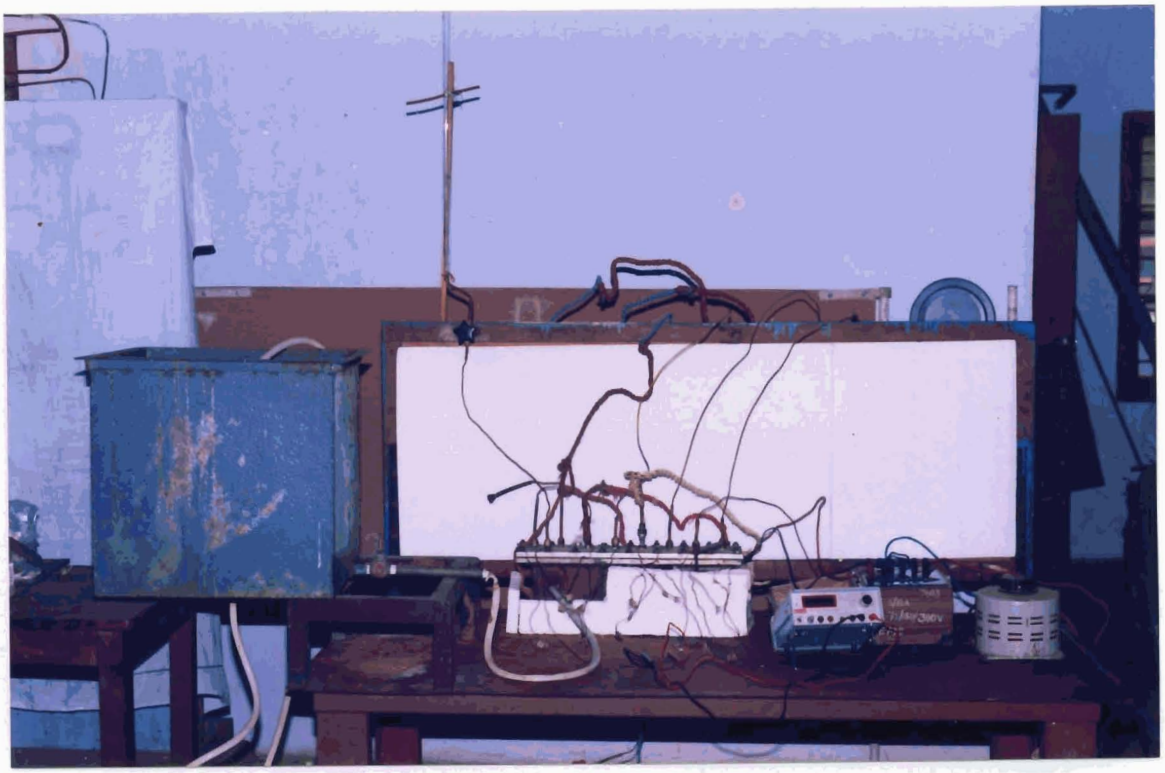

Fig.3.9 Photograph of Aluminium - Acetone Flat Heat Pipe Test Rig

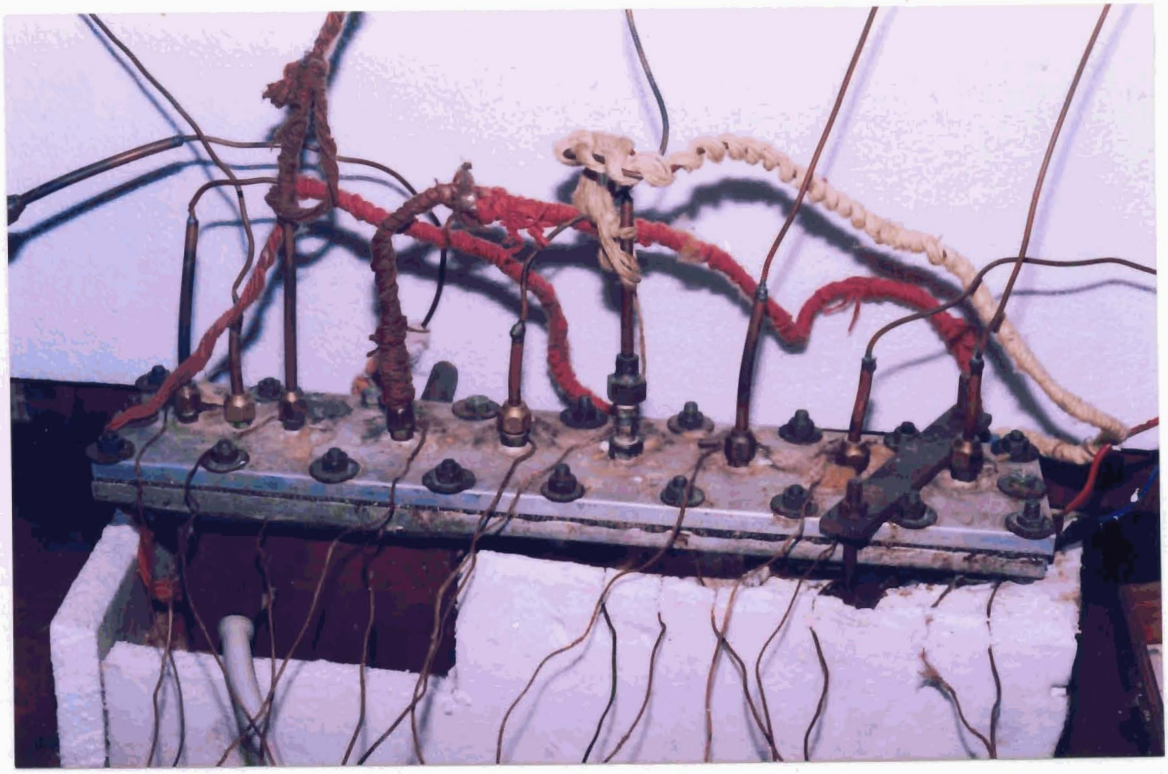

Fig.3.10 Photograph of Aluminium - Acetone Flat Heat Pipe Assembly

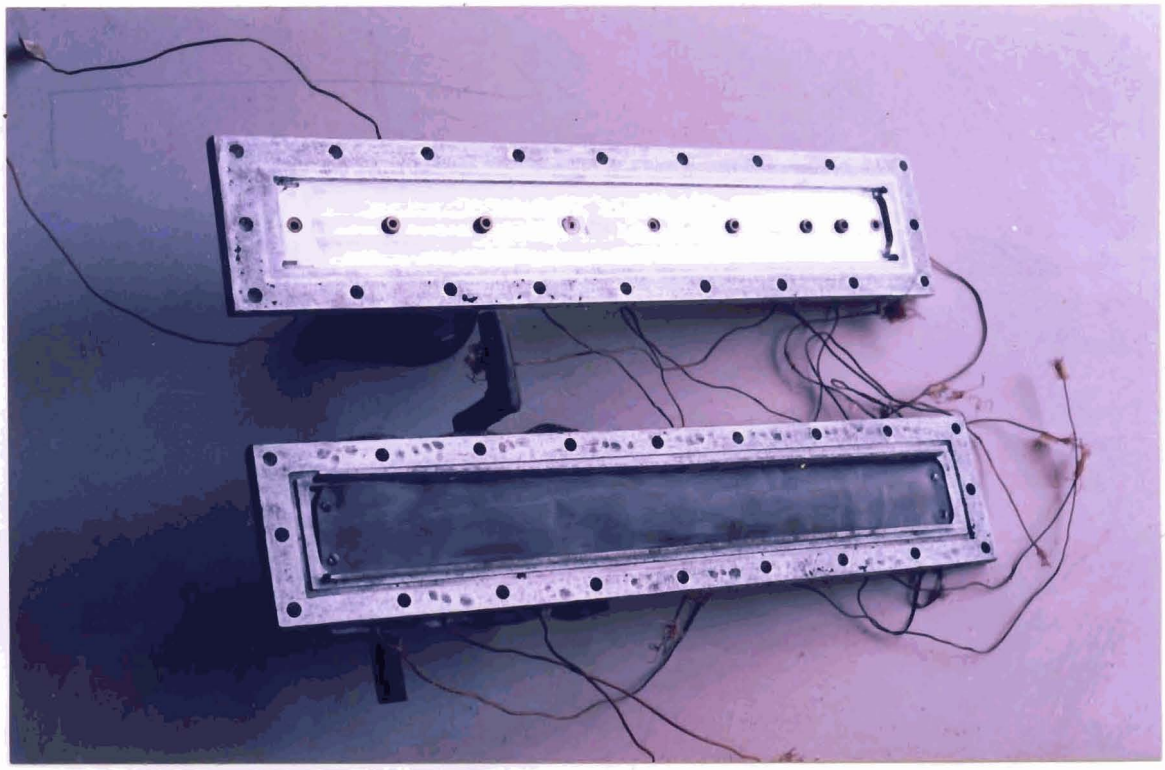

Fig.3.11 Photograph of Inner Details of Aluminium - Acetone Flat Heat Pipe

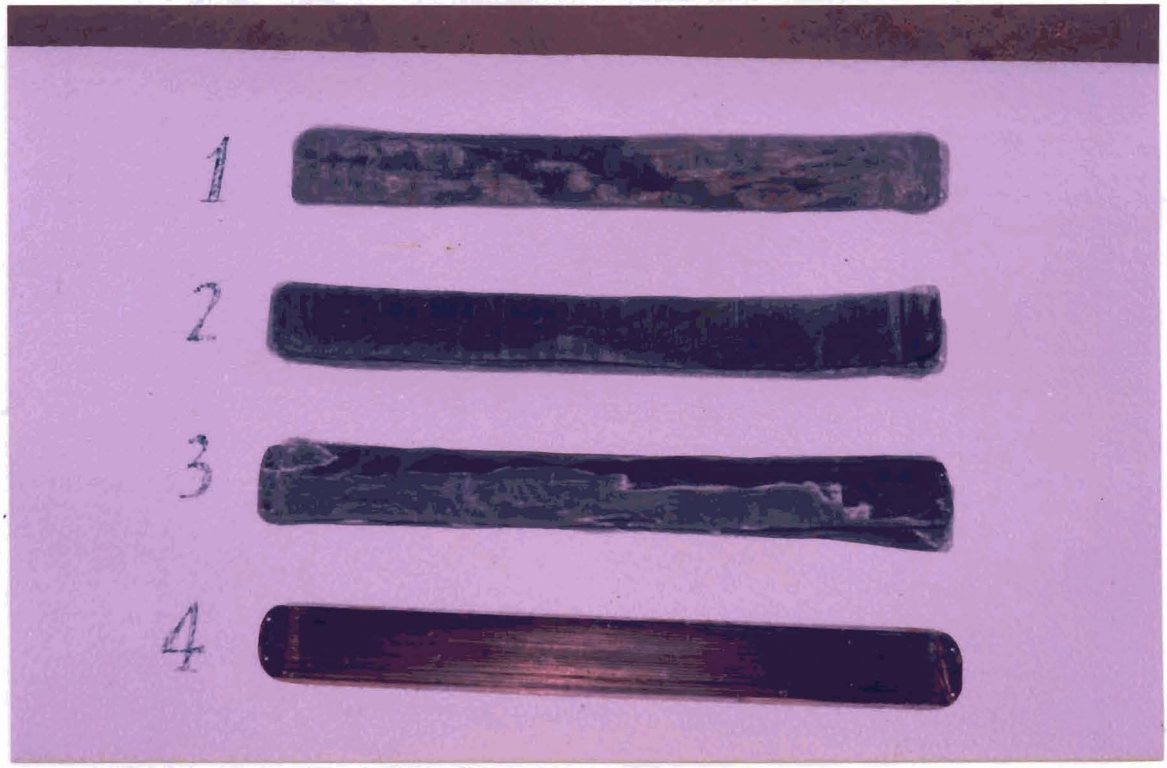

Fig.3.12 Photograph of Various Wicks Used in Aluminium-Acetone Heat Pipe

POISEUILLE MODEL

C. Muraleedharan “Heat transfer and fluid flow studies on flat heat pipe ” Thesis. Department of Mechanical Engineering, Calicut Regional Engineering College , University of Calicut, 2001

Chapter 4

POISEUILLE MODEL

4.1 Introduction

Heat pipe is a device to transport large amount of heat from one location to another by utilising the phase change phenomena of a working substance. The vapourised working fluid flows towards the condenser through the vapour core and the condensate returns to the evaporator through the wick. The heat pipe does not require any external power for its operation. Hence it can be called as a passive heat transport device. As the working fluid flows through the vapour core and along the porous wick, it experiences pressure drops. Poiseuille model is the simplest method to estimate these pressure drops.

4.2 The Pressure Balance of Working Fluid

During operation, the pressure of vapour developed at the evaporator end should be enough to overcome the pressure losses in the vapour core. The liquid from the condenser end is obtained by capillary action, in a horizontal heat pipe. If the heat pipe is vertical or inclined at an angle, the gravitational head either assists or resists the flow depending on whether the condenser is at a higher level or at a lower level with respect the evaporator.

For the heat pipe to operate, the maximum capillary pumping pressure p_c must be greater than the total pressure drop in the heat pipe.

i.e., $$p_c + p_g \geq \Delta p_l + \Delta p_v \quad (4.1)$$

where Δp_l is the pressure drop in the flow of liquid from the condenser to the evaporator through the wick,

Δp_v is the vapour pressure drop in the flow through the vapour channel from the evaporator to the condenser,

p_g is the gravitational pressure head which may be positive, zero or negative depending upon the position of the condenser above, at the same level or below the evaporator.

If this condition is not satisfied the wick will dry out in the evaporator and the heat pipe will not operate.

4.3 Capillary Pressure

The liquid, from the condenser zone to the evaporator section, is transported by capillary action of the wick structure in the heat pipe. The capillary pressure developed depends on the liquid surface tension of the working fluid (σ_l), the mean pore radius of the wick structure (r_c) and the contact angle (ϕ). The following equation gives the relation between them.

$$p_c = \frac{2\sigma_l}{r_c}\cos\phi \quad (4.2)$$

Assuming zero contact angle and r_c = w, for rectangular grooved wick Eq.(4.2) reduces to

$$p_c = \frac{2\sigma_l}{w} \quad (4.3)$$

4.4 Pressure Drop in the Vapour Phase by Poiseuille Model

Assuming the axial velocity of vapour v, is small compared to sonic velocity, the vapour flow can be treated as incompressible. In the evaporator section the vapour pressure gradient will be necessary to carry out two functions, namely

(i) to accelerate the vapour entering the evaporator section up to the axial velocity, v which may be treated as the inertial term , Δp_{vin} and

(ii) to overcome frictional drag forces at the inner surface of vapour core which may be treated as the viscous term, Δp_{vf}

Thus the total or static pressure profile, $\Delta p_y(y)$ can be expressed as,

$$\Delta p_v (y) = \Delta p_{vf}(y) + \Delta p_{vin}(y) \tag{4.4}$$

4.4.1 Frictional Pressure Drop

The flow in the vapour channel is considered as laminar and incompressible. Parabolic axial velocity profiles are assumed throughout the two dimensional vapour core. (see Appendix A). The two dimensional parabolic velocity distribution is represented by the following equation.

$$v(x,y) = \frac{3}{2} v_y \left[1 - \left(\frac{2x}{h_v} - 1 \right)^2 \right] \tag{4.5}$$

In the evaporator the average longitudinal velocity, v_y increases linearly with y and reaches a maximum value, v_a at the evaporator end. The frictional pressure drop $\Delta p_{vf}(y)$ has a quadratic profile, as given below.

$$\Delta p_{vf}(y) = \frac{6\mu_l v_a y^2}{h_v^2 l_e} \tag{4.6}$$

In the adiabatic section v_y is constant v_a and a linear profile is found, represented by the following equation.

$$\Delta p_{vf}(y) = \frac{12\mu_v v_a}{h_v^2}(y - l_c) \tag{4.7}$$

In the condenser, v_y decreases linearly with y, resulting in a shrinking quadratic profile as,

$$\Delta p_{vf}(y) = \frac{12\mu_v v_a l}{h_v^2 l_c}[y - (l_e + l_a)] + \frac{6\mu_{vv} v_a}{h_v^2 l_c}[y^2 - (l_e + l_a)^2] \tag{4.8}$$

4.4.2 Inertial Pressure Drop

The inertial pressure term is defined as the average momentum flux over the cross section given by,

$$\Delta p_{vin}(y) = \rho_v v_y^2 \tag{4.9}$$

For the evaporator this leads to a quadratic pressure contribution as

$$\Delta p_{vin}(y) = \frac{6}{5}\frac{\rho_v v_a^2 y^2}{l_e^2} \tag{4.10}$$

In the adiabatic zone a constant pressure profile is obtained by,

$$\Delta p_{vin}(y) = \frac{6}{5}\rho_v v_a^2 \tag{4.11}$$

In the condenser zone, the velocity decreases linearly with y and a shrinking quadratic profile for the acceleration term is obtained as

$$\Delta p_{vin}(y) = \frac{6}{5}\frac{\rho_v v_a^2}{l_c^2}(l - y)^2 \tag{4.12}$$

At the evaporator and condenser regions, there are mass flow in the direction perpendicular to the axis of the heat pipe, and the mass flow of vapour varies in these

regions. Therefore instead of the geometrical length of the wick an effective length, l_{eff}, is used for the mass flow calculations.

If the mass flow change per unit length is assumed to be constant, the total mass increases or decreases linearly along the evaporator and the condenser, respectively. Hence the length of the evaporator, l_e, and the length of the condenser, l_c, can be replaced by $l_e/2$ and $l_c/2$, respectively. Thus the effective length of the vapour flow path is given by

$$l_{eff} = l_e/2 + l_a + l_c/2 \tag{4.13}$$

The total pressure drop, Δp_v over the heat pipe by Poiseuille approximation model is obtained by summing up the various contributions in the three zones.

$$\Delta p_v = \frac{12\mu_v v_a}{h_v} l_{eff} \tag{4.14}$$

The average velocity at the adiabatic section v_a can be obtained as,

$$v_a = \frac{q}{\rho_v h_v W h_{fg}} \tag{4.15}$$

4.4.3 Pressure Build Up in the Condenser Zone

The axial momentum will be lost in the condenser zone as the vapour stream is brought to rest before setting condensed. Hence the inertial term will be negative. That is, there will be pressure recovery due to deceleration of the vapour in the condenser zone.

The ratio of inertial pressure drop to the frictional pressure drop at the evaporator is given by

$$\frac{\Delta p_{vin}}{\Delta p_{vf}} = \frac{Re_v}{5.0} \tag{4.16}$$

where $$Re_v = \frac{\rho_v u_o h_v}{\mu_v} \tag{4.17}$$

The two components of the pressure drop have opposite signs in the condenser region and for a value of 5.0 for Re, a constant pressure profile is obtained in this zone. For values of Re > 5.0, the acceleration term dominates, resulting in pressure build up in the zone. But practically it is not always possible to recover the inertial term in the condensing region.

The velocity of vapour, u_o at the wick – vapour interface is obtained from the relationship,

$$q = \rho_v \, l_e \, W \, u_o \, h_{fg} \tag{4.18}$$

i.e., $$u_o = \frac{q}{\rho_v \, l_e W \, h_{fg}} \tag{4.19}$$

4.5 Pressure Drop in the Wick

The flow of liquid working medium through the wick is assumed to be laminar. The pressure drop in the liquid flow through wick structure can be found out from Darcy's law.

$$\Delta p_{lf} = \frac{\mu_l}{K} y \, v_y \tag{4.20}$$

It is obvious, as in the vapour the velocity of liquid flow in the wick is also varying in the axial direction. In the condenser section the liquid velocity linearly increases in the direction of the liquid flow, in the adiabatic section the velocity is

uniform and in the evaporator zone the velocity decreases linearly. The increase in velocity of liquid flow in the condenser is due to the mass addition by condensation of vapour at the vapour core-wick interface and in the evaporator the mass depletion occurs due to continuous evaporation of liquid. So considering linear distribution of axial velocity in the wick, l_{eff} can be used to obtain the total liquid phase drop.

The total pressure drop in the liquid phase by Hagen – Poiseuille equation is as follows.

$$\Delta p_l = \frac{8\mu_l q l_{eff}}{h_w W r_c h_{fg} \varepsilon \rho_l} \tag{4.21}$$

where $\varepsilon = \frac{\text{volume of voids}}{\text{volume of wick}}$ and r_c is the capillary radius.

For flat rectangular heat pipe with axially grooved wick structure,

$$\Delta p_l = \frac{8\mu_l q l_{eff}}{h_w W w h_{fg} \varepsilon \rho_l} \tag{4.22}$$

where w is the groove width.

4.6 Gravitational Pressure Head

The gravitational pressure head, p_g is given by the following equation.

$$p_g = l_{eff} \rho_l g \sin\gamma \tag{4.23}$$

where γ is the angle of inclination of the heat pipe with respect to the horizontal direction. Gravitational pressure head can be positive, zero or negative depending upon the relative positions of the evaporator and the condenser. The flow of liquid in the heat pipe is gravity assisted, if the location of the evaporator is below the

condenser. While, if the condenser is below the evaporator, then the flow of liquid is against gravity.

4.7 Summary

Poiseuille theory is simple and can be employed as a first estimate for the velocity and pressure in the working medium. Figs. 4.1 - 4.3 and Fig.4.4 show the various pressure drops experienced by the working fluid and the fluid flow circuit in the heat pipe, respectively. The method for finding the pressure drop by this theory has been discussed in the present chapter. The basic Poiseuille theory is detailed in the Appendix A. The velocity distribution and pressure variation in the flow of vapour core and the liquid wick region are obtained. The results obtained using Poiseuille theory are presented in Chapter 6 (Section 6.3). The results thus obtained are compared with that of experimental and numerical studies.

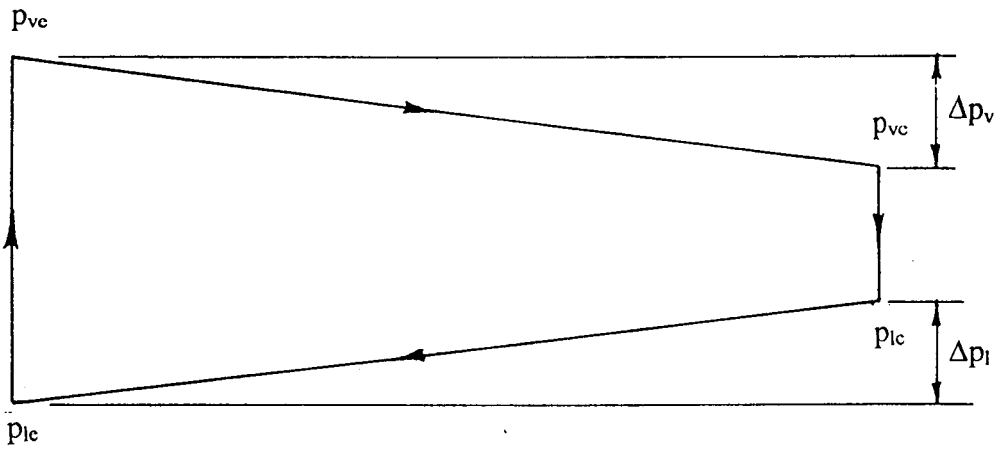

Fig.4.1 Variation of Working Fluid Pressure in Horizontal Heat Pipe

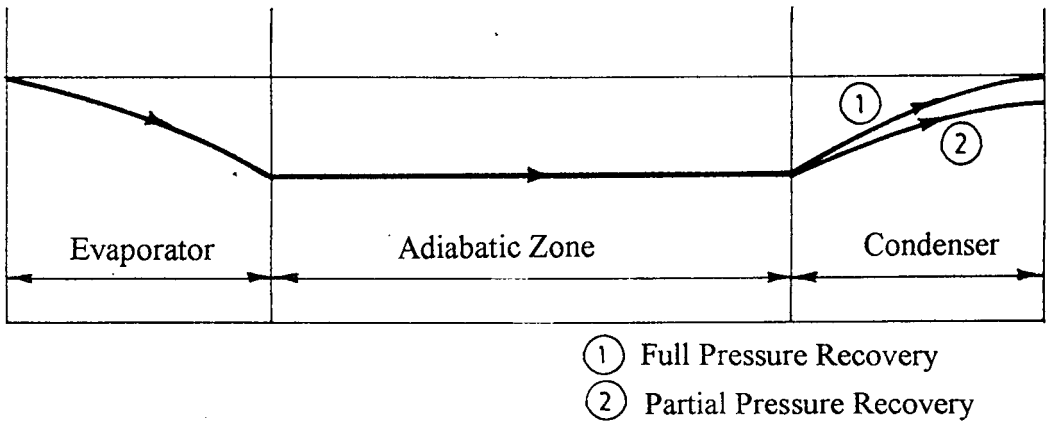

Fig.4.2 Vapour Pressure Variation Due to Velocity Variation

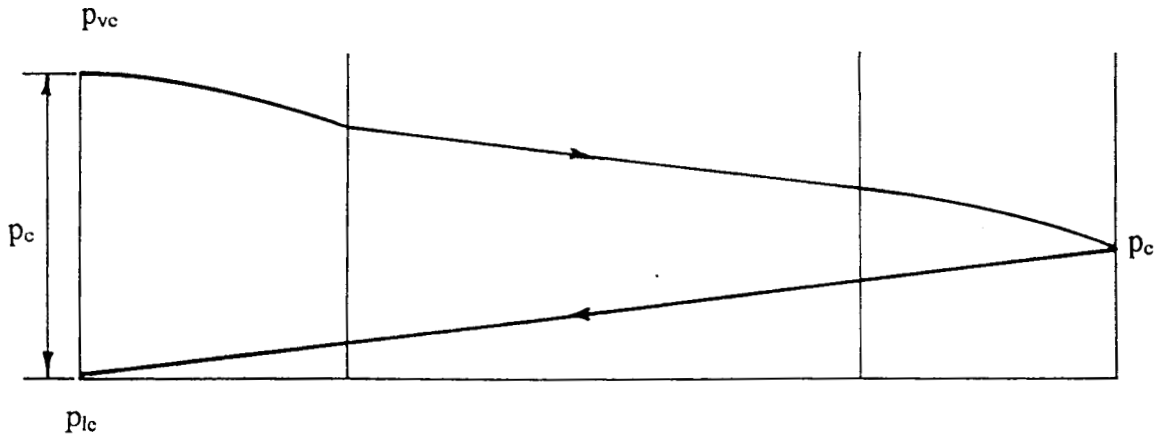

Fig.4.3 Variation of Working Fluid Pressure Considering Variation of Vapour Velocity

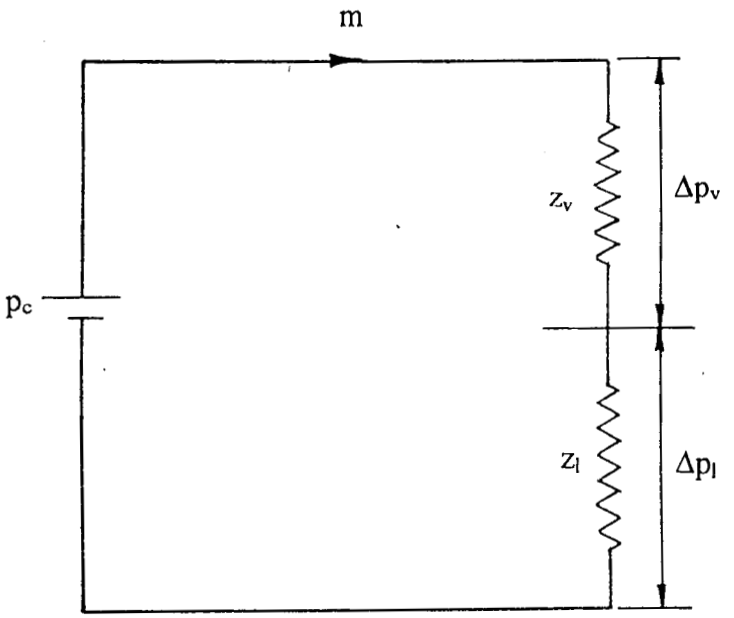

Fig.4.4 Fluid Flow Circuit for Heat Pipe

NUMERICAL MODEL

C. Muraleedharan “Heat transfer and fluid flow studies on flat heat pipe ” Thesis. Department of Mechanical Engineering, Calicut Regional Engineering College , University of Calicut, 2001

Chapter 5

NUMERICAL MODEL

5.1 Introduction

The heat pipe problem is a complex one. The longitudinal section of an asymmetric flat heat pipe is shown in Fig.5.1. In the heat pipe, by absorbing heat from the heat source the liquid working medium in the wick of the evaporator vaporises. The vapour which enters the vapour core flows to the condenser end through the vapour core of the heat pipe. At the condenser region the vapour condenses by rejecting heat to the heat sink. The condensate flows back to the evaporator along the capillary wick structure for reevaporation. In the present analysis the flow of vapour working medium through the vapour channel and the flow of the liquid medium in the wick structure in a nonsymmetrical flat rectangular heat pipe are separately analysed with common conditions at the interface.

5.2 Mathematical Formulation

In the numerical analysis of flow and thermal fields associated with any system, the conceived physical model is replaced by an equivalent mathematical model which is generally obtained by the application of thermophysical laws and by imposing appropriate supplementary conditions. For the analysis of the flat heat pipe, incorporating suitable assumptions, the dimensional and dimensionless governing partial differential equations along with boundary conditions both for primitive variables and stream function – vorticity formulations are presented. The strategy of

the numerical solution of the dimensionless stream function – vorticity transport equations and energy equation is also described.

5.3 Assumptions

The simulation of real physical model of heat pipe is quite complex. In order to obtain an equivalent mathematical model amenable to numerical solution aided with least computer storage and computing time without adversely affecting the results, it is usual practice to make certain simplifying assumptions. The appropriate assumptions made in the present study are:

(i) Flow is laminar and two dimensional.

(ii) Effect of compressibility is neglected.

(iii) The properties of the vapour and the liquid wick matrix are isotropic and homogeneous.

(iv) Body forces are neglected.

(v) Thermophysical properties of the fluid and the porous matrix are constant.

(vi) Axial heat conduction through the pipe wall is negligible.

(vii) As the temperature values involved are small, heat transfer due to radiation is neglected.

5.4 Modeling of Vapour Flow in a Flat Heat Pipe

As mentioned in Section 5.1, the flow of vapour working medium in the vapour core and the liquid through the porous wick structure in the flat heat pipe are separately analysed in the present study. The physical model of the vapour flow in the vapour space of a flat heat pipe is shown in Fig. 5.2. At the wick-vapour interface of the evaporator the liquid working medium vaporises by absorbing heat from the heat

source. This vapour flows through the vapour core to the condenser region at the interface of which it gets condensed by rejecting heat to the sink.

5.4.1 Governing Equations for Vapour Flow in Fundamental Variables

The equations governing the velocity and temperature fields within the vapour core of the heat pipe have been almost standardised. For a laminar, two dimensional incompressible flow in a heat pipe, these equations in primitive variables are

Mass:

$$\frac{\partial u}{\partial x}+\frac{\partial v}{\partial y}=0 \tag{5.1}$$

x– momentum:

$$\rho_v\left(\frac{\partial u}{\partial t}+u\frac{\partial u}{\partial x}+v\frac{\partial u}{\partial y}\right)=-\frac{\partial p}{\partial x}+\mu_v\left(\frac{\partial^2 u}{\partial x^2}+\frac{\partial^2 u}{\partial y^2}\right) \tag{5.2}$$

y – momentum:

$$\rho_v\left(\frac{\partial v}{\partial t}+u\frac{\partial v}{\partial x}+v\frac{\partial v}{\partial y}\right)=-\frac{\partial p}{\partial y}+\mu_v\left(\frac{\partial^2 v}{\partial x^2}+\frac{\partial^2 v}{\partial y^2}\right) \tag{5.3}$$

Energy:

$$\rho_v C_{pv}\left(\frac{\partial T}{\partial t}+u\frac{\partial T}{\partial x}+v\frac{\partial T}{\partial y}\right)=k_v\left(\frac{\partial^2 T}{\partial X^2}+\frac{\partial^2 T}{\partial Y^2}\right) \tag{5.4}$$

The system of equations (5.2) to (5.4) is parabolic in time and elliptic in space. It is mandatory to specify the boundary conditions on all the boundaries of the physical domain before solving these equations. Since only the steady state solution is intended, exact specification of initial condition is not important here. The most

appropriate initial and boundary conditions for the physical model shown in Fig.5.3 are

$$\text{For} \quad t \le 0 \quad u = 0 \quad v = 0 \quad T = T_c \quad p = p_c \tag{5.5}$$

For $t > 0$

$$\begin{aligned}
&y = 0, l \quad 0 < x < h_v \quad u = 0 \quad v = 0 \quad \frac{\partial T}{\partial y} = 0 \\
&x = 0 \quad 0 \le y \le l \quad u = 0 \quad v = 0 \quad \frac{\partial T}{\partial x} = 0 \\
&x = h_v \quad 0 \le y \le l_e \quad u = -u_o \quad v = 0 \quad \frac{\partial T}{\partial x} = \frac{\dot{q}}{k_v} \\
&\qquad l_e < y \le l_e + l_a \quad u = 0 \quad v = 0 \quad \frac{\partial T}{\partial x} = 0 \\
&\qquad l_e + l_a < y \le l \quad u = u_o \quad v = 0 \quad T = T_c
\end{aligned} \tag{5.6}$$

5.4.2 Dimensionless Representation of the Governing Equations for Vapour Flow

The sharp velocity and temperature gradients present in the flow and thermal fields usually introduce spurious oscillations, which finally may lead to instability problem in the numerical calculations .Non-dimensionalising the system of equations and corresponding initial and boundary conditions generally helps in resolving these gradients. In addition, in the process of non-dimensionalisation of the governing equations, it is easy to identify certain non-dimensional numbers of physical significance based on which the result can be predicted. The dimensionless variables used in the present analysis are

$$X = \frac{x}{h_v} \qquad Y = \frac{y}{h_v}$$

$$U = \frac{u}{u_o} \qquad V = \frac{v}{u_o}$$

$$\theta = \frac{T-T_\infty}{\left(\frac{\dot{q}h_v}{k_v}\right)} \qquad P = \frac{p-p_\infty}{\rho_v u_o^2} \tag{5.7}$$

$$Re = \frac{\rho_v u_o h_v}{\mu} \qquad Pr = \frac{\nu}{\alpha}$$

$$\tau = \frac{u_o t}{h_v}$$

By introducing the above dimensionless variables into the Eqs. (5.1) - (5.4) dimensionless equations of mass, momentum and energy in primitive variables are obtained as given below.

Mass :

$$\frac{\partial U}{\partial X} + \frac{\partial V}{\partial Y} = 0 \tag{5.8}$$

X-momentum :

$$\frac{\partial U}{\partial \tau} + U\frac{\partial U}{\partial X} + V\frac{\partial U}{\partial Y} = -\frac{\partial P}{\partial X} + \frac{1}{Re}\left(\frac{\partial^2 U}{\partial X^2} + \frac{\partial^2 U}{\partial Y^2}\right) \tag{5.9}$$

Y – momentum :

$$\frac{\partial V}{\partial \tau} + U\frac{\partial V}{\partial X} + V\frac{\partial V}{\partial Y} = -\frac{\partial P}{\partial Y} + \frac{1}{Re}\left(\frac{\partial^2 V}{\partial X^2} + \frac{\partial^2 V}{\partial Y^2}\right) \tag{5.10}$$

Energy:

$$\frac{\partial\theta}{\partial\tau}+U\frac{\partial\theta}{\partial X}+V\frac{\partial\theta}{\partial Y}=\frac{1}{\mathrm{Re\,Pr}}\left(\frac{\partial^2\theta}{\partial X^2}+\frac{\partial^2\theta}{\partial Y^2}\right) \tag{5.11}$$

The corresponding dimensionless initial and boundary conditions are:

For $\tau \le 0$ $\quad U=0 \quad V=0 \quad \theta=0$ (5.12)

For $\tau > 0$

$$\begin{array}{llllll}
Y=0,1/Ar & 0\le X<1 & U=0 & V=0 & \dfrac{\partial\theta}{\partial Y}=0 & \\
X=0 & 0 \le Y \le 1/Ar & U=0 & V=0 & \dfrac{\partial\theta}{\partial X}=0 & (5.13)\\
X=1 & 0 \le Y \le L_e & U=-1 & V=0 & \dfrac{\partial\theta}{\partial X}=1 & \\
 & L_e \le Y \le (L_e+L_a) & U=0 & V=0 & \dfrac{\partial\theta}{\partial X}=0 & \\
 & (L_e+L_a)\le Y \le 1/Ar & U=1 & V=0 & \dfrac{\partial\theta}{\partial X}=-1 &
\end{array}$$

5.4.3 Vorticity Transport Equations for Vapour Core

In the analysis of two dimensional incompressible flows, the stream function-vorticity formulation is the most popular approach. The most attractive feature of this formulation is that it does not require in information about the pressure field. In addition, the equation of continuity is automatically satisfied. The major disadvantage of this method is that it cannot be applied to three-dimensional flows. Also this method involves additional computation, if the pressure field is required as a part of the solution. The minor drawback of this formulation is that there is no direct boundary condition available for surface vorticity. For two dimensional laminar incompressible flow in rectangular geometry, the governing equations for stream function and vorticity are given below.

Stream Function

$$\frac{\partial \psi}{\partial \tau} = \Omega + \frac{\partial^2 \psi}{\partial X^2} + \frac{\partial^2 \psi}{\partial Y^2} \tag{5.14}$$

Vorticity Transport Equation

$$\frac{\partial \Omega}{\partial \tau} + U\frac{\partial \Omega}{\partial X} + V\frac{\partial \Omega}{\partial Y} = \frac{1}{Re}\left(\frac{\partial^2 \Omega}{\partial X^2} + \frac{\partial^2 \Omega}{\partial Y^2}\right) \tag{5.15}$$

Here the dimensionless stream function, ψ and vorticity, Ω are defined as

$$U = \frac{\partial \psi}{\partial Y} \qquad V = -\frac{\partial \psi}{\partial X} \qquad \Omega = \frac{\partial V}{\partial X} - \frac{\partial U}{\partial Y} \tag{5.16}$$

The imposed temporal and boundary conditions (shown in Fig. 5.4) are

$$\begin{aligned}
&Y = 0,\ 1/Ar \quad 0 \le X \le 1 && \psi = 0 && \Omega = -\frac{\partial^2 \psi}{\partial Y^2} \\
&X = 0 \quad 0 < Y < 1/Ar && \psi = 0 && \Omega = -\frac{\partial^2 \psi}{\partial X^2} \\
&X = 1 \quad 0 < Y < Le && \psi = -Y && \Omega = -\frac{\partial^2 \psi}{\partial X^2} \\
&Le \le Y \le (La + Le) && \psi = -Le && \Omega = -\frac{\partial^2 \psi}{\partial X^2} \\
&(Le + La) \le Y \le 1/Ar && \psi = (Y - 1/Ar) && \Omega = -\frac{\partial^2 \psi}{\partial X^2}
\end{aligned} \tag{5.17}$$

5.5 Modeling of Liquid Wick Region

Fig. 5.5 shows the physical model of the liquid wick region. At the vapour-wick interface of the condenser the vapour working fluid condenses by rejecting heat to the heat sink. The liquid condensate then flows through the porous wick to the evaporator where it gets vaporised by absorbing heat from the heat source.

5.5.1 Governing Equations for Liquid Wick Region in Fundamental Variables

For laminar, two dimensional, incompressible flow in a porous medium, the governing equations in primitive variables are given below.

Mass:

$$\frac{\partial u}{\partial x}+\frac{\partial v}{\partial y}=0 \tag{5.18}$$

X-momentum:

$$\frac{\rho_l}{\varepsilon}\left[\frac{\partial u}{\partial t}+u\frac{\partial u}{\partial x}+v\frac{\partial u}{\partial y}\right]=-\frac{\partial p}{\partial x}+\frac{\mu_l}{\varepsilon}\left[\frac{\partial^2 u}{\partial x^2}+\frac{\partial^2 u}{\partial y^2}\right]-\frac{\mu_l}{K}u-\frac{C_E}{\sqrt{K}}\rho_l|u|u \tag{5.19}$$

Y-momentum:

$$\frac{\rho_l}{\varepsilon}\left[\frac{\partial v}{\partial t}+u\frac{\partial v}{\partial x}+v\frac{\partial v}{\partial y}\right]=-\frac{\partial p}{\partial y}+\frac{\mu_l}{\varepsilon}\left[\frac{\partial^2 v}{\partial x^2}+\frac{\partial^2 v}{\partial y^2}\right]-\frac{\mu_l}{K}v-\frac{C_E}{\sqrt{K}}\rho_l|v|v \tag{5.20}$$

Energy:

$$(\rho_m C_m)\frac{\partial T}{\partial t}+(\rho_l C_l)\left[u\frac{\partial T}{\partial x}+v\frac{\partial T}{\partial y}\right]=k_m\left[\frac{\partial^2 T}{\partial x^2}+\frac{\partial^2 T}{\partial y^2}\right] \tag{5.21}$$

Here k_m is the effective thermal conductivity of the wick structure and is given by

$$k_m=(1-\varepsilon)k_w+\varepsilon k_l \tag{5.22}$$

This equation is applicable when the wick and working fluid are effectively parallel.

The initial and boundary conditions for the physical model, shown in Fig. 5.6, are:

For	$t \le 0$	$u=0$	$v=0$	$T=Tc$	(5.23)
For	$t > 0$				
x=0	$0 \le y \le l_e$	$u=-uo$	$v=0$	$\frac{\partial T}{\partial x}=\frac{q}{k_m}$	
	$l_e \le y \le (l_e+l_a)$	$u=0$	$v=0$	$\frac{\partial T}{\partial x}=0$	

	$(l_e + l_a) \le y \le l$	$u = uo$	$v = 0$	$T=Tc$
	$x = h_w \quad 0 \le y \le l_e$	$u = 0$	$v = 0$	$\frac{\partial T}{\partial x} = \frac{q}{k_m}$
	$l_e < y \le (l_e + l_a)$	$u = 0$	$v = 0$	$\frac{\partial T}{\partial x} = 0$
	$(l_e + l_a) < y \le l$	$u = 0$	$v = 0$	$\frac{\partial T}{\partial x} = -\frac{q}{k_m}$
$y=0$	$0<x<h_w$	$u = 0$	$v = 0$	$\frac{\partial T}{\partial y} = 0$
$y=l$	$0<x<h_w$	$u = 0$	$v = 0$	$\frac{\partial T}{\partial y} = 0$ (5.24)

5.5.2 Dimensionless Representation of the Governing Equations for Liquid Flow

The dimensionless variables used for the nondimensionalisation of the governing equations are listed below.

$$X = \frac{x}{h_w} \qquad Y = \frac{y}{h_w}$$

$$U = \frac{u}{u_o} \qquad V = \frac{v}{u_o}$$

$$\theta = \frac{T - T_c}{\left(\frac{qh_w}{k_m}\right)} \qquad P = \frac{(p - p_\infty)}{\rho_l u_o^2}$$

$$Re = \frac{\rho_l u_o h_w}{\mu_l} \qquad \tau = \frac{u_o t}{h_w}$$

$$Da = \frac{K}{h_w^2} \qquad C_E = 1.75\frac{\varepsilon^{\frac{2}{3}}}{\sqrt{150}}$$

$$RHC = \frac{(\rho_l C_l)}{(\rho_m C_m)} \qquad Pr = \frac{(\mu C_m)}{k_m} \tag{5.25}$$

Here ε is the porosity and C_E is the Ergun constant known also as dimensionless form drag constant. Earlier C_E was considered as a universal constant, with a value of approximately 0.55. However, later it was found that C_E does vary with the nature of the porous medium.

By introducing these dimensionless variables into the Eqs. (5.18) - (5.21), the dimensionless equations of mass, momentum and energy in primitive variables are obtained as given below.

Mass:

$$\frac{\partial U}{\partial X} + \frac{\partial V}{\partial Y} = 0 \tag{5.26}$$

X-momentum:

$$\frac{1}{\varepsilon}\left[\frac{\partial U}{\partial \tau} + U\frac{\partial U}{\partial X} + V\frac{\partial U}{\partial Y}\right] = -\frac{\partial P}{\partial X} + \frac{1}{\varepsilon\, Re}\left[\frac{\partial^2 U}{\partial X^2} + \frac{\partial^2 U}{\partial Y^2}\right] - \frac{U}{Re\, Da} - \frac{C_E}{\sqrt{Da}}|U|U \tag{5.27}$$

Y-momentum:

$$\frac{1}{\varepsilon}\left[\frac{\partial V}{\partial \tau} + U\frac{\partial V}{\partial X} + V\frac{\partial V}{\partial Y}\right] = -\frac{\partial P}{\partial Y} + \frac{1}{\varepsilon\, Re}\left[\frac{\partial^2 V}{\partial X^2} + \frac{\partial^2 V}{\partial Y^2}\right] - \frac{V}{Re\, Da} - \frac{C_E}{\sqrt{Da}}|V|V \tag{5.28}$$

Energy:

$$\frac{\partial \theta}{\partial \tau} + RHC\left[U\frac{\partial \theta}{\partial X} + V\frac{\partial \theta}{\partial Y}\right] = \frac{1}{Re\, Pr}\left[\frac{\partial^2 \theta}{\partial X^2} + \frac{\partial^2 \theta}{\partial Y^2}\right] \tag{5.29}$$

The dimensionless initial and boundary conditions are

For	$\tau \leq 0$	U= 0	V= 0	$\theta = 0$	(5.30)
For	$\tau > 0$				
X=0	$0 \leq Y \leq L_e$	U = -1	V = 0	$\frac{\partial \theta}{\partial X} = 1$	
	$L_e < Y \leq (L_e + L_a)$	U = 0	V = 0	$\frac{\partial \theta}{\partial X} = 0$	
	$(L_e + L_a) < Y < \frac{1}{Ar}$	U = 0	V = 0	$\theta = 0$	
X=1	$0 \leq Y \leq L_e$	U = 0	V = 0	$\frac{\partial \theta}{\partial X} = 1$	
	$L_e < Y \leq (L_e + L_a)$	U = 0	V = 0	$\frac{\partial \theta}{\partial X} = 0$	
	$(L_e + L_a) < Y \leq \frac{1}{Ar}$	U =1	V = 0	$\frac{\partial \theta}{\partial X} = -1$	
Y=0	$0 < X < 1$	U = 0	V = 0	$\frac{\partial \theta}{\partial Y} = 0$	
$Y=\frac{1}{Ar}$	$0 < X < 1$	U = 0	V = 0	$\frac{\partial \theta}{\partial Y} = 0$	(5.31)

5.5.3 Vorticity Transport Equations for the Liquid Wick Region

For two dimensional laminar incompressible flows in rectangular geometry, the governing equations for stream function and vorticity equation are

Stream Function

$$\frac{\partial \psi}{\partial \tau} = \Omega + \frac{\partial^2 \psi}{\partial X^2} + \frac{\partial^2 \psi}{\partial Y^2} \tag{5.32}$$

Vorticity Transport Equation

$$\frac{\partial\Omega}{\partial\tau}+U\frac{\partial\Omega}{\partial X}+V\frac{\partial\Omega}{\partial Y}=\frac{1}{Re}\left[\frac{\partial^2\Omega}{\partial X^2}+\frac{\partial^2\Omega}{\partial Y^2}\right]-\frac{\varepsilon\Omega}{Re\,Da}-\frac{\varepsilon C_E}{\sqrt{Da}}\left[V\frac{\partial|U|}{\partial X}-V\frac{\partial|U|}{\partial Y}+|U|\Omega\right] \quad (5.33)$$

Here the dimensionless stream function, ψ and vorticity, Ω are defined as

$$U=\frac{\partial\psi}{\partial Y} \qquad V=-\frac{\partial\psi}{\partial X} \qquad \Omega=\frac{\partial V}{\partial X}-\frac{\partial U}{\partial Y} \quad (5.34)$$

The modulus of U is obtained as

$$|U|=\sqrt{U^2+V^2}$$

The stream function - vorticity boundary conditions as shown in Fig.5.7 are

$$X=0 \qquad 0\le Y\le L_e \qquad \psi=-Y \qquad \Omega=-\frac{\partial^2\psi}{\partial X^2}$$

$$L_e<Y\le(L_e+L_a) \qquad \psi=-L_e \qquad \Omega=-\frac{\partial^2\psi}{\partial X^2}$$

$$(L_e+L_a)\le Y\le\frac{1}{Ar} \qquad \psi=(Y-\frac{1}{Ar}) \qquad \Omega=-\frac{\partial^2\psi}{\partial X^2}$$

$$X=1 \qquad 0\le Y\le\frac{1}{Ar} \qquad \psi=0 \qquad \Omega=-\frac{\partial^2\psi}{\partial X^2}$$

$$Y=0 \qquad 0<X<1 \qquad \psi=0 \qquad \Omega=-\frac{\partial^2\psi}{\partial Y^2}$$

$$Y=\frac{1}{Ar} \qquad 0<X<1 \qquad \psi=0 \qquad \Omega=-\frac{\partial^2\psi}{\partial Y^2} \quad (5.35)$$

5.6 Numerical Formulation

For most of the physical problems in engineering, the mathematical model obtained are generally in the form of non-linear partial differential equations subjected to complicated boundary conditions. Exact analytical solution of such equations are either not available or quite complex. With the availability of high-speed digital computers and advanced numerical methods in getting the near exact solution of such equations has become a reality. Finite difference method (FDM) is one of the most popular discretization methods mainly due to its computational economy and ease of coding.

In this method, the partial derivatives are replaced by approximate finite difference expressions leading to a set of equivalent algebraic equations generally known as finite difference equations. In FDM, different discretization schemes are available, such as explicit method, implicit method, Alternating Direction Implicit (ADI) scheme, etc. In the present study, the governing equations of stream function, vorticity and energy have been discretized using an ADI scheme. This scheme is unconditionally stable and results in an accuracy of $O(\Delta\tau^2, \Delta X^2, \Delta Y^2)$. In addition, the coefficient matrix corresponding to the system of algebraic equations obtained using this scheme forms a tridiagonal structure, which can be easily solved.

5.7 The Computational Grid System

In a two dimensional space, the finite difference grid system for the computational domain is presented in Fig.5.8. The computational domain is divided into unequal increments in the X and Y directions. These increments are known as the mesh size or grid size. The subscript indices i and j are used to represent the Cartesian

co-ordinates X and Y and the superscript index n is used to represent time. The origin of the computational domain is fixed at the top most left corner of the physical domain and it is represented as grid point (1,1). An increment of ΔX and ΔY in the X and Y directions respectively, increase i to i+1 and j to j+1. Also a small elapse of time by $\Delta\tau$ increases n to n+1. The maximum number of grid points in the X and Y directions are denoted by NX and NY respectively. Fig.5.9 depicts the grid system of n, n+1/2 and n+1 time level for ADI scheme.

5.8 Finite Difference Formulation

In Alternating Direction Implicit (ADI) scheme, for each time step $\Delta\tau$, two sets of finite difference equations are obtained each of which corresponding to half time step $\Delta\tau$. At any (n+1/2) time step, space derivatives are evaluated implicitly in one direction and explicitly in the other direction while at (n+1) time step these implicit and explicit evaluation of derivatives are reversed. Resulting two sets of tridiagonal simultaneous equations are solved in sequence by Thomas algorithm. This algorithm needs the least computer storage and computational time compared to other similar solution procedures.

5.9 Finite Difference Equations for the Vapour Flow

5.9.1 Stream Function

Finite difference form of the stream function equation (Eq.5.14) has been obtained by ADI scheme explained in Section 5.8. The most simplified form of the finite difference equations for stream function are given below.

At n+1/2 time step.

$$\left[\frac{\Delta\tau}{2(\Delta X)^2}\right]\psi_{i-1,j}^{n+1/2} - \left[\frac{\Delta\tau}{(\Delta X)^2}+1\right]\psi_{i,j}^{n+1/2} + \frac{\Delta\tau}{2(\Delta X)^2}\psi_{i+1,j}^{n+1/2}$$
$$= -\left[\frac{\Delta\tau}{2}\right]\Omega_{i,j}^{*} - \left[\frac{\Delta\tau}{2(\Delta Y)^2}\right]\left[\psi_{i,j+1}^{*} + \psi_{i,j-1}^{*}\right] + \left[\frac{\Delta\tau}{(\Delta Y)^2}-1\right]\psi_{i,j}^{*} \qquad (5.36)$$

At n+1 time step

$$\left[\frac{\Delta\tau}{2(\Delta Y)^2}\right]\psi_{i,j-1}^{n+1} - \left[\frac{\Delta\tau}{(\Delta Y)^2}+1\right]\psi_{i,j}^{n+1} + \left[\frac{\Delta\tau}{2(\Delta Y)^2}\right]\psi_{i,j+1}^{n+1}$$
$$= \left[\frac{\Delta\tau}{2}\right]\Omega_{i,j}^{*} - \left[\frac{\Delta\tau}{2(\Delta X)^2}\right]\left[\psi_{i+1,j}^{n+1/2} + \psi_{i-1,j}^{n+1/2}\right] + \left[\frac{\Delta\tau}{(\Delta X)^2}-1\right]\psi_{i,j}^{n+1/2} \qquad (5.37$$

The finite difference form of boundary conditions for stream function are

For j =1,NY	i =1.....NX	$\psi = 0$
For i =1	j = 2... NY-1	$\psi = 0$
For i =NX	j = 2... (Ne-1)	ψ = -Y
	j = Ne.....N2	ψ = -Le
	j = Na+1... NY-1	ψ = (Y-1/Ar) (5.38)

5.9.2 Vorticity

Using the ADI scheme explained in section 5.8, the vorticity transport equation (Eq. 5.15) is converted into finite difference equations for vorticity. After simplification, the finite difference equations for vorticity are rewritten as given below.

At n +1/2 time step

$$\left[\frac{\Delta\tau}{8\Delta X\Delta Y}\left(\overset{*}{\psi}_{i,j-1}-\overset{*}{\psi}_{i,j+1}\right)-\frac{\Delta\tau}{2(\Delta X)^2\,Re}\right]\Omega_{i-1,j}^{n+1/2}+\left[\frac{\Delta\tau}{(\Delta X)^2\,Re}+1\right]\Omega_{i,j}^{n+1/2}$$
$$+\left[\frac{\Delta\tau}{8\Delta X\Delta Y}\left(\overset{*}{\psi}_{i,j+1}-\overset{*}{\psi}_{i,j-1}\right)-\frac{\Delta\tau}{2(\Delta X)^2\,Re}\right]\Omega_{i+1,j}^{n+1/2}$$
$$=\left[1-\frac{\Delta\tau}{(\Delta Y)^2\,Re}\right]\overset{*}{\Omega}_{i,j}+\left[\frac{\Delta\tau}{8\Delta X\Delta Y}\left(\overset{*}{\psi}_{i+1,j}-\overset{*}{\psi}_{i-1,j}\right)+\frac{\Delta\tau}{2(\Delta Y)^2\,Re}\right]\overset{*}{\Omega}_{i,j+1}$$
$$-\left[\frac{\Delta\tau}{8\Delta X\Delta Y}\left(\overset{*}{\psi}_{i+1,j}-\overset{*}{\psi}_{i-1,j}\right)-\frac{\Delta\tau}{2(\Delta Y)^2\,Re}\right]\overset{*}{\Omega}_{i,j-1} \qquad (5.39)$$

At n +1 time step

$$\left[\frac{\Delta\tau}{8\Delta X\Delta Y}\left(\overset{*}{\psi}_{i+1,i}-\overset{*}{\psi}_{i-1,j}\right)-\frac{\Delta\tau}{2(\Delta Y)^2\,Re}\right]\Omega_{i,j-1}^{n+1}+\left[\frac{\Delta\tau}{(\Delta Y)^2\,Re}+1\right]\Omega_{i,j}^{n+1}$$
$$+\left[\frac{\Delta\tau}{8\Delta X\Delta Y}\left(\overset{*}{\psi}_{i-1,j}-\overset{*}{\psi}_{i+1,j}\right)-\frac{\Delta\tau}{2(\Delta Y)^2\,Re}\right]\Omega_{i,j+1}^{n+1}$$
$$=\left[1-\frac{\Delta\tau}{(\Delta X)^2\,Re}\right]\overset{*}{\Omega}_{i,j}+\left[\frac{\Delta\tau}{8\Delta X\Delta Y}\left(\overset{*}{\psi}_{i,j+1}-\overset{*}{\psi}_{i,j-1}\right)+\frac{\Delta\tau}{2(\Delta X)^2\,Re}\right]\overset{*}{\Omega}_{i-1,j} \qquad (5.40)$$
$$-\left[\frac{\Delta\tau}{8\Delta X\Delta Y}\left(\overset{*}{\psi}_{i,j+1}-\overset{*}{\psi}_{i,j-1}\right)-\frac{\Delta\tau}{2(\Delta X)^2\,Re}\right]\overset{*}{\Omega}_{i+1,j}$$

The finite difference form of vorticity boundary conditions are

i=1, j=2.....NY-1 $$\Omega_{i,j}=\frac{2\left(\overset{*}{\psi}_{i,j}-\overset{*}{\psi}_{i+1,j}\right)}{(\Delta X)^2}$$

i=NX, j=2.....NY-1 $$\Omega_{i,j}=\frac{2\left(\overset{*}{\psi}_{i,j}-\overset{*}{\psi}_{i-1,j}\right)}{(\Delta X)^2}$$

$$j=1, \qquad i=1\ldots\ldots NX \qquad \Omega_{i,j} = \frac{2\left(\overset{*}{\psi}_{i,j} - \overset{*}{\psi}_{i,j+1}\right)}{(\Delta Y)^2}$$

$$j=NY, \qquad i=1\ldots\ldots NX \qquad \Omega_{i,j} = \frac{2\left(\overset{*}{\psi}_{i,j} - \overset{*}{\psi}_{i,j-1}\right)}{(\Delta Y)^2} \tag{5.41}$$

5.9.3 Temperature

The energy equation (Eq. 5.11) has also been discretized using ADI schme. The simplified form of finite-difference equations for temperature are given below.

At n +1/2 time step

$$\left[\frac{\Delta\tau}{8\Delta X\Delta Y}\left(\Psi^{*}_{i,j-1} - \Psi^{*}_{i,j+1}\right) - \frac{\Delta\tau}{2(\Delta X)^2\,\mathrm{Re\,Pr}}\right]\theta^{n+1/2}_{i-1,j} + \left[\frac{\Delta\tau}{(\Delta X)^2\,\mathrm{Re\,Pr}} + 1\right]\theta^{n+1/2}_{i,j}$$
$$+\left[\frac{\Delta\tau}{8\Delta X\Delta Y}\left(\Psi^{*}_{i,j+1} - \Psi^{*}_{i,j-1}\right) - \frac{\Delta\tau}{2(\Delta X)^2\,\mathrm{Re\,Pr}}\right]\theta^{n+1/2}_{i+1,j}$$
$$=\left[1 - \frac{\Delta\tau}{(\Delta Y)^2\,\mathrm{Re\,Pr}}\right]\theta^{*}_{i,j} + \left[\frac{\Delta\tau}{8\Delta X\Delta Y}\left(\Psi^{*}_{i-1,j} - \Psi^{*}_{i+1,j}\right) + \frac{\Delta\tau}{2(\Delta Y)^2\,\mathrm{Re\,Pr}}\right]\theta^{*}_{i,j-1} \tag{5.42}$$
$$+\left[\frac{\Delta\tau}{8\Delta X\Delta Y}\left(\Psi^{*}_{i+1,j} - \Psi^{*}_{i-1,j}\right) + \frac{\Delta\tau}{2(\Delta Y)^2\,\mathrm{Re\,Pr}}\right]\theta^{*}_{i,j+1}$$

At n +1 time step

$$\left[\frac{\Delta\tau}{8\Delta X\Delta Y}\left(\Psi^{*}_{i+1,j}-\Psi^{*}_{i-1,j}\right)-\frac{\Delta\tau}{2(\Delta Y)^2\,\mathrm{Re\,Pr}}\right]\theta^{n+1}_{i,,j-1}+\left[\frac{\Delta\tau}{(\Delta Y)^2\,\mathrm{Re\,Pr}}+1\right]\theta^{n+1}_{i,j}$$
$$+\left[\frac{\Delta\tau}{8\Delta X\Delta Y}\left(\Psi^{*}_{i-1,j}-\Psi^{*}_{i+1,j}\right)-\frac{\Delta\tau}{2(\Delta Y)^2\,\mathrm{Re\,Pr}}\right]\theta^{n+1}_{i,j+1}$$
$$=\left[\frac{\Delta\tau}{8\Delta X\Delta Y}\left(\Psi^{*}_{i,j+1}-\Psi^{*}_{i,j-1}\right)+\frac{\Delta\tau}{2(\Delta X)^2\,\mathrm{Re\,Pr}}\right]\theta^{*}_{i-1,j}+\left[1-\frac{\Delta\tau}{(\Delta X)^2\,\mathrm{Re\,Pr}}\right]\theta^{*}_{i,j} \qquad (5.43)$$
$$+\left[\frac{\Delta\tau}{8\Delta X\Delta Y}\left(\Psi^{*}_{i,j-1}-\Psi^{*}_{i,j+1}\right)+\frac{\Delta\tau}{2(\Delta X)^2\,\mathrm{Re\,Pr}}\right]\theta^{*}_{i+1,j}$$

For i = 1 , j = 1.....NY

At n +1/2 time step

$$\left[\frac{\Delta\tau}{(\Delta X)^2\,\mathrm{Re\,Pr}}+1\right]\theta^{n+\frac{1}{2}}_{i,j}+\left[\frac{\Delta\tau}{(\Delta X)^2\,\mathrm{Re\,Pr}}\right]\theta^{n+\frac{1}{2}}_{i+1,j}$$
$$=\frac{\Delta\tau}{2(\Delta Y)^2\,\mathrm{Re\,Pr}}\left[\theta^{*}_{i,j+!}+\theta^{*}_{i,j-1}\right]+\left[\frac{\Delta\tau}{(\Delta Y)^2\,\mathrm{Re\,Pr}}-1\right]\theta^{*}_{i,j} \qquad (5.44)$$

At n +1 time step

$$\left[\frac{\Delta\tau}{2(\Delta Y)^2\,\mathrm{Re\,pr}}\right]\theta^{n+1}_{i,j-1}-\left[\frac{\Delta\tau}{(\Delta Y)^2\,\mathrm{Re\,pr}}+1\right]\theta^{n+1-}_{i,j}+\left[\frac{\Delta\tau}{2(\Delta Y)^2\,\mathrm{Re\,pr}}\right]\theta^{n+1}_{i,j+1}$$
$$=-\left[\frac{\Delta\tau}{(\Delta X)^2\,\mathrm{Re\,Pr}}\right]\theta^{*}_{i+1,j}+\left[\frac{\Delta\tau}{(\Delta X)^2\,\mathrm{Re\,pr}}-1\right]\theta^{*}_{i,j} \qquad (5.45)$$

For i = NX, j = 1.....Ne

At n +1/2 time step

$$\left[\frac{\Delta\tau}{(\Delta X)^2\,\mathrm{Re\,Pr}}\right]\theta_{i-1,j}^{n+\frac{1}{2}} - \left[\frac{\Delta\tau}{(\Delta X)^2\,\mathrm{Re\,Pr}} + 1\right]\theta_{i,j}^{n+\frac{1}{2}}$$

$$= -\Delta X\left[\frac{\Delta\tau}{(\Delta X)^2\,\mathrm{Re\,Pr}}\right] + 2(\Delta X)\left[\frac{\Delta\tau}{8\Delta X\Delta Y}\right]\left[\psi^{*}_{i,j+1} - \psi^{*}_{i,j-1}\right] \qquad (5.46)$$

$$-\frac{\Delta\tau}{2(\Delta Y)^2\,\mathrm{Re\,Pr}}\left[\theta^{*}_{i,j-1} + \theta^{*}_{i,j+1}\right] - \left[1 - \frac{\Delta\tau}{(\Delta Y)^2\,\mathrm{Re\,Pr}}\right]\theta^{*}_{i,j}$$

At n +1 time step

$$\left[\frac{\Delta\tau}{2(\Delta Y)^2\,\mathrm{Re\,Pr}}\right]\theta_{i,j-1}^{n+1} - \left[\frac{\Delta\tau}{(\Delta Y)^2\,\mathrm{Re\,Pr}} + 1\right]\theta_{i,j}^{n+1} + \left[\frac{\Delta\tau}{2(\Delta Y)^2\,\mathrm{Re\,Pr}}\right]\theta_{i,j+1}^{n+1}$$

$$= \left[\frac{\Delta\tau}{(\Delta X)^2\,\mathrm{Re\,Pr}} - 1\right]\theta^{*}_{i,j} - \left[\frac{\Delta\tau}{(\Delta X)^2\,\mathrm{Re\,Pr}}\right]\left[\Delta X + \theta^{*}_{i-1,j}\right]$$

$$-2(\Delta X)\frac{\Delta\tau}{8\Delta X\Delta Y}\left[\psi^{*}_{i,j-1} - \psi^{*}_{i,j+1}\right] \qquad (5.47)$$

For j = (Ne +1).....(Na-1)

At n +1/2 time step

$$\left[\frac{\Delta\tau}{(\Delta X)^2\,\mathrm{Re\,Pr}}\right]\theta_{i-1,j}^{n+\frac{1}{2}}-\left[\frac{\Delta\tau}{(\Delta X)^2\,\mathrm{Re\,Pr}}+1\right]\theta_{i,j}^{n+\frac{1}{2}}$$
$$=-\left[\frac{\Delta\tau}{2(\Delta Y)^2\,\mathrm{Re\,Pr}}\right]\left[\theta_{i,j-1}^{*}+\theta_{i,j+1}^{*}\right]-\left[1-\frac{\Delta\tau}{(\Delta Y)^2\,\mathrm{Re\,Pr}}\right]\theta_{i,j}^{*} \qquad (5.48)$$

At n +1 time step

$$\left[\frac{\Delta\tau}{2(\Delta Y)^2\,\mathrm{Re\,Pr}}\right]\theta_{i,j-1}^{n+1}-\left[\frac{\Delta\tau}{(\Delta Y)^2\,\mathrm{Re\,Pr}}+1\right]\theta_{i,j}^{n+1}+\left[\frac{\Delta\tau}{2(\Delta Y)^2\,\mathrm{Re\,Pr}}\right]\theta_{i,j+1}^{n+1}$$
$$=-\left[1-\frac{\Delta\tau}{(\Delta X)^2\,\mathrm{Re\,Pr}}\right]\theta_{i,j}^{*}-\left[\frac{\Delta\tau}{(\Delta X)^2\,\mathrm{Re\,Pr}}\right]\theta_{i-1,j}^{*} \qquad (5.49)$$

For j = N2 .....NY $\qquad \theta_{i,j}=0 \qquad (5.50)$

For j = 1, i = 2.....NX-1

At n +1/2 time step

$$\left[\frac{\Delta\tau}{2(\Delta X)^2\,\mathrm{Re\,Pr}}\right]\theta_{i-1,j}^{n+\frac{1}{2}}-\left[\frac{\Delta\tau}{(\Delta X)^2\,\mathrm{Re\,Pr}}+1\right]\theta_{i,j}^{n+\frac{1}{2}}+\left[\frac{\Delta\tau}{2(\Delta X)^2\,\mathrm{Re\,Pr}}\right]\theta_{i+1,j}^{n+\frac{1}{2}}$$
$$=-\left[\frac{\Delta\tau}{(\Delta Y)^2\,\mathrm{Re\,Pr}}\right]\theta_{i,j+1}^{*}+\left[\frac{\Delta\tau}{(\Delta Y)^2\,\mathrm{Re\,Pr}}-1\right]\theta_{i,j}^{*} \qquad (5.51)$$

At n +1 time step

$$-\left[\frac{\Delta\tau}{(\Delta Y)^2\,\mathrm{Re\,Pr}}+1\right]\theta_{i,j}^{n+1}+\left[\frac{\Delta\tau}{(\Delta Y)^2\,\mathrm{Re\,Pr}}\right]\theta_{i,j+1}^{n+1}$$
$$=-\left[\frac{\Delta\tau}{2(\Delta X)^2\,\mathrm{Re\,Pr}}\right]\left[\theta_{i+1,j}^{*}+\theta_{i-1,j}^{*}\right]+\left[\frac{\Delta\tau}{(\Delta X)^2\,\mathrm{Re\,Pr}}-1\right]\theta_{i,j}^{*} \qquad (5.52)$$

For j = NY i = 2.....NX-1

At n +1/2 time step

$$\frac{\Delta\tau}{2(\Delta X)^2\,\mathrm{Re\,Pr}}\theta_{i-1,j}^{n+\frac{1}{2}}-\left[\frac{\Delta\tau}{(\Delta X)^2\,\mathrm{Re\,Pr}}+1\right]\theta_{i,j}^{n+\frac{1}{2}}+\frac{\Delta\tau}{2(\Delta X)^2\,\mathrm{Re\,Pr}}\theta_{i+1,j}^{n+\frac{1}{2}}$$
$$=-\frac{\Delta\tau}{(\Delta Y)^2\,\mathrm{Re\,Pr}}\theta_{i,j-1}^{*}+\left[\frac{\Delta\tau}{(\Delta Y)^2\,\mathrm{Re\,Pr}}-1\right]\theta_{i,j}^{*} \qquad (5.53)$$

At n +1 time step

$$\left[\frac{\Delta\tau}{(\Delta Y)^2\,\mathrm{Re\,Pr}}\right]\theta_{i,j-1}^{n+1}-\left[\frac{\Delta\tau}{(\Delta Y)^2\,\mathrm{Re\,Pr}}+1\right]\theta_{i,j}^{n+1}$$
$$=-\left[\frac{\Delta\tau}{2(\Delta X)^2\,\mathrm{Re\,Pr}}\right]\left[\theta_{i+1,j}^{*}+\theta_{i-1,j}^{*}\right]+\left[\frac{\Delta\tau}{(\Delta X)^2\,\mathrm{Re\,Pr}}-1\right]\theta_{i,j}^{*} \qquad (5.54)$$

5.10 Finite Difference Equations for the Liquid Wick Region

5.10.1 Stream Function

Finite difference form of the stream function equation (Eq.5.32) has been by ADI scheme explained in Section 5.8. The most simplified form of the finite difference equations for stream function are given below.

At n +1/2 time step:

$$\left[\frac{\Delta\tau}{2(\Delta x^2)}\right]\psi_{i-1,.j}^{n+1/2}-\left[\frac{\Delta\tau}{2(\Delta X)^2}+1\right]\psi_{i,j}^{n+1/2}+\frac{\Delta\tau}{2(\Delta X)^2}\psi_{i+1,j}^{n+1/2}$$
$$=-\left[\frac{\Delta\tau}{2}\right]\Omega_{i,j}^{*}-\left[\frac{\Delta\tau}{2(\Delta Y)^2}\right]\left[\psi_{i,j+1}^{*}+\psi_{i,j-1}^{*}\right]+\left[\frac{\Delta\tau}{(\Delta Y)^2}-1\right]\psi_{i,j}^{*} \quad (5.55)$$

At n +1 time step

$$\left[\frac{\Delta\tau}{2(\Delta Y)^2}\right]\psi_{i,j-1}^{n+1}-\left[\frac{\Delta\tau}{(\Delta Y)^2}+1\right]\psi_{i,j}^{n+1}+\left[\frac{\Delta\tau}{2(\Delta Y)^2}\right]\psi_{i,j+1}^{n+1}$$
$$=-\left[\frac{\Delta\tau}{2}\right]\Omega_{i,j}^{*}-\left[\frac{\Delta\tau}{2(\Delta X)^2}\right]\left[\psi_{i+1,j}^{n+1/2}+\psi_{i-1,j}^{n+1/2}\right]+\left[\frac{\Delta\tau}{(\Delta X)^2}-1\right]\psi_{i,j}^{n+1/2} \quad (5.56)$$

The finite Difference form of boundary conditions for stream function are

For i = 1	j = 2 .....Ne	$\psi=-Y$
	j = (Ne+1) .....(Na)	$\psi=-Le$
	j = (Na+1) .....(NY-1)	$\psi=Y-\frac{1}{Ar}$
For i = NX	j = 2.....(NY-1).	$\psi=0$
For j = 1,NY	i = 1.....NX	$\psi=0$ (5.57)

5.10.2 Vorticity

Using the ADI scheme explained in Section 5.8, the vorticity transport equation (Eq.5.33) is converted into finite difference equations for vorticity. After simplification the finite difference equations for vorticity are rewritten as

At n +1/2 time step

$$\left[\frac{\Delta\tau}{8\Delta X\Delta Y}\left(\psi^{*}_{i,j-1}-\psi^{*}_{i,j+1}\right)-\frac{\Delta\tau}{2(\Delta X)^2\,\mathrm{Re}}\right]\Omega^{n+1/2}_{i-1,j}+\left[\frac{\Delta\tau}{(\Delta X)^2\,\mathrm{Re}}+1+\frac{\varepsilon}{\mathrm{Re\,Da}}+\frac{\varepsilon C_E}{\sqrt{\mathrm{Da}}}\mathrm{n6}\right]\Omega^{n+1/2}_{i,j}$$

$$\left[\frac{\Delta\tau}{8\Delta X\Delta Y}\left(\psi^{*}_{i,j+1}-\psi^{*}_{i,j-1}\right)-\frac{\Delta\tau}{2(\Delta X)^2\,\mathrm{Re}}\right]\Omega^{n+1/2}_{i+1,j}$$

$$=\left[1-\frac{\Delta\tau}{(\Delta Y)^2\,\mathrm{Re}}\right]\Omega^{*}_{i,j}+\left[\frac{\Delta\tau}{8\Delta X\Delta Y}(\psi^{*}_{i+1,j}-\psi^{*}_{i-1,j})+\frac{\Delta\tau}{2(\Delta Y)^2\,\mathrm{Re}}\right]\Omega^{*}_{i,j+1}$$

$$-\left[\frac{\Delta\tau}{8\Delta X\Delta Y}(\psi^{*}_{i+1,j}-\psi^{*}_{i-1,j})-\frac{\Delta\tau}{2(\Delta Y)^2\,\mathrm{Re}}\right]\Omega^{*}_{i,j-1}$$

$$+\frac{\varepsilon C_E}{\sqrt{\mathrm{Da}}}\left[\frac{(-\mathrm{n1})}{\mathrm{n6}}(\mathrm{n2}*\mathrm{n3}+\mathrm{n1}*\mathrm{n4})-\frac{\mathrm{n3}}{\mathrm{n6}}(\mathrm{n3}*\mathrm{n5}+\mathrm{n1}*\mathrm{n2})\right] \qquad (5.58)$$

At n +1 step

$$\left[\frac{\Delta\tau}{8\Delta X\Delta Y}\left(\psi^{*}_{i+1,j}-\psi^{*}_{i-1,j}\right)-\frac{\Delta\tau}{2(\Delta Y)^2\,\mathrm{Re}}\right]\Omega^{n+1}_{i,j-1}+\left[\frac{\Delta\tau}{(\Delta Y)^2\,\mathrm{Re}}+1+\frac{\varepsilon}{\mathrm{Re\,Da}}+\frac{C_E\varepsilon}{\sqrt{\mathrm{Da}}}\mathrm{n6}\right]\Omega^{n+1}_{i,j}$$

$$+\left[\frac{\Delta\tau}{8\Delta X\Delta Y}\left(\psi^{*}_{i-1,j}-\psi_{i+1,j)}\right)-\frac{\Delta\tau}{2(\Delta Y)^2\,\mathrm{Re}}\right]\Omega^{n+1}_{i,j+1}$$

$$=\left[1-\frac{\Delta\tau}{(\Delta X)^2\,\mathrm{Re}}\right]\Omega^{n+1}_{i,j}+\left[\frac{\Delta\tau}{8\Delta X\Delta Y}\left(\psi^{*}_{i,j+1}-\Psi^{*}_{i,j-1}\right)+\frac{\Delta\tau}{2(\Delta X)^2\,\mathrm{Re}}\right]\Omega^{*}_{i-1,j}$$

$$-\left[\frac{\Delta\tau}{8\Delta X\Delta Y}\left(\psi^{*}_{i,j+1}-\Psi^{*}_{i,j-1}\right)-\frac{\Delta\tau}{2(\Delta X)^2\,\mathrm{Re}}\right]\Omega^{*}_{i+1,j}$$

$$+\frac{C_E}{\sqrt{\mathrm{Da}}}*\frac{1}{\mathrm{n6}}\left[(-\mathrm{n1})*(\mathrm{n2}*\mathrm{n3}+\mathrm{n1}*\mathrm{n4})-\mathrm{n3}(\mathrm{n3}*\mathrm{n5}+\mathrm{n1}*\mathrm{n2})\right] \qquad (5.59)$$

where $$\mathrm{n1}=\left[\frac{\psi^{*}_{i+1,j}-\psi^{*}_{i-1,j}}{2\Delta X}\right]$$

$$\mathrm{n2}=\left[\frac{1}{4\Delta X\Delta Y}(\psi^{*}_{i+1,j+1}+\psi^{*}_{i-1,j-1}-\psi^{*}_{i+1,j-1}-\psi^{*}_{i-1,j+1})\right]$$

$$n3 = \left[\frac{\psi^*_{i,j+1} - \psi^*_{i,j-1}}{2\Delta Y} \right]$$

$$n4 = \left[\frac{\psi^*_{i-1,j} - 2*\psi^*_{i,j} + \psi^*_{i+1,j}}{(\Delta X)^2} \right]$$

$$n5 = \left[\frac{\psi^*_{i,j-1} - 2*\psi^*_{i,j} + \psi^*_{i,j+1}}{(\Delta Y)^2} \right]$$

$$n6 = \sqrt{\left((n3)^2 + (n1)^2\right)}$$

The finite difference form of voticity boundary conditions are as follows:

$$i = 1 \qquad j = 2.....(NY-1) \qquad \Omega_{i,j} = \frac{2\left(\psi^*_{i,j} - \psi^*_{i+1j}\right)}{(\Delta X)^2}$$

$$i = NX \qquad j = 2..... \quad (NY-1) \qquad \Omega_{i,j} = \frac{2\left(\psi^*_{i,j} - \psi^*_{i-1,j}\right)}{(\Delta X)^2}$$

$$j = 1 \qquad i = 1 .....NX \qquad \Omega_{i,j} = \frac{2\left(\psi^*_{ij} - \psi^*_{i,j+1}\right)}{(\Delta Y)^2}$$

$$j = NY \qquad i = 1.....NX \qquad \Omega_{i,j} = \frac{2\left(\psi^*_{ij} - \psi^*_{i,j-1}\right)}{(\Delta Y)^2} \qquad (5.60)$$

5.10.3 Temperature

The energy equation (Eq. 5.29) in the liquid wick region also has been discretized using ADI scheme. The simplified form of finite difference equations for temperature are obtained as below.

At n +1/2 time step

$$\left[\frac{\Delta\tau}{8\Delta X\Delta Y}\mathrm{RHC}\left(\psi^{*}_{i,j-1}-\psi^{*}_{i,j+1}\right)-\frac{\Delta\tau}{2(\Delta X)^{2}\,\mathrm{Re\,Pr}}\right]\theta^{n+1/2}_{i-1,j}+\left[1+\frac{\Delta\tau}{(\Delta X)^{2}\,\mathrm{Re\,Pr}}\right]\theta^{n+1/2}_{i,j}+$$
$$\left[\frac{\Delta\tau}{8\Delta X\Delta Y}\mathrm{RHC}\left(\psi^{*}_{i,j+1}-\psi^{*}_{i,j-1}\right)-\frac{\Delta\tau}{2(\Delta X)^{2}\,\mathrm{Re\,Pr}}\right]\theta^{n+1/2}_{i+1,j}$$
$$=\left[1-\frac{\Delta\tau}{(\Delta Y)^{2}\,\mathrm{Re\,Pr}}\right]\theta^{*}_{i,j}+\left[\frac{\Delta\tau}{8\Delta X\Delta Y}\mathrm{RHC}\left(\psi^{*}_{i-1,j}-\psi^{*}_{i+1,j}\right)+\frac{\Delta\tau}{2(\Delta Y)^{2}\,\mathrm{Re\,Pr}}\right]\theta^{*}_{i,j-1}$$
$$+\left[\frac{\Delta\tau}{8\Delta X\Delta Y}\mathrm{RHC}\left(\psi^{*}_{i+1,j}-\psi^{*}_{i-1,j}\right)+\frac{\Delta\tau}{2(\Delta Y)^{2}\,\mathrm{Re\,Pr}}\right]\theta^{*}_{i,j+1}\qquad(5.61)$$

At n +1 time step

$$\left[\frac{\Delta\tau}{8\Delta X\Delta Y}\mathrm{RHC}\left(\psi^{*}_{i+1,j}-\psi^{*}_{i-1,j}\right)-\frac{\Delta\tau}{2(\Delta Y)^{2}\,\mathrm{Re\,Pr}}\right]\theta^{n+1}_{i,j-1}+\left[1+\frac{\Delta\tau}{(\Delta Y)^{2}\,\mathrm{Re\,Pr}}\right]\theta^{n+1}_{i,j}+$$
$$\left[\frac{\Delta\tau}{8\Delta X\Delta Y}\mathrm{RHC}\left(\psi^{*}_{i-1,j}-\psi^{*}_{i+1,j}\right)-\frac{\Delta\tau}{2(\Delta Y)^{2}\,\mathrm{Re\,Pr}}\right]\theta^{n+1/2}_{i,j+1}$$
$$=\left[1-\frac{\Delta\tau}{(\Delta X)^{2}\,\mathrm{Re\,Pr}}\right]\theta^{*}_{i,j}+\left[\frac{\Delta\tau}{8\Delta X\Delta Y}\mathrm{RHC}\left(\psi^{*}_{i,j+1}-\psi^{*}_{i,j-1}\right)+\frac{\Delta\tau}{2(\Delta X)^{2}\,\mathrm{Re\,Pr}}\right]\theta^{*}_{i-1,j}$$
$$+\left[\frac{\Delta\tau}{8\Delta X\Delta Y}\mathrm{RHC}\left(\psi^{*}_{i,j-1}-\psi^{*}_{i,j+1}\right)+\frac{\Delta\tau}{2(\Delta X)^{2}\,\mathrm{Re\,Pr}}\right]\theta^{*}_{i+1,j}\qquad(5.62)$$

The finite difference forms of boundary conditions for energy equation are given below.

1) For i = 1

a) For j = 2 .....Ne

At n +1/2 step

$$-\left[\frac{\Delta\tau}{(\Delta X)^2\,\mathrm{Re}\,\mathrm{Pr}}+1\right]\theta_{i,j}^{n+1/2}+\left[\frac{\Delta\tau}{(\Delta X)^2\,\mathrm{Re}\,\mathrm{Pr}}\right]\theta_{i+1,j}^{n+1/2}$$
$$=\left[1-\frac{\Delta\tau}{(\Delta Y)^2\,\mathrm{Re}\,\mathrm{Pr}}\right]\theta_{i,j}^{*}+\left[\frac{\Delta\tau}{(\Delta Y)^2\,\mathrm{Re}\,\mathrm{Pr}}\right]\left[\theta_{i,j-1}^{*}+\theta_{i,j+1}^{*}\right]$$
$$+2\Delta X\left[\mathrm{RHC}\,\frac{\Delta\tau}{8\Delta X\Delta Y}\left(\psi_{i,j-1}^{*}-\psi_{i,j+1}^{*}\right)-\frac{\Delta\tau}{2(\Delta X)^2\,\mathrm{Re}\,\mathrm{Pr}}\right] \qquad (5.63)$$

At n +1 time step

$$\left[\frac{-\Delta\tau}{2(\Delta Y)^2\,\mathrm{Re}\,\mathrm{Pr}}\right]\theta_{i,j-1}^{n+1}+\left[\frac{\Delta\tau}{(\Delta Y)^2\,\mathrm{Re}\,\mathrm{Pr}}+1\right]\theta_{i,j}^{n+1}+\left[\frac{-\Delta\tau}{2(\Delta Y)^2\,\mathrm{Re}\,\mathrm{Pr}}\right]\theta_{i,j+1}^{n+1}$$
$$=\left[1-\frac{\Delta\tau}{(\Delta X)^2\,\mathrm{Re}\,\mathrm{Pr}}\right]\theta_{i,j}^{*}+\left[\frac{\Delta\tau}{(\Delta X)^2\,\mathrm{Re}\,\mathrm{Pr}}\right]\theta_{i+1,j}^{*}$$
$$-\left[\frac{\Delta\tau}{(\Delta X)^2\,\mathrm{Re}\,\mathrm{Pr}}\right]\Delta X-(2\Delta X)\left[\mathrm{RHC}\,\frac{\Delta\tau}{8\Delta X\Delta Y}\left(\psi_{i,j+1}^{*}-\psi_{i,j-1}^{*}\right)\right] \qquad (5.64)$$

j = (Ne+1).....(Na)

At n +1/2 time step

$$\left[\frac{-\Delta\tau}{(\Delta X)^2\,\mathrm{Re}\,\mathrm{Pr}}\right]\theta_{i+1,j}^{n+1/2}+\left[\frac{\Delta\tau}{(\Delta X)^2\,\mathrm{Re}\,\mathrm{Pr}}+1\right]\theta_{i,j}^{n+1/2}=\left[1-\frac{\Delta\tau}{(\Delta Y)^2\,\mathrm{Re}\,\mathrm{Pr}}\right]\theta_{i,j}^{*}+$$
$$\left[\frac{\Delta\tau}{2(\Delta Y)^2\,\mathrm{Re}\,\mathrm{Pr}}\right]\left[\theta_{i,j-1}^{*}+\theta_{i,j+1}^{*}\right] \qquad (5.65)$$

At n +1 time step

$$\left[\frac{-\Delta\tau}{2(\Delta Y)^2\,\mathrm{Re}\,\mathrm{Pr}}\right]\theta_{i,j-1}^{n+1}+\left[\frac{\Delta\tau}{(\Delta Y)^2\,\mathrm{Re}\,\mathrm{Pr}}+1\right]\theta_{i,j}^{n+1}$$
$$=\left[1-\frac{\Delta\tau}{(\Delta X)^2\,\mathrm{Re}\,\mathrm{Pr}}\right]\theta_{i,j}^{*}+ \qquad (5.66)$$
$$\left[\frac{\Delta\tau}{(\Delta X)^2\,\mathrm{Re}\,\mathrm{Pr}}\right]\left[\theta_{i+1,j}^{*}\right]$$

b) For j = (Na+1).....(NY-1)

At n +1/2 time step

$$\theta_{i,j}^{n+1/2} = 0 \tag{5.67}$$

At n +1 time step

$$\theta_{i,j}^{n+1} = 0 \tag{5.68}$$

2) For i = NX

a) For j = 2.....Ne

At n +1/2 time step

$$\left[\frac{-\Delta\tau}{(\Delta X)^2\,\mathrm{Re}\,\mathrm{Pr}}\right]\theta_{i-1,j}^{n+1/2} + \left[\frac{\Delta\tau}{(\Delta X)^2\,\mathrm{Re}\,\mathrm{Pr}} + 1\right]\theta_{i,j}^{n+1/2} = \left[1 - \frac{\Delta\tau}{(\Delta Y)^2\,\mathrm{Re}\,\mathrm{Pr}}\right]\theta_{i,j}^{*} + \left[\frac{\Delta\tau}{2(\Delta Y)^2\,\mathrm{Re}\,\mathrm{Pr}}\right]\left[\theta_{i,j-1}^{*} + \theta_{i,j+1}^{*}\right] - 2\Delta X\left[\mathrm{RHC}\frac{\Delta\tau}{8\Delta X\Delta Y}(\psi_{i,j+1}^{*} - \psi_{i,j-1}^{*}) - \frac{\Delta\tau}{2(\Delta X)^2\,\mathrm{Re}\,\mathrm{Pr}}\right] \tag{5.69}$$

At n +1 time step

$$\left[\frac{-\Delta\tau}{2(\Delta Y)^2\,\mathrm{Re}\,\mathrm{Pr}}\right]\theta_{i,j-1}^{n+1} + \left[\frac{\Delta\tau}{(\Delta Y)^2\,\mathrm{Re}\,\mathrm{Pr}} + 1\right]\theta_{i,j}^{n+1} + \left[\frac{-\Delta\tau}{2\Delta Y)^2\,\mathrm{Re}\,\mathrm{Pr}}\right]\theta_{i,j}^{n+1} = \left[1 - \frac{\Delta\tau}{(\Delta X)^2\,\mathrm{Re}\,\mathrm{Pr}}\right]\theta_{i,j}^{*} + \left[\frac{\Delta\tau}{(\Delta X)^2\,\mathrm{Re}\,\mathrm{Pr}}\right]\left[\theta_{i-1,j}^{*}\right] - 2\Delta X\left[\mathrm{RHC}\frac{\Delta\tau}{8\Delta X\Delta Y}(\psi_{i,j+1}^{*} - \psi_{i,j-1}^{*}) - \frac{\Delta\tau}{2(\Delta X)^2\,\mathrm{Re}\,\mathrm{Pr}}\right] \tag{5.70}$$

b) For j = (Ne+1).....(Na)

At n +1/2 time step

$$\left[\frac{-\Delta\tau}{(\Delta X)^2\,\mathrm{Re}\,\mathrm{Pr}}\right]\theta_{i-1,j}^{n+1/2}+\left[\frac{\Delta\tau}{(\Delta X)^2\,\mathrm{Re}\,\mathrm{Pr}}+1\right]\theta_{i,j}^{n+1/2}$$
$$=\left[1-\frac{\Delta\tau}{(\Delta Y)^2\,\mathrm{Re}\,\mathrm{Pr}}\right]\theta_{i,j}^{*}+\frac{\Delta\tau}{2(\Delta Y)^2\,\mathrm{Re}\,\mathrm{Pr}}\left[\theta_{i,j-1}^{*}+\theta_{i,j+1}^{*}\right] \tag{5.71}$$

At n +1 time step

$$\left[\frac{-\Delta\tau}{2(\Delta Y)^2\,\mathrm{Re}\,\mathrm{Pr}}\right]\theta_{i,j-1}^{n-1}+\left[\frac{\Delta\tau}{(\Delta Y)^2\,\mathrm{Re}\,\mathrm{Pr}}+1\right]\theta_{i,j}^{n+1}+\left[\frac{-\Delta\tau}{2(\Delta Y)^2\,\mathrm{Re}\,\mathrm{Pr}}\right]\theta_{i,j+1}^{n+1}$$
$$=\left[1-\frac{-\Delta\tau}{(\Delta X)^2\,\mathrm{Re}\,\mathrm{Pr}}\right]\theta_{i,j}^{*}+\frac{\Delta\tau}{(\Delta Y)^2\,\mathrm{Re}\,\mathrm{Pr}}\left[\theta_{i-1,j}^{*}\right] \tag{5.72}$$

c) For j = (Na+1) .....(NY-1)

At n +1/2 time step

$$\left[\frac{-\Delta\tau}{(\Delta X)^2\,\mathrm{Re}\,\mathrm{Pr}}\right]\theta_{i-1,j}^{n+1/2}+\left[\frac{\Delta\tau}{(\Delta X)^2\,\mathrm{Re}\,\mathrm{Pr}}+1\right]\theta_{i,j}^{n+1/2}$$
$$=\left[1-\frac{\Delta\tau}{(\Delta Y)^2\,\mathrm{Re}\,\mathrm{Pr}}\right]\theta_{i,j}^{*}+\frac{\Delta\tau}{2(\Delta Y)^2\,\mathrm{Re}\,\mathrm{Pr}}\left[\theta_{i,j-1}^{*}+\theta_{i,j+1}^{*}\right]$$
$$+2\Delta X\left[\frac{\Delta\tau}{8\Delta x\Delta Y}\mathrm{RHC}\left(\psi_{i,j+1}^{*}-\psi_{i,j-1}^{*}\right)-\frac{\Delta\tau}{2(\Delta X)^2\,\mathrm{Re}\,\mathrm{Pr}}\right] \tag{5.73}$$

At n +1 time step

$$\left[\frac{-\Delta\tau}{2(\Delta Y)^2\,\mathrm{Re}\,\mathrm{Pr}}\right]\theta_{i,j-1}^{n+1}+\left[\frac{\Delta\tau}{(\Delta Y)^2\,\mathrm{Re}\,\mathrm{Pr}}+1\right]\theta_{i,j}^{n+1}+\left[\frac{-\Delta\tau}{2(\Delta Y)^2\,\mathrm{Re}\,\mathrm{Pr}}\right]\theta_{i,j+1}^{n+1}$$
$$=\left[1-\frac{\Delta\tau}{(\Delta X)^2\,\mathrm{Re}\,\mathrm{Pr}}\right]\theta_{i,j}^{*}+\frac{\Delta\tau}{(\Delta X)\mathrm{Re}\,\mathrm{Pr}}\theta_{i-1,j}^{*} \qquad (5.74)$$
$$-2\Delta X\left[\frac{\Delta\tau}{8\Delta x\Delta Y}\mathrm{RHC}\left(\psi_{i,j-1}^{*}-\psi_{i,j+1}^{*}\right)+\frac{\Delta\tau}{2(\Delta X)^2\,\mathrm{Re}\,\mathrm{Pr}}\right]$$

3) For j=1 and i=1.....imax

At n +1/2 time step

$$\left[\frac{-\Delta\tau}{2(\Delta X)^2\,\mathrm{Re}\,\mathrm{Pr}}\right]\theta_{i-1,j}^{n+1/2}+\left[\frac{\Delta\tau}{(\Delta X)^2\,\mathrm{Re}\,\mathrm{Pr}}+1\right]\theta_{i,j}^{n+1/2}+\left[\frac{-\Delta\tau}{2(\Delta X)^2\,\mathrm{Re}\,\mathrm{Pr}}\right]\theta_{i+1,j}^{n+1/2}$$
$$=\left[1-\frac{\Delta\tau}{(\Delta Y)^2\,\mathrm{Re}\,\mathrm{Pr}}\right]\theta_{i,j}^{*}+\left[\frac{\Delta\tau}{(\Delta Y)^2\,\mathrm{Re}\,\mathrm{Pr}}\right]\theta_{i,j-1}^{*} \qquad (5.75)$$

At n +1 time step

$$-3\theta_{i,j}^{n+1}+4\theta_{i,j+1}^{n+1}-\theta_{i,j+2}^{n+1}=0 \qquad (5.76)$$

4) For j = NY i=1 .....NX

At n +1/2 time step

$$\left[\frac{-\Delta\tau}{2(\Delta X)^2\,\mathrm{Re}\,\mathrm{Pr}}\right]\theta_{i-1,j}^{n+1/2}+\left[\frac{\Delta\tau}{(\Delta X)^2\,\mathrm{Re}\,\mathrm{Pr}}+1\right]\theta_{i,j}^{n+1/2}+\left[\frac{-\Delta\tau}{2(\Delta X)^2\,\mathrm{Re}\,\mathrm{Pr}}\right]\theta_{i+1,j}^{n+1/2}$$
$$=\left[1-\frac{\Delta\tau}{(\Delta Y^2\,\mathrm{Re}\,\mathrm{Pr})}\right]\theta_{i,j}^{*}+\left[\frac{\Delta\tau}{(\Delta Y)^2\,\mathrm{Re}\,\mathrm{Pr}}\right]\theta_{i,j-1}^{*} \qquad (5.77)$$

At n +1 time step

$$\theta^{n+1}_{i,j} - \theta^{n+1}_{i,j-1} = 0 \qquad (5.78)$$

5.11 Solution Procedure

The step by step solution procedure for getting the solution of coupled partial differential equations of stream function, vorticity and temperature are given below.

Step 1: The values of the following parameters are given as inputs to start with.

a) Length of the heat pipe, l

b) Thickness of the vapour core or wick, h_v or h_w

c) Reynolds number, Re

d) Number of nodes in the X and Y directions, NX and NY.

e) Density, specific heat, thermal conductivity values of the fluid and the wick material, ρ, C and k.

Step 2: The values of $\psi^n{}_{i,j}, \Omega^n{}_{i,j}$ and $\theta^n{}_{i,j}$ for n=0 and all i and j are initialized to zeros.

Step 3: Using the known values of $\psi^n{}_{i,j}$ and $\Omega^n{}_{i,j}$ the values of $\psi^{n+\frac{1}{2}}{}_{i,j}$ are computed by sweeping in the i direction for all possible j.

Step 4: Using the known values of $\psi^{n+1/2}{}_{i,j}$ the values of $\psi^{n+1}{}_{i,j}$ are computed by sweeping in the j direction for all possible i.

Step5: Using the known values of $\psi^{n+1}{}_{i,j}$ and $\Omega^n{}_{i,j}$ the values of $\Omega^{n+1/2}{}_{i,j}$ are computed by sweeping in the i direction for all j.

Step 6: Using the known values of $\psi^{n+1}{}_{i,j}$ and $\Omega^{n+1/2}{}_{i,j}$ the value of $\Omega^{n+1}{}_{i,j}$ are computed by sweeping in j direction for all possible i.

Step 7: Using the known values of $\psi^{n+1}{}_{i,j}$ and $\theta^{n}{}_{i,j}$, the values of $\theta^{n+1/2}{}_{i,j}$ are computed by sweeping in the i direction for all possible j.

Step 8: Using the known values of $\psi^{n+1}{}_{i,j}$ and $\theta^{n+1/2}{}_{i,j}$ the values of $\theta^{n+1}{}_{i,j}$ are computed by sweeping in the j direction for all possible i.

Step 9: The values of $\left|\psi^{n}{}_{i,j}-\psi^{n+1}{}_{i,j}\right|$, $\left|\Omega^{n}{}_{i,j}-\Omega^{n+1}{}_{i,j}\right|$ and $\left|\theta^{n}{}_{i,j}-\theta^{n+1}{}_{i,j}\right|$ are compared with a very small value $E\left(O\left(10^{-4}\right)\right)$.

Step 10: The values of Vi,j and Ui,j are calculated from stream function.

Step 11: The pressure is calculated from the Y-momentum Equation.

5.12 Grid Convergence Test

The accuracy of the solution of a partial differential equation using finite difference method depends very much on the size of the finite difference mesh used. In order to obtain an accurate solution, an optimum finite difference mesh must be used. Optimum finite difference mesh is generally obtained by conducting a number of numerical experiments, through executing the developed code for the present study with different finite difference grids. The axial velocity profile in the vapour core at Y=5 and axial velocity variation in the wick region at X = 0.1 for different grid sizes are plotted. It is quite clear from the Figs.5.10 and 5.11 that, 19 x 29 for the vapour flow and 21 x 29 for liquid wick region are optimum grid sizes for the

present analysis. All the numerical results presented in Chapter 6 are obtained using these grid sizes only.

5.13 Summary

Numerical studies has a number of advantages in comparison with experimental analysis or analysis using simplified equations. The situation of the flow or heat transfer phenomenon can be achieved by using governing equations with proper boundary conditions. The heat transfer and fluid flow phenomena in the flat heat pipe are analysed in the present work. The flow of vapour from the evaporator to the condenser along the vapour core and the liquid flow through the porous wick structure are analysed separately here taking common interface conditions. In addition to the temperature distribution, velocity variation and pressure drop in the vapour core and wick region, the stream lines and velocity vector plots are also obtained. The various results along with the corresponding discussions are given in Chapter 6. A comparison of numerical results with that of experimental and Poiseuille theory is also detailed in the Section 6.5.

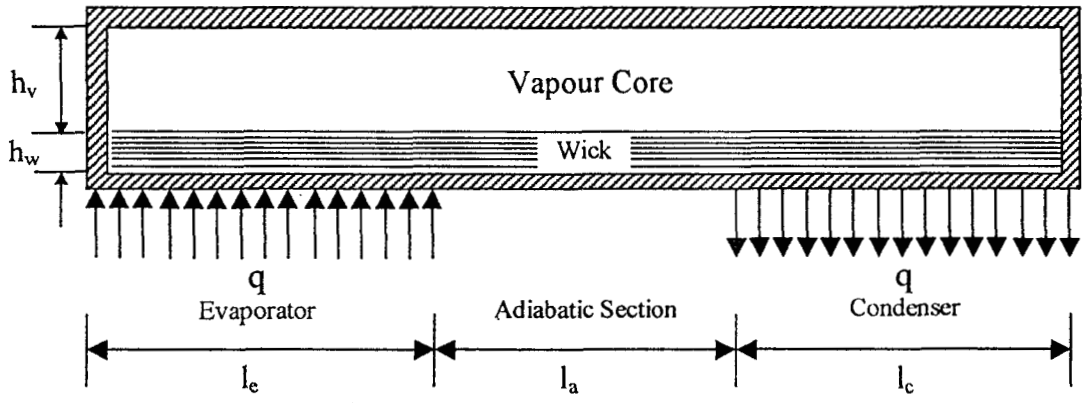

Fig. 5.1 Longitudinal Section of Heat Pipe

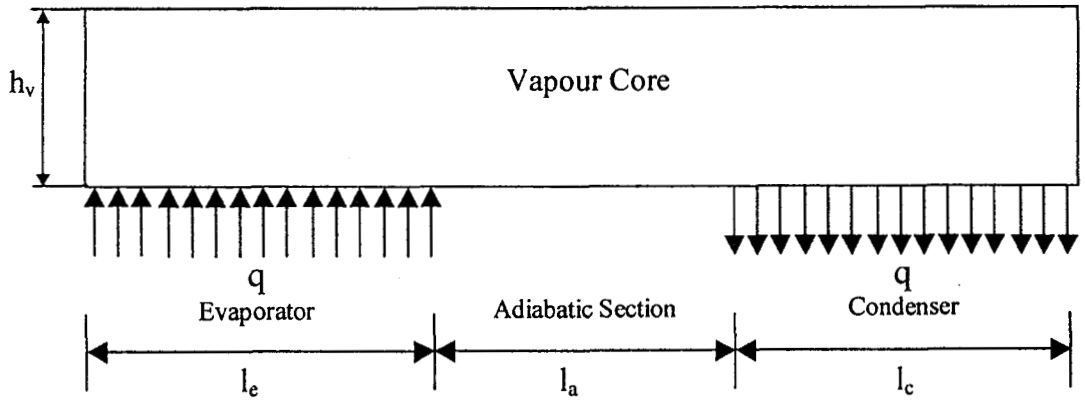

Fig. 5.2 Vapour Core of the Heat Pipe

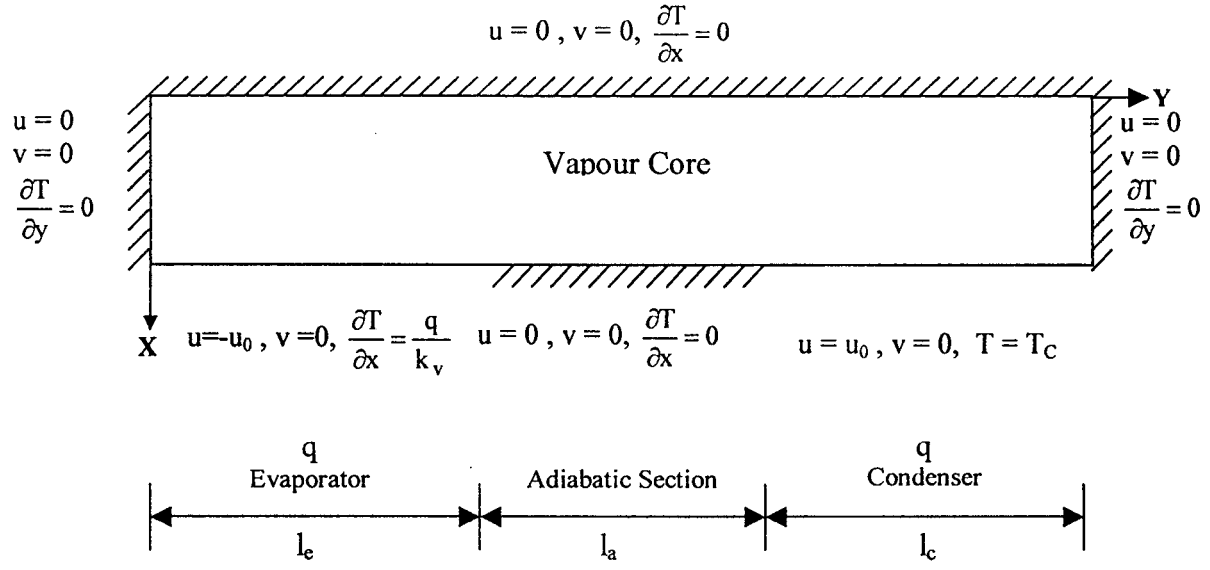

Fig. 5.3 Physical Domain (Vapour Core) with Boundary Conditions

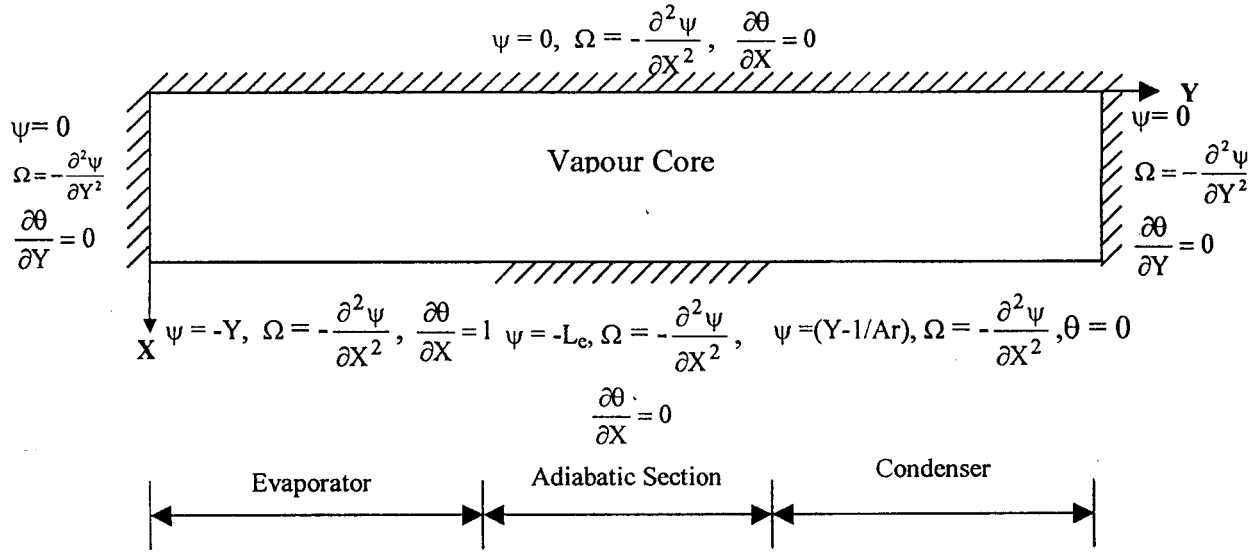

Fig. 5.4 Computational Domain (Vapour Core) with Boundary Conditions

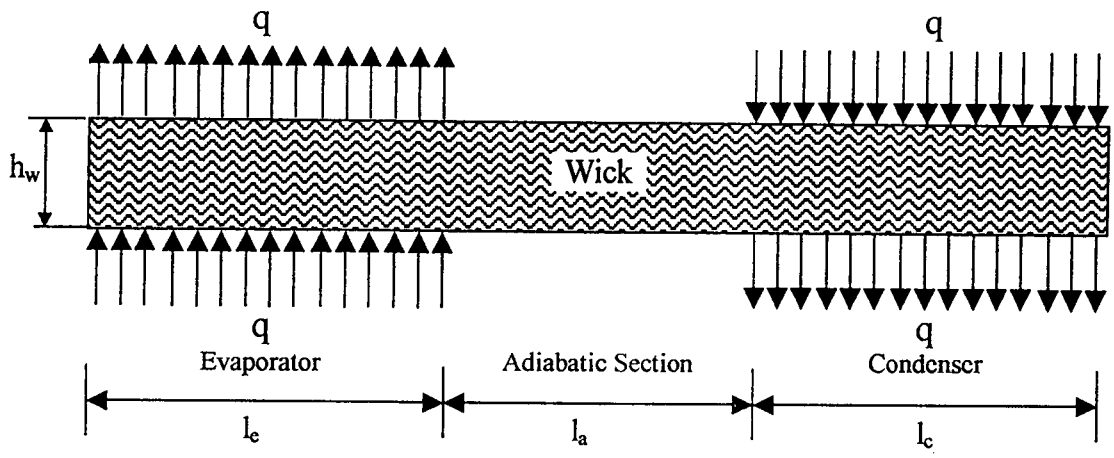

Fig. 5.5 Wick Region of the Heat Pipe

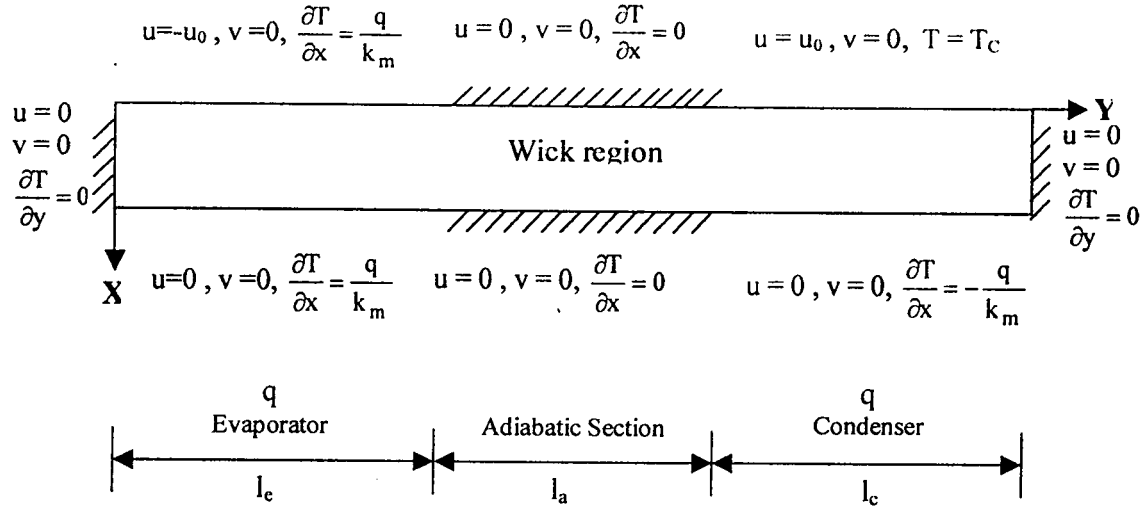

Fig. 5.6 Physical Domain (Wick Region) with Boundary Conditions

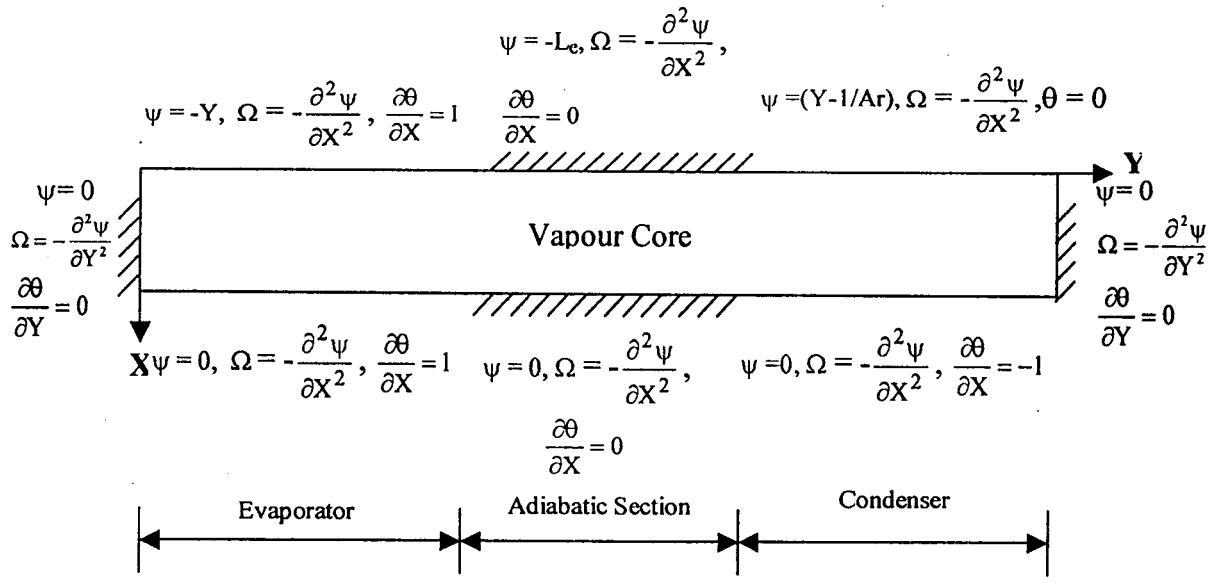

Fig. 5.7 Computational Domain (Wick Region) with Boundary Conditions

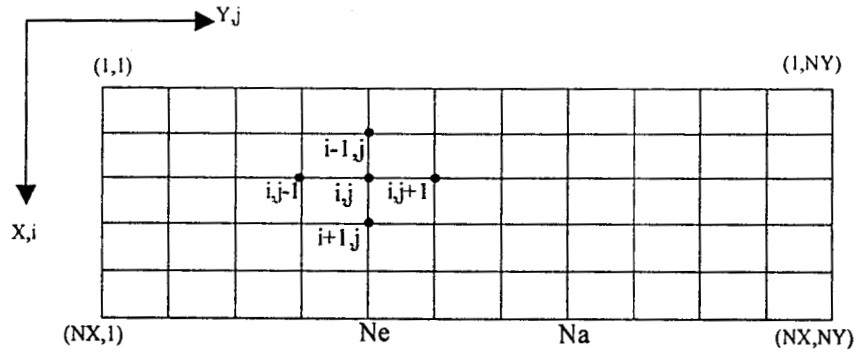

Fig. 5.8 Finite Difference Grid System

ADI METHOD

$$\text{X - Sweep} \quad \left(\frac{\partial\phi}{\partial\tau}\right)_{i,j}^{n+\frac{1}{2}} = \left(\frac{\partial^2\phi}{\partial X^2}\right)_{i,j}^{n+\frac{1}{2}} + \left(\frac{\partial^2\phi}{\partial Y^2}\right)_{i,j}^{n}$$

$$\text{Y - Sweep} \quad \left(\frac{\partial\phi}{\partial\tau}\right)_{i,j}^{n+1} = \left(\frac{\partial^2\phi}{\partial X^2}\right)_{i,j}^{n+\frac{1}{2}} + \left(\frac{\partial^2\phi}{\partial Y^2}\right)_{i,j}^{n+1}$$

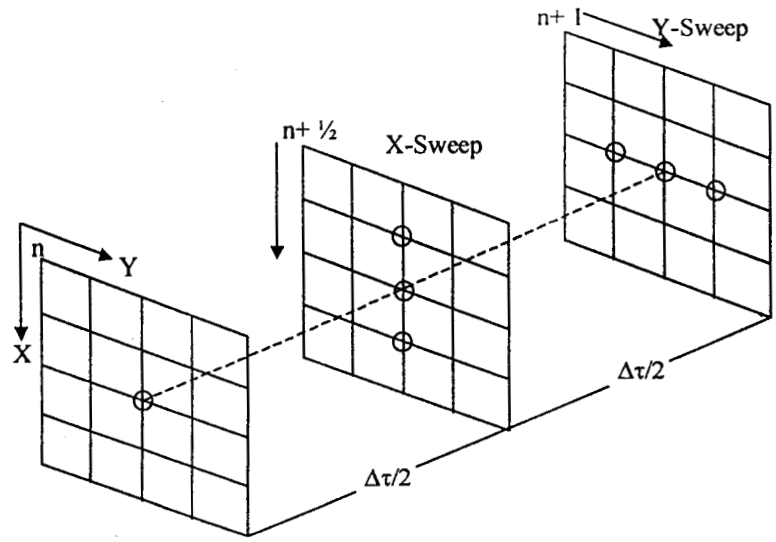

Fig. 5.9 ADI Finite Difference Scheme

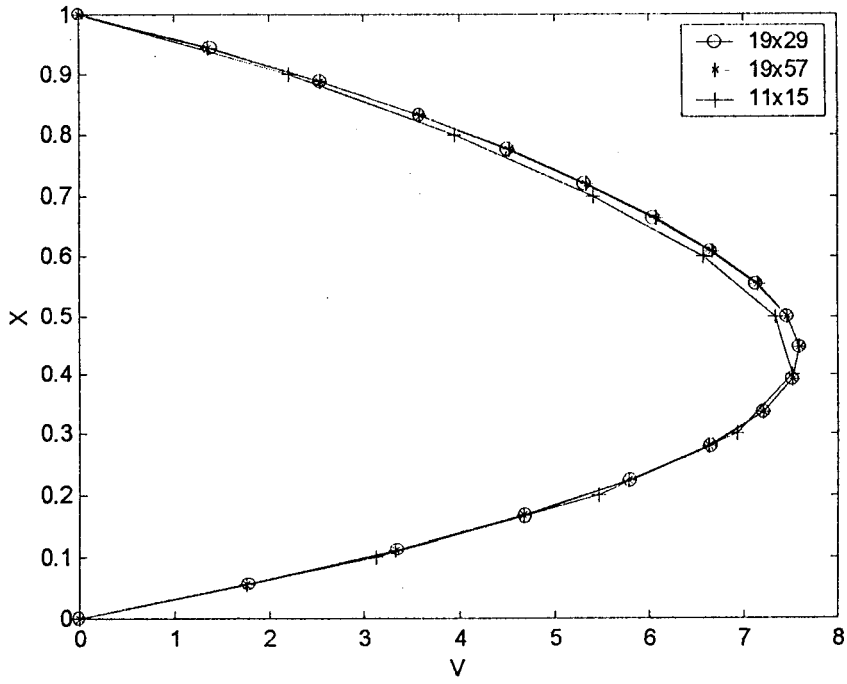

Fig.5.10 Grid Convergence Test for Vapour Flow (Y=5)

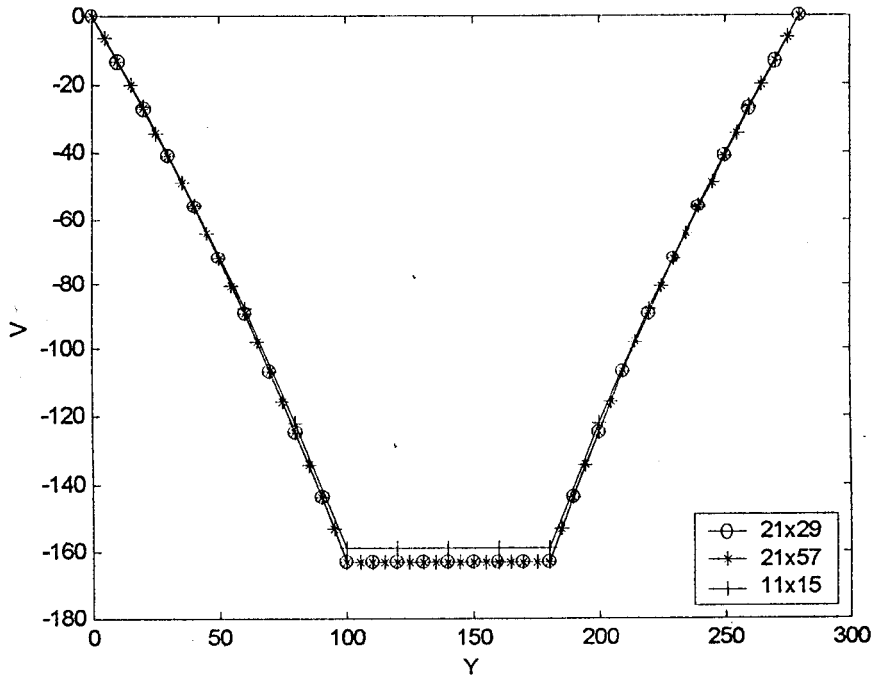

Fig.5.11 Grid Convergence Test for Liquid Flow (X = 0.1)

RESULTS AND DISCUSSION

C. Muraleedharan “Heat transfer and fluid flow studies on flat heat pipe ” Thesis. Department of Mechanical Engineering, Calicut Regional Engineering College , University of Calicut, 2001

Chapter 6

RESULTS AND DISCUSSION

6.1 Introduction

The present research work involves detailed theoretical and experimental investigations on flat heat pipes. The experimental studies are conducted on two different heat pipes. The temperature distribution and vapour pressure profiles are determined in a stainless steel flat heat pipe test set up. Water and acetone are used as working substances. The effect of fluid inventory on the heat pipe performance is also investigated on this heat pipe. The effect of the wick porosity is experimentally analysed in an aluminium flat heat pipe with acetone as working substance. The experimental data are obtained for both the heat pipes with different Reynolds number values.

The pressure drop in the liquid wick region and vapour core are estimated using the Poiseuille model. Results are obtained for different Re and porosity values. A detailed numerical analysis of flat heat pipes is also carried out as part of the present work. The vapour flow in the vapour core and liquid flow in the wick region are separately considered for the analysis. The longitudinal velocity distribution, transverse velocity profiles, temperature distribution and pressure profiles at various Re values are obtained for the flow of vapour. The fluid flow in the liquid wick is studied in detail. Similar results as that of the vapour core are also presented for the liquid wick region. The theoretical and experimental results obtained are presented

and discussed in this chapter. Also comparison of these results and with some available in the literature are detailed here.

6.2 Results of Experimental Studies

The present experiments are conducted on two different test rigs. The experiments on stainless steel flat heat pipe is done with both water and acetone as working substances, while only acetone is used as working fluid in the aluminium heat pipe. On both the experimental set ups a number of test runs are carried out in order to obtain repeated results. The temperature distribution along the heat pipe and pressure drop in the vapour core are obtained. The effect of the amount of working medium and the porosity of wick on heat pipe performance are also studied. The various test runs carried out on the experimental set ups have schematically been displayed in Figs.1.9 and 1.10.

6.2.1 Temperature Distribution Along the Stainless Steel Heat Pipe

The temperature variation along the top and bottom walls of the stainless steel flat heat pipe with water as working fluid are shown in Fig. 6.1. The thermal conductivity of the container material is significant and the wall thickness is very small. Hence the temperature along the bottom wall will be the temperature variation in the wick and the variation along the top wall can be considered as the temperature in the vapour core of the heat pipe. In the vapour core the temperature of the vapour drops continuously. At the evaporator and condenser sections the temperature drop is comparatively less than that at the adiabatic section (Fig.6.1a). The variation of nondimensional temperature in the wick region is almost uniform in every zone, even

though there is temperature drop between the zones (Fig.6.1b). In the adiabatic section a gradual variation of temperature is observed at comparatively low Re values. Though the thermal conductivity of stainless steel is relatively low (20W/m K) there will be axial conduction along the container wall at every Re values. At low Re values percentage of heat conduction along the wall is high compared to the heat flux through the heat pipe. Thus a temperature gradient exists at the adiabatic section along the length of the heat pipe. The temperature distribution in stainless steel heat pipe with acetone and water depicts similar nature (Fig.6.2). However, in this case, it is observed that the nondimensional surface temperature of the heat pipe is slightly higher especially at smaller Re values.

6.2.2 Temperature Distribution in the Aluminium Heat Pipe

The temperature variation in aluminium heat pipe with acetone as working fluid are shown in Figs.6.3 - 6.8 for various wick structures. The temperature in the wick and vapour core are found to be continuously varying from evaporator end to the condenser end irrespective of the heat flux values. This is due to the large thermal conductivity of the container material, which is aluminium. Aluminium has a thermal conductivity of 205 W/m K, which is more than ten times that of stainless steel. Hence, the amount of heat that is transmitted through the container is also quite high

6.2.3 Temperature Distribution at Various Porosity Values

The temperature variation along the aluminium heat pipe for various porosity values are shown in Figs. 6.9 and 6.10. It is observed that when porosity increases surface temperature of the heat pipe decreases at a particular Re value. When the porosity is large, more void is present in the wick structure which will lead into more

amount of liquid contained within the porous wick structure. As liquid has more specific heat than the solid wick material, more heat is required to increase the temperature. Hence, for a particular heat flux, the wick structure which has more porosity is showing less surface temperature.

6.2.4 Influence of Fluid Inventory on the Temperature of the Heat Pipe

One of the important objectives of the present work is to investigate the effect of working fluid charged on the performance of the heat pipe. Performance of both the stainless steel and aluminium heat pipes are analysed with different quantities of the working fluid. The normal or adequately required charge for a heat pipe can be calculated using the dimensions of the heat pipe. The normal charge is the amount of working fluid required just to saturate the capillary structure and to fill the vapour space. Difference in the performance of the heat pipe can be expected when it is forced to work with undercharge or overcharge compared to the normal charge. It has been observed in almost all the cases, the surface temperature of the heat pipe is minimum when operating with the normal charge. The experimental data obtained with different working fluid inventory are tabulated (Tables 6.1 – 6.25).

Figs. 6.11 and 6.12 show the variation of average evaporator temperature of the stainless steel heat pipe with Reynolds number at the same amounts of working fluids namely acetone and water. In both the cases, the evaporator temperature with normal charge is found to be minimum. The reason for this performance could be that, when the heat pipe is operating with undercharge, the thermodynamic properties of the wick structure will be dominating in the operation of the heat pipe. The wick material has less specific heat and more thermal conductivity. When the heat is

transmitted through the dry wick, the temperature rise of it will be more than that of the wick which is saturated with the liquid. When the wick is overcharged, there is excess liquid available which forms an additional layer over the wick structure. This liquid layer will create additional resistance for the heat to flow. This phenomena is prominent in the condenser section of the heat pipe leading to an increase in the condenser temperature. This will be propagated to other regions as well and corresponding increase in temperature will be exhibited in other sections too. Fig. 6.13 shows the variation of the effective thermal conductance of the stainless steel heat pipe with water as the working fluid. It can be observed in this figure that the maximum effective conductance is obtained when the heat pipe operates with normal charge.

6.2.5 Pressure Drop in the Vapour Core

The pressure drop in the vapour core is measured as part of the present experimental studies. The pressure in the liquid wick region could not be measured by utilising the available facility. The pressure profiles are obtained by direct measurement of the vapour pressure at various locations in the vapour core. The pressure profiles are also presented by calculating the pressure from the temperature using Clausius-Clapeyron relations. Both the pressure profiles obtained in the stainless steel heat pipe are shown in Figs. 6.14 and 6.15. The pressure drop estimated using Clausius-Clapeyron relations is observed as larger in magnitude compared with the measured value. The vapour pressure measured at the evaporator shows that it is in superheated state while at the condenser the pressure is greater than that at saturated conditions. Hence, the experimental pressure drop is found to be less

compared to that estimated assuming saturated conditions. When water is used as working fluid, maximum Re vlaue attained is about 5 (Fig.6.14). Hence no pressure build up is expected in this case. However, in one profile a small pressure recovery is observed which can be attributed to error in the measurements. Pressure profiles obtained using the temperature variation do not show any considerable pressure recovery. However, when acetone is used as the working fluid in the stainless steel heat pipe there is pressure build up observed as shown in Fig. 6.15.

6.3 Results of Poiseuille Model

Poiseuille model can be used to estimate the velocity at any point and pressure drop that occurs during the flow of the working medium in the flat heat pipe. The velocity distribution and pressure drop, both in the flow of liquid and vapour working fluid are obtained. The flow of vapour through the vapour core of the heat pipe and liquid through the porous wick are considered as two dimensional, by assuming the width of the heat pipe is very large compared to the thickness of the heat pipe. The fluid is assumed to be Newtonian in nature and the flow is considered as laminar and incompressibe.

6.3.1 Flow of Vapour Through the Vapour Core

In the flat heat pipe, at the interface of the evaporator region vapour will be formed from the liquid working medium by absorbing heat from the heat source. The vapour formed will flow from the evaporator zone to the condenser zone along the vapour space. At the condenser zone the vapour will get condensed by rejecting heat to the heat sink.

6.3.1.1 Velocity Distribution : At the liquid wick and vapour core interface of the evaporator, evaporation of the liquid working medium occurs. The vapour molecules will escape into the vapour core of the evaporator section continuously at the interface. Assuming uniform distribution of the heat source, the temperature is also expected to be uniform at the evaporator zone. The mass of vapour accumulated in the vapour core of evaporator increases linearly due to continuous mass injection by evaporation along the direction of flow of the working fluid. A maximum value is attained at the end of the evaporator zone which is the beginning of the adiabatic zone. In the evaporator section, $0 < y < l_e$, the velocity profile is parabolic in nature. The adiabatic section of the heat pipe is fully insulated, so that theoretically no heat transfer occurs in this section. Since it is assumed that the container and wick materials have low thermal conductivity, conduction heat transfer through these are also can be considered negligible compared to the heat carried by the vapour. The velocity profile is parabolic and identical to that at the beginning of the adiabatic section and the velocity distribution remains unchanged in this zone ($l_e < y < l_e + l_a$). The phenomenon that occurs in the condenser is just reverse of that occurs in the evaporator. In the condenser section, continuously vapour is removed from the vapour core by condensation and the liquid condensate is absorbed by the wick. The liquid working medium comes back to the evaporator through the wick. The velocity profile is parabolic here ($l_e + l_a < y < l$) also. However, the velocity variation here is of diminishing type in the direction of flow unlike that in the evaporator section.

6.3.1.2 Vapour Pressure Drop : As the vapour working medium flows from the evaporator to the condenser end, it experiences a pressure drop. This pressure drop is caused by friction between the vapour and the internal surface of the heat pipe, as well as due to the acceleration of the vapour in the vapour space. Fig.6.16 depicts the vapour pressure variation along the stainless steel heat pipe at various Re values (Re = 0.89, 1.52, 2.04, 2.85, 3.99 and 5.26). The frictional pressure drop is proportional to the velocity of the medium. In the evaporator section it has a parabolic variation. In the adiabatic section the frictional pressure drop linearly varies as the velocity is more or less constant. Similar to that of evaporator zone, pressure drops parabolically in the condenser zone. Though the inertial pressure drops in the evaporator zone causing acceleration of the fluid, it will be increasing in the condenser region due to deceleration. Along the adiabatic section, the inertial pressure is a constant value. As the inertial pressure has opposite sign in the condenser zone compared to that in the evaporator zone, pressure build up is expected here. It is observed that when Re value is greater than 5.0, there is pressure recovery (Fig.6.16f). In the present analysis, when acetone is used in stainless steel heat pipe, Re values are greater than 5.

Fig. 6.17 shows the nondimensional pressure drop corresponding to various Reynolds numbers (Re = 0.89, 1.52, 2.04, 2.85, 3.99 and 5.26). This figure shows the compiled form of the total pressure drop which are shown in Figs. 6.16 (a – e). Fig.6.18 shows the ratio of total pressure drop to the effective pressure drop corresponding to the same Re values. The effective pressure drop is caused by the frictional term only as the inertial term has opposite signs in the evaporator and condenser zones. The maximum value of the pressure ratio is unity which occurs at the condenser end. All the curves are observed as meeting at the same point

corresponding to evaporator end ($P^+ = 0$) and condenser end ($P^+ = 1$) as seen from Fig.6.18. Similar graphs are also obtained in stainless steel heat pipe with acetone as working fluid (Figs. 6.19 - 6.21). Here, pressure build up can be noticed when Re value is greater than 5.

6.3.2 Flow of Liquid in the Porous Wick Structure

In the heat pipe the flow of liquid working medium occurs through the porous wick structure. At the vapour wick interface of the condenser section the vapour gets condensed by rejecting heat to the heat sink. The condensed working fluid flows back along the wick towards the evaporator. At the evaporator again the same liquid will be vaporised and this cycle repeats as the heat pipe operates continuously. The velocity distribution in the liquid wick region also can be determined by using the Poiseuille approach. The pressure drop for different Re values and for different porosity values are estimated by using Darcy's formula. Since the velocity is negligibly small in the wick region the inertial term is not taken in to consideration.

6.3.2.1 Velocity Distribution in the Wick Region: The mean velocity distributions of the liquid working fluid for different Re values in the wick region are shown in Fig.6.22. The velocity distribution is expressed in its nondimensional form. It can be observed in Fig. 6.22 that the velocity of the liquid working medium increases linearly in the condenser zone due to mass addition by condensation of vapour and heat is rejected to the sink (cooling water). At the evaporator zone the velocity decreases linearly due to depletion of liquid medium by evaporation, while in the adiabatic zone velocity remains constant (see Fig. 6.22).

6.3.2.2 Pressure Drop in the Liquid Wick Region: The pressure drop in the liquid medium is estimated by Darcy's formula (Eq. 4.20). Since the velocity of the liquid in the porous wick structure is very small, only the viscous term need to be considered (neglecting the inertial pressure drop). The pressure profile for various Re values are shown in Fig.6.23. The pressure drop increases as the Reynolds number increases as expected. It is interesting to note that the increase in pressure drop is quite appreciable in the Reynolds number range 20<Re<30 compared to that in 10<Re<20.

6.4 Results of Numerical Analysis

The problem of fluid flow and heat transfer analysis in heat pipes is highly complex. The basic physical problems involved in the flat heat pipe are the flow of vapour working medium from the evaporator zone (where it is formed by absorbing heat from the source) to the condenser section. It should be kept in mind that this vapour is generated continuously throughout the evaporator region by absorbing heat from the source. The flow of vapour from the evaporator to condenser occurs through the vapour core of the heat pipe. At the condenser section the vapour becomes liquid by rejecting heat to the heat sink. The condensed liquid returns to the evaporator through the porous wick structure for re-evaporation. In order to reduce the complexity of analysis, the flow of vapour along the vapour core and flow of liquid in the wick structure are modeled separately in the present analysis with common interfacial conditions.

6.4.1 Results for Vapour Flow Through the Vapour Core

Solution of the governing equations for flow of vapour working medium through the vapour space of the flat heat pipe has been obtained by solving Eqs.5.11, 5.14 and 5.15. Results are obtained with water as working fluid in a nonsymmetrical stainless steel flat heat pipe at different Reynolds number values. Stream lines, axial velocity profiles, axial velocity distribution, interfacial temperature distribution and pressure profiles are plotted.

6.4.1.1 Stream Lines for Vapour Flow: Stream lines for Re = 1, 5, 10 and 12.50 are shown in Fig.6.24 corresponding to an aspect ratio value of 0.014. Uniform evaporation and condensation boundaries are visible in every stream line plot. The stream lines are perpendicular to the interface boundary at the evaporator and condenser sections. At the evaporator the stream lines tend to move towards the adiabatic top wall, while at the condenser the trend is in the opposite direction. At the adiabatic region the stream lines are parallel to each other and almost horizontal at low value of Reynolds number ($Re \leq 5$). At higher Re values the stream lines in the evaporator and condenser zones are strongly coupled. It is obvious from the stream line plots that the adiabatic section has influence on the heat pipe performance. When the Re value increases ($Re > 12.5$), reverse flow is observed in the condenser zone. It is also noticed during computation that further increase of Reynolds number leads to the formation of a recirculation zone at the condenser region. Results are presented here up to Re = 12.5 only, considering the fact that the practical Re values in the flat heat pipes will be quite less.

6.4.1.2 Vector Plots for Vapour Flow : Fig.6.25 shows the vector plots for four different Reynolds number values (Re = 1, 5, 10 and 12.50). By these vector plots it is possible to realise both the magnitude and direction of the fluid flow. These vector plots also convey the flow phenomenon in the flow passage. The vector plots corresponding to Re = 1 and 5 (Figs.6.25a and 6.25b), indicate that the flow is smooth. But when Re increases further to say, Re = 10, majority of the fluid flow from the evaporator to the condenser zone shifts closer to the interface. A similar trend is available for Re = 12.50 also (Fig. 6.25d) and tendency of flow reversal is observed at this Re value (See Fig.6.24d also). The velocity terms are nondimensionalised by the vertical velocity at the interface. As the Reynolds number increases, there will be considerable increase in the velocity at the interface. It affects the velocity vector plots also.

6.4.1.3 Axial Velocity Distribution in the Vapour Space : The velocity distribution in the vapour channel along the axial direction is shown in Fig.6.26 for different Re values (Re = 1, 2, 5, 10, 12.5 and 15). It is observed that the variation of the velocity at the evaporator and condenser regions linearly increases and decreases respectively at low Re values. However, at increased Reynolds number values, in addition to the deviation from linear variation, a sudden increase at the end of evaporator zone and decrease at the beginning of condenser zone are observed (See Fig 6.26). This signifies the fact that, due to high temperature at the evaporator, more vapour is formed leading to an increase in the average axial velocity at this section. At the condenser section the phenomenon is just the reverse, due to the effect of sudden cooling taking place there. As far as, the vertical component of velocity is concerned, there will be a corresponding opposite trend. However, at the adiabatic section, the

velocity remains more or less horizontal which does not have much effect with respect to Reynolds number value (except for high Re, say Re=15, as shown in Fig.6.26). Fig. 6.27 shows the variation of axial velocity of vapour at two different values of X (X = 0.056 and 0.50) corresponding to Re=5. As expected, the magnitude of V is higher as the distance from the solid wall increases. The velocity distribution has similarity with Poiseuille theory at low Re values.

6.4.1.4 Axial Velocity Profile : Figs. 6.28 - 6.32 show the axial velocity profiles for Re = 1, 2, 5, 10 and 12.5 respectively, in the vapour core corresponding to the aspect ratio, Ar = 0.014. At low values of Re the axial velocity profile is found as parabolic (Fig.6.28), showing similarity with Poiseuille flow. However, when the heat flux increases, or at higher Re values, an upward shift of the velocity maxima from the centre line of the vapour core is observed (Figs.6.29 and 6.30) in the condenser section. The reason for this is the inertia of the vapour formed in changing the direction. When Re is high, more vapour is formed. At the beginning, the vapour has only vertical component and after some displacement along the vertical direction it gets diverted by the upper wall of the heat pipe container. Thus, it achieves the increased axial component to flow in the direction of the condenser. At the condenser section the nature of the axial velocity profile is entirely different. Though the profile is parabolic at low Re values, the velocity maxima shift to bottom side of the axis of the channel. The tendency of flow reversal is observed at the condenser zone when Re = 12.50 (Fig. 6.32). When Re > 10, very high velocity maxima are observed which attain very near to the interface of the condenser zone.

The most important and interesting observation is that at Re >12.50, the flow reversal phenomena occurs (see Fig.6.32A). This Reynolds number (Re=12.50) has significance, in the sense that it corresponds to the capillary limitation with respect to the given heat flux. All the vapour formed at the evaporator zone will not be getting condensed at the condenser zone. The accumulation of the vapour at the condenser zone causes the flow reversal. The lack of full condensation of the vapour at the condenser zone affects the mass flow of the liquid through the porous wick to the evaporator zone. This can cause starvation of liquid in the evaporator zone at times. The heat pipe can not take away the supplied heat at the evaporator section and hence lead to eventual ceasure of operation of the heat pipe. A comparison of axial velocity profiles for two different Re values (Re=1.0 and 5.0) is shown in Fig. 6.33, both in the condenser and evaporator sections. At the evaporator section larger peak value of velocity is achieved at higher Re values (Fig.6.33a) where as opposite is the case at the condenser section (Fig.6.33b).

6.4.1.5 Temperature Distribution : The nondimensional temperature distribution along the wick - vapour core interface is obtained and shown in Fig.6.34 for various Re values (Re = 2.0, 5.0, 10.0 and 20.0) corresponding to Ar = 0.014. It is observed that at the interface the temperature remains almost uniform at the respective sections. The nondimensional temperature value decreases at the evaporator with respect to increase in the Reynolds number value. But the dimensional temperature increases with Re values. The decrease in nondimensional temperature in the heat pipe indicates that as Re increases, the same amount of heat flux is transferred with lower temperature gradient.

6.4.1.6 Pressure Profiles in Vapour Channel : In the present analysis, the pressure profile along the vapour core of flat heat pipe has more significance. In majority of the low capacity heat pipe designs, the vapour pressure drop is neglected. The pressure drop along the vapour core of the heat pipe is shown in Fig.6.35. Even at low Re values the pressure drop obtained is greater than that estimated by the Poiseuille model. At Re = 5.26, no pressure recovery is observed at the condenser. But at Re = 10 and 20, pressure build up is noticed at the condenser zone (Fig.6.35). It may also be added here that in the heat pipe designs the pressure drop in the vapour core should be considered, especially when the capacity is large and cross sectional area is small.

6.4.2 Results for Liquid Flow Through the Porous Wick Structure

6.4.2.1 Stream lines in the Liquid Wick Region : Stream lines in the liquid wick region are shown in Fig.6.36 corresponding to Ar = 0.0036 and Re = 0.1, 1, 10 and 20. At all Re values the stream lines obtained are smooth and well defined. At the condenser section and evaporator section all stream lines are found to be perpendicular to the interface, indicating no flow along the interface. At low Re values the stream lines are well distributed in the whole domain (Figs. 6.36a and 6.36b). While at higher Re values the stream lines are found to be nearer to the interface showing concentration of mass flow closer to the interface (Figs 6.36c and 6.36d). Stream lines for different wick structure having porosity, ε = 0.75, 0.70 and 0.65 corresponding to Re = 10 are shown in Figs.6.37a, 6.38a and 6.39a respectively. Unlike the vapour core stream lines, the stream lines do not indicate any flow reversals even at higher Re values.

6.4.2.2 Velocity Vector Plots: Stream lines are the imaginary lines at any point on which the tangent will give the direction of velocity. However, the velocity vector plots will exhibit the flow phenomenon realistically, that occurs in the respective regions. Figs. 6.37b, 6.38b and 6.39b show the vector plots corresponding to the stream lines at Re = 10, for various wick structures with ε = 0.75, 0.70 and 0.65 respectively. Since the difference in velocity is not much, only slight difference is noticeable between these plots. At the interface of the condenser zone only vertical component of velocity exists, that too in the downward direction due to condensation of vapour which is assumed to be taking place at the interface itself. The direction of the velocity vector gradually changes to the horizontal giving rise to the axial velocity component and decrease in vertical component. At the adiabatic section only axial component of velocity exists. At the evaporator region also the magnitude of the axial velocity decreases and as the interface is reached, only vertical component remains (see Figs. 6.37b, 6.38b and 6.39b).

6.4.2.3 Axial Velocity Distribution in the Liquid Wick Region: Fig. 6.40 shows the axial velocity distribution in the wick region for various Re values (Re = 0.1, 1, 10 and 20) with Ar = 0.0036 and ε = 0.5. Flow of liquid in the porous wick structure is from the condenser zone to the evaporator region. It is observed that for all Re values the non-dimensional mean axial velocity distribution has similarity with that obtained using the Poiseuille model (see Fig.6.22). At the condenser section, the axial velocity increases due to addition of liquid mass to the wick by condensation of vapour at the vapour - wick interface. This increase in axial velocity occurs up to the end of the condenser zone. The variation of the velocity is not found to be strictly linear as the

vertical component is not included in predicting the distribution. At the adiabatic section, the axial velocity distribution is parallel to the interface and bottom wall showing no addition or removal of liquid in the region. In the evaporator region, due to uniform evaporation of liquid, mass depletion occurs in the wick. Hence the axial velocity decreases gradually along the direction and reaches zero when Y = 0 (See Fig.6.40).

Fig.6.41 shows the axial distribution for Re = 5 at various longitudinal sections. In the porous wick the axial velocity can be uniform at every cross section (or at any Y). But the figure shows that there is variation with respect to transverse distance. It is observed that the velocity nearer to the interface is higher and when Re = 10 and 20, the velocity is extremely high nearer to the interface showing that the flow concentrated very near to the wick – vapour interface. Figs.6.42a and 6.42b show the axial velocity distribution for different wick structure at Re = 10. The porosity values considered to obtain these data are 0.75, 0.70 and 0.65. Fig.6.42a is plotted at X = 0.1 where as Fig.6.42b is plotted at X = 0.5 (middle of the liquid wick). Though the nondimensional axial velocity distribution is similar, the actual velocity will be different. As the porosity increases, the axial velocity decreases due to the effective increase in area of flow. When the porosity decreases velocity increases. Fig.6.43a shows the mean axial velocity distribution at different porosity values (ε = 0.75, 0.70 and 0.65). Only small difference is observed in the velocity values. Fig.6.43b shows the velocity distribution for different porosity values (ε = 0.75, 0.70 and 0.65) when the wire diameter of the different wicks is assumed constant. Slight variation of the velocity is observed comparing with Fig.6.42b in which the practical case is considered where wire diameters are different.

6.4.2.4 Axial Velocity Profile in the Liquid Wick Region : Visualising the axial velocity profiles of the liquid flow through the porous wick can lead to interesting conclusions. Normally the velocity in porous wick is assumed to be uniform at every cross section corresponding to one dimensional flow. An attempt is made here to plot the two dimensional axial velocity profiles at various cross sections along the longitudinal direction of the heat pipe (Figs.6.44 – 6.46). But the axial velocity profiles shown in Figs.6.44 - 6.46 convey the deviations of the velocity profile highly different from the one dimensional flow assumption. It is observed that the velocity nearer to the interface is maximum.Velocity profiles are not strictly parabolic and satisfying the no slip boundary conditions at the solid wall and liquid - vapour interface. The magnitude of the velocity increases as the fluid moves away from the extreme ends of the heat pipe (See Figs.644 – 6.46). The axial velocity profiles shown in Fig.6.47 display a comparison between the velocity values obtained for different Re values (Re = 1 and 10) at constant porosity (ε=0.50) and aspect ratio (Ar = 0.0036). Fig.6.48 shows similar comparison for different ε values (ε =0.65, 0.70 and 0.75) at constant Reynolds number (Re=10) and aspect ratio (Ar = 0.0023). For plotting Figs. 6.47 and 6.48, two different locations of the heat pipe along its axial direction are selected (Y = 40 and Y =340). The former is corresponding to the practical case where the wire diameter is different in different wire screens while the latter is for the same wire diameter.

6.4.2.5 Isotherms in the Liquid Wick Region : The actual heat transfer pattern within the liquid wick can be explicitly seen with the help of isotherms. The isotherms plotted with Re = 1 and 10 are shown in Fig.6.49. The heat flux applied at

the bottom boundary of the evaporator is transmitted into the interior regions of the porous wick. The temperature gradient near the container wall is higher compared to that near the interface. The thermal gradients are responsible for the heat transfer. In the evaporator zone the isotherms are closer to each other because of the large thermal gradients prevailing there. Uniform temperature distribution is found along the evaporator section (Fig.6.49). At the ends of the adiabatic section of the heat pipe, the isotherms are perpendicular to the wall indicating no heat transfer. As the exterior of the adiabatic zone is considered as insulated, no heat transfer will occur through the wall. In the interfacial regions of the adiabatic section, the isotherms are perpendicular for the same reason. The temperature decreases in the axial direction of the heat pipe, even though constant temperature is noticed with respect to any Y in the evaporator and condenser sections. Marginal change in the isotherm pattern is observed with respect to the Reynolds number (see Figs.6.49a and 6.49b).

6.4.2.6 Temperature Distribution: The temperature variation in the longitudinal direction along the container wall is shown in Figs. 6.50 and 6.51 for different Re values with $\varepsilon = 0.50$ and $Ar = 0.0036$. In the evaporator section, heat will be transported to the liquid surface partly by conduction through the wick material and liquid and partly by convection. Evaporation is assumed to occur at the liquid wick surface. However actually in the heat pipe, as the heat flux is increased, the liquid in contact with the wall will become progressively superheated and bubbles will form at the nucleation sites. The vapour bubbles will transport some energy to the surface by latent heat of vaporization and will greatly enhance the convective heat transfer within the wick domain. In the condenser section vapour is assumed to condense at the

liquid surface in the interface. However, in the actual situation, condensation can occur in two ways. First the condensing vapour forms a continuous liquid surface (film condensation) and second it can form a large number of drops (drop wise condensation). Experimental studies indicate that mostly film condensation occurs within heat pipe. The total temperature drop in the heat pipe is equal to the sum of the temperature drops at the evaporator, vapour flow passage and the condenser. Figs.6.50 and 6.51 indicate that the temperature decreases along the longitudinal direction of the heat pipe. However the temperature virtually remains constant in the evaporator, adiabatic and condenser zones. As Re increases the temperature gradient along the heat pipe decreases showing an increase in the heat flux. Hence, with the heat pipe having same dimensions, larger heat fluxes can be transported at higher Re values.

Fig.6.52 indicates the temperature variation along the heat pipe for different porosity values (ε = 0.75, 0.70 and 0.65) at Re = 10 and Ar = 0.0036. As porosity increases, void area increases and hence volume occupied by the fluid is more than that occupied at lower porosity. Since the fluid specific heat is more than that of the solid matrix, at higher porosity, the fluid content is more and hence in order to have a change in temperature more heat is to be supplied than that is required at lower porosity. This indicates that as the porosity value decreases temperature of the wick matrix should increase (see Fig. 6.52).

6.4.2.7 Pressure Variation in the Liquid Wick Region: When the working medium flows in the heat pipe it experiences two types of pressure drops. They are the pressure drop in the vapour core and the pressure drop in the liquid phase. Out of

these the latter is larger in magnitude. The pressure drop that occurs in the liquid phase when flowing through the porous wick is determined. Fig.6.53 shows the pressure drop in the liquid wick region for different Re values with respect to the pressure at the evaporator end (Y =0) . As Re increases, velocity of flow increases, and pressure drop also increases. Moreover, as the porosity of the wick structure decreases, the velocity increases, and correspondingly increase will be occurring in the pressure drop. Figs. 6.54a and 6.54b show the pressure drop in the liquid phase for Re = 0.05 and Re = 10 respectively at different porosity values (ε = 0.75, 0.70 and 0.65). It is observed that the pressure drop increases with decrease in porosity of the wick structure which is caused by the increase in the velocity of liquid flow.

6.5 Comparison of Results

The objectives of the present work are the experimental and theoretical analyses of the flat heat pipe performance. As explained, the experimental studies are conducted on two different flat heat pipes. One flat heat pipe is made up of stainless steel and the working substances used in this are water and acetone. The other set up contains an aluminium flat heat pipe which employs acetone as the working fluid. The temperature distribution and pressure drop are studied on these heat pipes. The influence of the amount of working fluid, porosity of the wick structure and thermal conductivity of the container material are also investigated as part of the present work. Poiseuille model can be used to estimate the velocity distribution and thus pressure variation along the heat pipe. The velocity variation and pressure drop in the vapour core are calculated by using Poiseuille theory, while the pressure drop in the liquid wick region is calculated by employing the Darcy's equation. Vapour flow in the

vapour channel of the heat pipe and flow of liquid through the porous wick are analysed numerically in detail using common interfacial conditions. The two dimensional governing equations are solved using stream function-vorticity approach by employing ADI finite difference scheme. The stream lines, velocity vector plots, velocity distribution, velocity profile, temperature distribution and pressure variation in the domains are obtained. Some of the results obtained by these three different methods and that available from the previous literature are compared. The original idea for determining the vapour pressure drop and temperature characteristics was emanated from the work published by van Ooijen (1981). The temperature distribution and pressure profiles were plotted both experimentally and theoretically by van Ooijen (1981). The average adiabatic temperature measured by him was around 15°C. In the present work the average adiabatic temperature obtained was more than 40°C. The temperature distribution and pressure profiles from the present work and that of van Ooijen are compared in the following sections.

6.5.1. Temperature Distribution

The temperature distribution in stainless steel flat heat pipe with water as working fluid obtained by van Ooijen (1981) and that from the present study are shown in Fig.6.55. It should be noted that the magnitude of the temperature in the heat pipe used for the present anlysis is high. Fig.6.56 shows the comparison of temperature distribution obtained from numerical and experimental results. The surface temperature at the evaporator of the heat pipe is for two Re values (Re corresponding to two heat flux values). Eventhough the container material is stainless steel there will be axial heat conduction along the heat pipe wall. This causes the

condenser temperature also to increase. Hence, effectively there is an increase in the whole surface temperature of the heat pipe. However, except for very low heat flux values the temperature at every zone remains uniform in the present experiments. This observation has similarity with that reported by van Ooijen (1981) as shown in Fig.6.55.

The temperature distribution will not be uniform in the heat pipe when highly conducting materials like copper, aluminium, etc. are used. Sobhan *et al.* (1997) numerically obtained the temperature variation along the heat pipe including axial heat conduction and the effect of porosity of the wick structure. In the present work the temperature distribution with aluminium as the container material is obtained. It is observed that there exists a continuous temperature gradient from the evaporator end to the condenser end which causes significant axial heat conduction.

The temperature distribution obtained in the present case is similar to that reported by Sobhan *et al.* (1997, 2000). The variation of temperature shown in Fig.6.55 is for stainless steel flat heat pipe. Since stainless steel has low thermal conductivity, negligible temperature gradient exists along the heat pipe. Therefore, temperature is uniform at the respective zones of the stainless steel flat heat pipe. But it is observed that as the porosity of the wick decreases, the temperature of the wick increases. Though the temperature profiles obtained are somewhat different from that obtained by Sobhan *et al.*, the above trend is repeated for the present case also.

6.5.2 Pressure Profiles

The pressure of vapour will be depending upon the corresponding temperature of the medium. The pressure variation along the vapour core is obtained in the present work by experimental method, Poiseuille theory and by numerical analysis. Fig. 6.57

shows a comparison between these pressure profiles corresponding to Re = 2.04 and Re = 5.26. In both the cases (Figs. 6.57a and 6.57b) the pressure drop estimated by Poiseuille method has the smallest magnitude. However, the experimental and numerical values are comparable in magnitude. It is inferred that the Poiseuille method is too large an approximation to estimate the pressure drop in the flow of the working medium in the heat pipe. Hence for a better design of heat pipes (especially in the case of flat heat pipes which carry large heat capacities) vapour pressure drop should be taken into account and numerical method is suggested. While incorporating the pressure drop in the vapour core, the maximum heat transport capability of the stainless steel flat heat pipe used in the present work, reduces to about two third of the value obtained without vapour pressure drop.

6.6 Summary

The most important section of this report is the presentation of results and the corresponding explanations. The present research contains three different divisions. In each part, the various performance characteristics of the flat heat pipe are analysed using a different method. The characteristics obtained by these different methods are discussed in detail. In addition, some of the characteristics determined by the different methods are compiled and compared. The comparison infers that the vapour pressure drop in the vapour should be considered for designing the heat pipe. It also leads to the conclusion that there is effect of fluid quantity on the heat pipe performance. Moreover, the performance is influenced by the porosity of the wick structure and the thermal conductivity of the heat pipe container material. The derived inferences are detailed in the next concluding section of this thesis.

Table 6.1 Stainless Steel-Water Heat Pipe (∀: 28cc)

No.	q, W	Re_v	Re_l	T_e, °C	T_c, °C	ko	Δq,W
1	47	0.91	0.009	53.72	33.55	265	2.51
2	70	1.35	0.013	57.74	33.19	318	2.57
3	107	2.06	0.021	59.53	33.19	451	3.51
4	132	2.54	0.025	61.83	33.91	517	1.84
5	205	3.95	0.039	68.28	35.00	666	2.26
6	270	5.20	0.052	88.23	36.10	622	3.15

Table 6.2 Stainless Steel-Water Heat Pipe (∀: 34cc)

1	51	0.89	0.009	53.9	31.92	263	2.93
2	79	1.52	0.015	52.34	33.67	457	1.90
3	106	2.04	0.020	56.34	32.15	491	3.32
4	148	2.85	0.029	59.18	33.14	621	3.45
5	207	3.99	0.040	66.98	35.19	700	1.98
6	273	5.26	0.053	82.98	35.65	619	2.75

Table 6.3 Stainless Steel-Water Heat Pipe (∀: 40cc)

1	41	0.79	0.008	56.71	32.11	191	2.62
2	95	1.83	0.018	58.42	32.78	409	2.97
3	112	2.16	0.022	61.65	33.28	434	3.24
4	145	2.79	0.028	62.97	33.28	533	3.32
5	202	3.89	0.039	67.50	34.75	663	2.05
6	274	5.28	0.053	83.30	35.23	614	2.75

Table 6.4 Stainless Steel-Acetone Flat Heat Pipe (∀: 28cc)

1	46	4.91	0.098	55.40	32.06	229	2.74
2	61	6.52	0.13	58.50	32.83	288	3.0
3	70	7.48	0.15	61.30	32.96	279	3.12
4	98	10.47	0.208	68.38	33.42	298	3.63

Table 6.5 Stainless Steel-Acetone Flat Heat Pipe (∀: 34cc)

1	47	5.02	0.10	53.58	33.04	255	1.74
2	58	6.20	0.124	57.45	33.22	265	2.54
3	71	7.59	0.152	61.41	33.00	278	3.47
4	95	10.15	0.202	66.36	33.44	307	3.48

Table 6.6 Stainless Steel-Acetone Flat Heat Pipe (∀: 40cc)

1	47	5.02	0.10	56.44	31.70	217	2.89
2	59	6.30	0.126	59.62	31.52	240	3.31
3	68	7.26	0.144	62.90	32.11	254	3.66
4	100	10.68	0.212	67.28	33.93	319	3.37

Table 6.7 Aluminium-Acetone Heat Pipe–Wire Screen Wick, MN100 (∀: 16cc)

Sl. No.	q, W	Re_v	Re_l	T_e, °C	T_c, °C	Δq, W
1	5	2.14	0.004	54.73	38.62	15
2	17	7.27	0.012	61.05	44.65	13
3	22	9.40	0.016	69.56	47.2	18

Table 6.8 Aluminium-Acetone Heat Pipe–Wire Screen Wick, MN100 (∀: 21cc)

1	10	4.27	0.007	44.19	32.53	10
2	16	6.84	0.001	52.55	36.39	14
3	22	9.40	0.016	62.56	41.41	18

Table 6.9 Aluminium-Acetone Heat Pipe–Wire Screen Wick, MN100 (∀: 26cc)

1	7	2.99	0.005	45.17	29.21	13
2	12	5.13	0.008	51.57	29.74	18
3	18	7.69	0.013	56.54	29.32	22
4	23	9.83	0.016	63.45	30.44	27

Table 6.10 Aluminium-Acetone Heat Pipe–Wire Screen Wick, MN100 (∀: 31cc)

1	10	4.70	0.007	45.55	33.28	10
2	17	7.27	0.012	53.38	37.49	13
3	22	9.40	0.016	60.6	39.68	18

Table 6.11 Aluminium -Acetone Flat Heat Pipe–Wire Screen , MN200 (∀: 16cc)

1	3	1.28	0.002	53.90	37.41	17
2	10	4.27	0.007	65.95	42.31	20

Table 6.12 Aluminium -Acetone Flat Heat Pipe–Wire Screen, MN200 (∀: 21cc)

1	8	3.42	0.006	47.20	33.35	12
2	10	4.27	0.007	58.04	35.61	20

Table 6.13 Aluminium -Acetone Flat Heat Pipe–Wire Screen, MN200 (∀: 26cc)

1	4	1.71	0.0030	49.54	35.16	16
2	12	5.13	0.0092	54.35	37.96	18

Table 6.14 Aluminium-Acetone Flat Heat Pipe–Wire Screen , MN300 (∀: 16cc)

1	4	1.71	0.0032	57.36	38.40	16

Table 6.15 Aluminium-Acetone Flat Heat Pipe–Wire Screen, MN300(∀: 21cc)

1	4	1.71	0.0032	56.84	37.80	16
2	7	2.99	0.0057	74.60	45.78	23

Table 6.16 Aluminium-Acetone Flat Heat Pipe–Wire Screen , MN300(∀: 26cc)

1	5	2.14	0.0042	53.45	37.12	15

Table 6.17 Aluminium-Acetone Flat Heat Pipe, Axial Grooves(∀: 12cc)

1	20	7.89	0.0426	63.25	34.00
2	31	12.23	0.066	68.07	34.75
3	39	15.38	0.084	82.58	35.42

Table 6.18 Aluminium-Acetone Flat Heat Pipe, Axial Grooves (∀: 17cc)

1	26	10.26	0.0554	63.24	32.00
2	36	14.20	0.0766	73.31	34.74
3	42	16.57	0.894	80.98	35.18

Table 6.19 Aluminium-Acetone Flat Heat Pipe, Axial Grooves (∀: 22cc)

1	26	10.26	0.0554	62.83	32.39
2	32	12.62	0.068	76.77	35.35
3	38	14.99	0.0808	84.77	36.53

Table 6.20 Composite Wick (∀: 13cc)

1	25	9.86	0.0532	64.52	33.99
2	32	12.62	0.068	76.34	35.54
3	40	15.77	0.085	83.24	36.77

Table 6.21 Composite Wick (∀: 18cc)

1	20	7.89	0.0426	55.34	35.99
2	30	11.83	0.0638	66.36	37.17
3	38	14.99	0.0808	76.57	38.53

Table 6.22 Composite Wick (∀: 23cc)

1	17	6.71	0.0362	58.99	35.75
2	27	10.65	0.0574	65.65	37.09
3	36	14.20	0.0766	83.15	39.26

Table 6.23 Screen Wick, MN100 (∀: 33cc)

1	23	9.07	0.033	61.04	33.15
2	35	13.81	0.0496	70.37	35.02
3	48	18.93	0.0681	78.15	36.37

Table 6.24 Screen Wick, MN100(∀: 38cc)

1	26	10.26	0.036	60.50	33.41
2	33	13.02	0.0468	69.28	34.95
3	45	17.75	0.0639	74.88	36.16

Table 6.25 Screen Wick, MN100 (∀: 43cc)

1	24	9.47	0.034	60.48	33.43
2	33	13.02	0.0468	69.81	34.93
3	44	17.36	0.0624	83.90	36.83

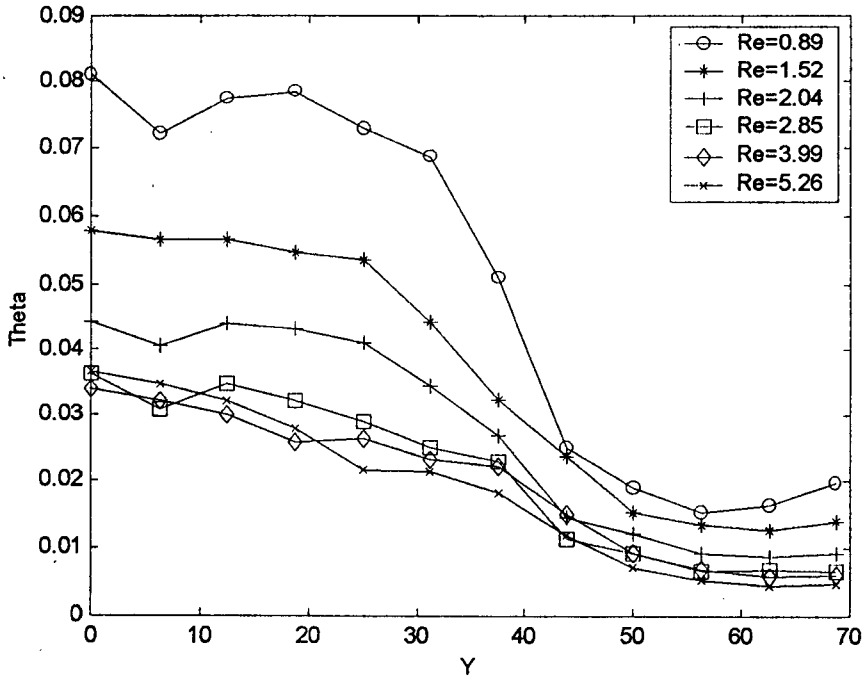

(a) Along Top Wall

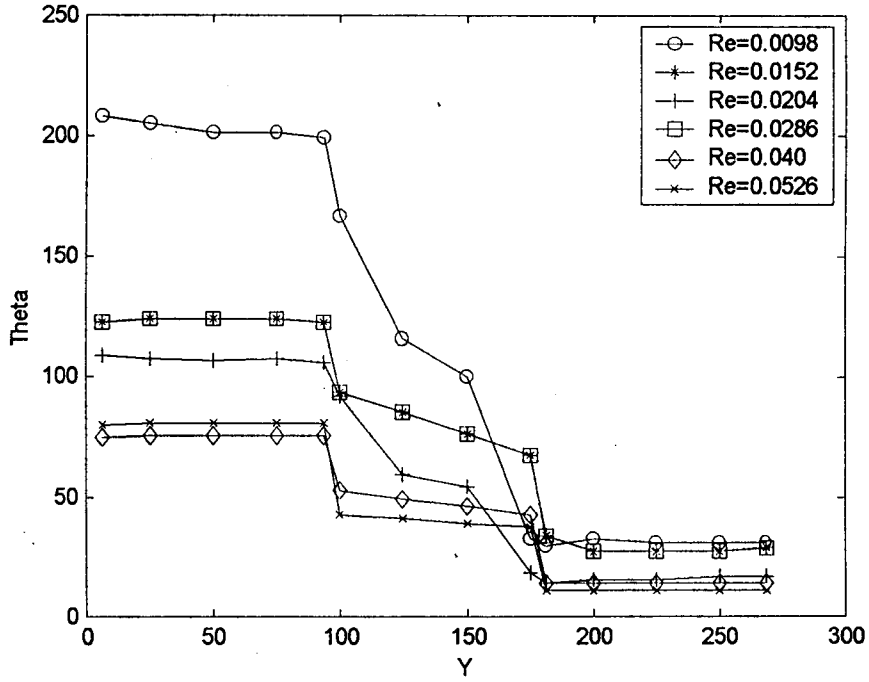

(b) Along Bottom Wall

Fig. 6.1 Temperature Distribution in Stainless Steel-Water Heat Pipe
(∀ : 34cc)

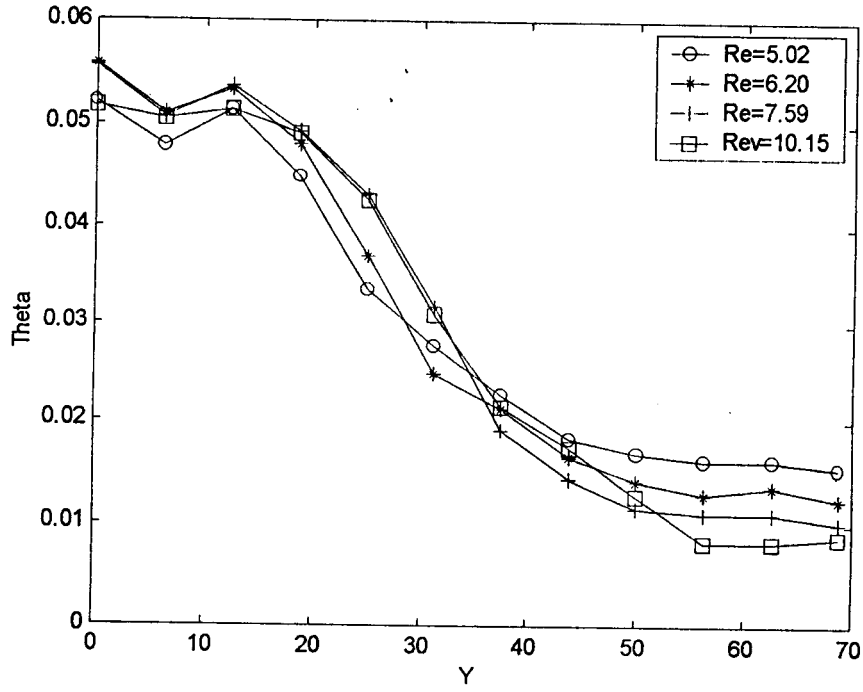

(a) Along Top Wall

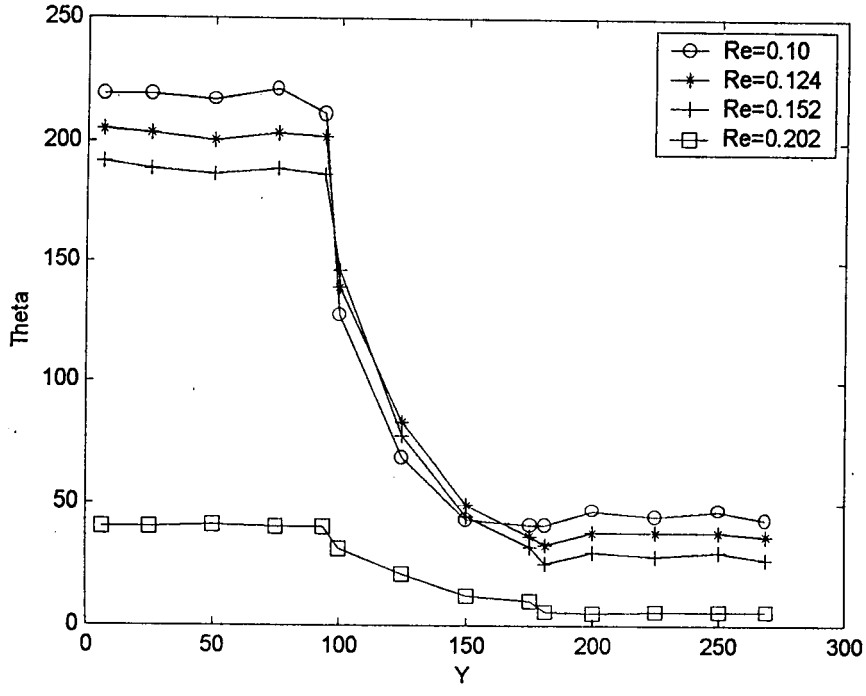

(b) Along Bottom Wall

Fig. 6.2 Temperature Distribution in Stainless Steel-Acetone Heat Pipe
($\forall$: 34cc)

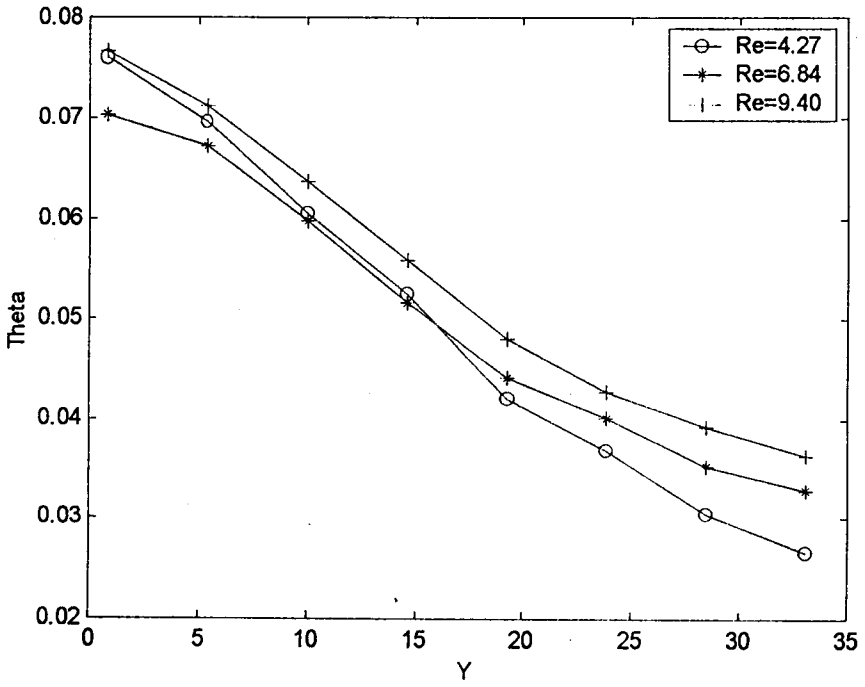

(a) Along Top Wall

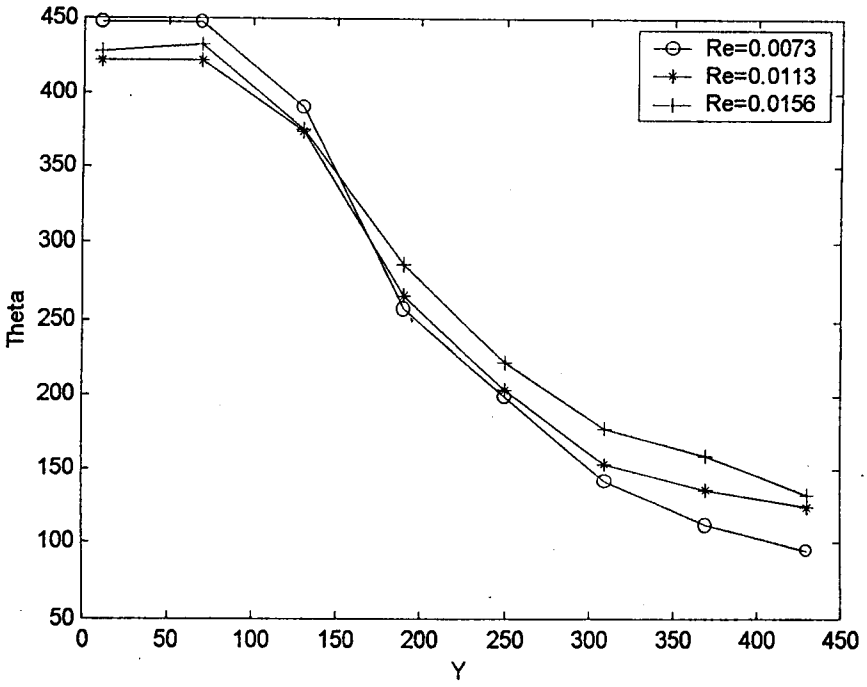

(b) Along Bottom Wall

Fig. 6.3 Temperature Distribution in Aluminium-Acetone Heat Pipe With Wire Screen ($\forall$: 21cc, ε=0.75)

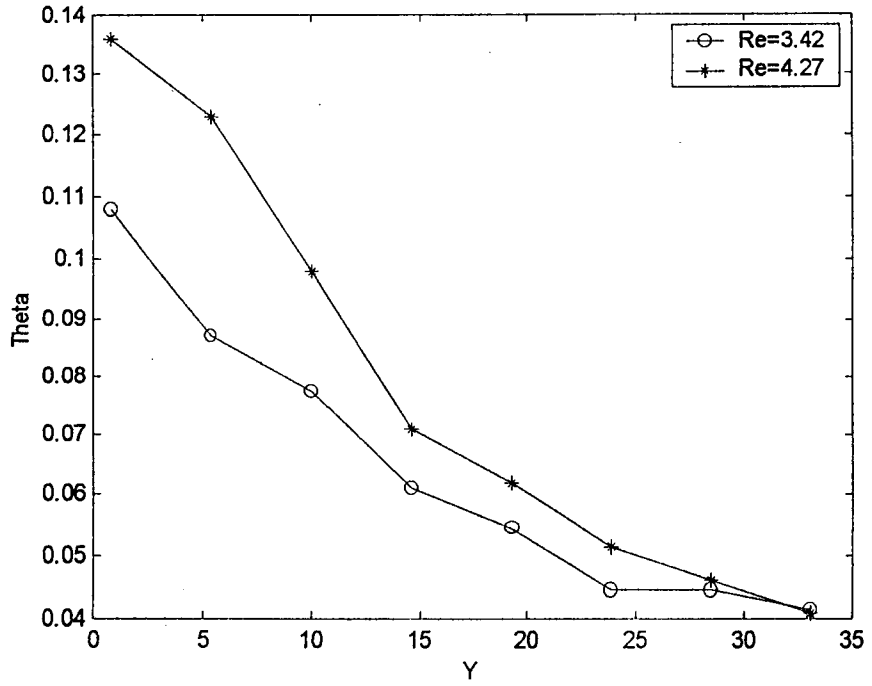

(b) Along Top Wall

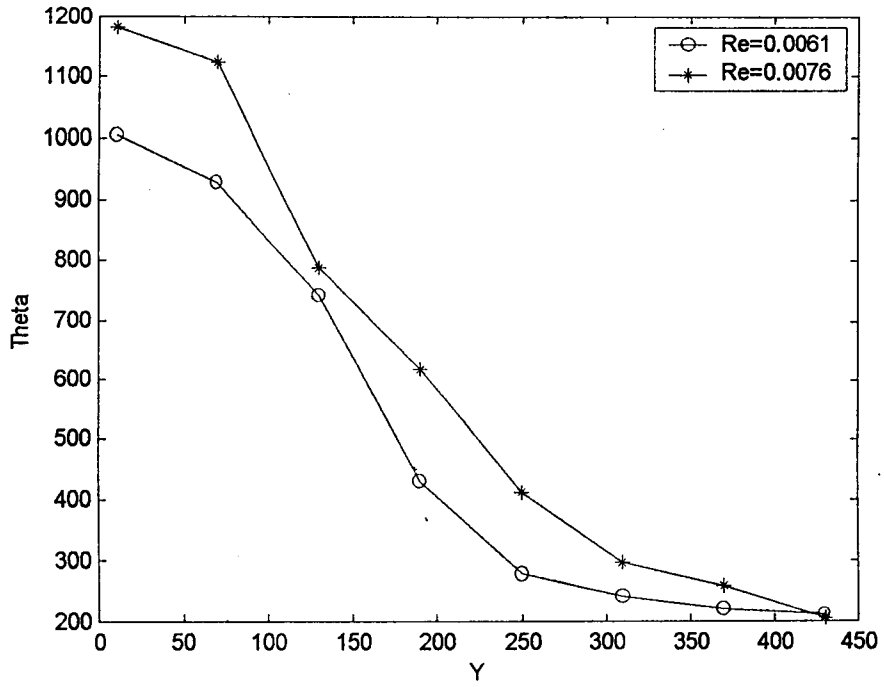

(b) Along Bottom Wall

Fig. 6.4 Temperature Distribution in Aluminium-Acetone Heat Pipe With Wire Screen ($\forall$:21cc, ε=0.70)

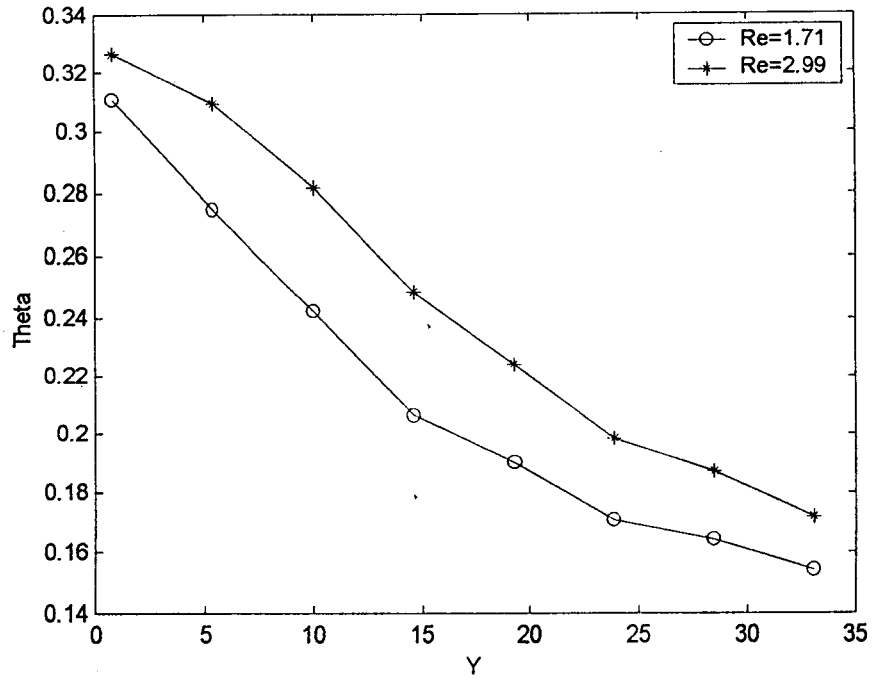

(b) Along Top Wall

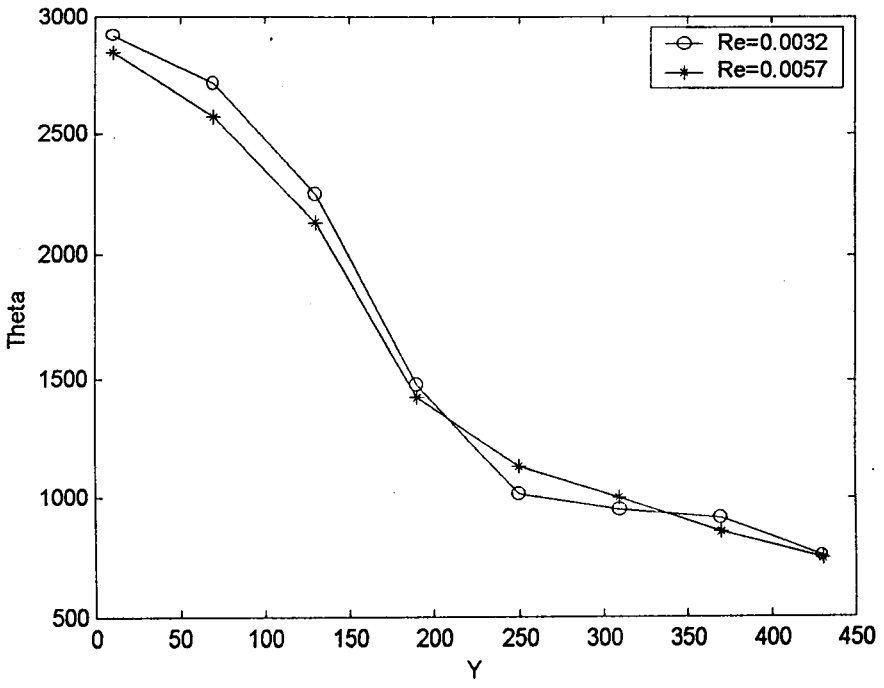

(b) Along Bottom Wall

Fig. 6.5 Temperature Distribution in Aluminium-Acetone Heat Pipe With Wire Screen ($\forall$: 21cc, ε=0.65)

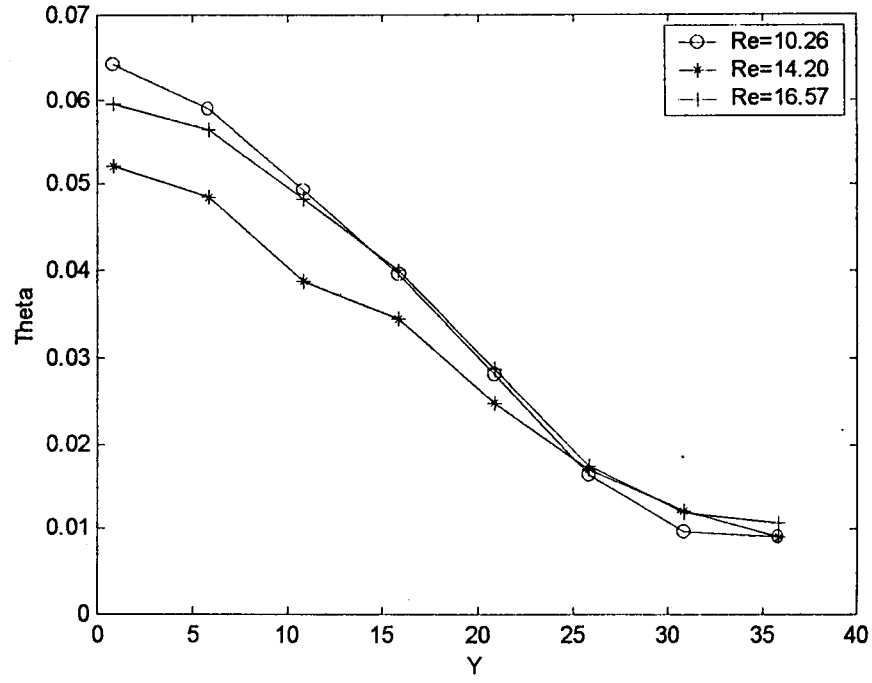

(b) Along Top Wall

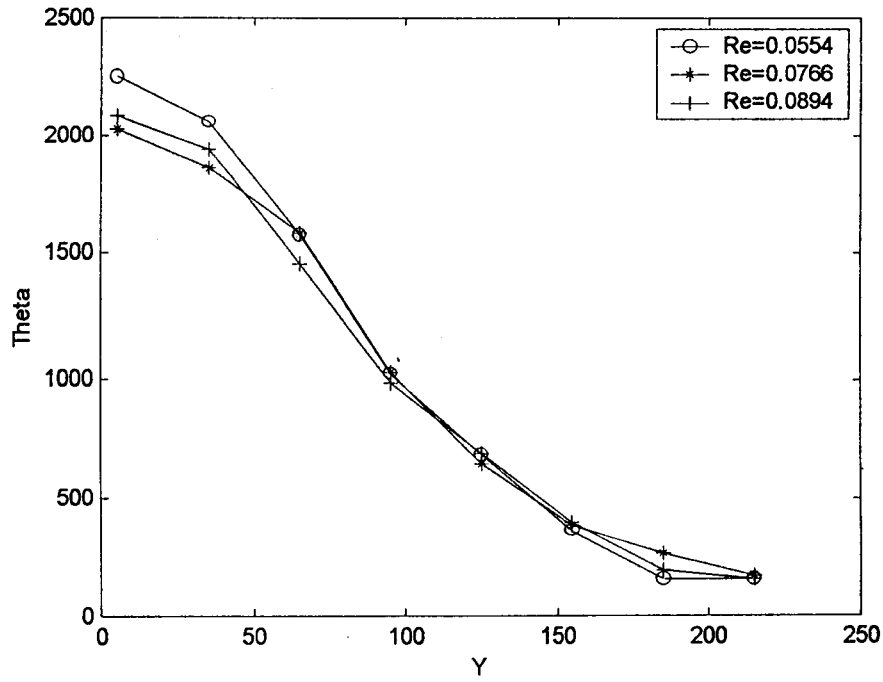

(b) Along Bottom Wall

Fig. 6.6 Temperature Distribution in Aluminium-Acetone Heat Pipe With Axial Grooves ($\forall$: 17cc, ε=0.50)

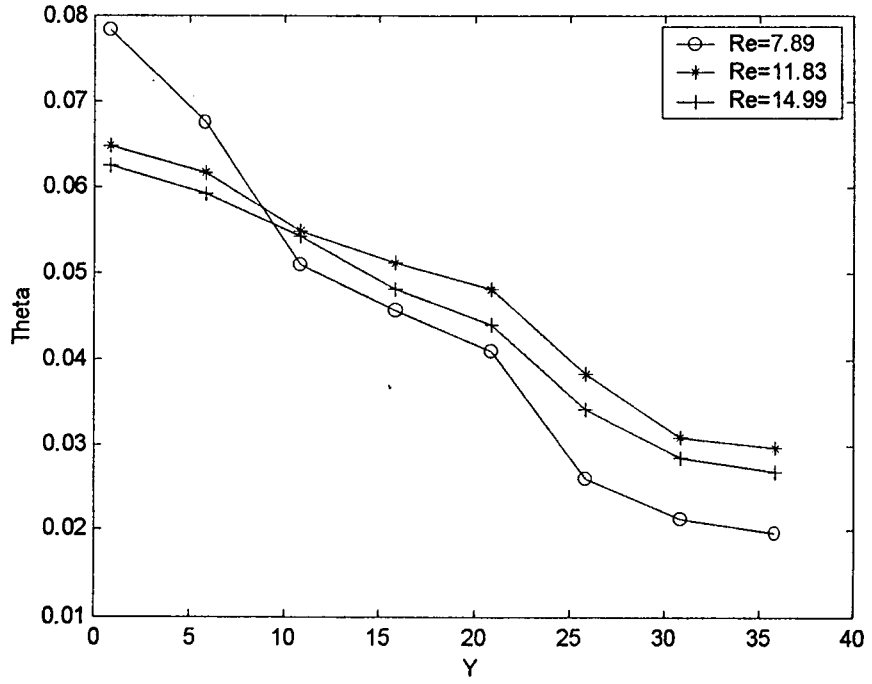

(b) Along Top Wall

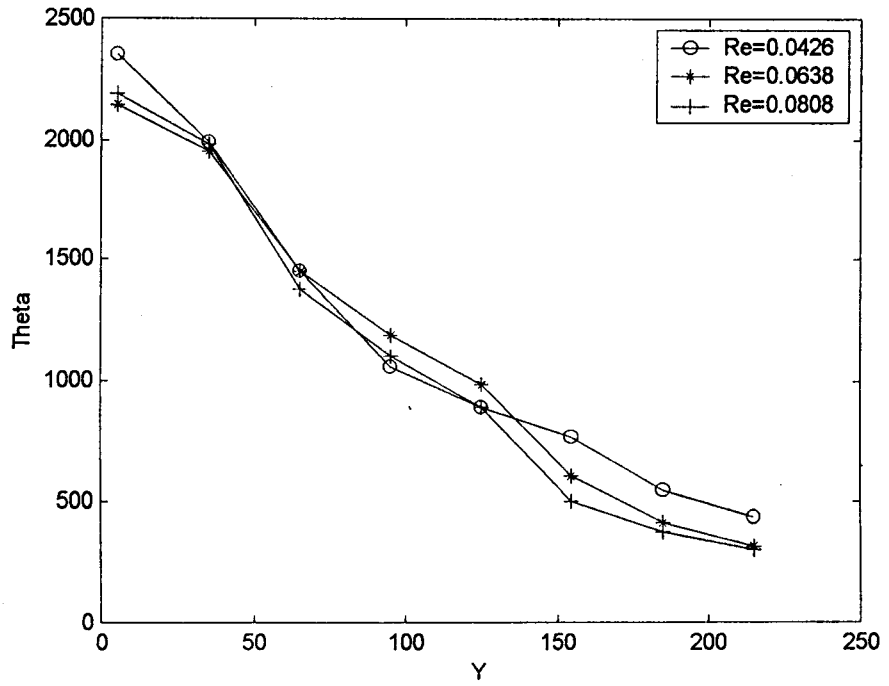

(b) Along Bottom Wall

Fig. 6.7 Temperature Distribution in Aluminium-Acetone Heat Pipe With CompositeWick ($\forall$: 18cc, ε=0.50)

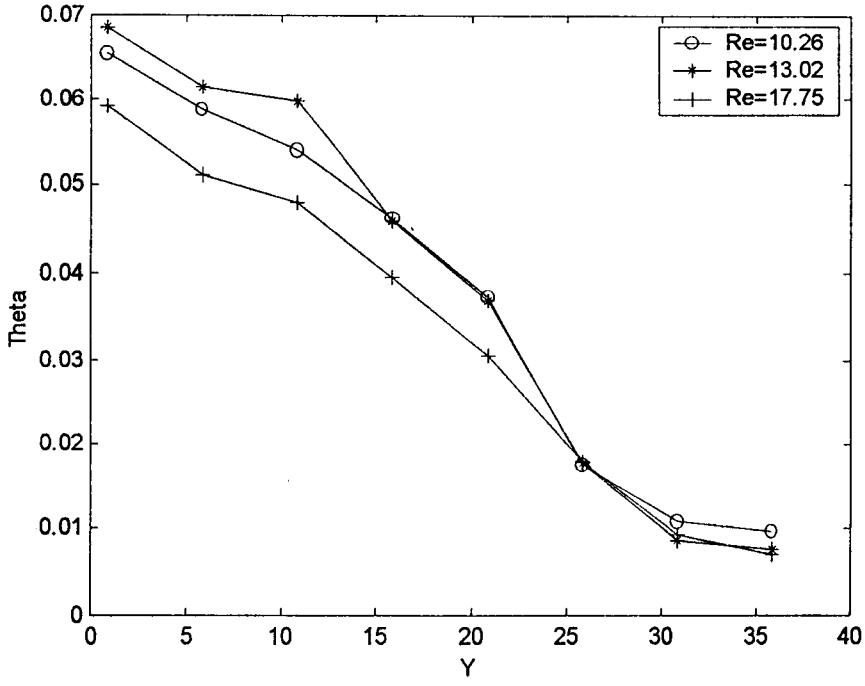

(b) Along Top Wall

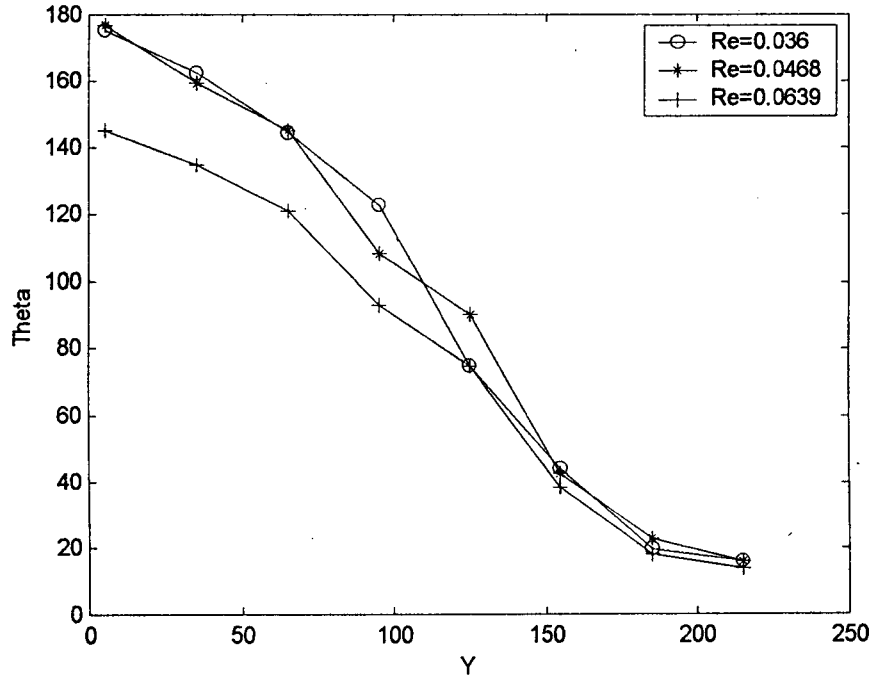

(b) Along Bottom Wall

Fig. 6.8 Temperature Distribution in Aluminium-Acetone Heat Pipe With Wire Screen ($\forall$: 38cc, ε=0.75)

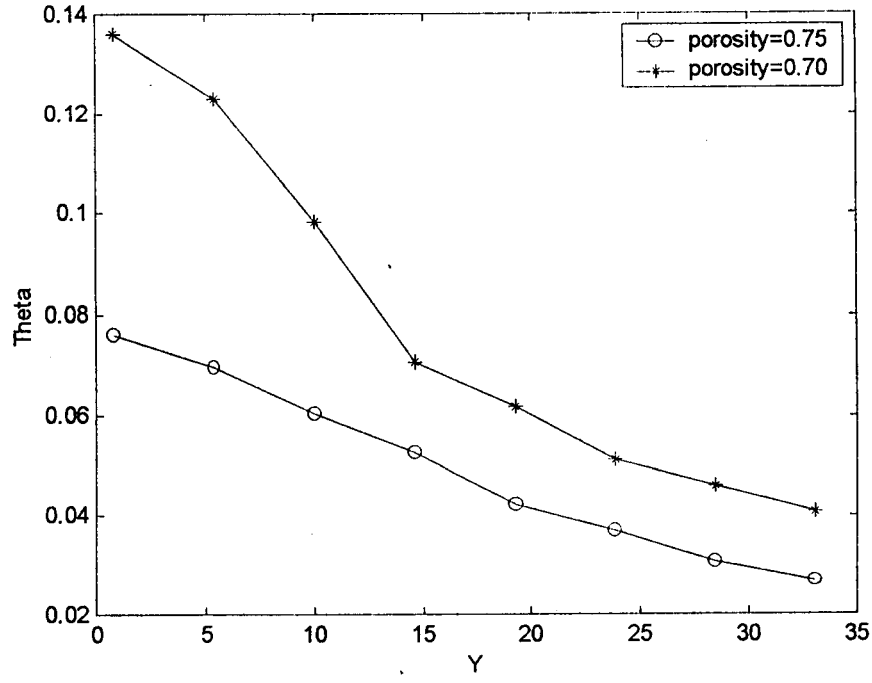

(a) Along Top Wall

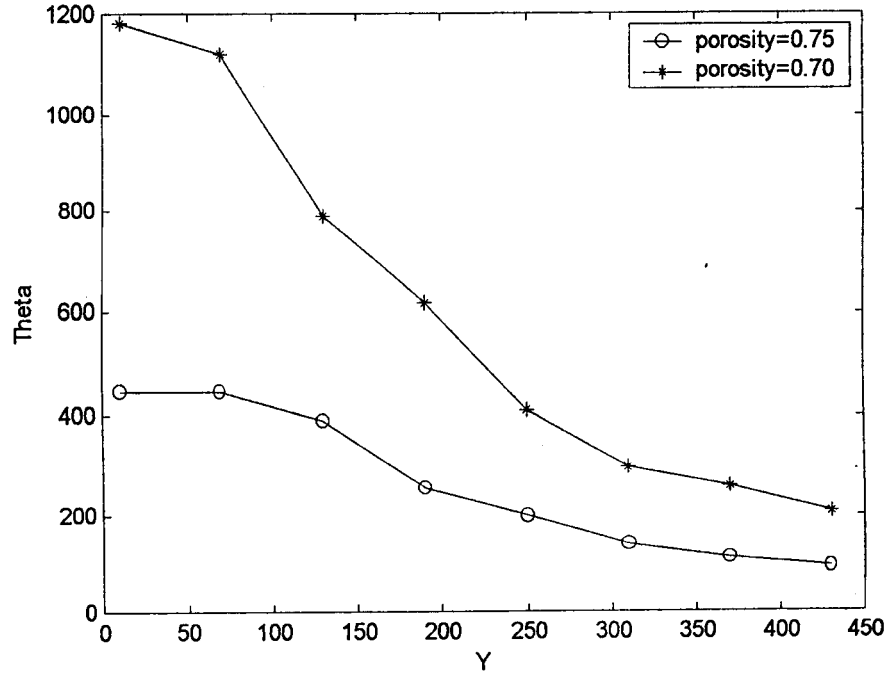

(b) Along Bottom Wall

Fig. 6.9 Comparison of Temperature Distribution at Various Porosities ($\varepsilon = 0.75$ and 0.70)

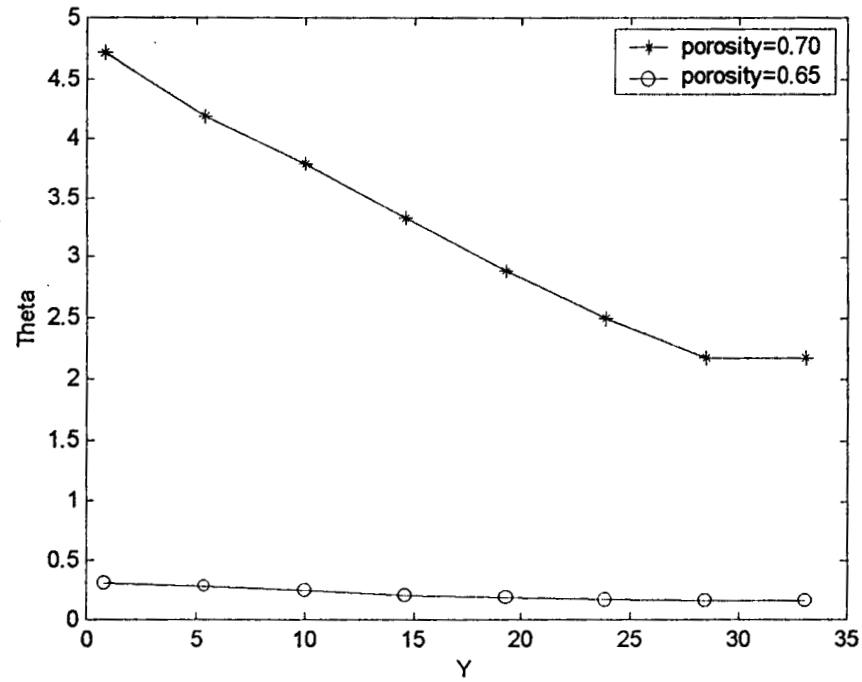

(a) Along Top Wall

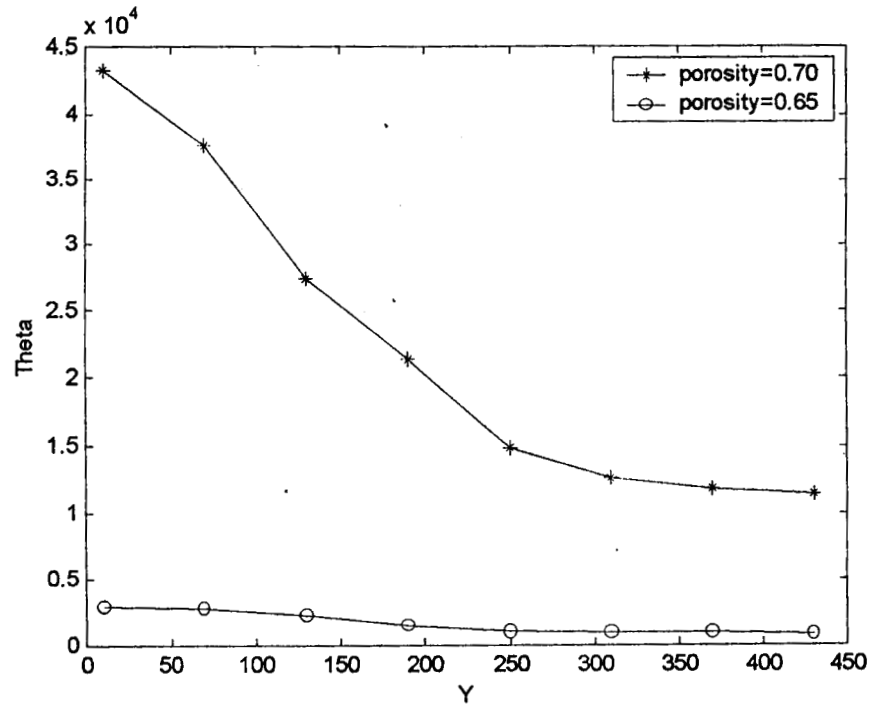

(b) Along Bottom Wall

Fig. 6.10 Comparison of Temperature Distribution at Various Porosities ($\varepsilon = 0.70$ and 0.65)

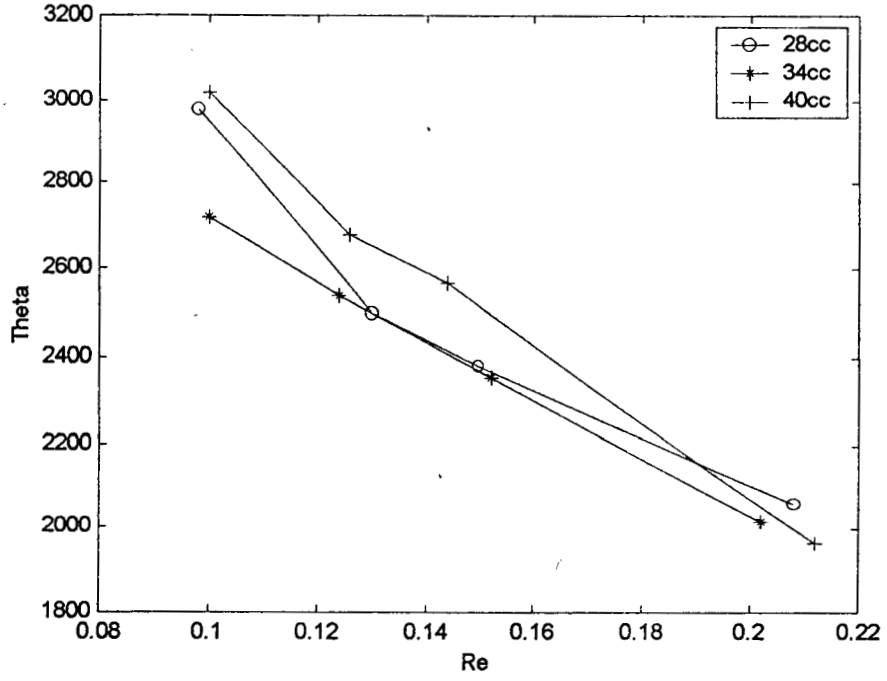

Fig. 6.11 Variation of Evaporator Temperature with Acetone as Working Fluid

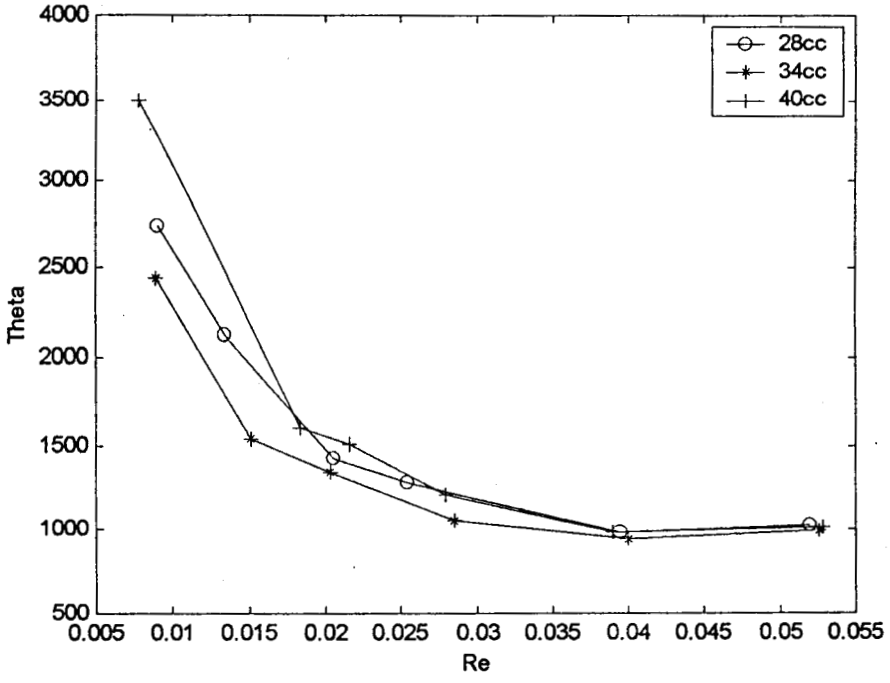

Fig. 6.12 Variation of Evaporator Temperature with Water as Working Fluid

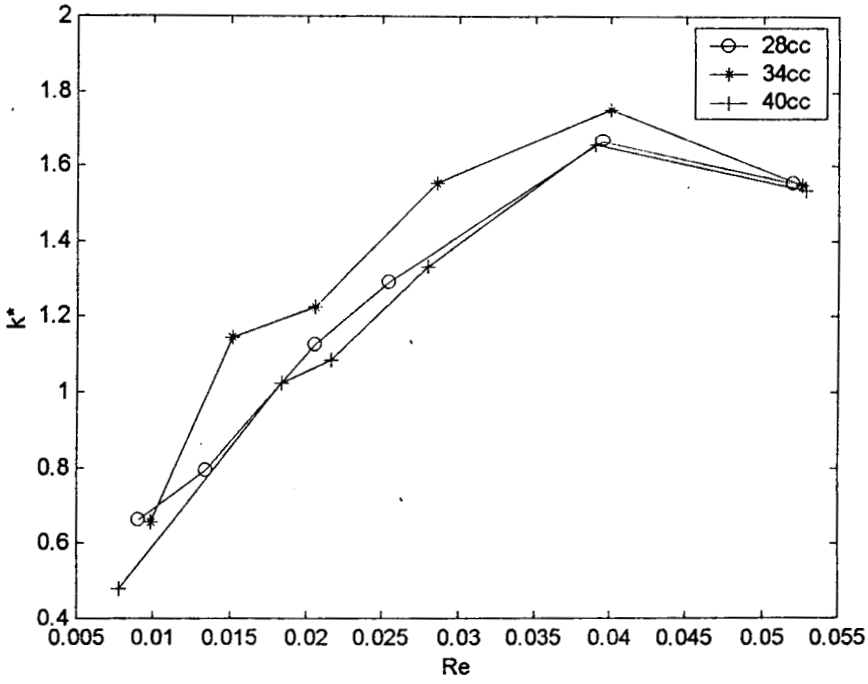

Fig. 6. 13 Variation of Effective Conductance at Different Charges

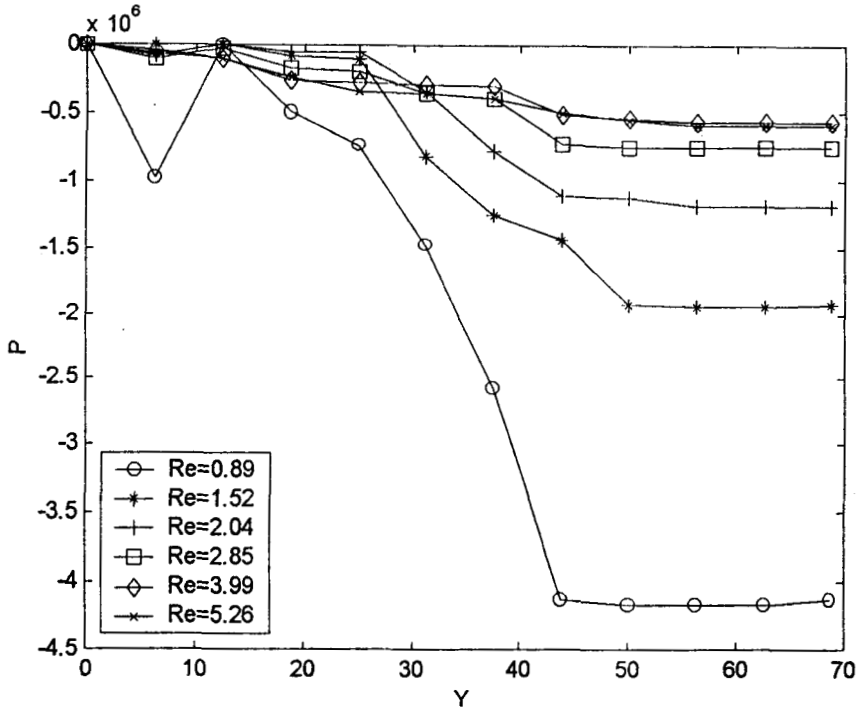

Fig. 6.14 (a) Vapour Pressure Profiles Obtained Using Clausius-Clapeyron Equation in Stainless Steel-Water Heat Pipe ($\forall$: 34cc)

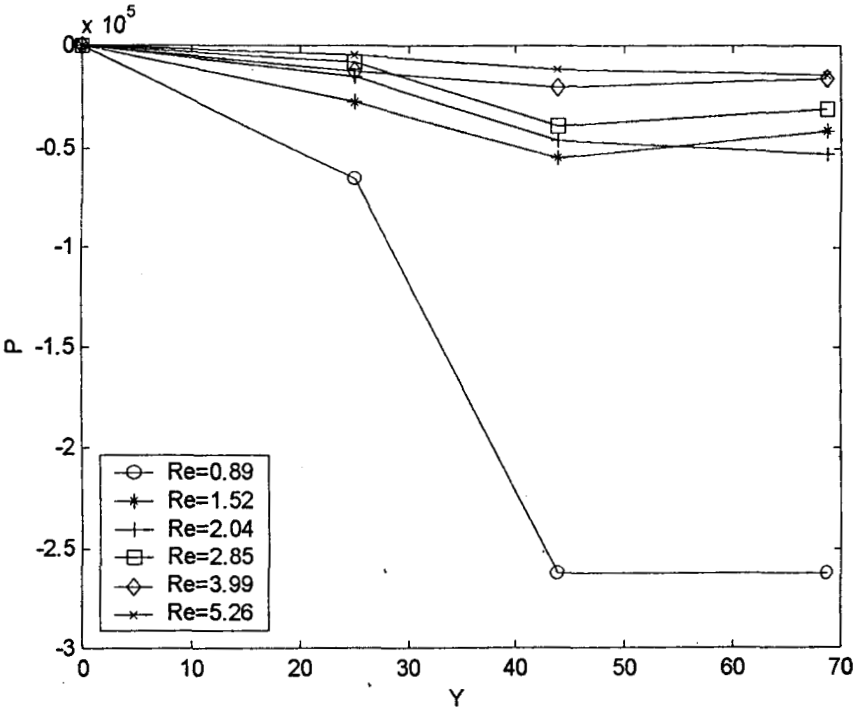

Fig. 6.14 (b) Experimental Vapour Pressure Profiles in Stainless Steel-Water Heat Pipe ($\forall$: 34cc)

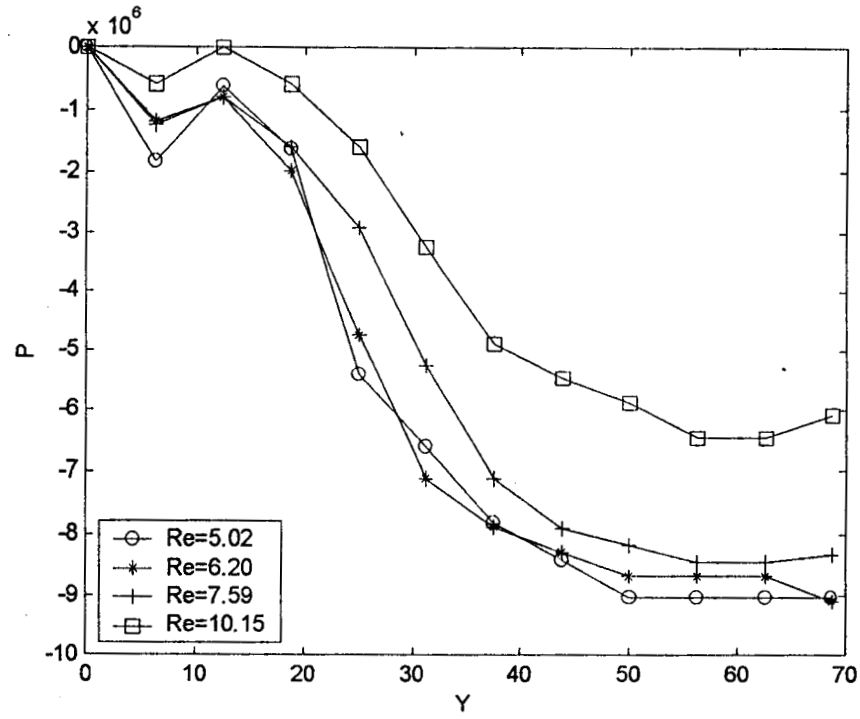

Fig. 6.15(a) Vapour Pressure Profiles Obtained Using Clausius-Clapeyron Equation in Stainless Steel-Acetone Heat Pipe ($\forall$: 34cc)

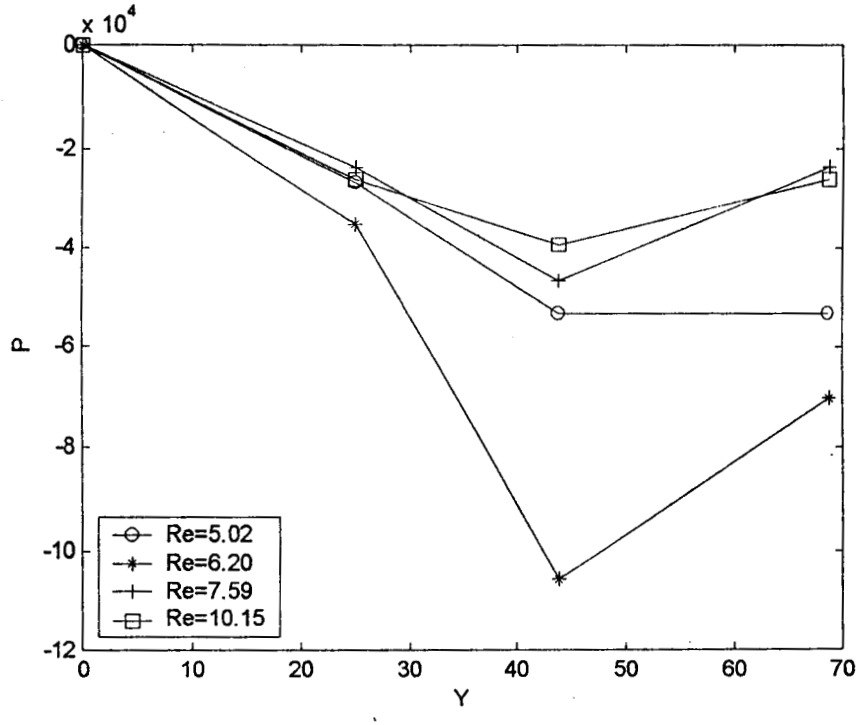

Fig. 6.15 (b) Experimental Vapour Pressure Profiles in Stainless Steel-Acetone Heat Pipe($\forall$: 34cc)

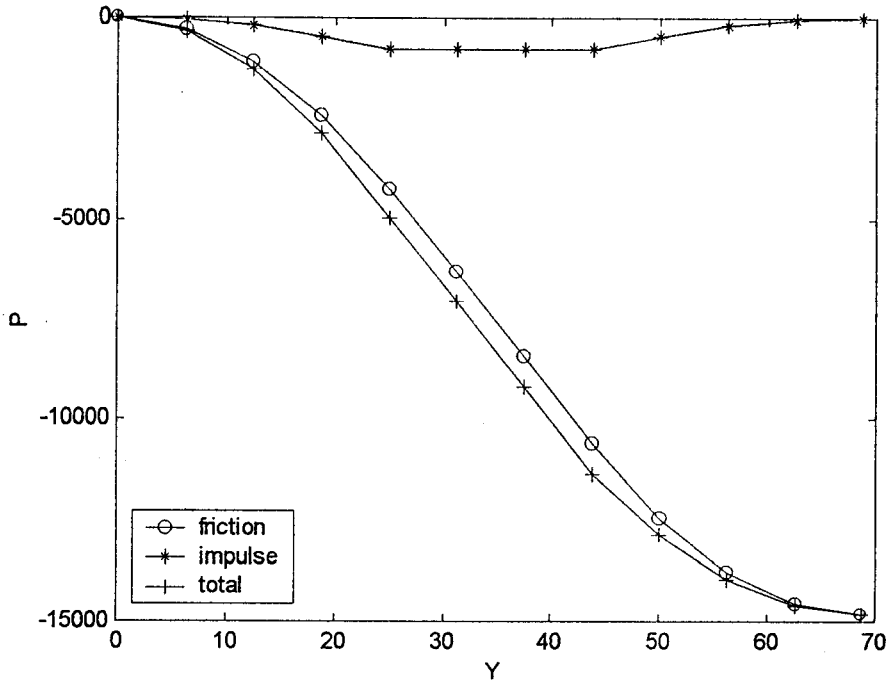

(a) Re=0.89

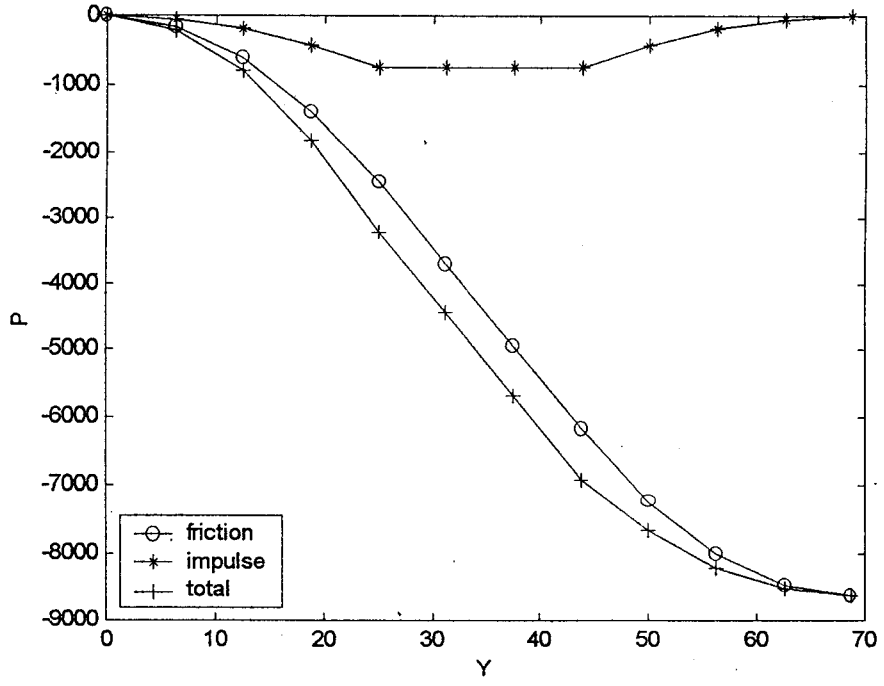

(b) Re=1.52

Fig. 6.16 Vapour Pressure Variation Along Stainless Steel-Water Flat Heat Pipe Obtained Using Poiseuille Model ($\forall$: 34cc)

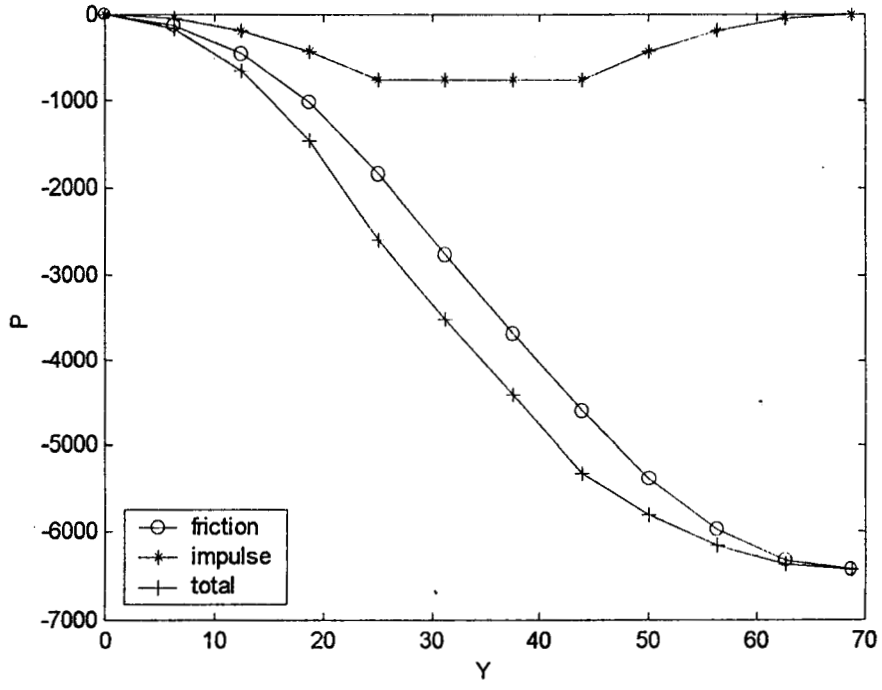

(c) Re=2.04

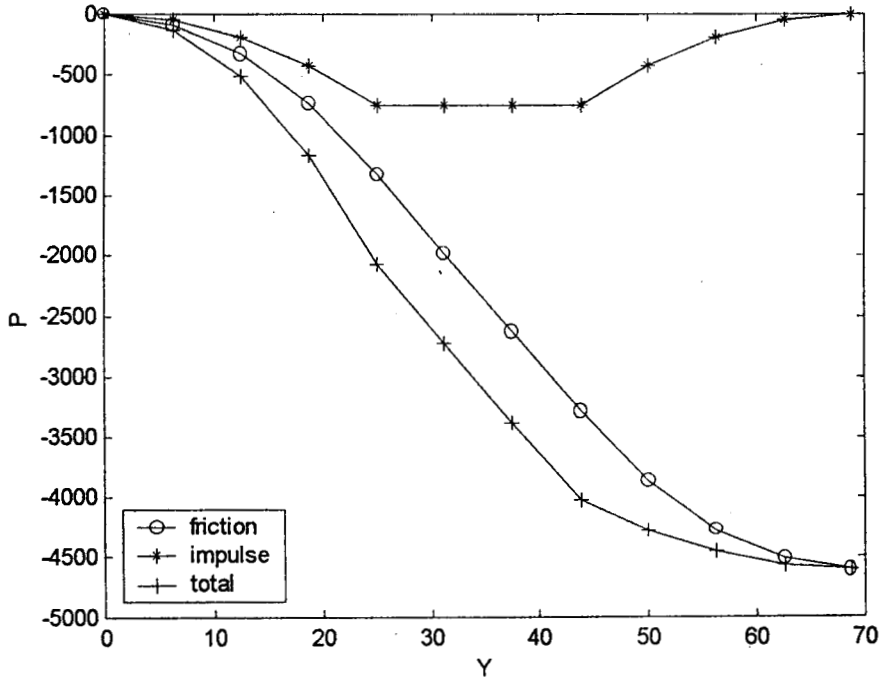

(d) Re=2.85

Fig. 6.16 Vapour Pressure Variation Along Stainless Steel-Water Flat Heat Pipe Obtained Using Poiseuille Model ($\forall$: 34cc)

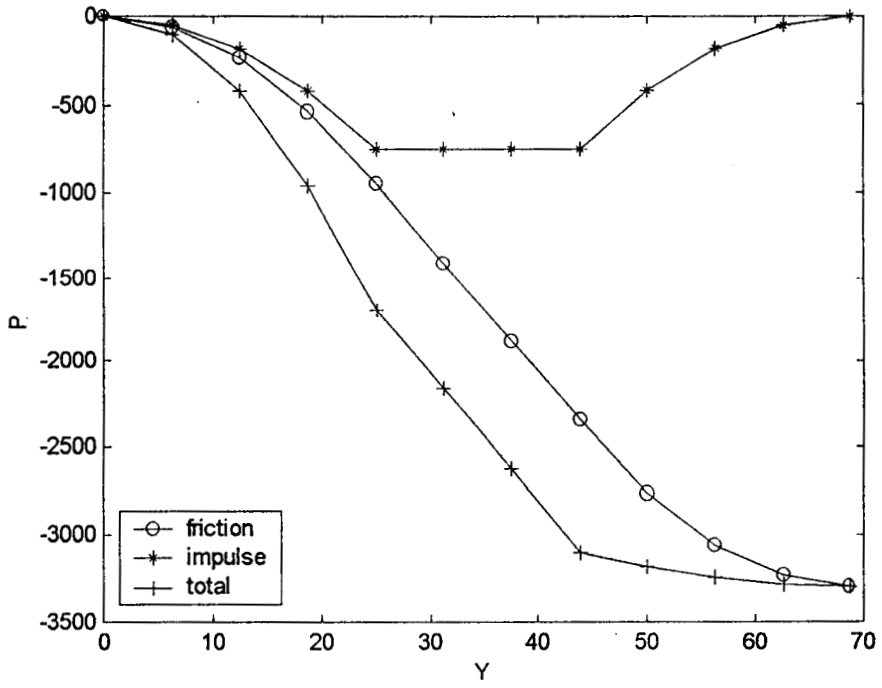

(e) Re=3.99

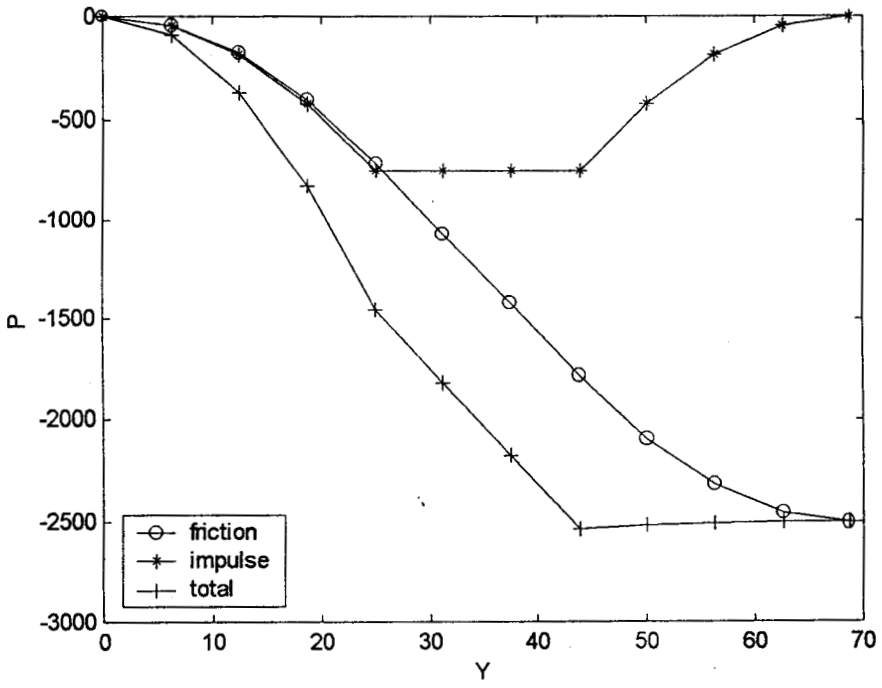

(f) Re=5.26

Fig. 6.16 Vapour Pressure Variation Along Stainless Steel-Water Flat Heat Pipe Obtained Using Poiseuille Model ($\forall$: 34cc)

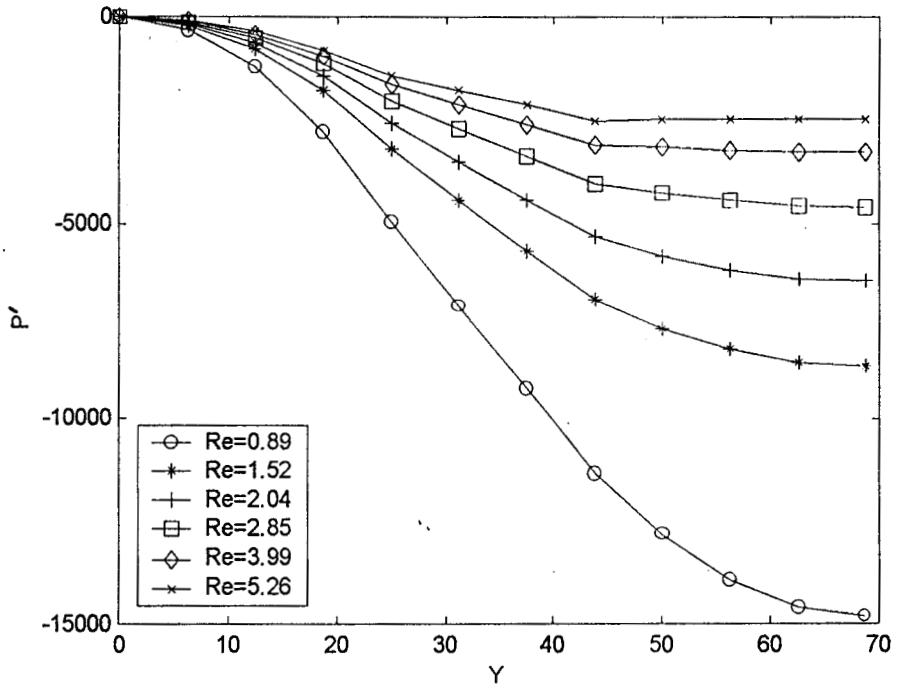

Fig. 6.17 Static Vapour Pressure Variation Along Stainless Steel-Water Flat Heat Pipe ($\forall$: 34cc)

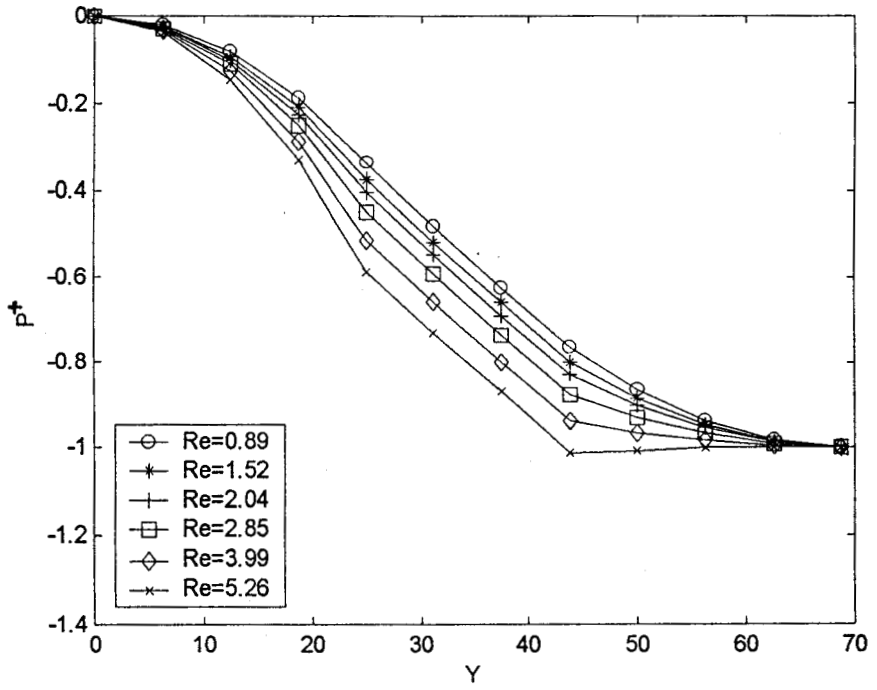

Fig. 6.18 Static Vapour Pressure Variation With Respect to Effective Pressure Drop Along Stainless Steel-Water Flat Heat Pipe ($\forall$: 34cc)

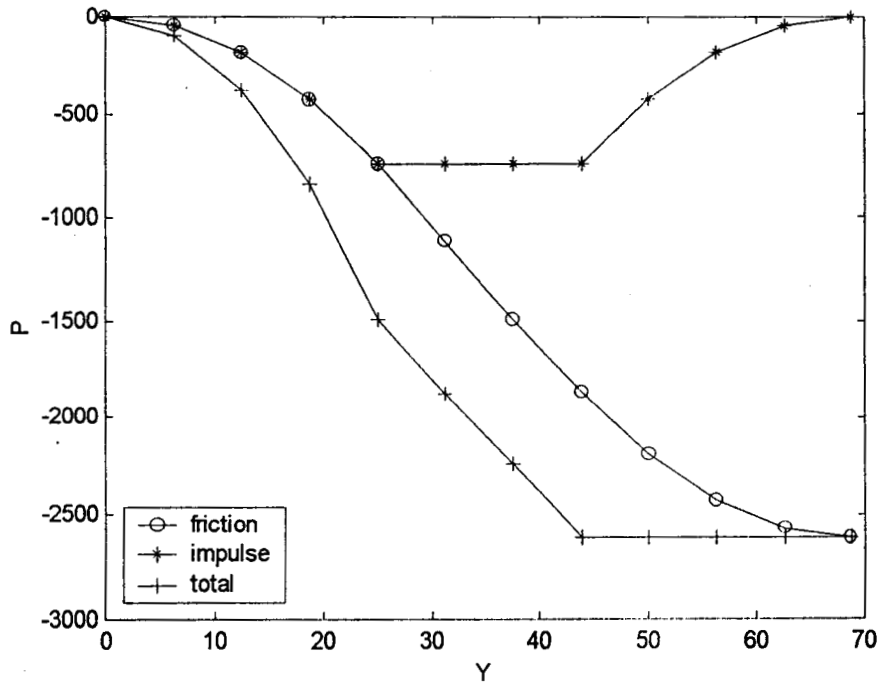

(a) Re=5.02

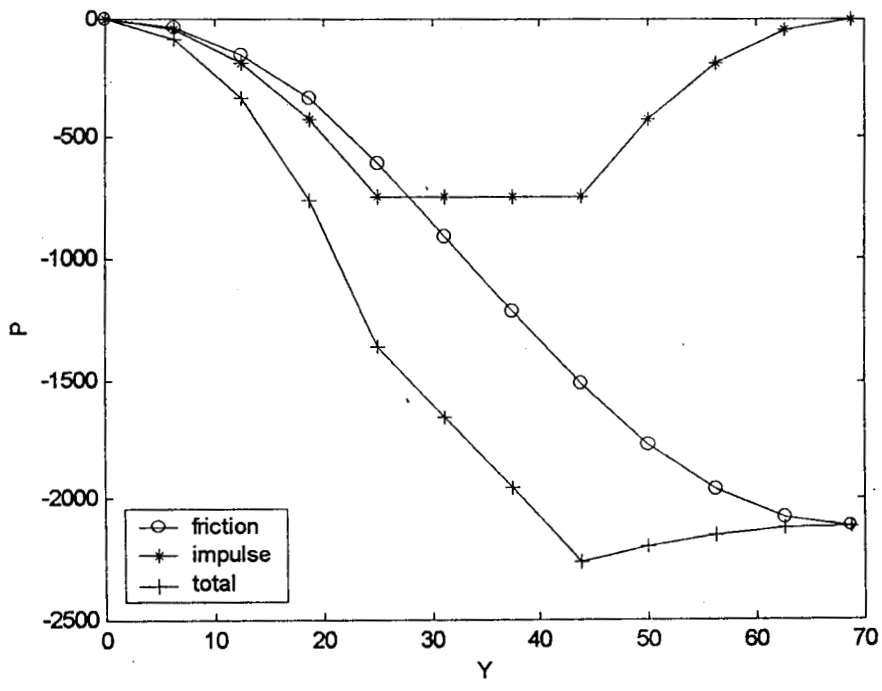

(b) Re=6.20

Fig. 6.19 Vapour Pressure Variation Along Stainless Steel-Acetone Flat Heat Pipe Obtained Using Poiseuille Model ($\forall$: 34cc)

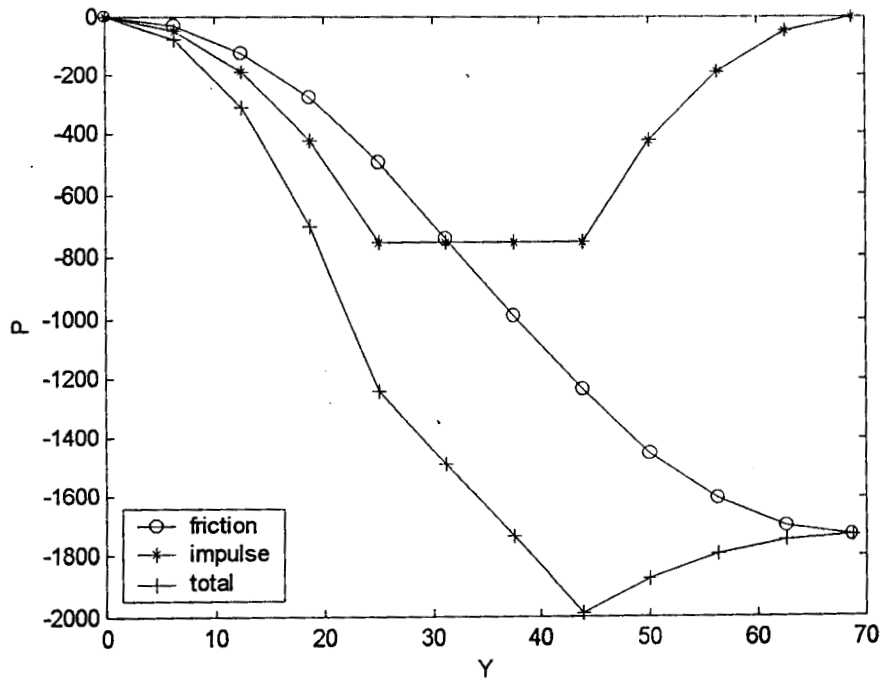

(c) Re=7.59

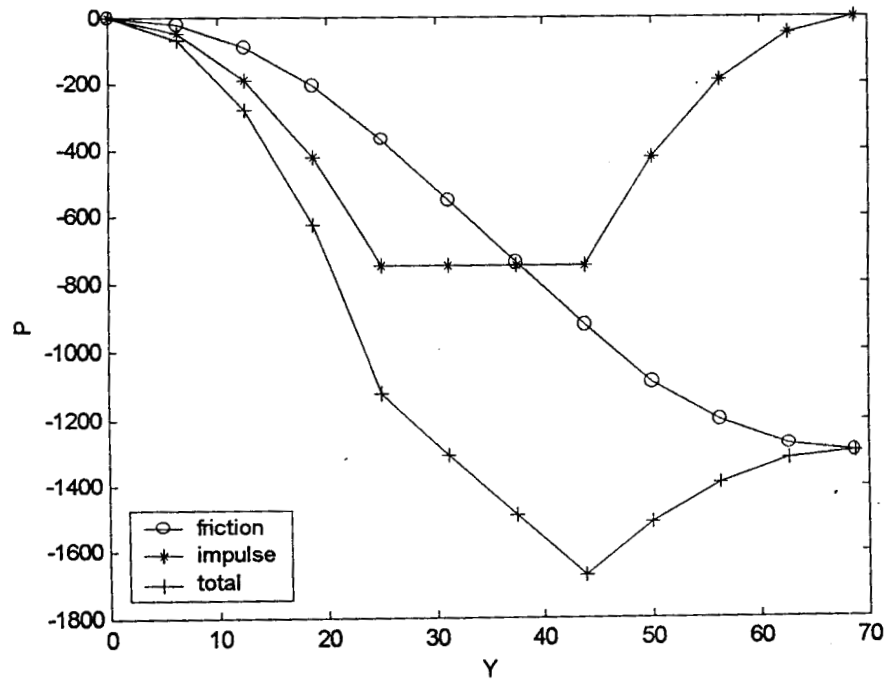

(d) Re=10.15

Fig. 6.19 Vapour Pressure Variation Along Stainless Steel-Acetone Flat Heat Pipe Obtained Using Poiseuille Model ($\forall$: 34cc)

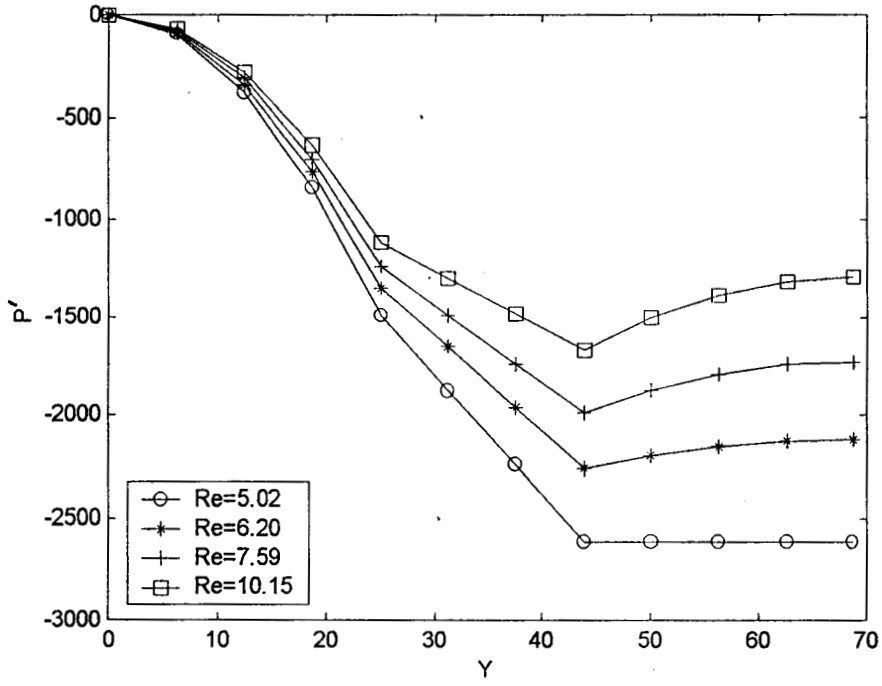

Fig 6.20 Static Vapour Pressure Variation Along Stainless Steel-Acetone Flat Heat Pipe ($\forall$: 34cc)

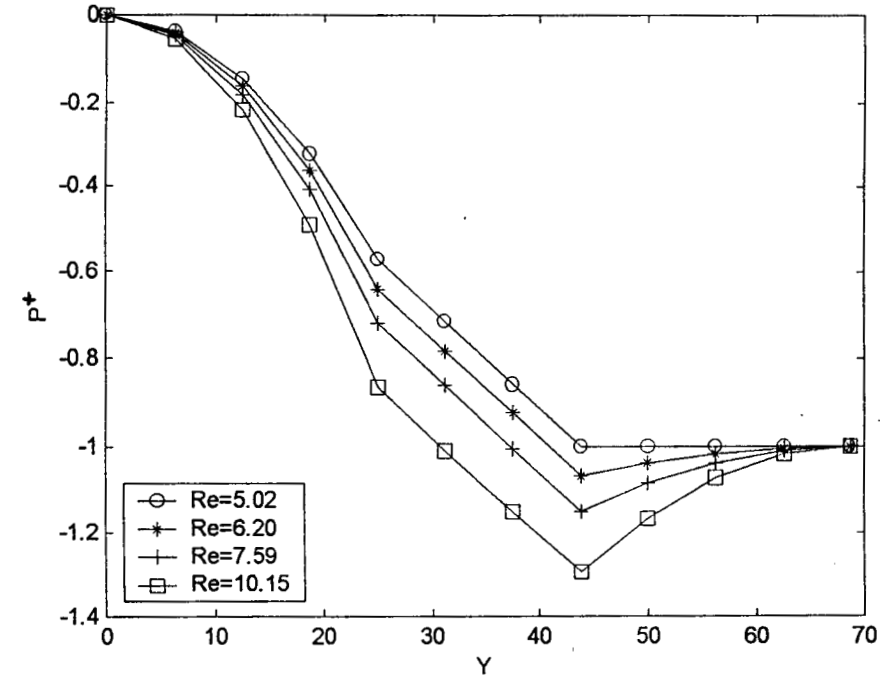

Fig. 6.21 Static Vapour Pressure Variation With Respect to Effective Pressure Drop Along Stainless Steel-Acetone Flat Heat Pipe ($\forall$: 34cc)

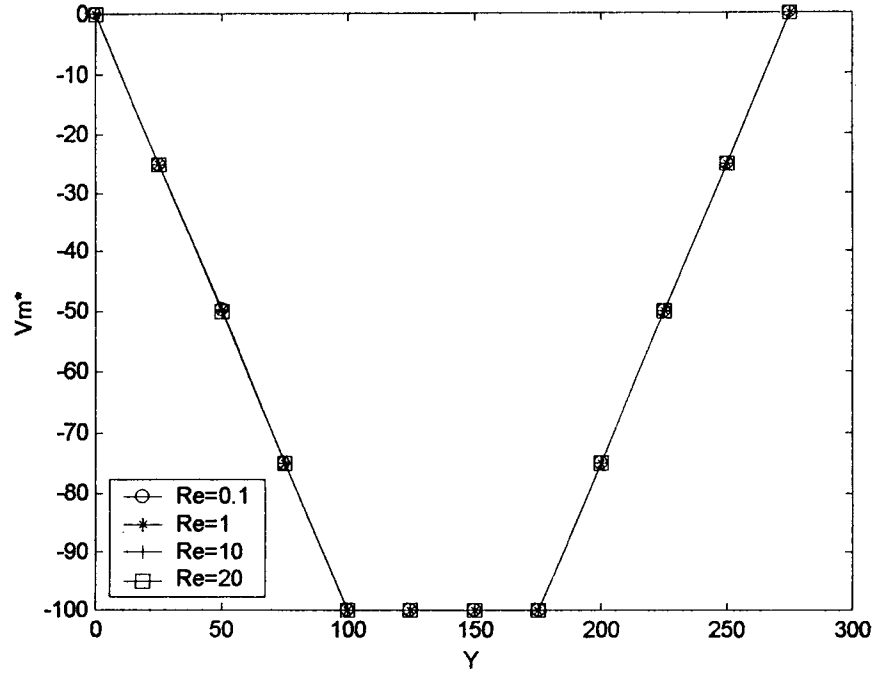

Fig. 6.22 Mean Velocity Variation of Liquid in the Wick Region Obtained Using Poiseuille Model (Ar=0.0036, ε=0.50)

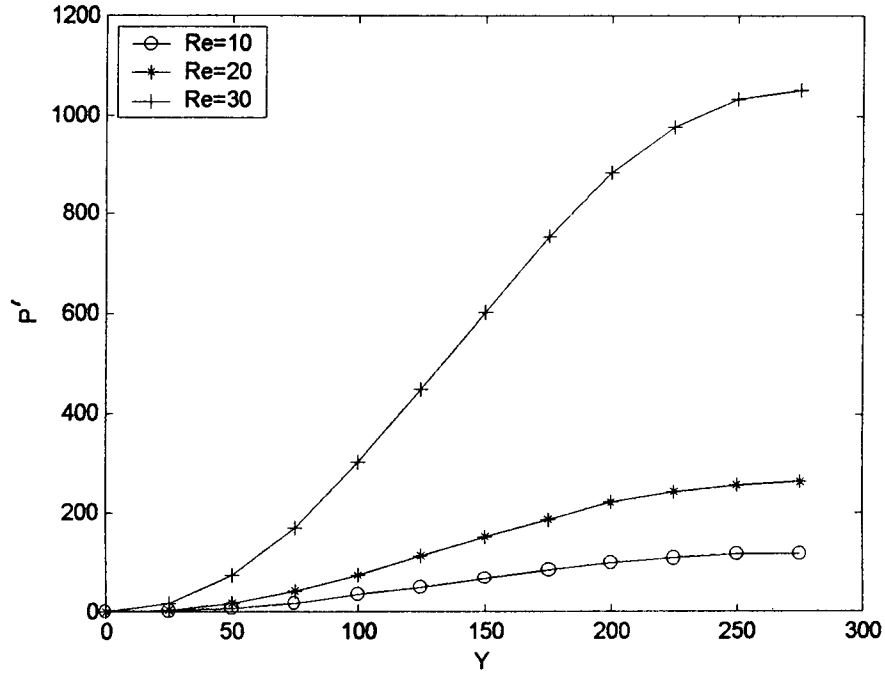

Fig. 6.23 Pressure Variation in the Liquid Wick Region Obtained Using Darcy's Equation (Ar=0.0036, ε=0.50)

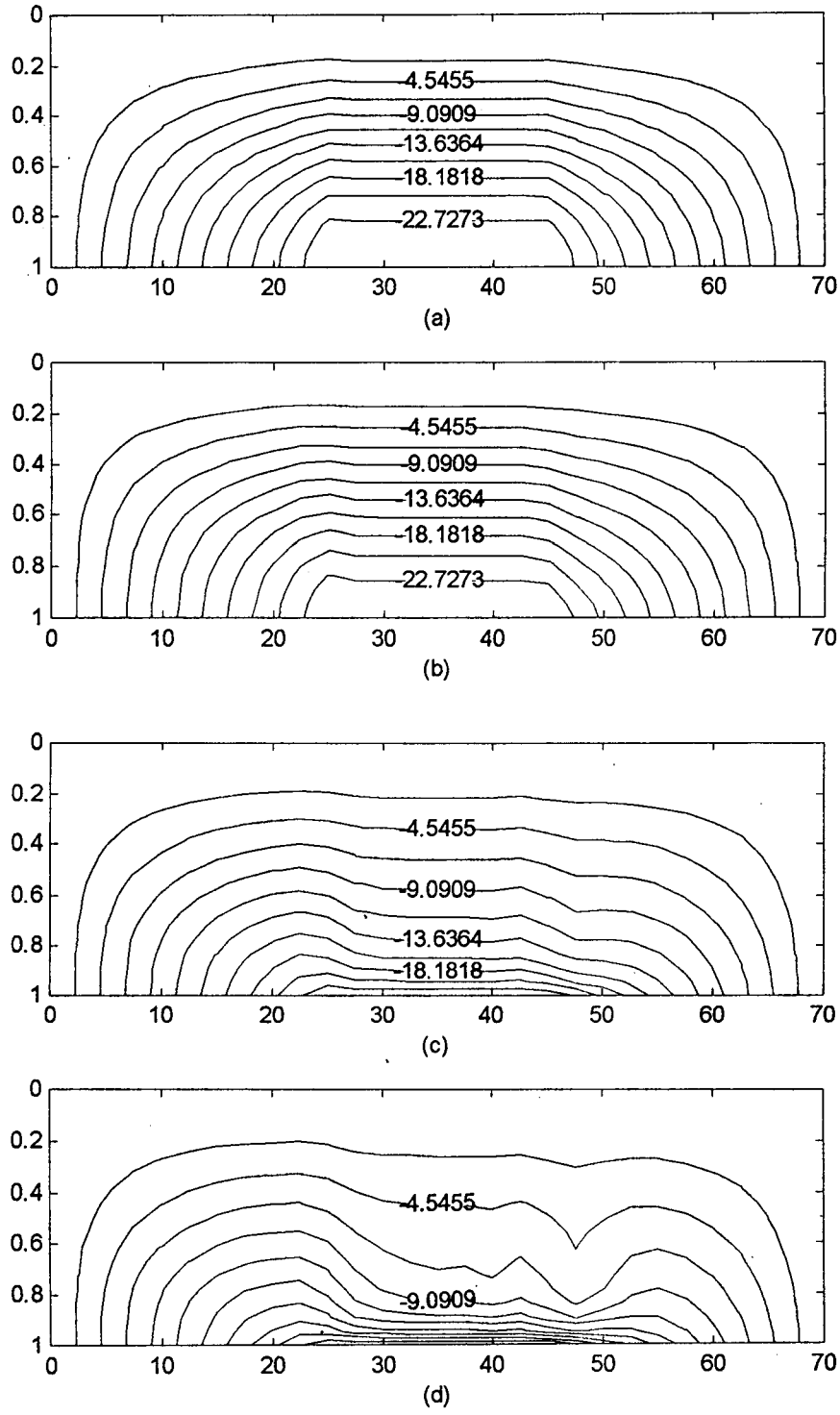

Fig. 6.24 Stream Lines in Vapour Core Region (Ar=0.014)
(a) Re=1.0, (b) Re=5.0, (c) Re=10.0, (d) Re=12.5

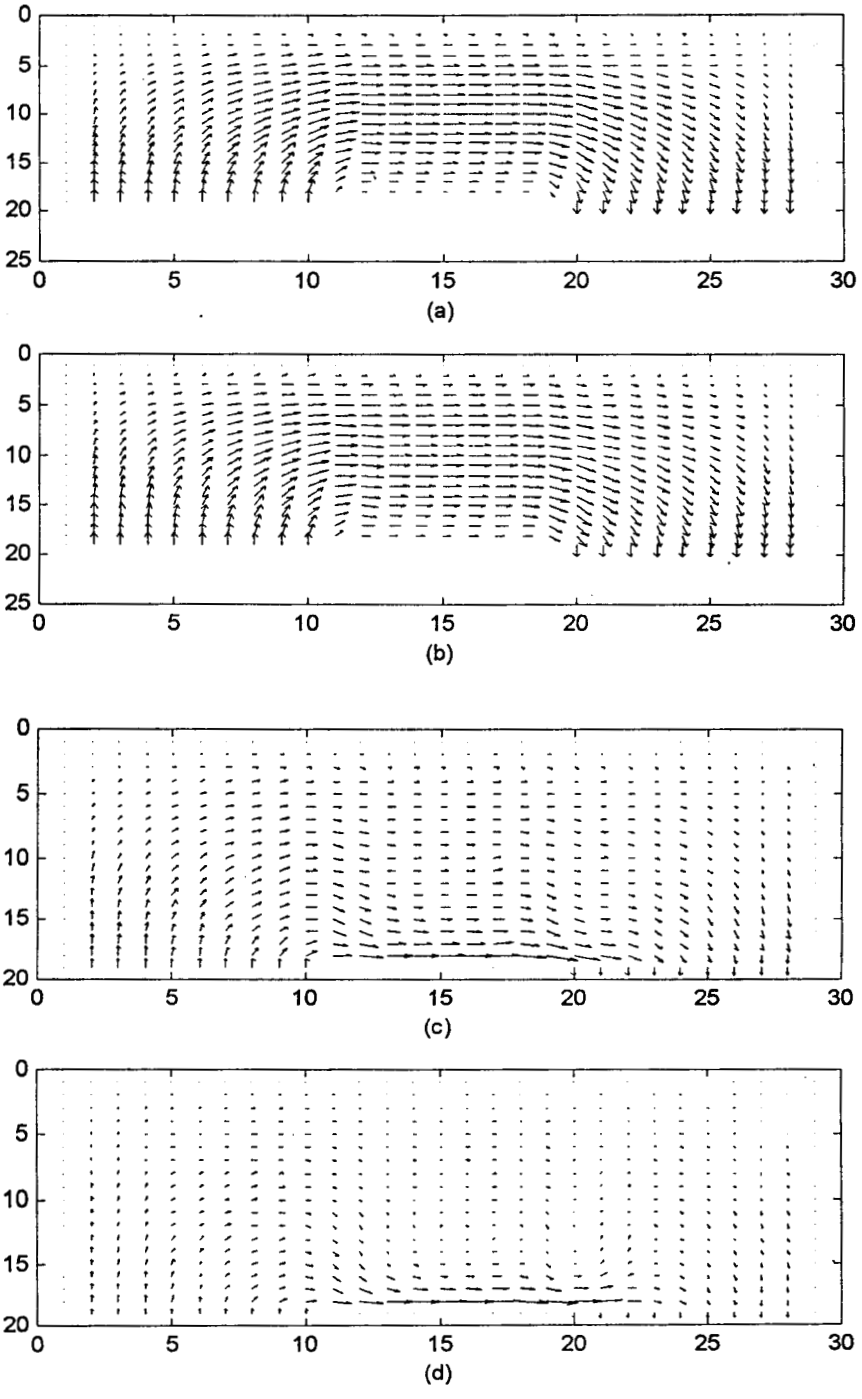

Fig. 6.25 Vector Plots for Vapour Core Region (Ar=0.014)
(a) Re=1.0, (b) Re=5.0, (c) Re=10.0, (d) Re=12.5

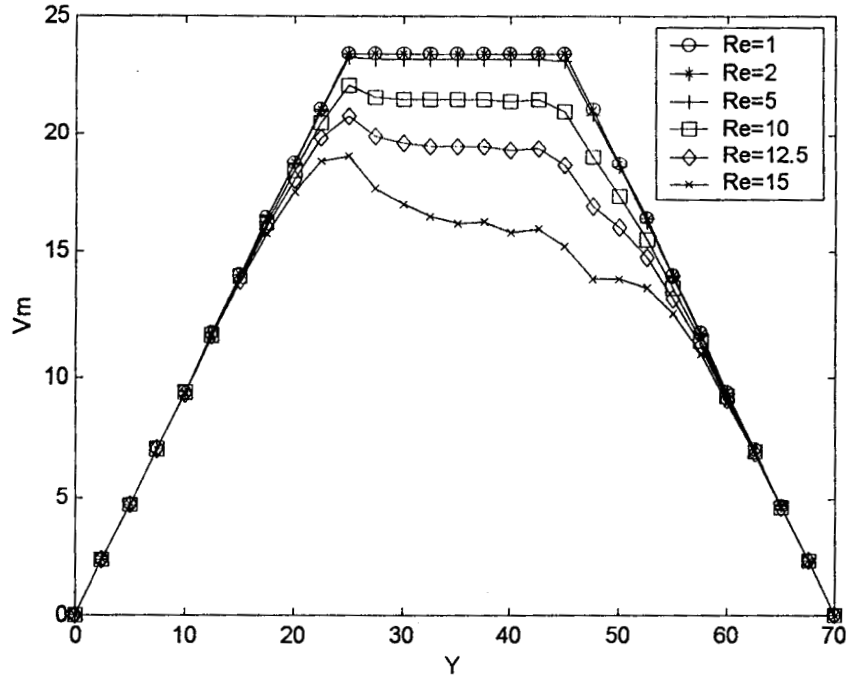

Fig. 6.26 Variation of Mean Axial Velocity of Vapour in the Vapour Core With Respect to Re (Ar=0.014)

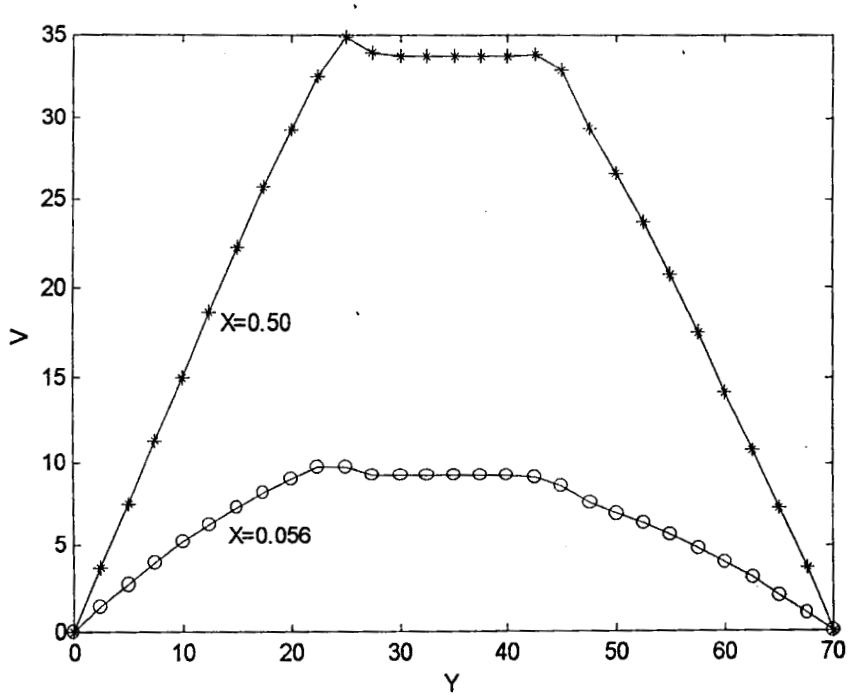

Fig. 6.27 Variation of Axial Velocity of Vapour in the Vapour Core With Respect to X (Re=5.0, Ar=0.014)

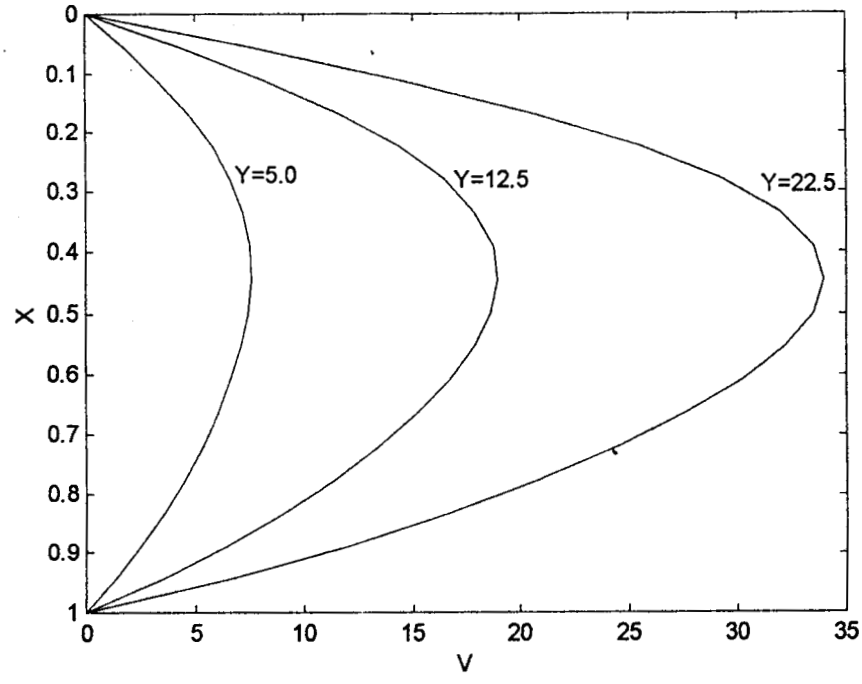

(a) In the Evaporator Zone

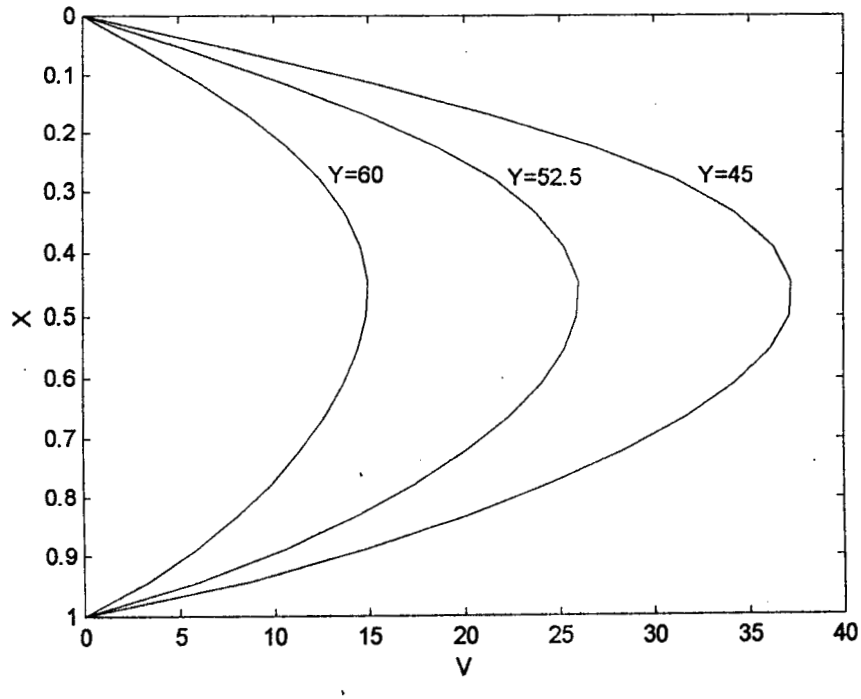

(b) In the Condenser Zone

Fig. 6.28 Axial Velocity Profiles in the Vapour Core
(Re =1.0, Ar = 0.014)

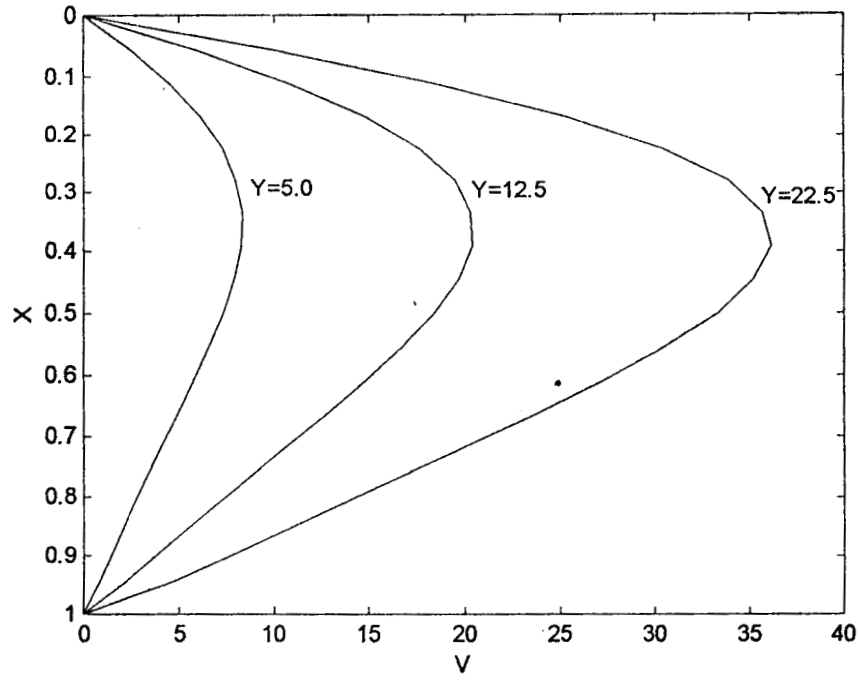

(a) In the Evaporator Zone

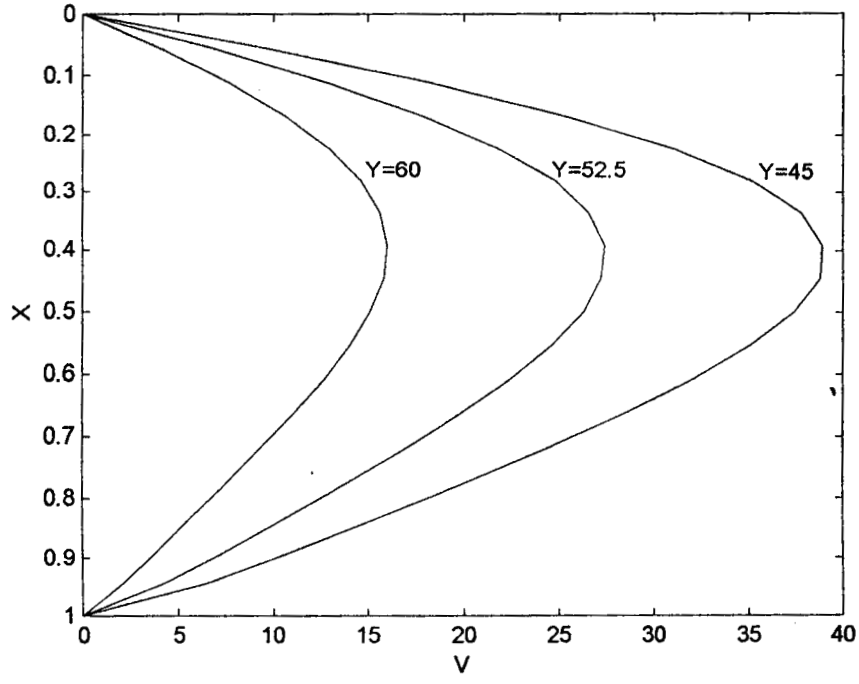

(b) In the Condenser Zone

Fig. 6.29 Axial Velocity Profiles in the Vapour Core
(Re =2.0, Ar = 0.014)

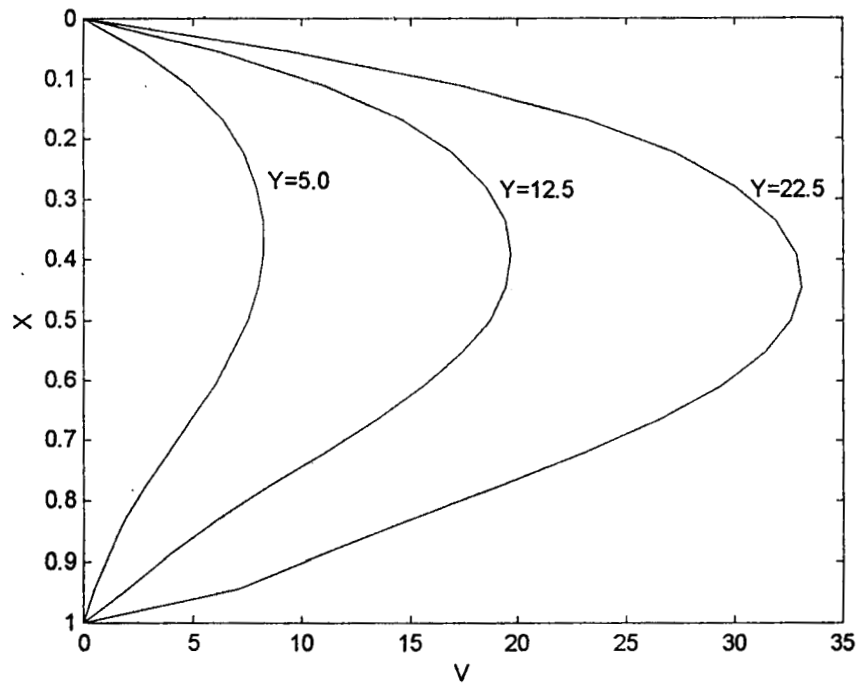

(a) In the Evaporator Zone

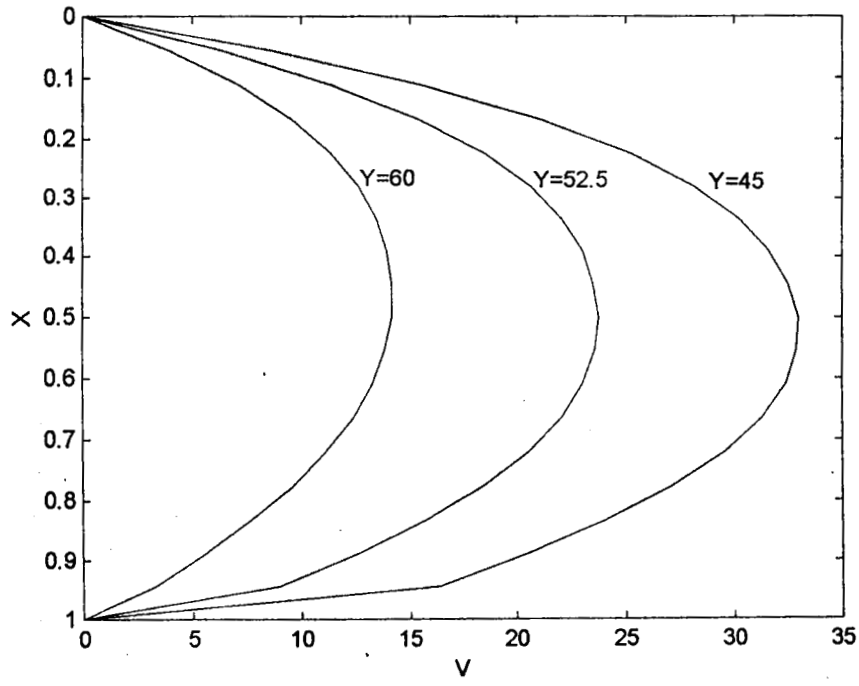

(b) In the Condenser Zone

Fig. 6.30 Axial Velocity Profiles in the Vapour Core
(Re =5.0, Ar = 0.014)

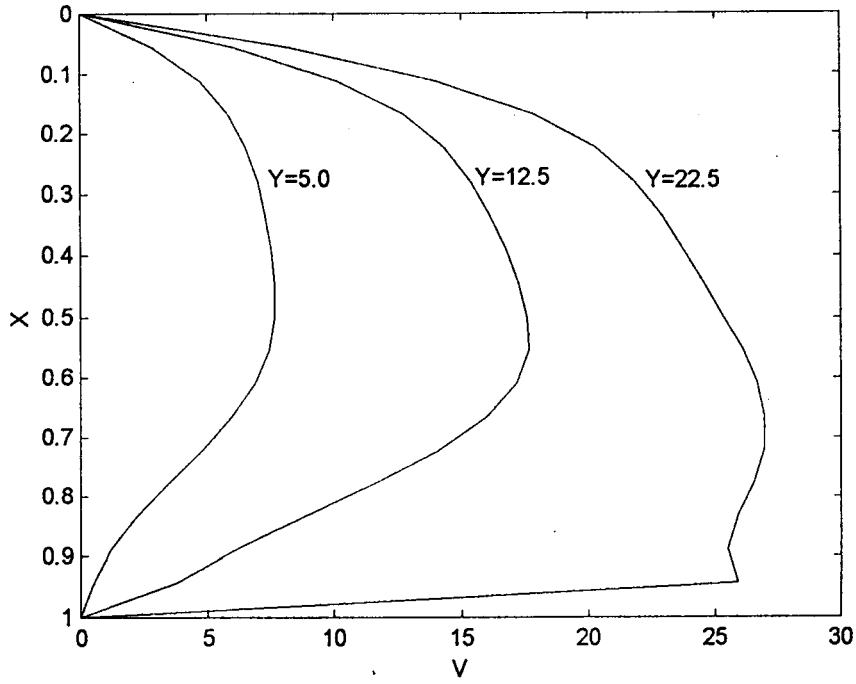

(a) In the Evaporator Zone

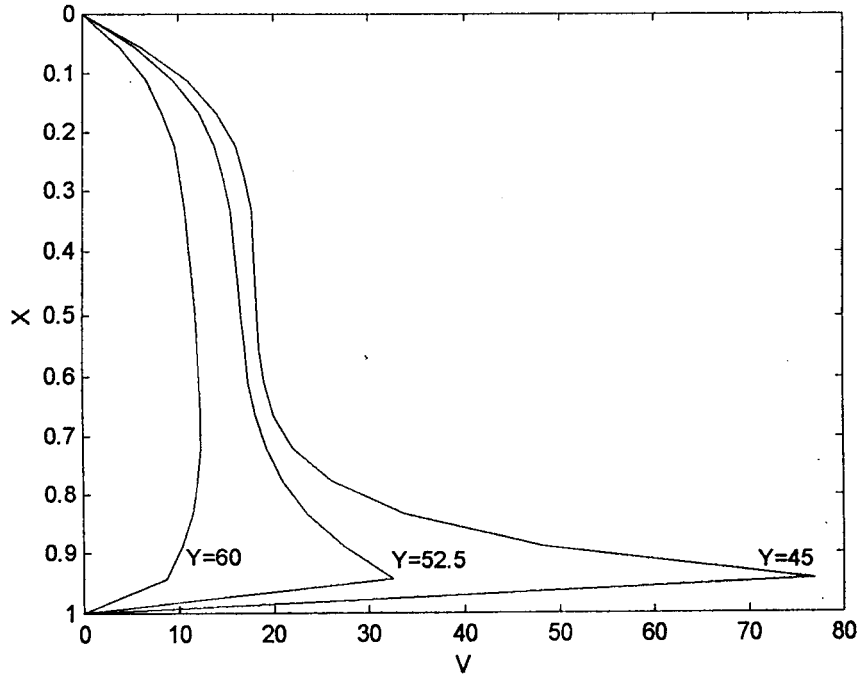

(b) In the Condenser Zone

Fig. 6.31 Axial Velocity Profiles in the Vapour Core
(Re =10, Ar = 0.014)

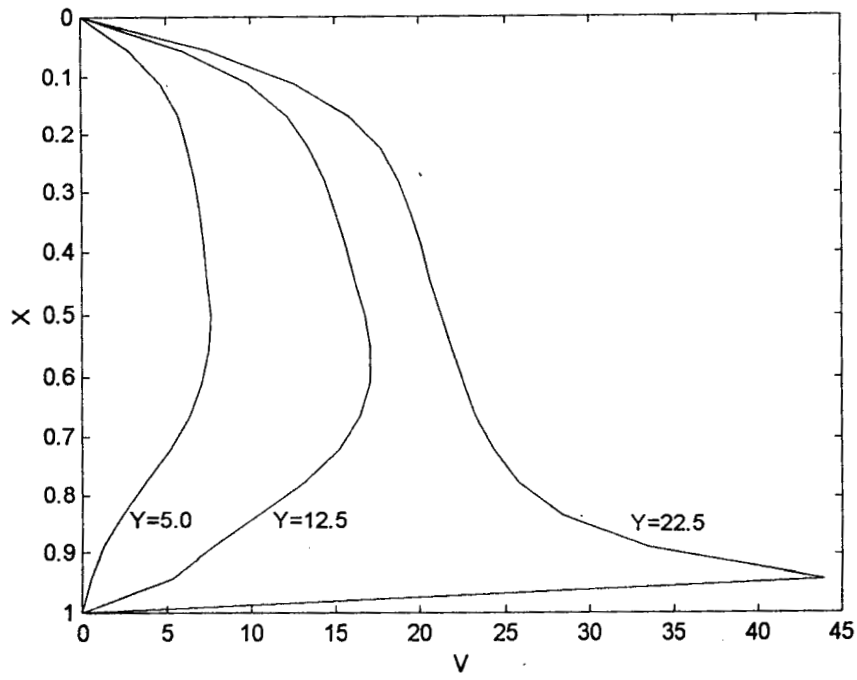

(a) In the Evaporator Zone

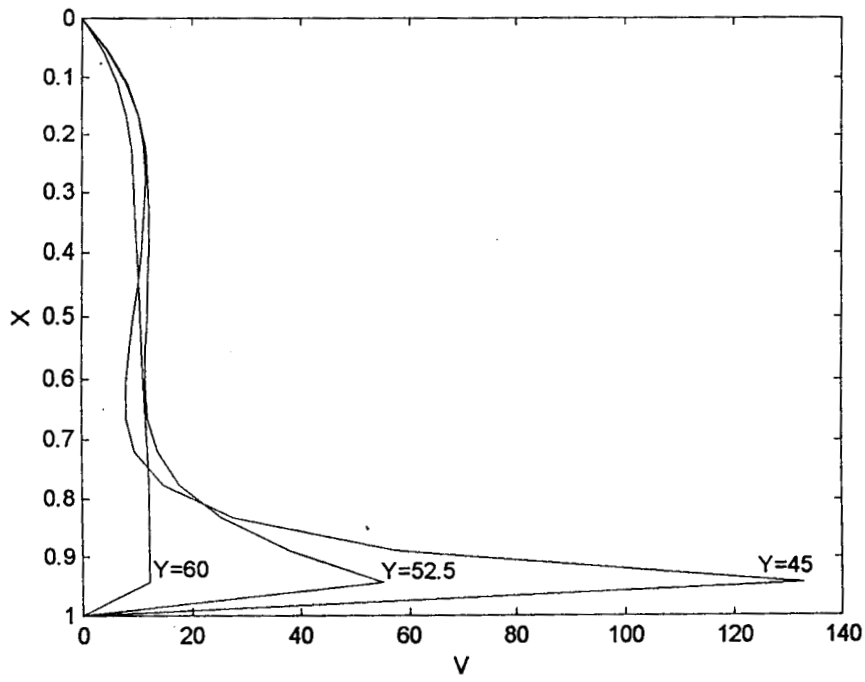

(b) In the Condenser Zone

Fig. 6.32 Axial Velocity Profiles in the Vapour Core
(Re =12.5, Ar = 0.014)

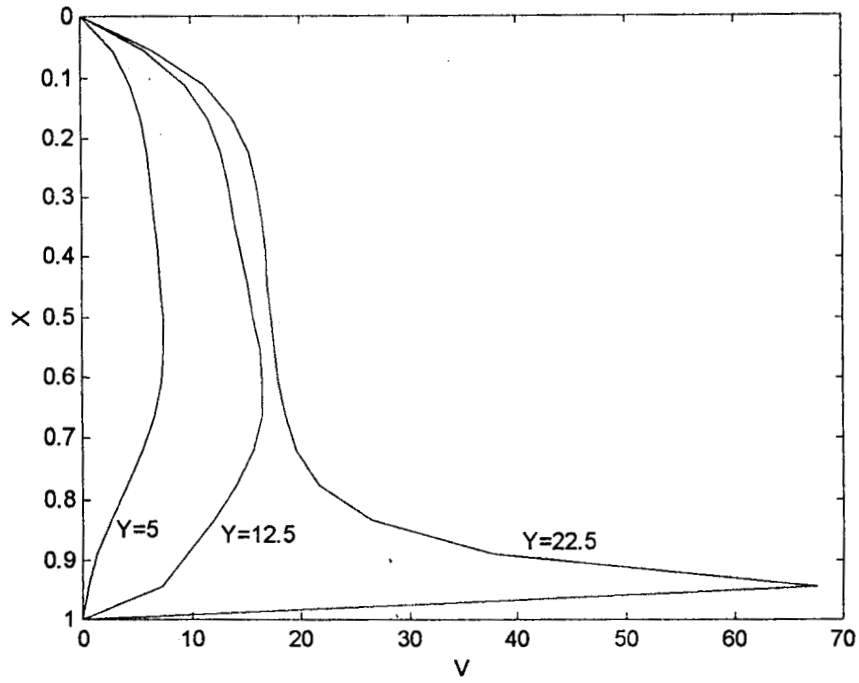

(b) In the Evaporator Section

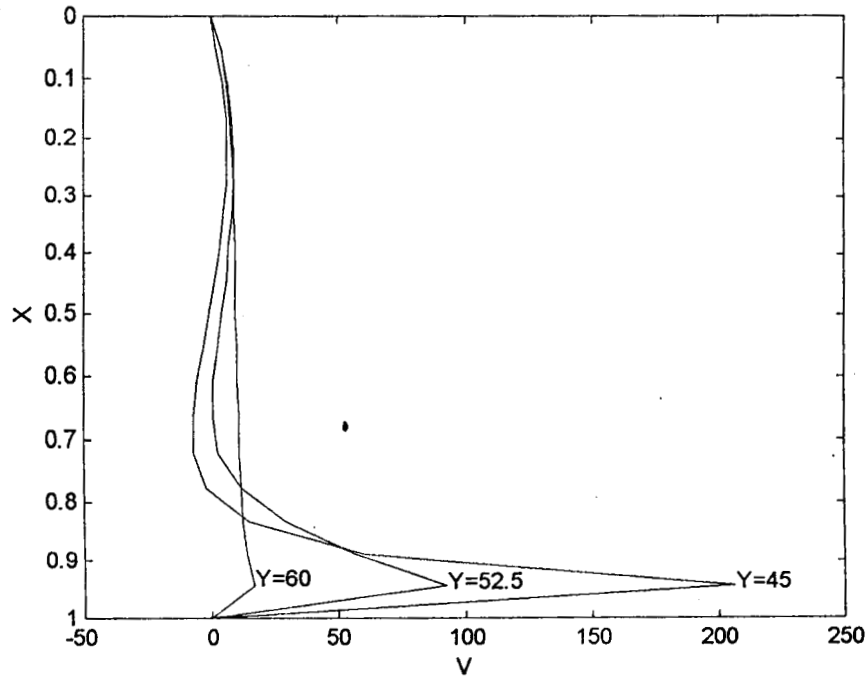

(b) In the Condenser Section

Fig. 32A Axial Velocity Profiles in the Vapour Core
(Re=15, Ar=0.014)

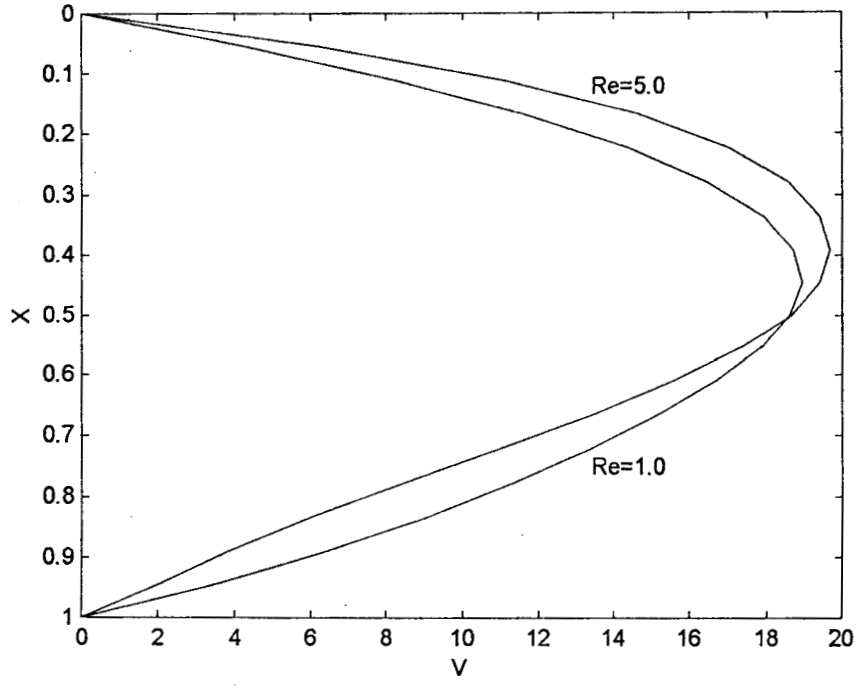

(a) In the Evaporator Zone (Y=12.5)

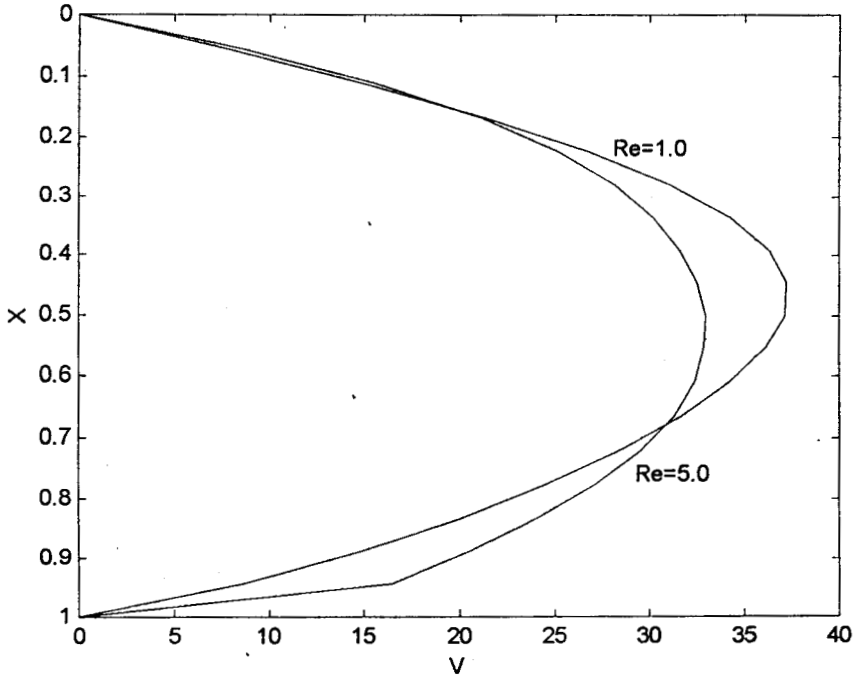

(b) In the Condenser Zone (Y= 45)

Fig. 6.33 Comparison of Axial Velocity Profiles in the Vapour Core At Two Different Re Values (Ar = 0.014)

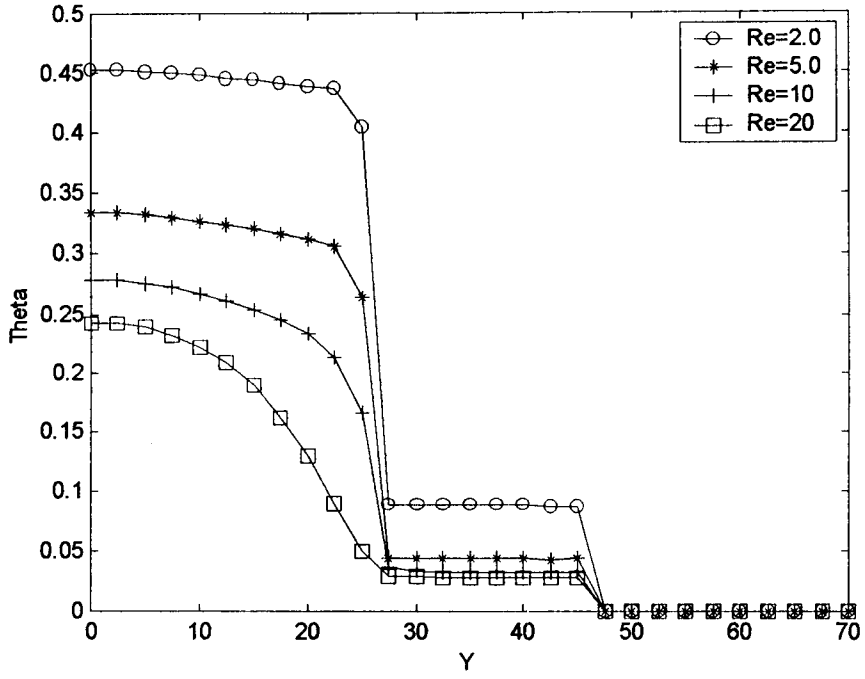

Fig. 6.34 Temperature Distribution Along the Wick-Vapour Interface (Ar = 0.014)

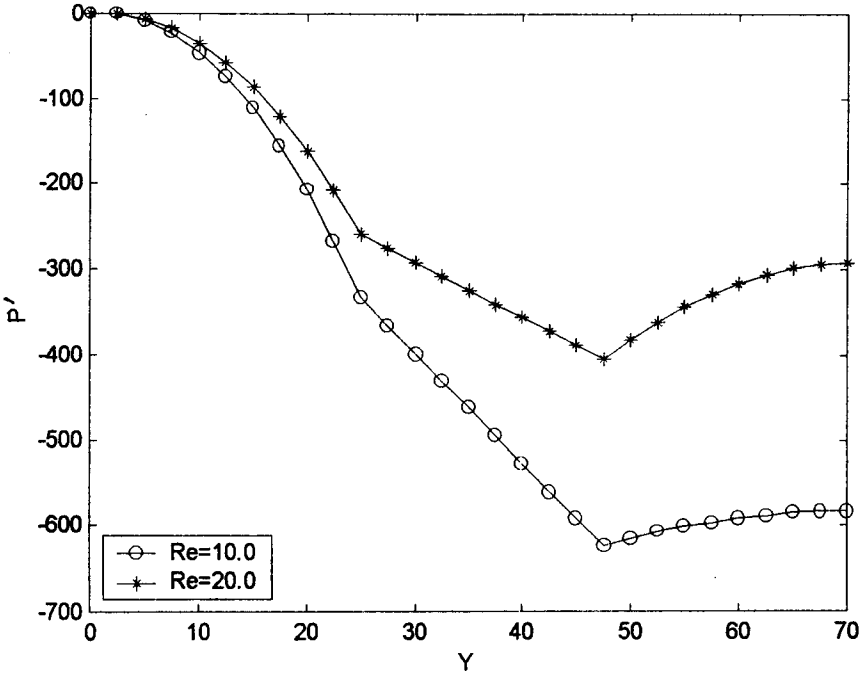

Fig. 6.35 Mean Pressure Variation Along the Vapour Core (Ar = 0.014)

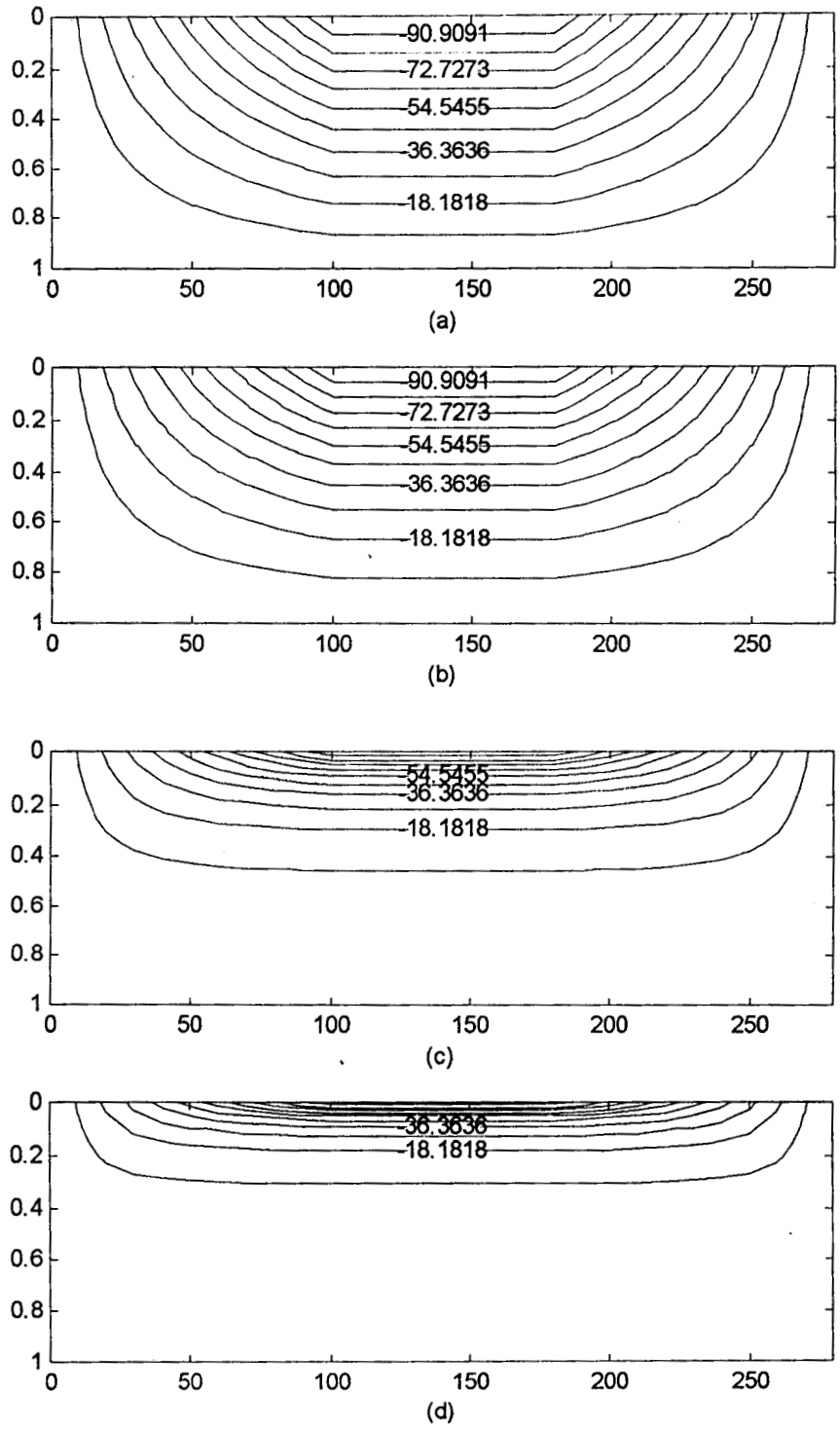

Fig. 6.36 Stream Lines in the Liquid Wick Region (Ar=0.0036)
(a) Re=0.10, (b) Re=1.0, (c) Re=10, (d) Re=20

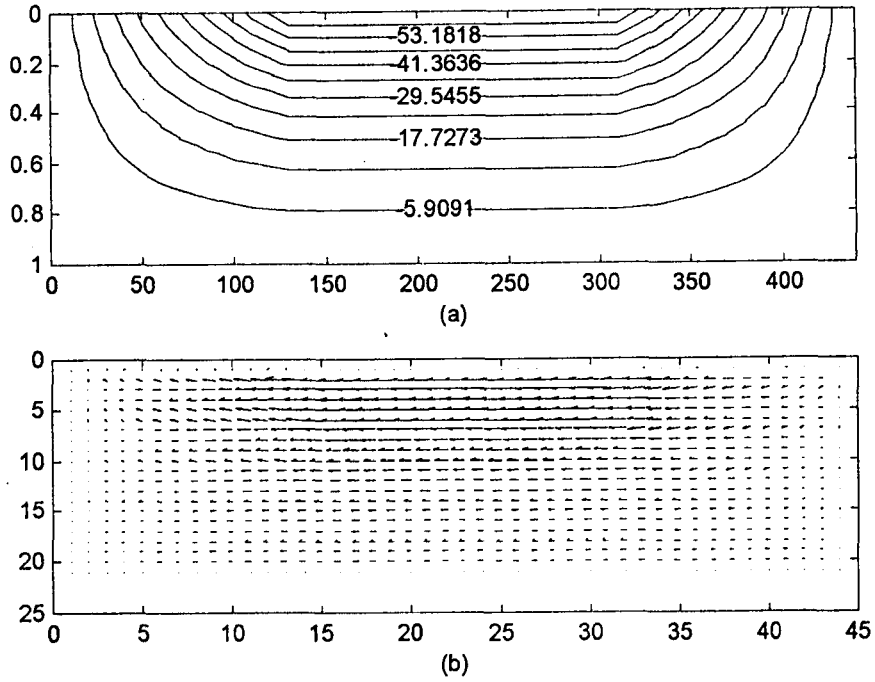

Fig. 6.37 (a) Stream Lines and (b) Vector Plot in the Liquid Wick Region (Re=10, Ar=0.0023, ε=0.75)

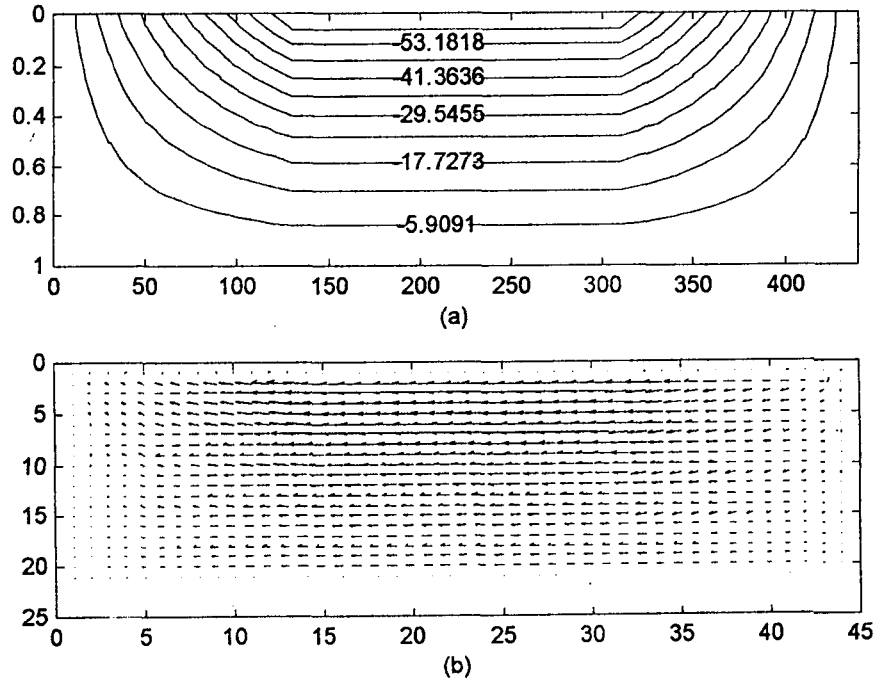

Fig. 6.38 (a) Stream Lines and (b) Vector Plot in the Liquid Wick Region (Re=10, Ar=0.0023, ε=0.70)

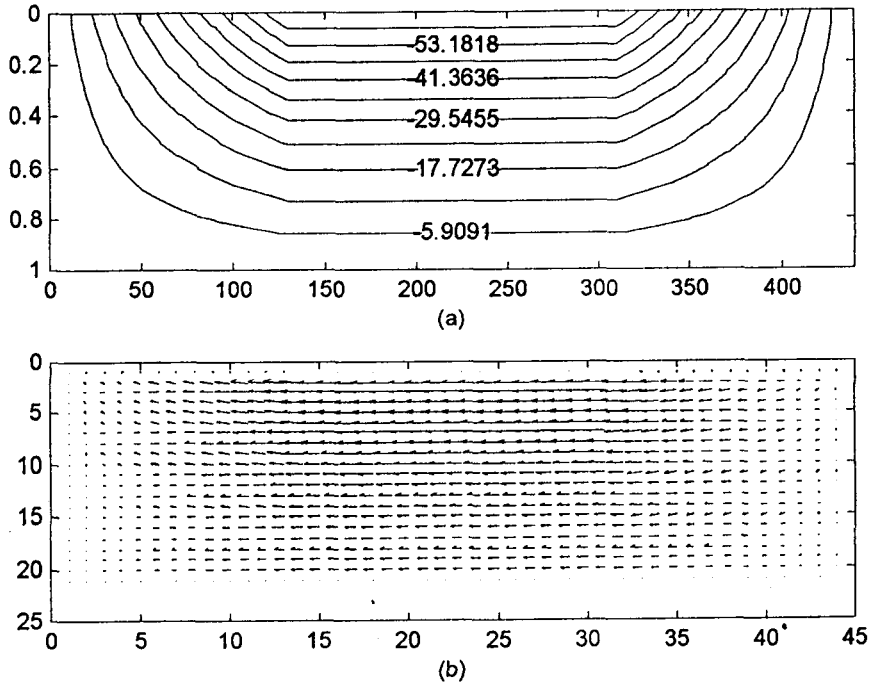

Fig. 6.39 (a) Stream Lines and (b) Vector Plot in the Liquid Wick Region (Re=10, Ar=0.0023, ε=0.65)

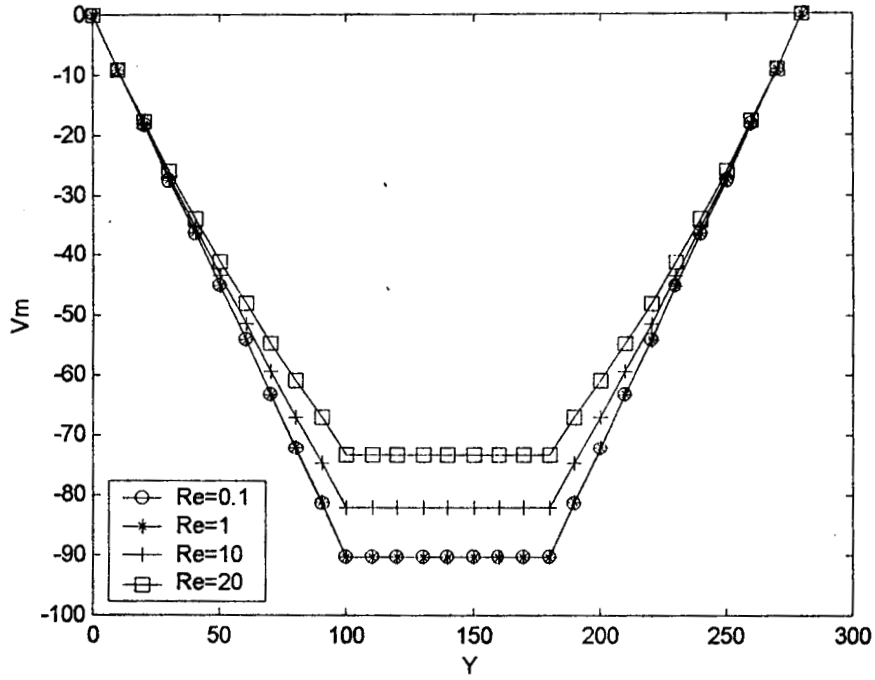

Fig. 6.40 Variation of Mean Axial Velocity of Liquid in the Wick Region (Ar=0.0036, ε=0.50)

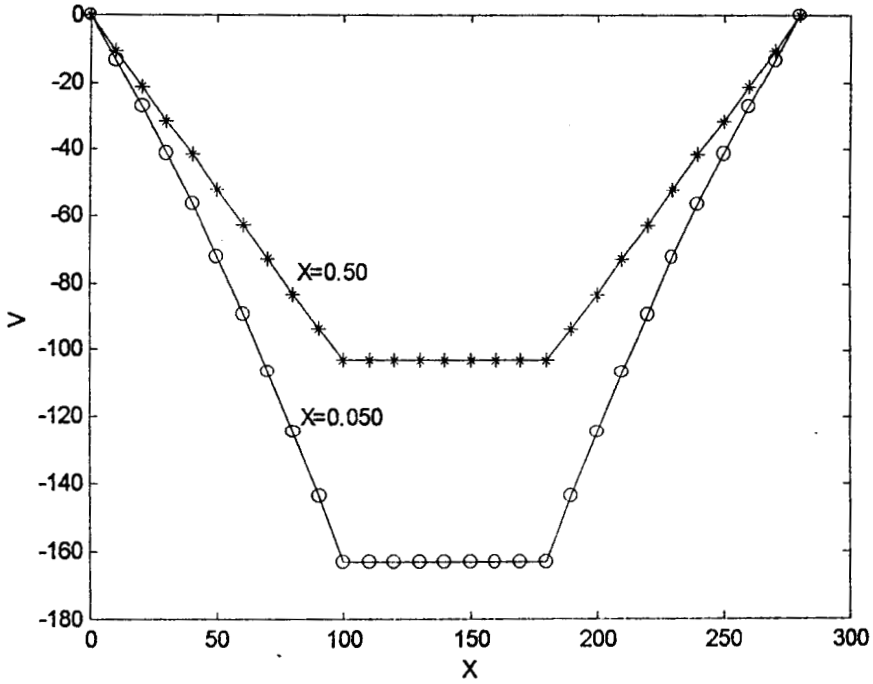

Fig. 6.41 Variation of Axial Velocity of Liquid in the Wick Region (Re=5.0, Ar=0.0036, ε=0.50)

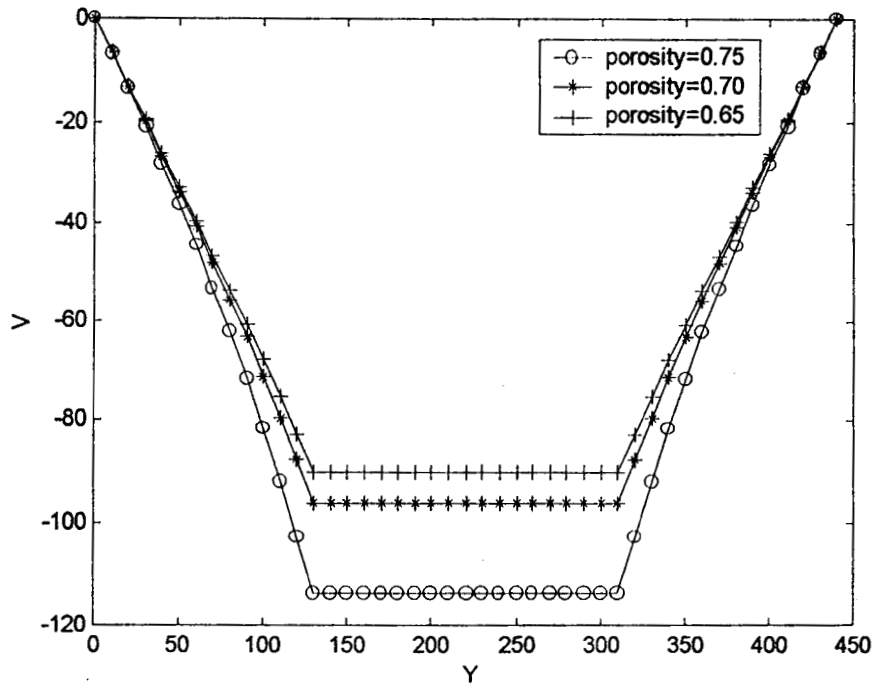

Fig. 6.42 (a) Comparison of Axial Velocities for Different Porosity Values (Re=10, X=0.10, Ar=0.0023)

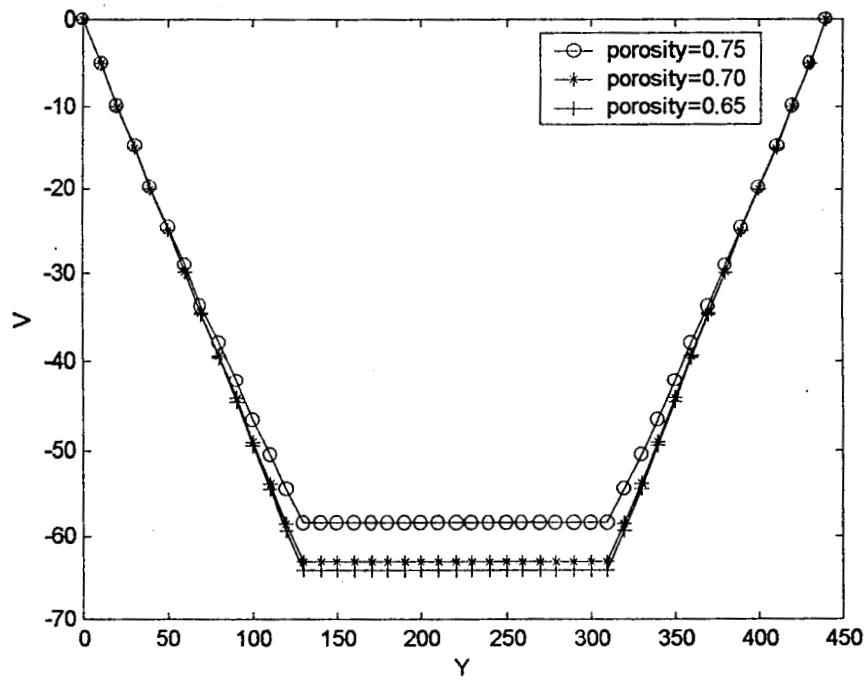

Fig. 6.42 (b) Comparison of Axial Velocities for Different Porosity Values (Re=10, X=0.50, Ar=0.0023)

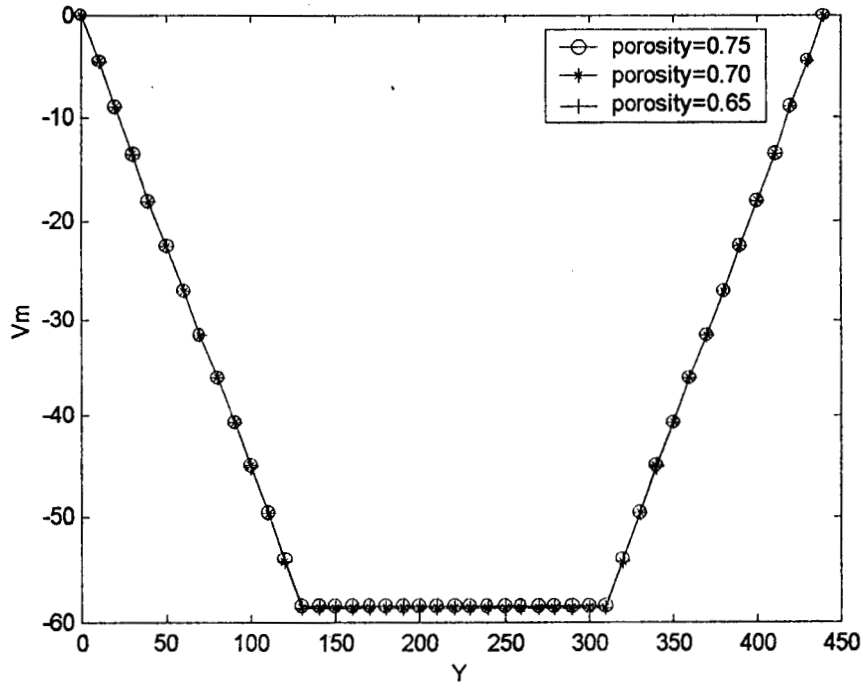

Fig. 6.43 (a) Comparison of Mean Axial Velocities for Different Porosity Values (Re=10, Ar=0.0023)

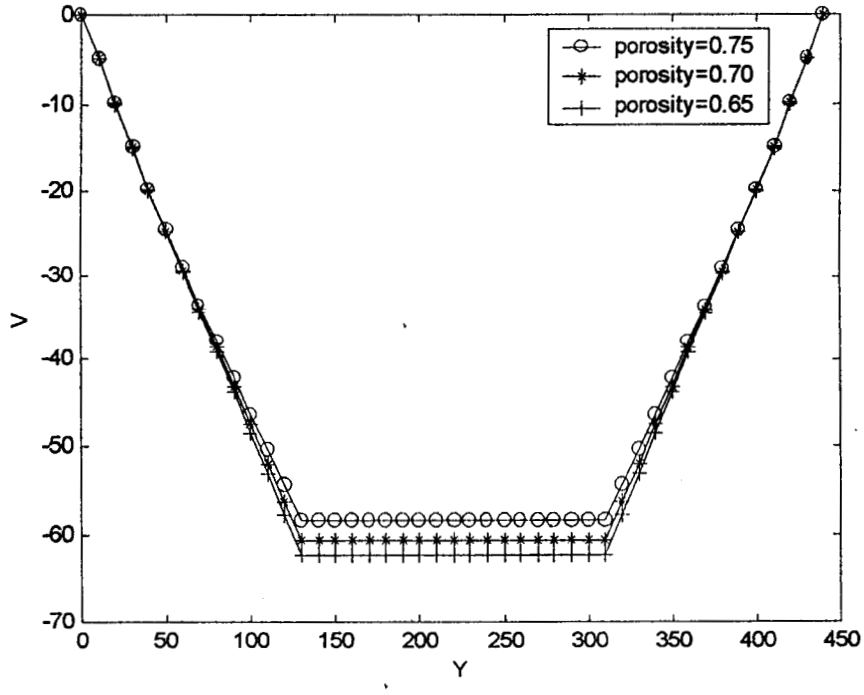

Fig. 6.43 (b) Comparison of Mean Axial Velocities for Different Porosity Values (Re=10, Ar=0.0023, Same Wire Diameter)

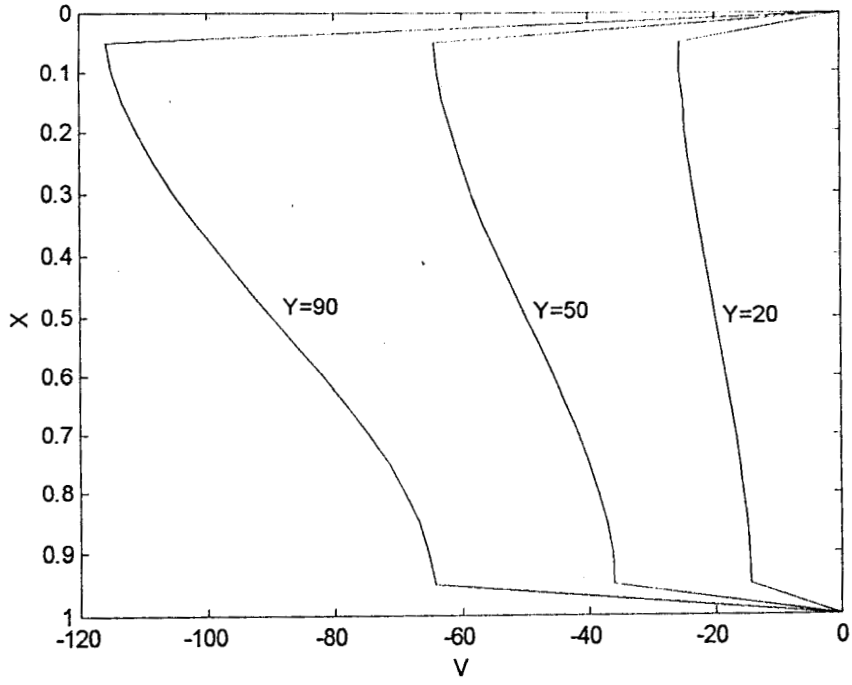

(a) In the Evaporator Zone

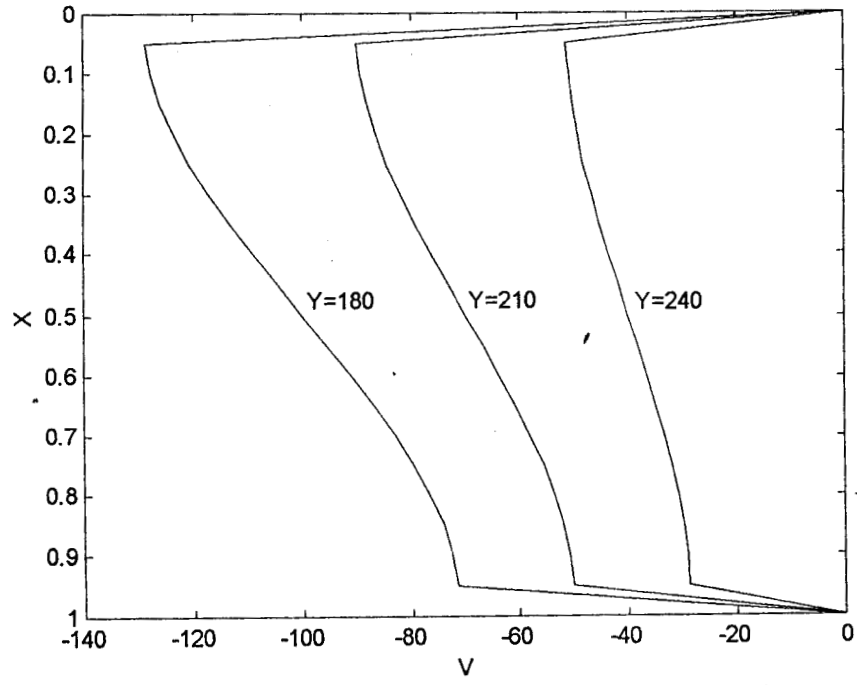

(b) In the Condenser Zone

Fig. 6.44 Axial Velocity Profiles of Liquid in the Wick Region
(Re=0.025, Ar=0.0036, ε=0.50)

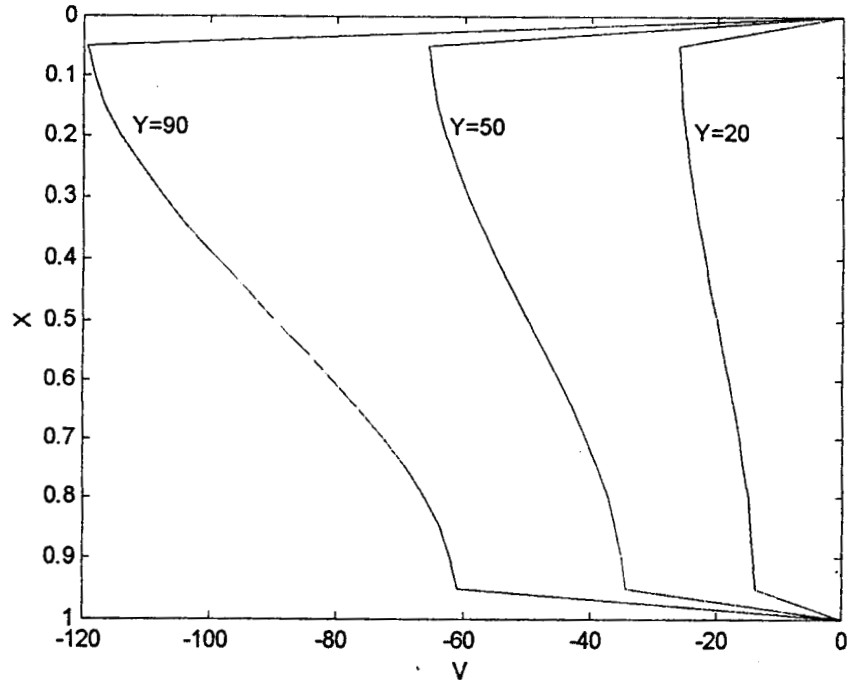

(a) In the Evaporator Zone

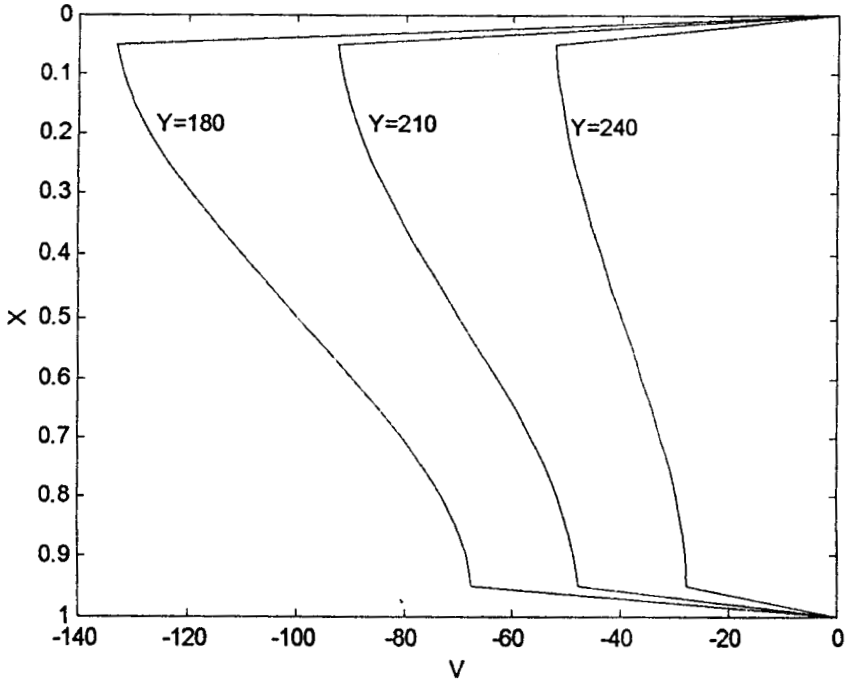

(b) In the Condenser Zone

Fig. 6.44A Axial Velocity Profiles of Liquid in the Wick Region
(Re=0.10, Ar=0.0036, ε=0.50)

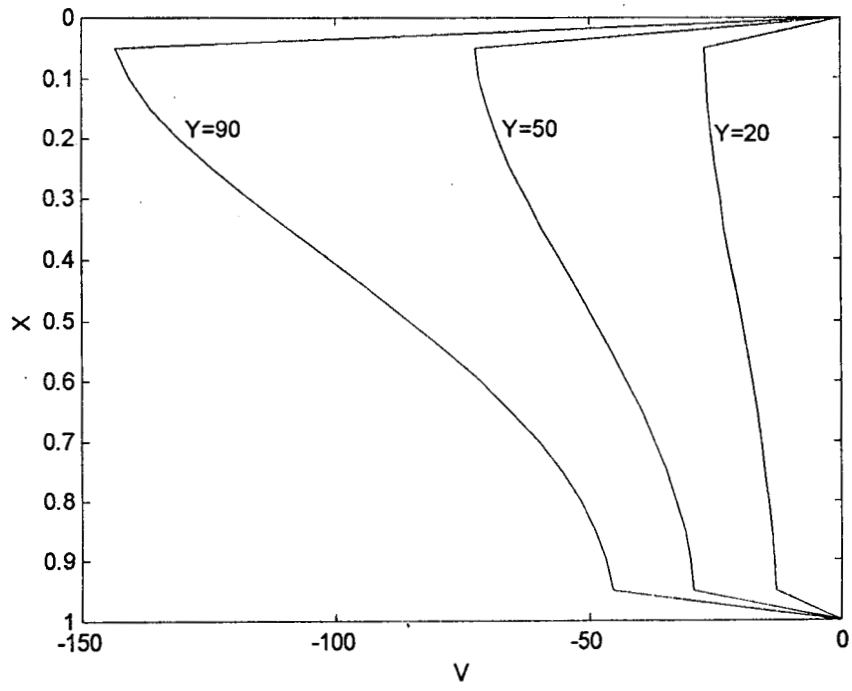

(a) In the Evaporator Zone

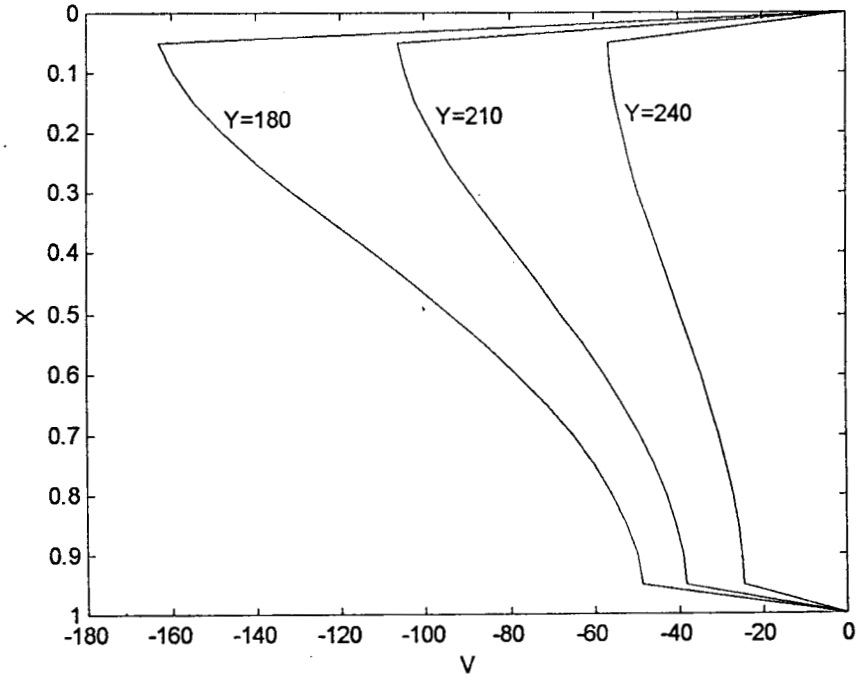

(b) In the Condenser Zone

Fig. 6.45 Axial Velocity Profiles of Liquid in the Wick Region (Re=1.0, Ar=0.0036, ε=0.50)

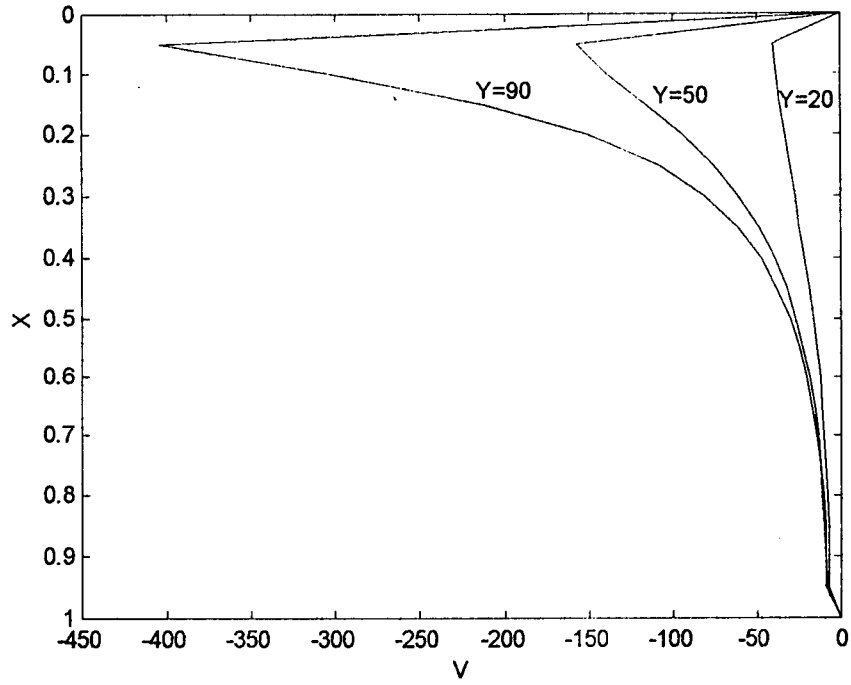

(a) In the Evaporator Zone

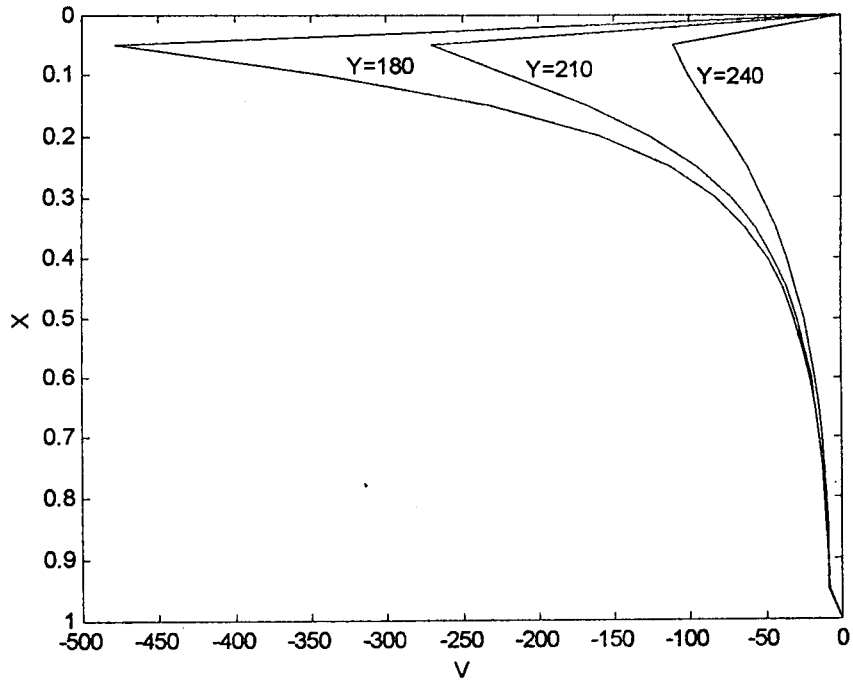

(b) In the Condenser Zone

Fig. 6.46 Axial Velocity Profiles of Liquid in the Wick Region (Re=10, Ar=0.0036, ε=0.50)

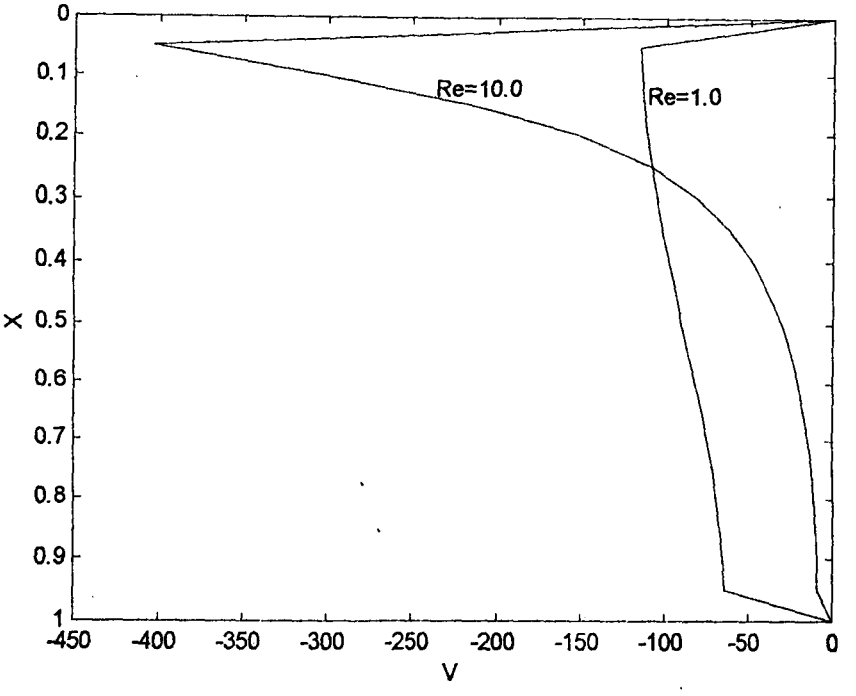

(a) In the Evaporator Zone (Y=90)

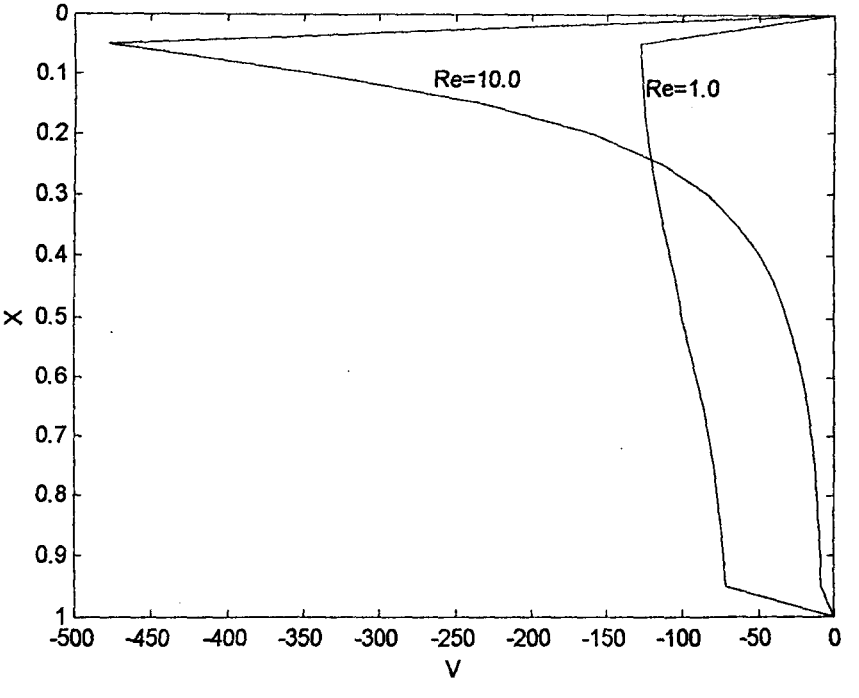

(b) In the Condenser Section (Y=180)

Fig. 6.47 Comparison of Axial Velocities of Liquid in the Wick Region (Ar=0.0036, ε=0.50)

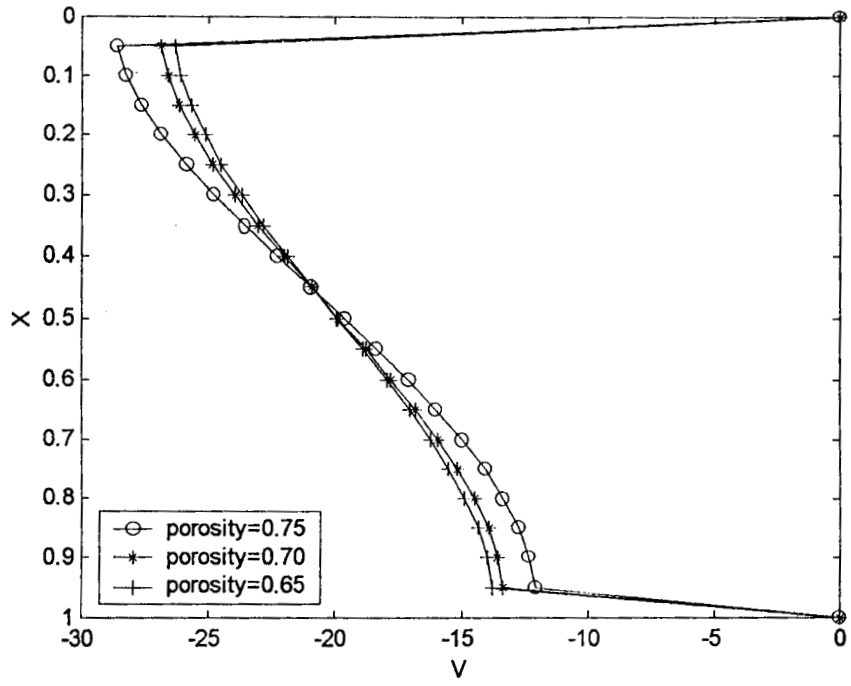

(a) In the Evaporator Zone (Y=40)

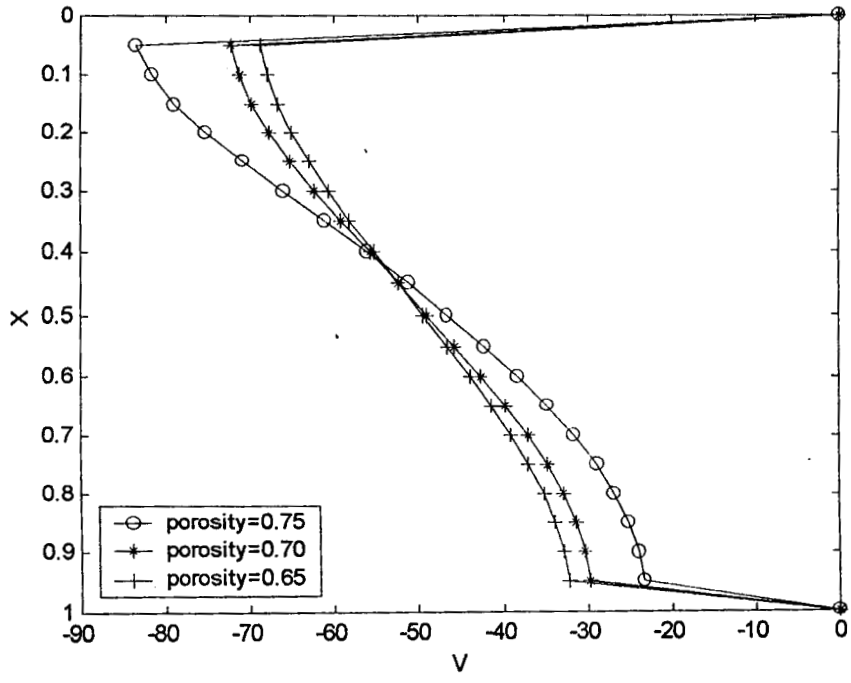

(b) In the Condenser Zone (Y=340)

Fig. 6.48 A Comparison of Axial Velocities in the Liquid Wick Region for Different Porosity Value (Re=10, Ar=0.0023)

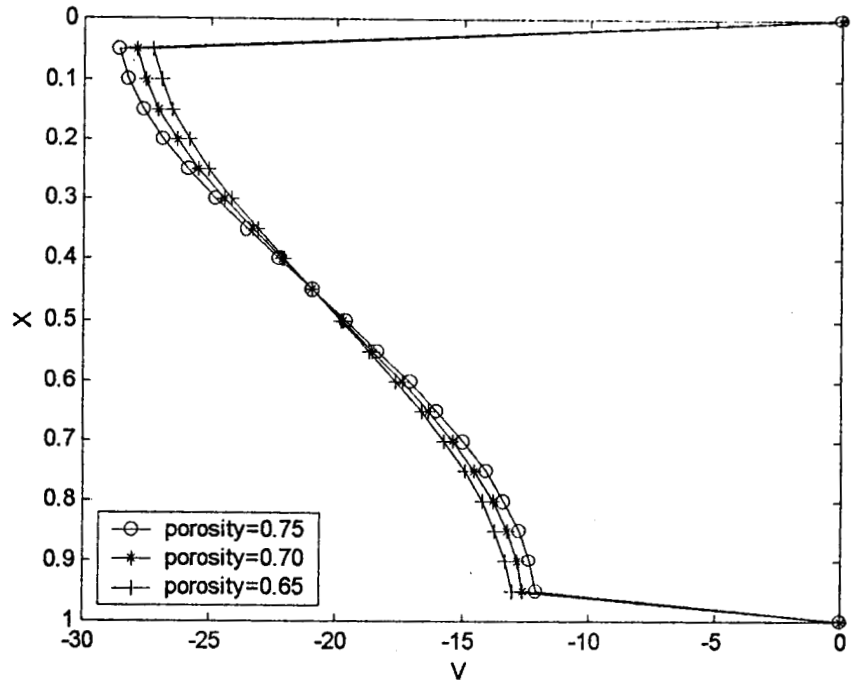

(a) In the Evaporator Zone (Y=40)

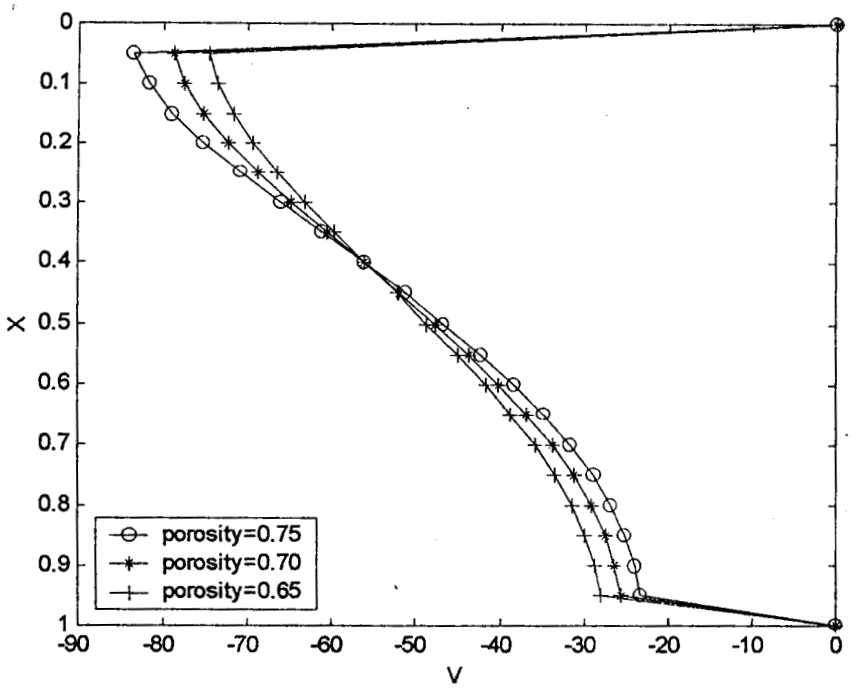

(b) In the Condenser Zone (Y=340)

Fig. 6.48 B Comparison of Axial Velocities for Different Porosity Values (Re=10, Ar=0.0023, Same Wire Diameter)

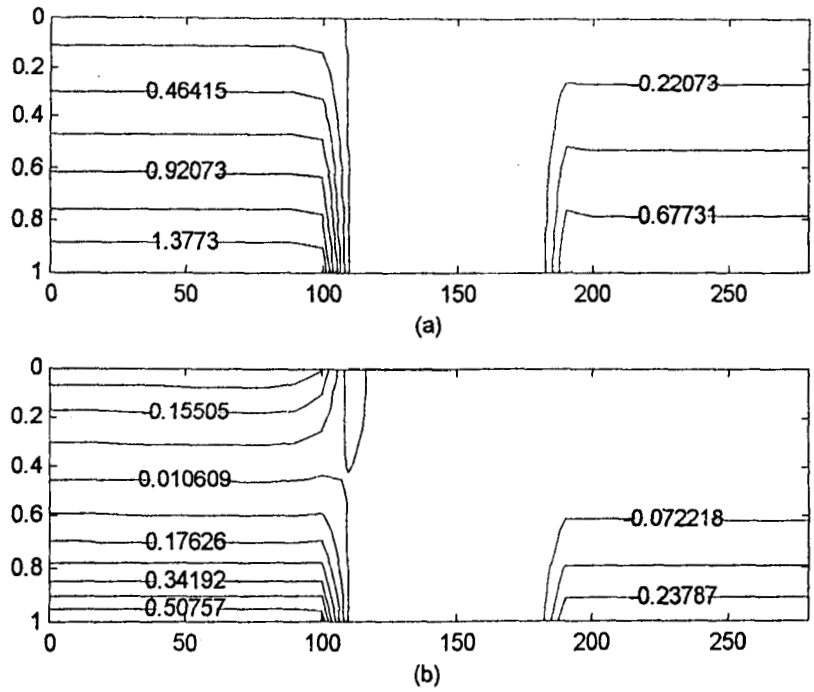

Fig. 6.49 Isotherms in Liquid Wick region (a) Re=1.0, (b) Re=10.0 (Ar=0.0036, ε=0.50)

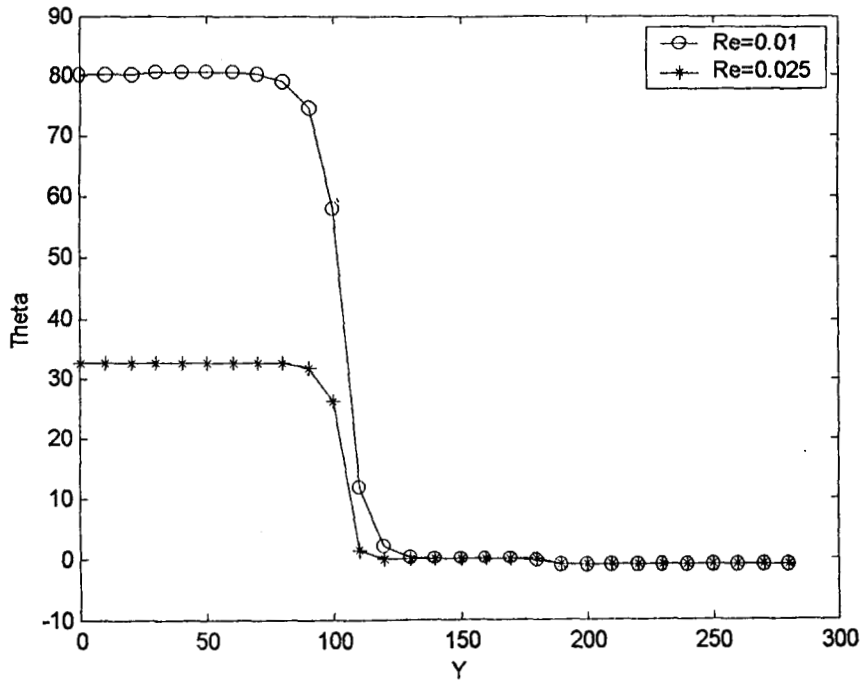

Fig. 6.50 Temperature Distribution Along the Wick Region (X=1, Ar=0.0036, ε=0.50)

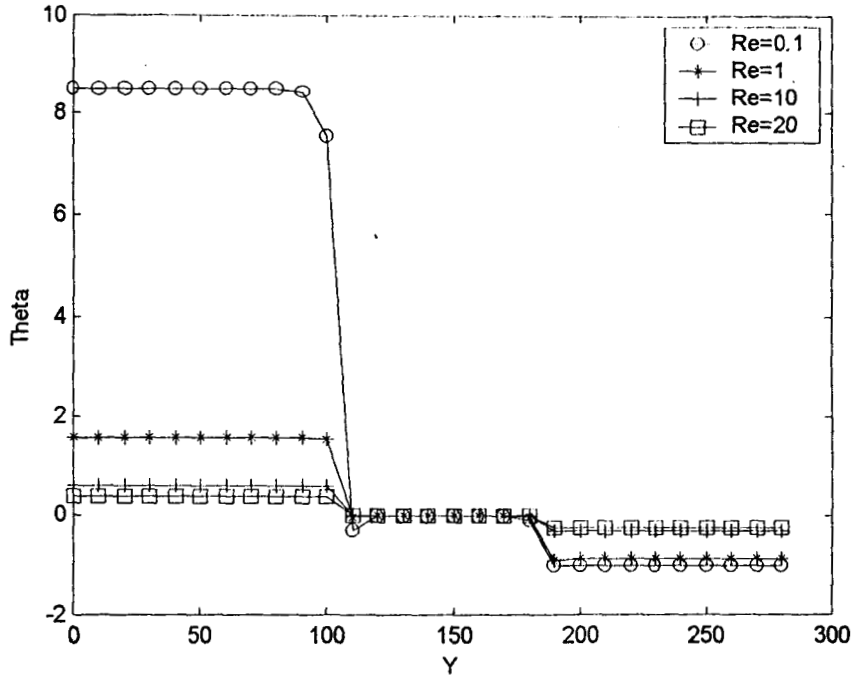

Fig. 6.51 Temperature Distribution Along the Wick Region (X=1, Ar=0.0036, ε=0.50)

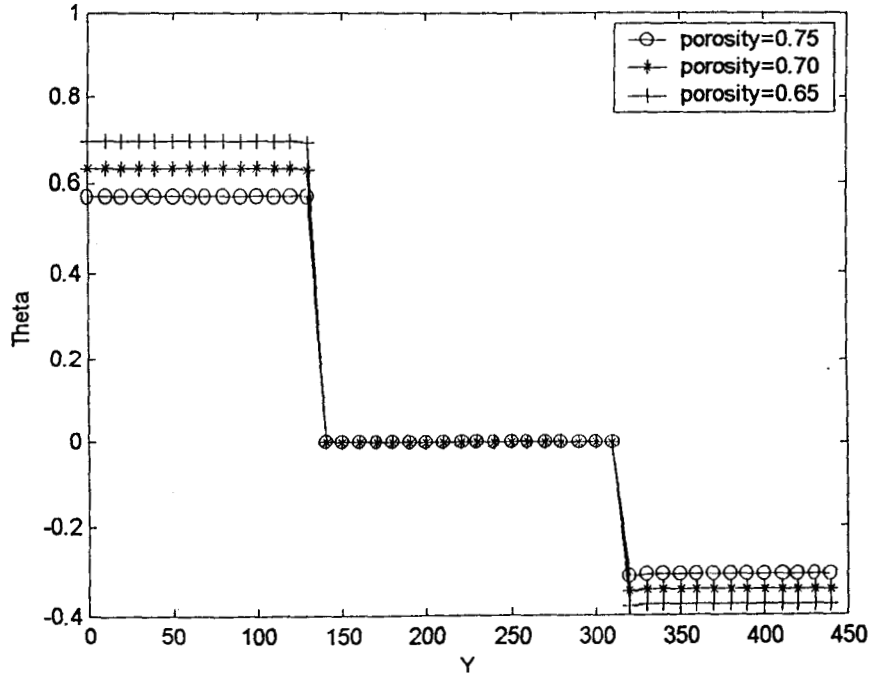

Fig. 6.52 Temperature Distribution Along the Bottom Wall of the Wick Region for Different Porosity Values (Re = 10, Ar=0.0036)

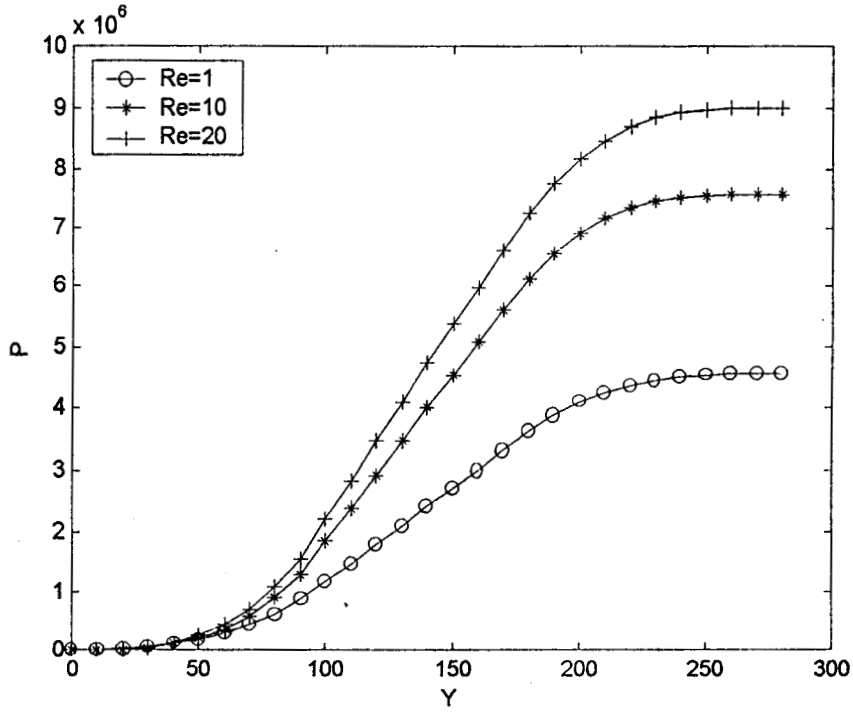

Fig. 6.53 Pressure Variation in the Liquid Wick Region With Respect to Reynolds Number (Ar=0.0036, ε=0.50)

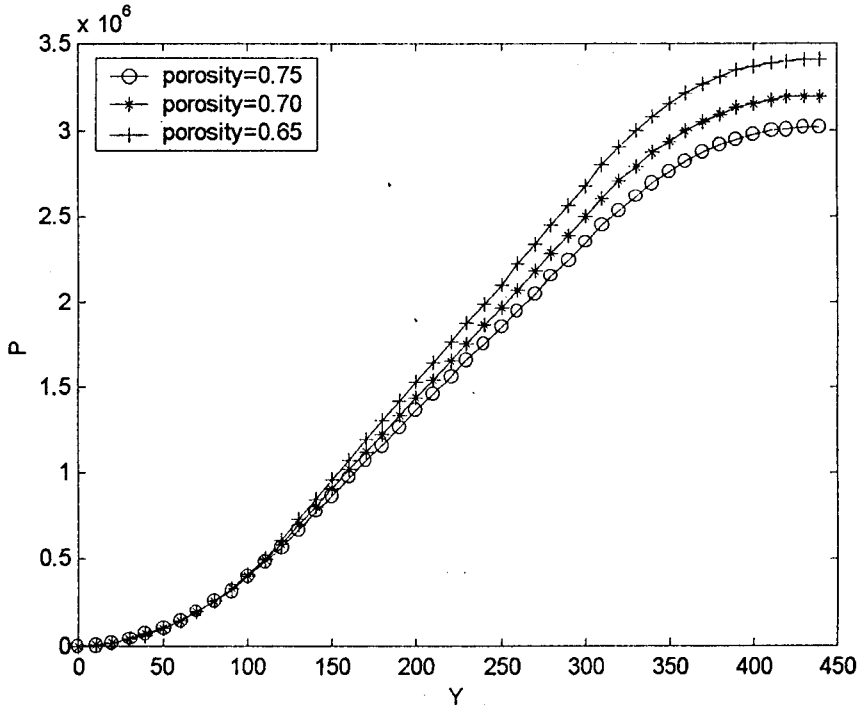

(a) Re=0.05

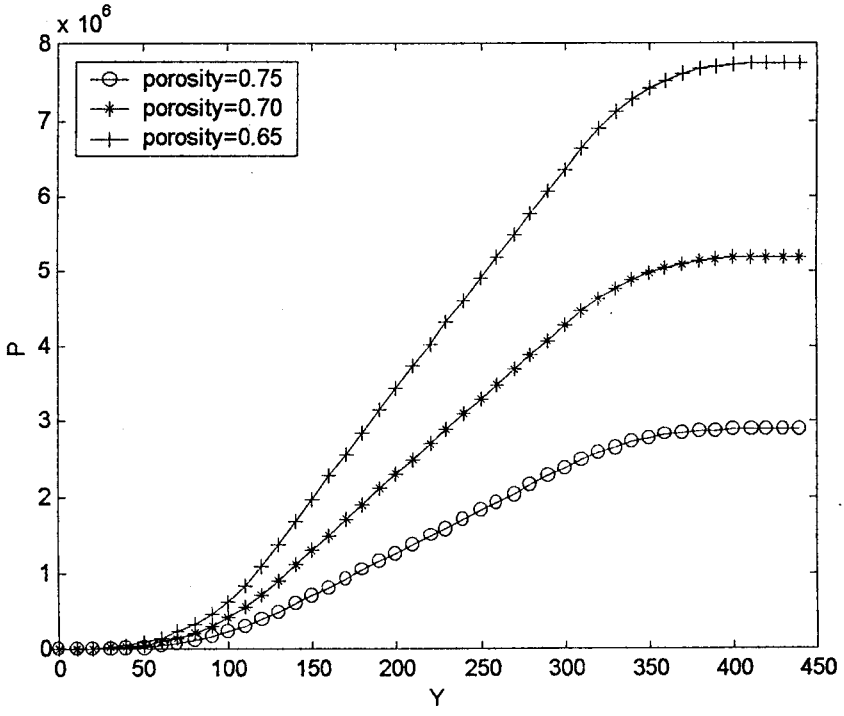

(b) Re=10.0

Fig. 6.54 Pressure Variation in the Liquid Wick Region With Respect to Porosity Values (Ar=0.0023)

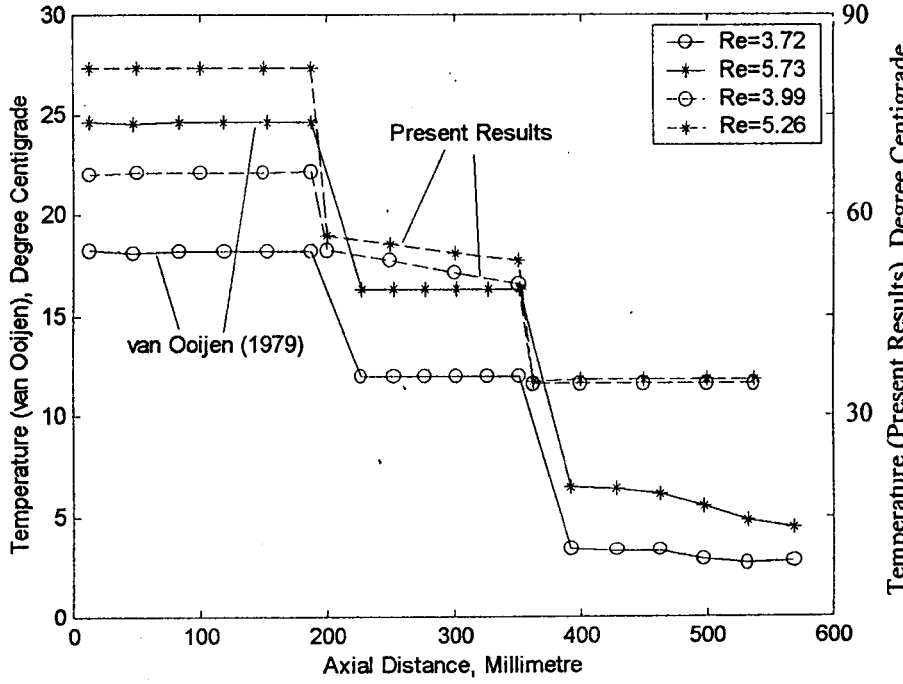

Fig. 6.55 Comparison of Temperature Distribution Obtained With that of van Ooijen (1981)

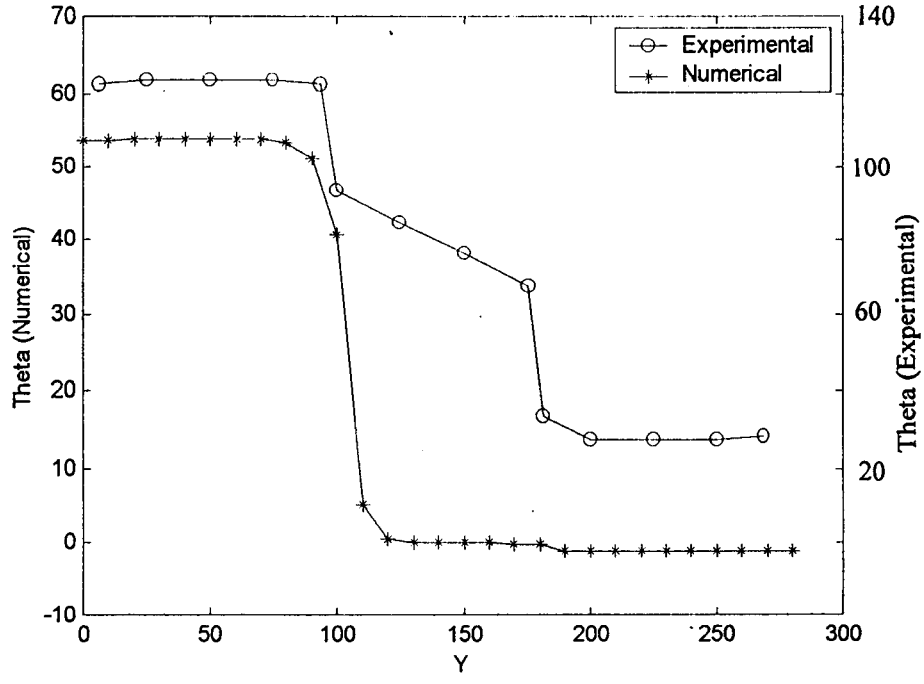

(a) Re (Liquid) = 0.0152

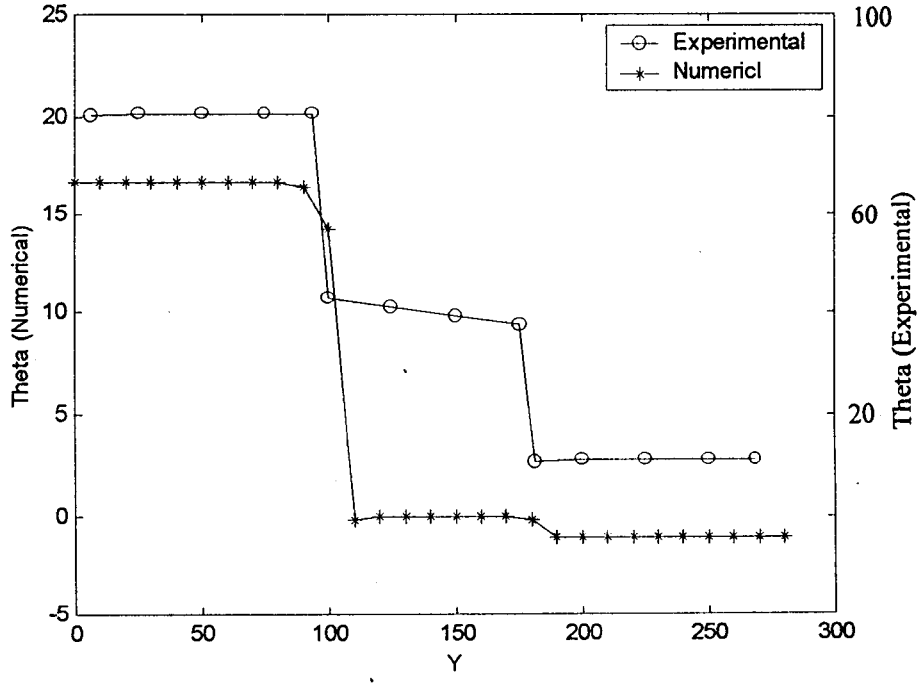

(b) Re (Liquid) = 0.0526

Fig. 6.56 Comparison of Temperature Distribution Obtained Experimentally and Numerically in Stainless Steel Flat Heat Pipe

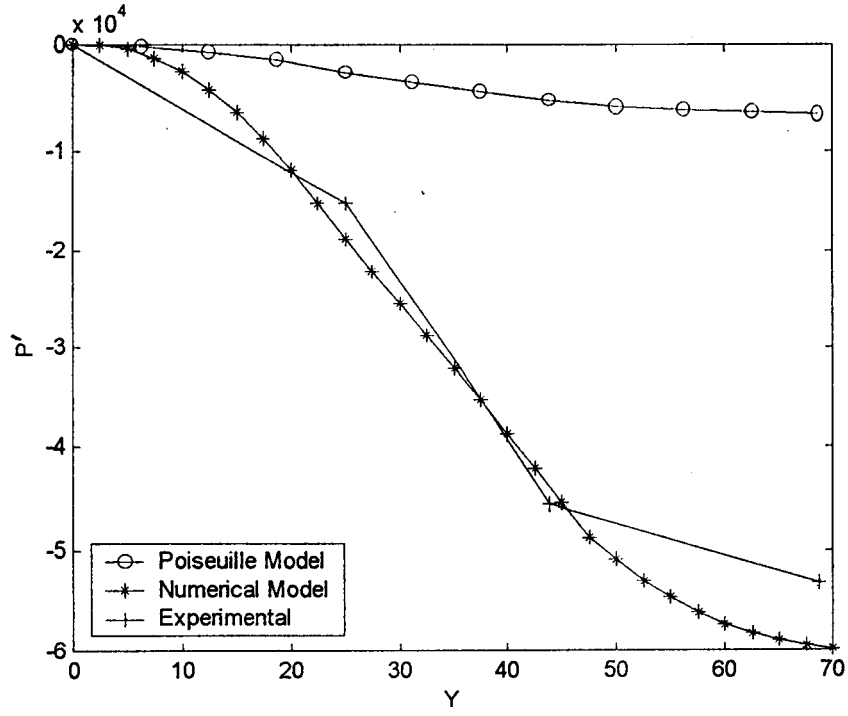

(a) Re=2.04

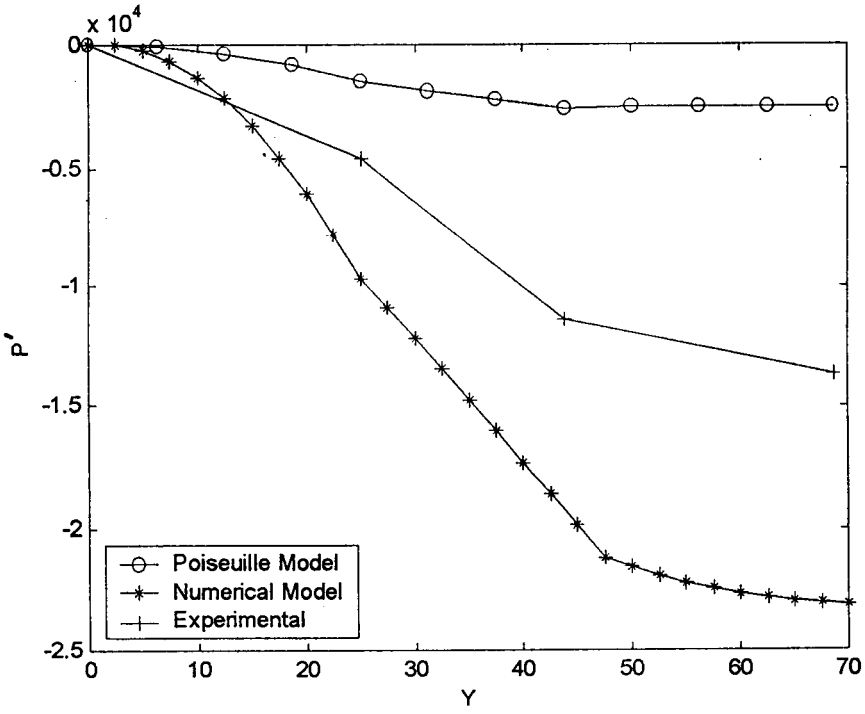

(b) Re=5.26

Fig. 6.57 Comparison of Pressure Drop in the Vapour Core

CONCLUSIONS

C. Muraleedharan “Heat transfer and fluid flow studies on flat heat pipe ” Thesis. Department of Mechanical Engineering, Calicut Regional Engineering College , University of Calicut, 2001

Chapter 7

CONCLUSIONS

7.1 Conclusions

Though the heat pipe is a simple heat transporting device, the fluid flow and heat transfer phenomena occurring within the heat pipe are quite complex in nature. Hence the analysis of heat transfer and fluid flow within the heat pipe is an involved task. In the present work, an attempt has been made to analyse the heat transfer and fluid flow in the flat heat pipe, both experimentally and theoretically. Experimental investigations have been conducted on stainless steel flat heat pipe with water and acetone as working substances. The performance characteristics of an aluminium flat heat pipe have also been obtained with acetone as the working fluid. The temperature variation in the heat pipe and the pressure profile along the vapour core have been studied. Both the vapour flow in the vapour space and liquid flow through the porous wick have been determined by the Poiseuille theory. A detailed numerical analysis was conducted and two dimensional model for the vapour flow through the vapour channel and liquid flow in the wick region have been presented with common interface conditions. The stream lines and velocity vector plots have also been obtained in addition to the velocity distribution, velocity profile, temperature variation and pressure drop for both vapour and liquid sides. The conclusions derived, from the extensive experimental and theoretical studies and the comparison of results, are detailed below.

- The vapour in the evaporator zone of vapour core in the heat pipe is in the superheated condition.

- The evaporator temperature increases with Reynolds number. The temperature difference between the evaporator and condenser also increases with Reynolds number.

- Experimentally temperature is found to be remaining almost constant at the evaporator, adiabatic and condenser zones when stainless steel is used for the heat pipe container wall except in low heat transfer rates. At low heat transport capacities a temperature gradient exists at the adiabatic section.

- The temperature of the heat pipe continuously varies from the evaporator end to the condenser end when high thermal conductivity material like aluminium is used as container material.

- The surface temperature of the heat pipe is found to be increasing with decrease in porosity of the wick structure.

- Surface temperature of the heat pipe is found to be minimum when the heat pipe is operating with the adequate charge of the working substance. This must be giving the best performance for the heat pipe and so can be considered as optimum charge of the working fluid.

- The vapour pressure drop increases with increasing Reynolds number. The vapour pressure drop is significant and thus should be taken into account in the compact design of heat pipes.

- Pressure build up is observed at high Reynolds number values, with acetone as working fluid.

- Eventhough Poiseuille model is too simple and can be used to obtain a first estimate, it is quite inadequate for pressure calculations within the heat pipe.

- The vapour flow characteristics obtained numerically have similarity with Poiseuille flow at low Reynolds number values ($Re < 5$).

- Reverse flow at the condenser was observed at high Reynolds number values ($Re \geq 12.50$). $Re=12.50$ corresponds to the capillary limit of the present heat pipe.

- At high values of Reynolds number, velocity maxima for vapour shift to top and bottom of the centre line in the evaporator and condenser zones, respectively within the vapour core.

- The temperature distribution along the vapour – wick interface is virtually uniform at every section when stainless steel is used as container material.

- The vapour pressure drop is significant and comparable with experimental results. At high Reynolds number values pressure build up has been observed.
- The liquid velocity distribution has similarity with Poiseuille flow.
- The velocity maxima have been observed closer to the wick – vapour interface.
- The temperature distribution in the wick is found to be uniform at every zone eventhough there is temperature drop between the zones. The temperature distribution has similarity with that of experimental results and that of the numerical results for vapour flow.
- The surface temperature of the heat pipe is found to be increasing with decrease in porosity.
- The nondimensional temperature difference between the evaporator and the condenser decreases as Reynolds number increases, causing high heat transfer rates.
- Pressure drop in the wick increases with decrease in porosity.
- No pressure build up has been observed in liquid wick region.

7.2 Scope for Future Work

In the present work detailed theoretical and experimental analyses of flat heat pipe have been brought out. In the numerical analysis of the flat heat pipe majority of the common conditions have been included. Still a few more parameters and conditions can be incorporated to achieve the actual physical situation. Some of them are described below:

- Multiphase flow effects may be investigated.
- Dry out limits for different types of wick structures may be predicted.
- Conjugate analysis of the heat pipe shall be done including axial heat conduction along the container wall.
- The effect of variable thermophysical properties may be incorporated in the analysis.

7.3 Contributions of Present Work

Theoretical and experimental studies have been conducted to bring out the various performance characteristics of the flat heat pipe. Based on the detailed analysis of the flat heat pipe the following important contributions are identified.

- Application of stream function- vorticity approach in the vapour core and liquid wick region of the flat heat pipe.
- Detailed analysis of liquid flow in flat heat pipe which is not much studied.
- Matching of temperature distributions between numerical and experimental studies.
- Numerical and experimental validation of temperature distribution at various porosity values.
- Experimental establishment for including axial conduction along the container wall when highly conducting material is used for the container of the heat pipe.

REFERENCES

1. Abhat, A and Seban, R.A, "Boiling and Evaporation from Heat Pipe Wicks With Water and Acetone", J. Heat Transfer, pp. 331-337, 1974.

2. Acton, A, "Correlating Equations for the Properties of Metal-Felt Wicks", Proc. 4th Int. Heat Pipe Conf., London, pp. 279-288, September 1981.

3. Ahmad, W and Khan, M, "A Digital Technique for Measurement of Differential Pressure and Flow", IEEE Trans. on Industrial Electronics and Control Instrumentation, Vol. IECI-25, No.1, pp. 26-29, 1978.

4. Anderson, D.A and Tannehill, J.C, Pletcher, R.H, "Computational Fluid Mechanics and Heat Transfer", Hemisphere Publishing Corporation, McGraw-Hill Book Company, 1984.

5. Bairamov, R and Toiliev, K, "Heat Pipes in Solar Collectors", Proc. of 4th Int. Heat Pipe Conf., pp. 47-54, London, September 1981.

6. Bankston, C.A and Smith, H.J, "Vapour Flow in Cylindrical Heat Pipes", J. of Heat Transfer, pp. 371-376, 1973.

7. Bear, J, "Dynamics of Fluids in Porous Media", American Elsevier Publishing Company Inc. New York, 1972.

8. Bilegan, I.C and Fetcu, D, "Performance Characteristics of Gravity Assisted Aluminium Extruded Heat Pipes", Proc. of 4th Int. Heat Pipe Conf., pp. 89-94, London, September 1981.

9. Bowman, J.W and Beran, P.S, "Implicit Heat Pipe Vapour Model", J. of Thermophysics, Vol. 8, No.1, Technical Notes, pp 187-190, 1993.

10. Busse, C.A, "Pressure Drop in the Vapour Phase of Long Heat Pipes", Thermionic Conversion Specialist Conf., Palo Alto, California, pp. 391-398, October 1967.

11. Busse, C.A, "Theory of the Ultimate Heat Transfer Limit of Cylindrical Heat Pipes", Int. J. of Heat and Mass Transfer, Vol.16, pp. 169-186, Pergamon Press, 1973.

12. Busse, C.A, "Theory of the Axial Dry-out Heat Flow of Gravity – Assist Heat Pipes with Capillary Flow", Advances in Heat Pipe Technology, Pergamon Press, pp. 297-312, 1982.

13. Busse, C.A, Geiger, F and Quataert, D, "Status of Emitter Heat Pipe Development at ISPRA", Thermionic Conversion Specialist Conf., Miami, Florida, pp. 550-555, October 1970.

14. Busse, C.A and Kemme, J.E, "Dry – out Phenomena in Gravity Assist Heat Pipes with Capillary Flow", Int. J. of Heat and Mass Transfer, Vol. 23, pp. 643-654, 1980.

15. Busse, C.A and Loehrke, R.I, "Subsonic Pressure Recovery in Cylindrical Condensers", J.of Heat Transfer, Vol.111, pp. 533-537, 1989.

16. Cao, Y and Faghri, A, "A Numerical Analysis of Phase – Change Problems Including Natural Convection", Trans. of the ASME, Vol. 112, pp. 812-816, 1990.

17. Cao, Y and Faghri, A, "Transient Two-Dimensional Compressible Analysis for High-Temperature Heat Pipes With Pulsed Heat Input", Numerical Heat Transfer, Part – A, Vol.18, pp 483-502, 1990.

18. Chen, M.M and Faghri, A "An Analysis of the Vapour Flow and Heat Conduction Through the Liquid Wick and Pipe Wall in a Heat Pipe with Single and Multiple Heat Sources", Int. J. of Heat and Mass Transfer, Vol.33, No.9, pp. 1945-1955, 1990.

19. Chi, S.W, "Heat Pipe Theory and Practice – A Source Book", Hemisphere Publishing Corporation, 1976.

20. Chun, K.R, "Some Experiments on Screen Wick Dry-Out Limits", J. of Heat Transfer, pp. 1-6, 1972.

21. Dunn, P.D and Reay, D.A, "Heat Pipes", Third Edition, Pergamon Press, 1982.

22. El-Genk, M.S and Huang, L, "An Experimental Investigation of the Transient Response of Water Heat Pipe", Int. J. of Heat and Mass Transfer, Vol. 36, No.15, pp. 3823-3830, 1993.

23. Faghri, A and Buchko, M, "Experimental and Numerical Analysis of Low Temperature Heat Pipes with Multiple Heat Sources", Trans. of ASME, Vol. 113, pp. 728-732, 1991.

24. Faghri, A and Harley, C, "Transient Lumped Heat Pipe Analyses", Heat Recovery Systems and CHP, Vol.14, No.4, pp. 351-363, 1994.

25. Faghri, A and Thomas, S, "Performance Characteristics of a Concentric Annular Heat Pipe, Part – I – Experimental Prediction and Analysis of the Capillary Limit, Trans. of ASME, Vol.111, pp 844-850, 1989.

26. Feldman Jr. K.J and Kenney, D.D, "The Compatibility of Mild Steel and Water in a Heat Pipe Application", Proc. of 4th Int. Heat Pipe Conf., pp. 439-450, London, September 1981.

27. Hall, M.L and Doster, M.J, "A Sensitivity Study of the Effects of Evaporation/Condensation Accommodation Coefficients on Transient Heat Pipe Modeling", Int. J. of Heat and Mass Transfer, Vol.33, No.3, pp. 465-481, 1990.

28. Hariharan, P.S, "Vapour Pressure Drop Studies in Flat Heat Pipe", M.Tech. Thesis, University of Calicut, 1991.

29. Harley, C and Faghri, A, "Transient Two - Dimensional Gas Loaded Heat Pipe Analysis", J. of Heat Transfer, Vol.116, pp. 716-723, 1994.

30. Hsiao, S.W, Chen, C.K and Cheng, P., A Numerical Solution for Natural Convection in an Inclined Porous Cavity with a Discrete Heat Source on One Wall", Int. J. of Heat and Mass Transfer, Vol.37, No.15, pp. 2193-2201, 1994.

31. Imura, H, Kozai, H and Ikeda, Y "The Effective Pore Radius of Screen Wicks", Heat Transfer Engineering, Vol.15, No.4, pp. 1994.

32. Issacci, F, Catton, I and Ghoniem, N.M, "Vapour Dynamics of Heat Pipe Start Up", J. of Heat Transfer, Vol.113, pp. 985-994, 1991.

33. Jang, J.H, Faghri, A and Chang, W.S, "Analysis of the One – Dimensional Transient Compressible Vapour Flow in Heat Pipes", Int. J. of Heat and Mass Transfer, Vol.14, No.8, pp. 2029-2037, 1991.

34. Jayee, K, Varghese, "An Investigation of Temperature Profile and Vapour Pressure Drop in a Flat Heat Pipe", M.Tech. Thesis, University of Calicut, 1994.

35. Kaviany, M, "Principles of Heat Transfer in Porous Media", Springer – Verlag, 1991.

36. Khrustalev, D and Faghri, A, "Heat Transfer During Evaporation on Capillary- Grooved Structures of Heat Pipes", J. of Heat Transfer, Vol. 117, pp. 740-747, 1995.

37. Kobayashi, Y, Ikeda, S and Iwasa, M, "Evaporative Heat Transfer at the Evaporative Section of a Grooved Heat Pipe", J. of Thermophysics and Heat Transfer, Vol.10, No.1, pp. 1996.

38. Krishna Prasad, G.N.V, "Steady State Analysis of Liquid Flow in Flat Heat Pipes", M.Tech. Thesis, University of Calicut, 2001.

39. Krishna Priya, G.S, "Steady State Analysis of Vapour Flow in Flat Heat Pipes", M.Tech. Thesis, University of Calicut, 2000.

40. Larkin, B.S, "An Experimental Study of the Temperature Profiles and Heat Transfer Coefficients in a Heat Pipe for a Heat Exchanger", Proc. of 4th Int. Heat Pipe Conf., pp. 177-191, London, September 1981.

41. Li, H.M, Liu, C.Y and Damodaran, M, "Analytical Study of the Flow and Heat Transfer in a Rotating Heat Pipe", Heat Recovery System and CHP, Vol.13, No.2, pp. 115-122, 1993.

42. Littwin, D.A and McCurley, J, "Heat Pipe Waste Heat Recovery Boilers", Proc. of 4th Int. Heat Pipe Conf., pp. 213-224, London, September 1981.

43. Longtin, J.P, Badran, B and Gerner, F.M, "A One - Dimensional Model of a Micro Heat Pipe during Steady State Operation", J. of Heat Transfer, Vol.116, pp. 709-715, 1994.

44. Munzel, W.D and Krahling, H, "Life Test Investigations with Stainless Steel / Water Heat Pipes", Proc. of 4th Int. Heat Pipe Conf., pp. 459-469, London, September 1981.

45. Muralidhar, K and Sundararajan, T, "Computational Fluid Flow and Heat Transfer", Narosa Publishing House, 1995.

46. Nield, D.A and Bejan, A, "Convection in Porous Media", Springer-Verlag, New York Inc., 1992.

47. Peretz, R, "Heat Transfer Effectiveness of Heat Pipe", Proc. of 4th Int. Heat Pipe Conf., pp. 201-211, London, September 1981.

48. Petrick, S.W, "Hydrogen Gas Generation in Water/Stainless Steel Heat Pipes", ASME Winter Annual Meeting, New York, pp. 1-7, November 1972.

49. Rao, Y.F and Wang, B.X, "Natural Convection in Vertical Porous Enclosures with Internal Heat Generation", Int. J. of Heat and Mass Transfer, Vol.34, No.1, pp. 247-252, 1991.

50. Richter, R and Gottschlich, J.M, "Thermodynamic Aspects of Heat Pipe Operation", J. of Thermodynamics and Heat Transfer, Vo.8, No.2, pp. 334-340, 1994.

51. Robert Samuel, C, "Heat Pipe Applications for Dissipating Heat from the Equipment Bay of Remote Piloted Vehicles", Final Report on the Research Project (No: 443) on Air Craft Systems Panel of A.R.D.B., Govt. of India, 1991.

52. Shibayama, S and Morooka, S, "Study on Heat Pipe, Bulletin of JSME, Vol. 22, No.171, pp. 1243-1250, 1979.

53. Shibayama, S and Morooka, S, "Study on a Heat Pipe", Int. J. of Heat and Mass Transfer, Vol.23, pp. 1003-1013, Pergamon Press, 1980.

54. Smirnov, G.F and Afanasiev, B.A, "Investigation of Vapourisation in Screen Wick Capillary Structures", Proc. of 4th Int. Heat Pipe Conf., London, pp. 405-413, September 1981.

55. Sobhan, C.B, Garimella, S.V and Unnikrishnan, V.V, "A Computational Model for the Transient Analysis of Flat Heat Pipes", 7th ITHERM 2000, Las Vegas, Nevada, Vol.2, pp. 106-113, 2000.

56. Soumitra Mahato, "Effect of Wick Structure on Heat Carrying Capacity in Flat Heat Pipe", M.Tech. Thesis, University of Calicut, 2000.

57. Sun, K.H, Liu, C.Y and Leong, K.C, "The Effective Length of a Flat Plate Heat Pipe Covered Partially by a Strip Heater on the Evaporator Section", Heat Recovery Systems and CHP, Vol.15, No.4, pp. 383-388, 1995.

58. Tien, C.L and Rohani, A.R, "Theory of Two-component Heat Pipes", J. of Heat transfer, pp. 479-484, 1972.

59. Tien, C.L and Rohani, A.R, "Analysis of the Effect of Vapour Pressure Drop on Heat Pipe Performance", Int. J. of Heat and Mass Transfer, Vol.17, pp. 61-67, Pergamon Press, 1974.

60. Tournier, J.M and El-Genk, M.S, "A Heat Pipe Transient Analysis Model", Int. J. of Heat and Mass Transfer, Vol.37, No.5, pp. 753-762, 1994.

61. Tournier, J.M and El-Genk, M.S, "A Vapour Flow Model for Analysis of Liquid – Metal Heat Pipe Start Up from a Frozen State", Int. J. of Heat and Mass Transfer, Vol.39, No.18, pp. 3767-3780, 1996.

62. Unnikrishnan, V.V and Sobhan, C.B, "Finite Difference Analysis of the Transient Performance of a Flat Heat Pipe", 10th Int. Conf. on Numerical Methods in Thermal Problems, Swansea, UK, pp. 391-400, 1997.

63. Unnikrishnan, V.V, Garimella, S.V and Sobhan, C.B, "Characterization of the Performance of Flat Heat Pipes for Electronic Applications", EEP, Vol.28, Packaging of Electronic and Photonic Devices, ASME, pp. 261-268, November 2000.

64. Vafai, K and Wang, W, "Analysis of Flow and Heat Transfer Characteristics of Asymmetrical Flat Plate Heat Pipe", Int. J.of Heat and Mass Transfer, Vol.35, No.9, pp. 2087-2099. 1992.

65. Vafai, K, Zhu, N and Wang,W, "Analysis of Asymmetric Disk-Shaped and Flat-Plate Heat Pipes", J. of Heat Transfer, Vol.117, pp. 209-218, 1995.

66. van Ooijen, H and Hoogendoorn, C.J, "Vapour Flow Calculations in a Flat Plate Heat Pipe", AIAA Jounral, Vol. 17, No.11, pp. 1251-1259, 1979.

67. van Ooijen, H and Hoogendoorn, C.J, "Experimental Pressure Profiles Along the Vapour Channel of a Flat – Plate Heat Pipe", Proc. of 4th Int. Heat Pipe Conf., pp. 415-426, September 1981.

68. Vasiliev, L.L, Grakovich, L.P and Khrustalev, D.K, "Low Temperature Axially Grooved Heat Pipes", Proc. of 4th Int. Heat Pipe Conf., London, pp. 337-348, September 1981.

69. Vasiliev, L.L and Konev, S.V, "Thermodynamic Analysis of Heat Pipe Operation", Proc. of 4th Int. Heat Pipe Conf., pp. 313-325, September 1981.

70. Wang, Y and Vafai, K, "Transient Characterization of Flat Plate Heat Pipes During Startup and Shut Down Operations", Int. J. of Heat and Mass Transfer, (43), pp. 2641-2655, 2000.

71. Wang, Y and Vafai, K, "An Experimental Investigation of the Thermal Performance of an Asymmetrical Flat Plate Heat Pipe", Int. J. of Heat and Mass Transfer, (43), pp. 2657-2668, 2000.

72. Wang, Y and Vafai, K, "An Experimental Investigation of the Transient Characteristics on a Flat - Plate Heat Pipe During Startup and Shut Down Operations", J. of Heat Transfer, Vol.122, pp. 525-535, 2000.

73. Zhu, N and Vafai, K, "Vapour and Liquid Flow in an Asymmetrical Flat Plate Heat Pipe: A Three Dimensional Analytical and Numerical Investigation", Int. J. of Heat and Mass Transfer, Vol.41, No.1, pp. 159-174, 1998.

74. Zuo, N and Faghri, A, "A Network Thermodynamic Analysis of the Heat Pipe", Int. J. of Heat and Mass Transfer, Vol.41, No.11, pp. 1473-1484, 1998.

75. Zhu, N and Vafai, K, "Analytical Modeling of the Startup Characteristics of Asymmetrical Flat – Plate and Disk – Shaped Heat Pipes", Int. J. of Heat and Mass Transfer, Vol.41, No.17, pp. 2619-2637, 1998.

LIST OF TECHNICAL PAPERS

1. Jayaraj, S, Muraleedharan, C and Jilani G, "Modeling of Vapour Flow in Flat Heat Pipes", Proc. of 24th National Systems Conf., Bangalore, pp. 111-120, December 2000.

2. Jilani, G, Muraleedharan, C and Jayaraj, S, "A Finite Difference Scheme for Vapour Dynamics Calculations in Flat Heat Pipes", Proc. of 27th National Conf. on Fluid Mechanics and Fluid Power, Palakkad, pp. 221-228, December 2000.

3. Muraleedharan, C, Jayaraj, S and Jilani, G, "An Experimental Investigation on the Performance of Flat Heat Pipes", Proc. of 24th National Systems Conf., Bangalore, pp. 134-140, December 2000.

4. Muraleedharan, C, Jayaraj, S and Jilani, G, "Modeling of Liquid Flow in Flat Heat Pipes", Int. Conf. on Fluid Mechanics, Heat Transfer and Thermodynamics, South Africa, April 2002 (Accepted).

5. Muraleedharan, C, Jayaraj, S and Jilani, G, " Steady State Analysis of Liquid Flow in Flat Heat Pipe", 25th National Systems Conf., Coimbatore, December 2001 (Communicated).

6. Muraleedharan, C, Jayaraj, S and Jilani, G, "Heat Transfer and Fluid Flow Studies With Flat Heat Pipes", AIAA J. Thermophysics (Communicated).

Appendix A

POISEUILLE APPROXIMATION MODEL

A.1 Poiseuille Theory Applied to Flat Heat Pipe

Consider the flow through the flat heat pipe as shown in Fig. A.1. In this heat pipe, the working fluid attains vapour state absorbing heat from the heat source. This vapour flows from the evaporator to the condenser through the vapour core. The vapour, condenses at the condenser zone rejecting heat to the heat sink. The condensate is returned from the condenser to the evaporator through the porous wick.

In ordinary heat pipes, which make use of working fluids other than the metallic working fluids, both the vapour flow and liquid flow will be laminar. The width of the channel is assumed to be very large compared with the height of the passage to create a two-dimensional situation by neglecting end effects. Both vapour flow and liquid flow, in the heat pipe are assumed to be two dimensional, steady and laminar.

Considering the fluid element, shown in Fig. A.2, as a free body, the various forces acting on the element are the frictional force and the pressure force. The shear force will resist the motion of the free body while a pressure gradient will be maintained in the direction of flow to overcome the frictional resistance and to continue the flow. For equilibrium in steady flow, the summation of all the forces acting on the body must be zero.

i.e., $$p\delta x - \left[p + \frac{dp}{dy}\delta y\right]\delta x - \tau\delta y + \left[\tau + \frac{d\tau}{dx}\delta x\right]\delta y = 0 \qquad \text{A.1}$$

$$-\frac{dp}{dy}\delta y\delta x = -\frac{d\tau}{dx}\delta x\delta y \qquad \text{A.2}$$

$$\frac{dp}{dy} = \frac{d\tau}{dx} \qquad \text{A.3}$$

That is, the pressure gradient in y direction is equal to the shear gradient in x direction.

A.2 Velocity Profile in the Vapour Core of Flat Heat Pipe

For the purpose of obtaining the velocity profile, following two important assumptions are made.

(i) Fluid is Newtonian

(ii) There is no slip of fluid particles at the solid boundary

$$\int d\tau = \frac{dp}{dy}\int dx \qquad \text{A.4}$$

$$\tau = \frac{dp}{dy}x + C_1 \qquad \text{A.5}$$

From the first assumption,

$$\tau = \mu_v \frac{\partial v}{dx} \qquad \text{A.6}$$

and the second assumption gives,

at $x = 0, \quad v = 0$

$x = h_v, \quad v = 0$ A.7

$$dv = \frac{1}{\mu_v}\left(\frac{dp}{dy}\right)(x + C_1)dx \qquad \text{A.8}$$

Integrating and applying proper boundary conditions,

$$v = \frac{1}{\mu_v}\left(-\frac{dp}{dy}\right)\left(h_v x - x^2\right) \qquad \text{A.9}$$

A.3 Maximum Velocity and Average Velocity

Corresponding to maximum velocity the condition to be satisfied is,

$$dv/dx = 0$$

It can be easily shown that maximum velocity occurs at $x = h_v/2$.

i.e.,
$$v_{max} = \frac{1}{8\mu_v}\left(-\frac{dp}{dy}\right)h_v^2 \qquad \text{A.10}$$

The rate of flow is given by

$$q = \int u\, dx \qquad \text{A.11}$$

$$= \int_0^{h_v} \frac{1}{2\mu_v}\left(-\frac{dp}{dy}\right)\left(h_v x - x^2\right) \qquad \text{A.12}$$

or
$$q = \frac{1}{12\mu_v}\left(-\frac{dp}{dy}\right)h_v^3 \qquad \text{A.13}$$

$$= v_y h_v \qquad \text{A.14}$$

Hence the average velocity will be

$$v_y = \frac{1}{12\mu_v}\left(-\frac{dp}{dy}\right)h_v^2 \qquad \text{A.15}$$

$$= 2/3\ v_{max} \qquad \text{A.16}$$

A.4 Local Velocity

The expression for the local velocity is

$$v_{(x,y)} = \frac{1}{2\mu_v}\left(-\frac{dp}{dy}\right)\left(h_v x - x^2\right)$$

$$= \frac{4}{8}\cdot\frac{1}{\mu_v}\left(-\frac{dp}{dy}\right)h_v^2\left[\frac{4x}{h_v} - \frac{4x^2}{h_v^2}\right]$$

$$= v_{max}\left[1-\left(\frac{2x}{h_v}-1\right)^2\right] \qquad \text{A.17}$$

i.e.,

$$v(x,y) = \frac{3}{2}v_y\left[1-\left(\frac{2x}{h_v}-1\right)^2\right] \qquad \text{A.18}$$

A.5 Pressure Drop in the Vapour Core of Flat Heat Pipe

The pressure drop in the vapour core of the flat heat pipe is given by the following expression,

$$-\frac{dp}{dy} = \frac{12\mu_v}{h_v^2}\,v_y \qquad \text{A.19}$$

In the evaporator section the liquid working fluid absorbs heat, and is converted into vapour state. From y = 0 to y = l_e, there is continuous and uniform mass injection to the vapour core and a linear velocity variation can be assumed as shown in Fig.A.3.

$$\frac{v_a}{l_e} = \frac{v_y}{y} \qquad \text{A.20}$$

i.e.,

$$v_y = v_a \frac{y}{l_e} \qquad \text{A.21}$$

Substituting this in Eq. A.19 we get

$$-dp = 12\mu_v \frac{v_a\ y}{h_v^2\ le} dy \qquad \text{A.22}$$

Integrating between 0 and y,

$$\Delta p_{f(y)} = -12\mu_v \frac{v_a\ y^2}{2h_v^2\ le} \qquad \text{A.23}$$

Case (i) Evaporator Section, y < le:

$$\Delta p_{f(y)} = -12\mu_v \frac{v_a}{h_v^{\ 2}} \left(\frac{y^2}{2l_e}\right) \qquad \text{A.24}$$

$$\dot{m} = \frac{q}{h_{fg}} = \rho_v\ a_v\ v_a \qquad \text{A.25}$$

i.e.,

$$v_a = \frac{q}{\rho_v h_v W h_{fg}} \qquad \text{A.26}$$

$$\Delta p_{f(y)} = -\frac{12\mu_v\ q}{h_v^{\ 3}\ \rho_v\ W h_{fg}} \left(\frac{y^2}{2l_e}\right) \qquad \text{A.27}$$

When $y = l_e$,

$$\Delta p_{f(y)} = -\frac{6\mu_v\ q\ l_e}{h_v^2\ \rho_v\ W\ h_{fg}} \qquad \text{A.28}$$

Case (ii) Adiabatic Section, le < x < le + la:

$$\Delta p_{f(y)} = \Delta p_{f(l_e)} + \int_{l_e}^{y} -\frac{12\mu_v\ v_a}{h_v}\ dy \qquad \text{A.29}$$

$$= \frac{-6\mu_v\ v_a\ l_e}{h_v^2} - \frac{12\mu\ v_a}{h_v^2}[y]_{l_e}^{y} \qquad \text{A.30}$$

$$\Delta p_{f(y)} = -\frac{12\mu_v\, v_a}{h_v^2}\left[\frac{l_e}{2} + (y - l_e)\right] \quad \text{A.31}$$

$$= -\frac{12\mu_v\, v_a}{h_v^2}\left[y - l_e/2\right] \quad \text{A.32}$$

Case (iii) Condenser Section, le + la < x < l:

$$v_y = \frac{(l-y)}{lc}.v_a \quad \text{A.33}$$

$$\Delta p_{f(y)} = \Delta p_{f(l_e+l_a)} + \int_{l_c+l_a}^{y} -\frac{12\mu_v(l-y)}{h_v^2\, lc}\, v_a dy \quad \text{A.34}$$

$$= \Delta p_{f(l_c+l_a)} - \frac{12\mu_v l\, v_a}{h_v^2 l_c}\left[y - (l_e + l_a)\right] + \frac{12\mu_v v_a}{h_v{}^2 l_c}\left[\frac{y^2}{2} - \frac{(l_e+l_a)^2}{2}\right] \quad \text{A.35}$$

A.6 Inertial Pressure Drop

The total pressure drop in the flow is the sum of the frictional pressure drop and inertial pressure drop. During the flow of the working fluid along the vapour core of the heat pipe, it experiences continuous acceleration in the evaporator and deceleration in the condenser. While in the adiabatic section the velocity can be found to be unchanged. The inertial pressure can be calculated form the impulse by the following equation

$$\Delta p_{in(y)} = \rho_v v_y{}^2 \quad \text{A.36}$$

Including the momentum correction, for the flow of fluid through rectangular channels, which is ,

$$\beta = \frac{\int_0^{h_v} \rho_v v^2_{(x,y)}\, dx}{\rho_v v_y{}^2 h_v} = 6/5 \quad \text{A.37}$$

Case (i) Evaporator Section:

$$\Delta p_{in(y)} = \frac{6}{5}\rho_v v_a^{\,2}\frac{y^2}{l_e^{\,2}} \qquad \text{A.38}$$

Case (ii) Adiabatic Section:

$$\Delta p_{in(y)} = \frac{6}{5}\rho_v v_a^{\,2} \qquad \text{A.39}$$

Case (iii) Condenser Section:

$$\Delta p_{in(y)} = \frac{6}{5}\rho_v v_a^{\,2}\frac{(1-y)^2}{l_c^{\,2}} \qquad \text{A.40}$$

A.7 Total Pressure Drop

The total pressure drop is the sum of the pressure drop due to friction and the inertial pressure.

$$\Delta p_v = \Delta p_{vf} + \Delta p_{vin}$$

The effective pressure drop is due to friction only because the inertial pressure has opposite sign in the evaporator and condenser regions.

A.8 Pressure Drop in the Liquid Wick Region

Flow of the liquid through the porous wick is highly laminar. The value of Reynolds number can be found to be considerably low. The flow of the liquid through the wick is from the condenser towards the evaporator. In the condenser section mass is continuously added due to condensation of vapour and the evaporator zone depletes from liquid due to evaporation. Here also, it is convenient to assume a linearly increasing velocity distribution at the condenser zone and linearly decreasing one at the evaporator. The velocity at the adiabatic zone will remain unchanged.

Since the density of the liquid is considerably high compared to that of the vapour, the velocity of liquid flow will be very low and hence the inertial term is neglected. The pressure drop in the liquid flow can be found from Darcian approach.

$$\Delta p_{lf(y)} = \frac{\mu_l}{K} y v_y \qquad \text{A.41}$$

The variation of velocity in the liquid wick region is similar to that in the vapour core, in the opposite direction.

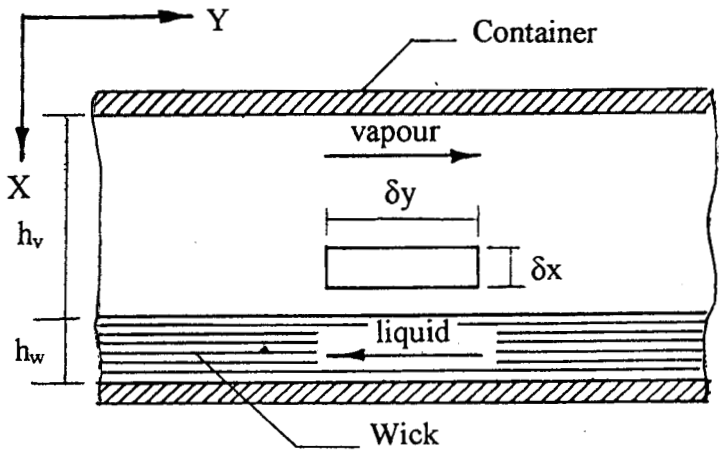

Fig A.1 Flow of Working Fluid in the Flat Heat Pipe

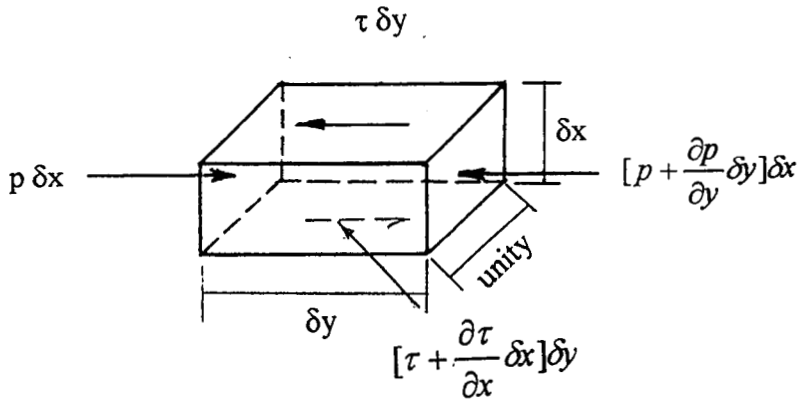

Fig.A.2 Forces Acting on the Fluid Element

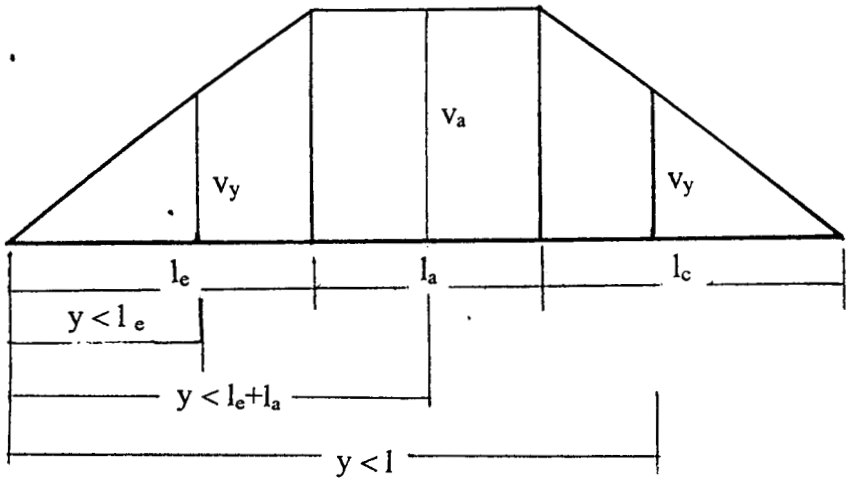

Fig.A.3 Velocity Distribution of Vapour Along the Flat Heat Pipe

Appendix B

A DIGITAL TYPE DIFFERENTIAL PRESSURE METER

A simple device for the accurate measurement of differential pressure has been developed by Wasim and Khan (1978). Based on the technique a differential pressure meter has been fabricated and used for the measurement.

The construction details of the pressure meter are shown in Fig. B.1. .There are three leads A, B and C (A and B are in mercury which are made of iron and C in water made of copper).

For any value of differential pressure with in the possible limits of the variation, the value of $L_1 + L_2$ is constant. If an a.c voltage (of zero average value and suitable rms value, V) is applied across the leads A and B, the voltage across A and C is given by,

$$V_P = L\frac{L_1}{L_1 + L_2} \tag{B.1}$$

and for a fixed value of V and L_1+L_2

$$V_P = K\,L_1 \tag{B.2}$$

V_P can be taken as a measure of the differential pressure p_1-p_2. Fig. B.2 shows the plot of V_P against p_1-p_2 obtained experimentally for the pressure meter. The a.c voltage V supplied to the transducer is 6 volts. It is observed that the relationship is linear. The difference between the theoretical and actual voltage is due to the nonsimilarity of the two water columns. It is found that if the voltmeter used is of millivolt accuracy, the differential pressure 0.02mm of mercury can be measured.

A modified form of astable multivibrator, shown in Fig. B.3, can be used to convert the output of the pressure meter into pulse numbers for direct measurements using counting technique.

If the supply voltage to the circuit is a symmetrical square wave a.c signal of suitable amplitude and frequency (3V and 200Hz square wave a.c), the circuit oscillates only during the positive half portion of a cycle and the number of output pulses per cycle of the supply voltage can be given by:

$$N = \frac{1}{4fRC}\frac{R_1}{R_1 + R_2} \tag{B.3}$$

where R_1 and R_2 are the resistances of water columns of length L_1 and L_2 respectively.

In this case $$N = \frac{1}{4fRC}\frac{L_1}{L_1 + L_2} \tag{B.4}$$

Therefore N can be taken as a measure of this differential pressure. For the circuit shown theoretical value of $N = 1.1\ L_1$. For the supply voltage a square wave audio oscillator or a square wave generator is used. It is experimentally found that the circuit performance remains independent of the supply voltage if it is kept between 1.3V and 4V. The pressure meter fabricated could not be used for the entire study because of sucking of mercury in and evaporation of mercury.

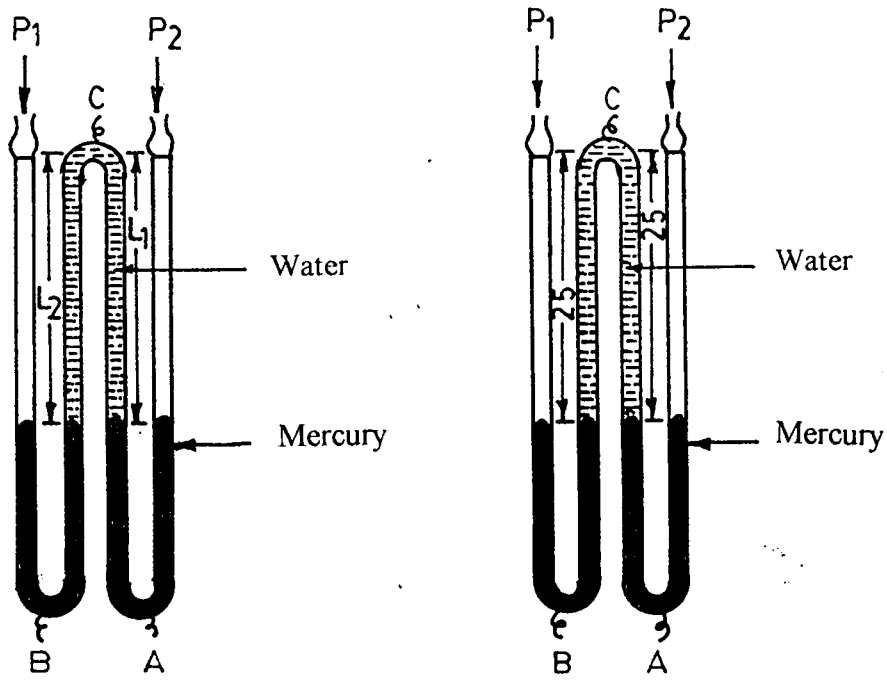

Fig.B.1 Constructional Details of Differential Pressuremeter

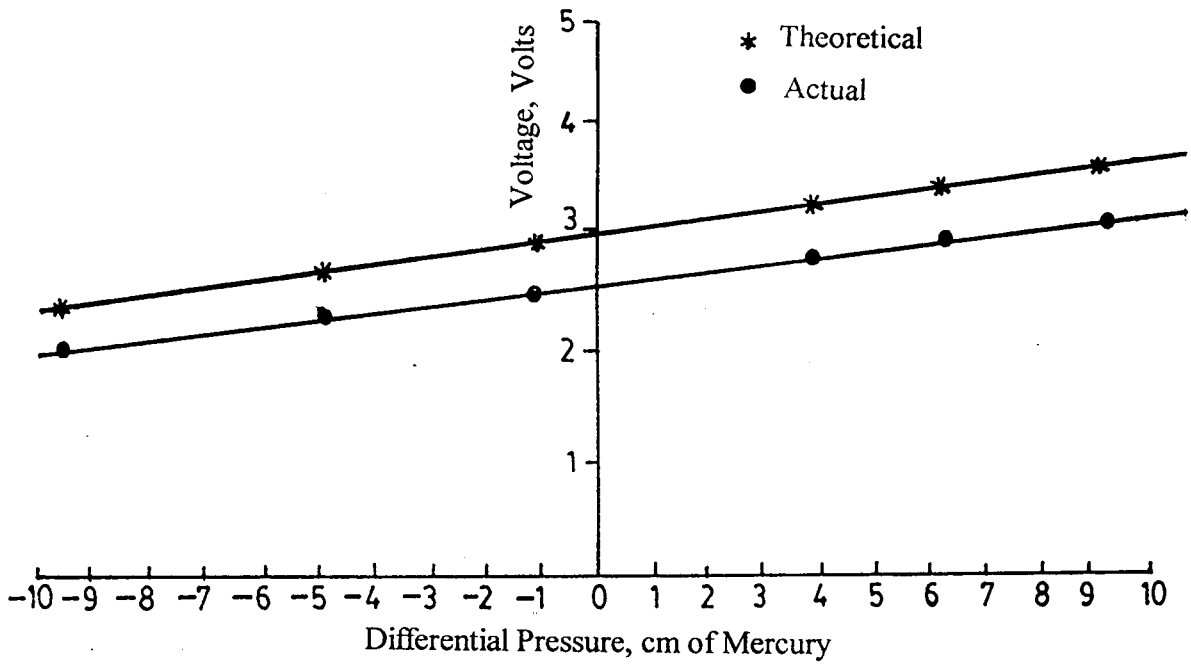

Fig.B.2 Relation Between Voltage and Differential Pressure

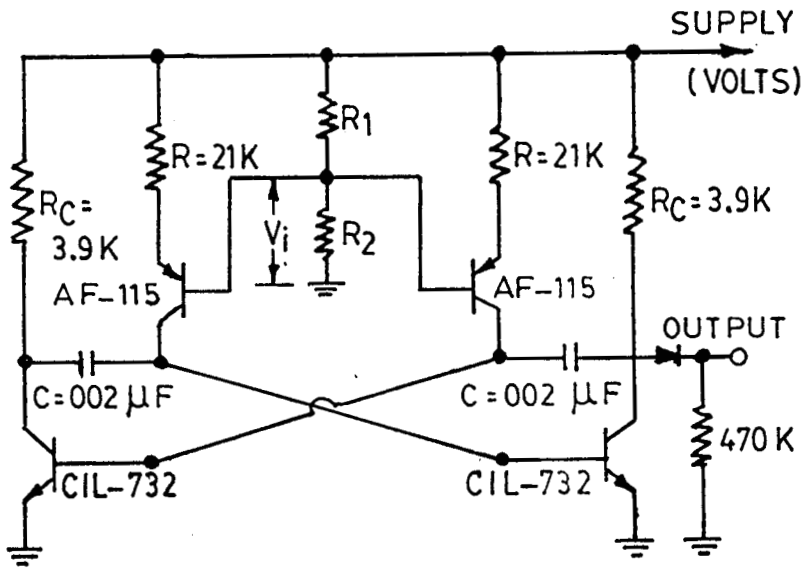

Fig.B.3 Modified Astable Multivibrator

Appendix C

PROPERTIES OF ACETONE AND WATER

Table C.1 Thermophysical Properties of Acetone

Tem	Latent Heat	Liquid Density	Vapour Density	Liquid Thermal Conduc-tivity	Liquid Visco-sity	Vapour Visco-. sity	Vapour Press-ure	Vapour Specific Heat	Liquid Surface Tension
K	KJ/kg	kg/m^3	kg/m^3	W/mK	cP	$cPx10^2$	Bar	kJ/kgK	$N/mx10^2$
233	660.0	860.0	0.03	0.200	0.800	0.68	0.01	2.00	3.10
253	615.6	845.0	0.10	0.189	0.500	0.73	0.03	2.06	2.76
273	564.0	812.0	0.26	0.183	0.395	0.78	0.10	2.11	2.62
293	552.0	790.0	0.64	0.181	0.323	0.82	0.27	2.16	2.37
313	536.0	768.0	1.05	0.175	0.269	0.86	0.60	2.22	2.12
333	517.0	744.0	2.37	0.168	0.226	0.90	1.15	2.28	1.86
353	495.0	719.0	4.30	0.160	0.192	0.95	2.15	2.34	1.62
373	472.0	689.6	6.94	0.148	0.170	0.98	4.43	2.39	1.34
393	426.1	660.3	11.02	0.135	0.148	0.99	6.70	2.45	1.07
413	394.4	631.8	18.61	0.126	0.132	1.03	10.49	2.50	0.81

Table C.2 Thermophysical Properties of Water

293	2448	998.2	0.02	0.603	1.00	0.96	0.02	1.81	7.28
313	2402	992.3	0.05	0.630	0.65	1.04	0.07	1.89	6.96
333	2359	983.0	0.13	0.649	0.47	1.12	0.20	1.91	6.62
353	2309	972.0	0.29	0.668	0.36	1.19	0.47	1.95	6.26
373	2258	958.0	0.60	0.680	0.28	1.27	1.01	2.01	5.89
393	2200	945.0	1.12	0.682	0.23	1.34	2.02	2.09	5.50
413	2139	928.0	1.99	0.683	0.20	1.41	3.90	2.21	5.06
433	2074	909.0	3.27	0.679	0.17	1.49	6.44	2.38	4.66
453	2003	888.0	5.16	0.669	0.15	1.57	10.04	2.62	4.29
473	1967	865.0	7.87	0.659	0.14	1.65	16.19	2.91	3.89